UMinho | 2013

Vítor Emanuel da Silva Matos

A Bio-inspired architecture for adaptive
quadruped locomotion over irregular terrain

Universidade do Minho
Escola de Engenharia

Vítor Emanuel da Silva Matos

A Bio-inspired architecture for adaptive quadruped locomotion over irregular terrain

Outubro de 2013

Universidade do Minho
Escola de Engenharia

Vítor Emanuel da Silva Matos

A Bio-inspired architecture for adaptive quadruped locomotion over irregular terrain

Tese de Doutoramento
Programa Doutoral em
Engenharia Electrónica e de Computadores

Trabalho efectuado sob a orientação da
Professora Doutora Cristina Manuela Peixoto Santos

Outubro de 2013

DECLARAÇÃO

Vítor Emanuel da Silva Matos

Endereço electrónico: vmatos@dei.uminhopt Telefone: _9149623222

Número do Bilhete de Identidade: 12955116

Título tese:

A Bio-inspired architecture for adaptive quadruped locomotion over irregular terrain

Orientadora:

Professora Doutora Cristina Manuela Peixoto Santos

Ano de conclusão: _2013

Designação do Ramo de Conhecimento do Doutoramento:

Programa Doutoral em Engenharia Electrónica e de Computadores

Nos exemplares das teses de doutoramento ou de mestrado ou de outros trabalhos entregues para prestação de provas públicas nas universidades ou outros estabelecimentos de ensino, e dos quais é obrigatoriamente enviado um exemplar para depósito legal na Biblioteca Nacional e, pelo menos outro para a biblioteca da universidade respectiva, deve constar uma das seguintes declarações:

> É AUTORIZADA A REPRODUÇÃO INTEGRAL DESTA TESE APENAS PARA EFEITOS DE INVESTIGAÇÃO, MEDIANTE DECLARAÇÃO ESCRITA DO INTERESSADO, QUE A TAL SE COMPROMETE.

Universidade do Minho, _24_/_10_/_2013_

Assinatura: ____

ACKNOWLEDGEMENTS

I would like to thank the many wonderful people I had the pleasure of meeting and working with during the pursuit my thesis.

First and foremost, I would like to thank my advisor Cristina Santos by allowing me to integrate this research group and inviting me to pursue this project under her guidance. I am extremely grateful for the dedication and support towards her students despite tight schedules of a researcher with many projects, the fruitful discussions, and the constant motivation to pursue intellectual challenging topics. The help and advice I received was invaluable on the execution of the present work, by providing suggestions and pushing me forward when I got stuck, by inviting me to take on new research problems, and by participating very closely on the completion of many publications.

Every day of these four years were joyful thanks to everybody in the lab, who have made a good working experience despite the tight space. I am especially grateful to the other permanent residents of the lab, Miguel, Jorge, Carolina, Pedro and Maria, for all the friendship and companionship.

I would like to thank Miguel Oliveira for all the help when I first came to the lab, introducing me to the simulation tools, controllers and the basic workflow with the robots, and for his help and discussions on how to improve the performance of our solutions and on the design of optimizations in the robots. Jorge Silva for the constant discussions on dynamical systems approach to robotics, on how, and if, they can be applied in robotics, for the insight on stability of nonlinear systems and the mutual interest on understanding the behavior of the Landau-Stuart oscillator when constantly modulated. Pedro Silva, who I share many common interests, the spurring philosophical debates on computing and open-source, though provoking discussions on a broad range of topics, from artificial intelligence to machine learning.

I would like to express my gratitude to Vincent Padois and Joseph Salini by the opportunity to learn new topics in robotics, and collaborating on the whole-body control framework. It was also a great pleasure to visit and work in ISIR for one week, where they received me with open arms.

I am grateful to Auke Ijspeert for accepting to collaborate with us, and for receiving me on Biorob's lab. I would like to thank all members, since everybody was equally welcoming, friendly and helpful, making me feel like I was part of the group and were always available to clarify any doubt or help on any problem I had. I truly enjoyed working for three months in such a dynamic environment, full of great students and researchers.

Finally, I must thank my dearest friends and family, for their constant support, love and encouragement.

The presented work was possible thanks to the support by the Portuguese Science and Technology Foundation through the PhD grant SFRH/BD/62047/2009.

ABSTRACT

This thesis presents a tentative advancement on walking control of small quadruped and humanoid position controlled robots, addressing the problem of walk generation by combining dynamical systems approach to motor control, insights from neuroethology research on vertebrate motor control and computational neuroscience.

Legged locomotion is a complex dynamical process, despite the seemingly easy and natural behavior of the constantly present proficiency of legged animals. Research on locomotion and motor control in vertebrate animals from the last decades has brought to the attention of roboticists, the potential of the nature's solutions to robot applications. Recent knowledge on the organization of complex motor generation and on mechanics and dynamics of locomotion has been successfully exploited to pursue agile robot locomotion.

The work presented on this manuscript is part of an effort on the pursuit in devising a general, model free solution, for the generation of robust and adaptable walking behaviors. It strives to devise a practical solution applicable to real robots, such as the Sony's quadruped AIBO and Robotis' DARwIn-OP humanoid. The discussed solutions are inspired on the functional description of the vertebrate neural systems, especially on the concept of Central Pattern Generators (CPGs), their structure and organization, components and sensorimotor interactions. They use a dynamical systems approach for the implementation of the controller, especially on the use of nonlinear oscillators and exploitation of their properties.

The main topics of this thesis are divided into three parts.

The first part concerns quadruped locomotion, extending a previous CPG solution using nonlinear oscillators, and discussing an organization on three hierarchical levels of abstraction, sharing the purpose and knowledge of other works. It proposes a CPG solution which generates the walking motion for the whole-leg, which is then organized in a network for the production of quadrupedal gaits. The devised solution is able to produce goal-oriented locomotion and navigation as directed through high-level commands from local planning methods. In this part, active balance on a standing quadruped is also addressed, proposing a method based on dynamical systems approach, exploring the integration of parallel postural mechanisms from several sensory modalities. The solutions are all successfully tested on the quadruped AIBO robot.

In the second part, is addressed bipedal walking for humanoid robots. A CPG solution for biped walking based on the concept of motion primitives is proposed, loosely based on the idea of synergistic organization of vertebrate motor control. A set of motion primitives is shown to produce the basis of simple biped walking, and generalizable to goal-oriented walking. Using the proposed CPG, the inclusion of feedback mechanisms is investigated, for modulation and adaptation of walking, through phase transition control according to foot load information. The proposed solution is validated on the humanoid DARwIn-OP, and its application is evaluated within a whole-body control framework.

The third part sidesteps a little from the other two topics. It discusses the CPG as having an alternative role to direct motor generation in locomotion, serving instead as a processor of sensory information for a feedback based motor generation. In this work a reflex based walking controller is devised for the compliant quadruped Oncilla robot, to serve as purely feedback based walking generation. The capabilities of the reflex network are shown in simulations, followed by a brief discussion on its limitations, and how they could be improved by the inclusion of a CPG.

Keywords: Legged robots, locomotion, central pattern generators, oscillators, dynamical systems, reflexes

SUMÁRIO

Esta tese apresenta uma tentativa de avanço no controlo de locomoção para pequenos robôs quadrúpedes e bipedes controlados por posição, endereçando o problema de geração motora através da combinação da abordagem de sistemas dinâmicos para o controlo motor, e perspectivas de investigação neuroetologia no controlo motor vertebrado e neurociência computacional.

Andar é um processo dinâmico e complexo, apesar de parecer um comportamento fácil e natural devido à presença constante de animais proficientes em locomoção terrestre. Investigação na área da locomoção e controlo motor em animais vertebrados nas últimas decadas, trouxe à atenção dos roboticistas o potencial das soluções encontradas pela natureza aplicadas a aplicações robóticas. Conhecimento recente relativo à geração de comportamentos motores complexos e da mecânica da locomoção tem sido explorada com sucesso na procura de locomoção ágil na robótica.

O trabalho apresentado neste documento é parte de um esforço no desenho de uma solução geral, e independente de modelos, para a geração robusta e adaptável de comportamentos locomotores. O foco é desenhar uma solução prática, aplicável a robôs reais, tal como o quadrúpede Sony AIBO e o humanóide DARwIn-OP. As soluções discutidas são inspiradas na descrição funcional do sistema nervoso vertebrado, especialmente no conceito de *Central Pattern Generators* (CPGs), a sua estrutura e organização, componentes e interacção sensorimotora. Estas soluções são implementadas usando uma abordagem em sistemas dinâmicos, focandos o uso de osciladores não lineares e a explorando as suas propriedades.

Os tópicos principais desta tese estão divididos em três partes.

A primeira parte explora o tema de locomoção quadrúpede, expandindo soluções prévias de CPGs usando osciladores não lineares, e discutindo uma organização em três níveis de abstracção, partilhando as ideias de outros trabalhos. Propõe uma solução de CPG que gera os movimentos locomotores para uma perna, que é depois organizado numa rede, para a produção de marcha quadrúpede. A solução concebida é capaz de produzir locomoção e navegação, comandada através de comandos de alto nível, produzidos por métodos de planeamento local. Nesta parte também endereçado o problema da manutenção do equilíbrio num robô quadrúpede parado, propondo um método baseado na abordagem em sistemas dinâmicos, explorando a integração de mecanismos posturais em paralelo, provenientes de várias modalidades sensoriais. As soluções são todas testadas com sucesso no robô quadrupede AIBO.

Na segunda parte é endereçado o problema de locomoção bípede. É proposto um CPG baseado no conceito de *motion primitives*, baseadas na ideia de uma organização sinergética do controlo motor vertebrado. Um conjunto de *motion primitives* é usado para produzir a base de uma locomoção bípede simples e generalizável para navegação. Esta proposta de CPG é usada para de seguida se investigar a inclusão de mecanismos de *feedback* para modulação e adaptação da marcha, através do controlo de transições entre fases, de acordo com a informação de carga dos pés. A solução proposta é validada no robô humanóide DARwIn-OP, e a sua aplicação no contexto do *framework* de *whole-body control* é também avaliada.

A terceira parte desvia um pouco dos outros dois tópicos. Discute o CPG como tendo um papel alternativo ao controlo motor directo, servindo em vez como um processador de informação sensorial para um mecanismo de locomoção puramente em *feedback*. Neste trabalho é desenhado um controlador baseado em reflexos para a geração da marcha de um quadrúpede *compliant*. As suas capacidades são demonstradas em simulação, seguidas por uma breve discussão nas suas limitações, e como estas podem ser ultrapassadas pela inclusão de um CPG.

Palavras-chave: Locomoção robótica, central pattern generators, osciladores, sistemas dinâmicos, reflexos

TABLE OF CONTENTS

Acknowledgements **iii**

Abstract **v**

Sumário **vii**

Table of Contents **ix**

1 Introduction **1**
1.1 List of publications related to this thesis 4

2 Context and related work **7**
2.1 Legged robot locomotion 7
2.1.1 Characteristics of quadrupedal and bipedal walking 9
2.1.2 Static balanced locomotion 11
2.1.3 Dynamic balanced locomotion 12
2.1.4 Bio-inspired robotic locomotion 13
2.2 Central Pattern Generators 14
2.2.1 Sensory modulation and adaptation 16
2.2.2 Interesting features for robot motor control 18
2.3 Central Pattern Generators in robotics 19
2.3.1 Robot locomotion and motor control 19
2.3.2 Level of abstraction 20
2.3.3 Locomotion in legged robots 20
2.3.4 CPG modeling and implementation 21
2.3.5 Feedback mechanisms in CPG based controllers 23
2.4 Dynamical systems approach 25

3 Modeling Central Pattern Generators **27**
3.1 CPG model of distributed unit generators 28
3.1.1 Landau-Stuart oscillator 29
3.1.2 Oscillator coupling 32
3.1.3 Discrete dynamical system 34

3.2 Two layer CPG model . . . 35
3.2.1 Rhythm generator . . . 36
3.2.2 Motion pattern generator . . . 37

4 Quadruped locomotion 39
4.1 Related works . . . 39
4.2 Quadruped CPG approach . . . 41
4.2.1 Generation level . . . 42
4.2.2 Regulation level . . . 50
4.3 Omnidirectional walking experiments . . . 56
4.3.1 Steering . . . 57
4.3.2 Diagonal walk . . . 58
4.3.3 Walking laterally . . . 59
4.3.4 Steering diagonally . . . 59
4.3.5 Remarks on omnidirectional walking . . . 65
4.4 Navigation application . . . 65
4.4.1 Heading direction dynamics . . . 66
4.4.2 Velocity dynamics . . . 67
4.4.3 Simulations . . . 68
4.4.4 Remarks on quadruped navigation . . . 72
4.5 Entrainment of pendular effects . . . 72
4.5.1 Revisiting the locomotor system . . . 73
4.5.2 Robot phase coupling . . . 73
4.5.3 Simulations . . . 75
4.5.4 Remarks on entrainment of pendular effects . . . 80
4.6 Standing postural control . . . 81
4.6.1 Postural control . . . 81
4.6.2 Revisiting the CPG model . . . 82
4.6.3 Postural control system . . . 83
4.6.4 Experimental results . . . 89
4.6.5 Remarks on standing postural control . . . 96
4.7 Discussion . . . 96

5 Biped locomotion 99
5.1 Bipedal CPG approach . . . 99
5.1.1 Rhythm generator . . . 101
5.1.2 Motion pattern generator . . . 102
5.2 Motion primitives . . . 103
5.2.1 Balancing motion . . . 104
5.2.2 Flexion motion . . . 104
5.2.3 Compass motion . . . 106
5.2.4 Turning motion . . . 109
5.2.5 Knee yielding motion . . . 109
5.2.6 Pelvis rotation motion . . . 109
5.2.7 Motion summary . . . 111
5.2.8 Other locomotor behaviors . . . 111
5.3 Bipedal walking demonstrations . . . 112
5.3.1 Motion primitive parametrization . . . 112

5.3.2 Forward walking 119
5.3.3 Turning 120
5.3.4 Ball following 120
5.3.5 Comparison with ZMP walking 122
5.3.6 Remarks on bipedal walking 132
5.4 Phase regulation 132
5.4.1 Phase regulation mechanism 133
5.4.2 Simulations with HOAP-2 137
5.4.3 DARwIn-OP experiments 139
5.4.4 Remarks on phase regulation 142
5.5 Open-loop CPG within LQP whole-body control 142
5.5.1 Whole-body control 143
5.5.2 CPG based walking on Whole-body control 145
5.5.3 Simulations 146
5.5.4 Remarks on CPG within whole-body control framework 156
5.6 Discussion 156

6 Reflex-based quadruped walking **159**
6.1 Related works 160
6.1.1 Summary of reflexes 164
6.2 Modeling and implementation 164
6.2.1 Neuron model 166
6.2.2 Sensory inputs 166
6.2.3 Reflex network 166
6.3 Simulations 168
6.3.1 Hind legs 169
6.3.2 Fore legs 175
6.3.3 Fore and hind legs 178
6.4 Remarks on reflex-based quadruped walking 180
6.4.1 Integration of the reflex network with a CPG 180

7 Conclusions **183**

Bibliography **187**

A Landau-Stuart oscillator **203**
A.1 Behavior and stability of the oscillator 203
A.2 Phase coupling into Landau-Stuart oscillator 206

B Phase oscillator coupling **207**

CHAPTER 1

INTRODUCTION

The present manuscript describes the work the author developed throughout his doctoral studies while integrated in the Adaptive System Behaviour Group at Universidade do Minho. This work addresses the problem of walk generation for legged robots by combining insights of dynamical systems theory, concepts from computational neuroscience and robotics. It presents a tentative advancement for walking control on small quadruped and humanoid position controlled robots through the application of concepts from neuroethology research on vertebrate motor control and the concept of Central Pattern Generator (CPG).

Motivation Legged locomotion is characterized by a discrete sequence of support points for support of the body and progression on the environment. The ability to explicit choose support points present several advantages over other forms of robot locomotion, presenting a better alternative for mobility on certain tasks on unstructured environments. It has the advantage of minimal environment impact, high maneuverability on unstructured terrains with the possibility of negotiating obstacles and terrains' features, while enabling to decouple between the base and the ground, providing attitude manipulation.

However, to achieve agile robot legged locomotion, many challenging problems and requirements must be addressed. Broad research topics are included in robot walking, including the problems related with mechanical design, such as energy efficiency and actuation method, or problems related with the control of walking, dealing with environment perception, planning and high redundancy of the closed-loop kinematics. Agile locomotion requires the control of the dynamical interactions between the robot and the environment, possibly partially unknown and subject to unperceived perturbations. Generated motions are required to provide support for the body's weight, while producing the necessary propulsion and maintaining the balance as it negotiates the varied terrain features, where each foot placement is a potential disturbance to the robot stability. As a partially solved problem with a great potential for mobility and autonomy, legged locomotion is a very interesting research field related to dynamic motor control in robotics.

One usually does not realize the complexity of legged locomotion unless one ponders on it, especially because walking, running and climbing are ubiquitous abilities in one's life experience. Legged animals are proficient walkers on unstructured terrains and are able to generalize their ability to unexplored terrains by choosing appropriate strategies on the fly within their motor abilities. These abilities have always roused the interest of researchers on understanding the neural mechanisms governing motor behavior. Research in the last decades has brought many insights on vertebrate motor control, on the organization of the central nervous system (CNS), on the control of voluntary movements and on the centers responsible for the production of rhythmic motor actions, the CPG, including those of locomotion.

Inspiration from the concept of CPGs and the dynamic interactions of sensory feedback processes have been used for a while in the design of robotic solutions. It is believed that if reaching an understanding of the mechanisms at play in the control of locomotion, one can design a better controller able to achieve flexible and adaptive robot walking.

Goals and methods The work herein presented is part of a wider team project which endeavors to achieve general and autonomous robot walking by designing a controller capable of generating purposeful, robust locomotion for unknown and irregular terrains. The project focus the research on the use of the CPG concept and on a dynamical systems approach for the design of a walking control mechanism for small quadruped and small biped robots.

In the present work is chosen an abstract approach for the design of a walking controller based on the concept of CPGs, such that the proposed models are better suited for robotic implementation. It addresses the problem from an engineering perspective, rather than trying to faithfully model the neuronal circuits and organization, it takes inspiration from the functional description of the vertebrate CNS, CPGs, their structure and organization, components and sensorimotor interactions.

The proposed solution relies on the dynamical systems approach for the implementation of the controller, especially on the use of nonlinear oscillators and exploitation of their properties. The dynamical systems approach has proven to be successful in several robotic applications [44, 91, 94, 189, 192, 198], providing desirable features for dynamic motor control. Furthermore, the proposed model extends other's [44, 174] and the team's related work on: postural control [36]; locomotion-induced head movement minimization [186]; gait transition [131] and a drumming task [46]. This choice allows to apply previously proposed mechanisms and solutions, and enables the sharing of the advancements within the framework.

The goal is to devise a general model free solution using the discussed framework, capable of arbitrarily generate complex movements for the execution of different locomotor behaviors. The used framework allows the inclusion of feedback mechanisms, enabling the influence of sensory information from multiple modalities for the correction and adaptation of the produced rhythmic motions, to achieve a more robust, flexible and adaptive walking. It aims to design a solution which achieves a correct coordination and timing of motor patterns, posture and behavior selection to environment and body changes through feedback mechanisms.

The present work strives to devise a practical solution applicable to real robots, such as the Sony's quadruped AIBO and Robotis' DARwIn-OP humanoid.

Contribution The contributions of the present work relates to the advancement and expansion of capabilities of current solutions based on the concept of CPGs and dynamical systems for the control of walking robots. It addresses the problem of quadruped and biped walking by proposing two solutions which are based on two current views on the possible organization of vertebrate CPGs.

Purposeful, goal-oriented quadruped omnidirectional locomotion has been accomplished on a CPG based solution. The proposed organization of interconnected oscillators within a CPG allows for whole coordinated leg control, requiring no explicit low-level planning. The proposed CPG is capable of producing rhythmic and discrete motions for all three joints in a leg, including double peak motions for the knee joint, reducing the dimensionality of the low-level control of the end effectors. Furthermore, quadrupedal gaits are achieved as a result of the coordinated interaction among the CPGs, enabling the performance of different quadruped gaits. The proposed solution successfully decouples low-level planning and trajectory generation from high-level planning of the walking task, as demonstrated in simulated and real quadruped robots [184, 185].

A method for active balance on a standing quadruped was also proposed. Based on the features of dynamical systems approach, it accomplishes the integration of parallel postural mechanisms from several sensory modalities. It was demonstrated in simulation and in a quadruped platform that the robot satisfyingly maintains stability and does not fall when subject to different perturbations.

In the topic of biped locomotion, a distinct view on the CPG organization was used, since the problem is slightly more challenging in matters of balance and trajectory generation on a biped walker. The proposed CPG solution is based on the idea of two separate layers, one for rhythm generation and other for pattern generation. The solution exploits the idea of motion primitives for a modular construction of the robot's motor abilities. A successful identification of a minimum required set of motion primitives for a capable goal-oriented walking was also achieved. This is demonstrated in a small humanoid DARwIn-OP and in simulation for several robot models, including on the iCub model where it is achieved the integration of the CPG within a method for whole-body control [182].

A feedback mechanisms was proposed for the regulation of the timing of the step phases. These phase regulation mechanisms adapt the produced motions depending on the current step phase and current sensory information, coupling the controller to the exhibited behavior and environment. The application of phase regulation mechanisms has been demonstrated to achieve adaptation to small unperceived slopes on the DARwIn-OP robot [130].

Lastly, a reflex based controller is presented in an effort to explore a possible alternative role of the CPG in the generation of legged locomotion. It aims to promote the discussion on the role of the CPG as a filter, or process coordinator of a motor reflex chain, instead of having a role as explicit motor generator.

After a survey on motor reflexes observed in animal locomotion and a review of reflex based solutions in simulation and legged robot control, it is defined a generalized set of reflexes elicited from sensory events, to be implemented in a reflex chain network. The proposed reflex chain network produces locomotor patterns in the compliant quadruped robot Oncilla according to sensory information and sensory events. It is then used to discuss the possible integration of the CPG and its role on top of the reflex network.

Outline After the introductory notes on the motivation, goals and contributions, the context of legged locomotion is presented in chapter 2. It covers some important concepts of legged robot locomotion and legged locomotion in general. The concept of CPG is clarified, providing some insight on the role of sensory information within locomotion generation, and reviews its interesting features for robot locomotor control. A small survey of CPG application on robotics is then presented, explaining its approaches, characteristics and interpreting its results. Chapter 3 presents the methodology and framework employed in this thesis, presenting two method for modeling CPGs. These CPG models are employed for the formulation of quadruped (chapter 4) and biped walking (chapter 5) generation, and is demonstrated its application in goal-oriented scenarios. Chapter 6 discusses an alternative role for the CPG within locomotion generation, and presents a reflex based walking generator for the compliant quadruped robot Oncilla. A summary and discussion of the results of this thesis is presented in chapter 7.

A list of movies pertaining to this thesis is available at `http://asbg.dei.uminho.pt/user/1`.

1.1 List of publications related to this thesis

Journal articles

- Cristina P. Santos and Vítor Matos, *CPG modulation for navigation and omnidirectional quadruped locomotion*, Robotics and Autonomous Systems, Volume 60, Issue 6, June 2012, Pages 912-927
- Cristina P. Santos and Vítor Matos, *Gait Transition and modulation in a quadruped robot: A brainstem-like modulation approach*, Robotics and Autonomous Systems, Volume 59, Issue 9, September 2011, Pages 620-634

Conference papers

- Miguel Oliveira, Vitor Matos, Cristina Santos and Lino Costa, *Multi-objective Parameter CPG Optimization for Gait Generation of a Biped Robot*, IEEE International Conference on Robotics and Automation, Karlsruhe, Germany, May 6 - 10, 2013.
- Vitor Matos and Cristina Santos, *Central Pattern Generators with Phase Regulation for the Control of Humanoid Locomotion*, IEEE-RAS International Conference on Humanoid Robots, Osaka, Japan, November 29th - December 1st, 2012.
- Pedro Silva, Vitor Matos, Cristina Santos, *Adaptive Quadruped Locomotion: Learning to Detect and Avoid an Obstacle*, From animals to animats 12: Proc. Int. Conf. Simulation of Adaptive Behaviour, 2012.
- Vitor Matos and Cristina Santos, *Omnidirectional Locomotion in a Quadruped Robot: A CPG-Based Approach*, 2010 IEEE/RSJ International Conference on Intelligent Robots and Systems, Taipei, Taiwan, October 18th-2th, 2010.

- João Sousa, Vitor Matos and Cristina Santos, *A Bio-Inspired Postural Control for a Quadruped Robot: An Attractor-Based Dynamics*, 2010 IEEE/RSJ International Conference on Intelligent Robots and Systems, Taipei, Taiwan, October 18th-2th, 2010.
- Jorge Bruno Silva, Vitor Matos and Cristina Santos, *Generating Trajectories With Temporal Constraints for an Autonomous Robot*, 8th IEEE International Workshop on Safety, Security & Rescue Robotics (SSRR - 2010)
- Jorge Bruno Silva, Vitor Matos and Cristina Santos, *Timed Trajectory generation for a toy-like wheeled robot*, IECON-2010, in 36th Annual Conference of the IEEE Indus- trial Electronics Society
- Ricardo Campos, Vitor Matos, Miguel Oliveira and Cristina Santos, *Gait generation for a simulated hexapod robot: a nonlinear systems approach*, Controlo - 9th Portuguese conference on automatic control, 2010.
- Cristina Santos, Miguel Oliveira, Vitor Matos, Ana Maria Rocha and Lino Costa, *Combining Central Pattern Generators with the Electromagnetism-like Algorithm for Head Motion Stabilization during Quadruped Robot Locomotion*, 2009 IEEE/RSJ International Conference on Intelligent Robots and Systems, St. Louis, USA, October 11th-15th, 2009.

Poster communications

- *Attractor-based postural control for a quadruped robot*, International Workshop on Bio-inspired Robots, Ecole des Mines de Nantes, April 6th to April 8th, 2011.
- *Bio-inspired postural control for a standing quadruped robot*, 9th International Congress of Neuroethology, Salamanca, Spain, August 2nd-7th, 2010.

CHAPTER 2

CONTEXT AND RELATED WORK

Mobility in autonomous robots can be a means to alternate and move between distant task locations, or can play a very important role on the execution of the task itself, e.g. carrying cargo, explore environments, human interaction as in the case of humanoid robots.

The goal of research on legged robot locomotion is to create mechanisms providing for the improvement of the performance on their mobility and autonomy. Locomotion performance in legged robots is often defined by energy efficiency, locomotion smoothness and stability, walking velocity, adaptability to the terrain and robustness to unforeseen perturbations. Performance requirements from walking robots ought to be defined by the required mobility, largely influenced by the task and the environment the robot must navigate.

The final result of legged robot research would be to have a robot capable of achieving a locomotion performance similar to humans and other legged animals, which excel in walking and running, especially when innately generalizing their abilities to novel environments or rough terrains.

In this chapter is presented an overview of the first defining works in the field of legged robot locomotion. Having this overview one can have a better understanding of following and current research, what kind of problems face, how are addressed and accompanying technological advances. This description will allow for framing the discussion around locomotion solutions based on Central Pattern Generators (CPGs).

After a small description of CPGs and their role in the production of locomotion within the Central Nervous System, the most interesting features are aggregated and presented as basis of the motivation of recent works applying the CPG concept to legged robots. These works are discussed regarding the target platform, design methodology and implementation, and the feedback mechanisms employed.

2.1 Legged robot locomotion

Terrestrial animal locomotion is rich in its diversity and variety, and it provides an immense research subject in several fields, from biomechanics to neuroscience. Focus is herein placed in bipedal and quadrupedal terrestrial locomotion, as it is argued that knowledge from these subjects could help in improving current legged robot locomotion capabilities. Studying, understanding and simulating the animals' locomotion mechanisms can be an efficient method for advancing current state of the art on robot mechanical designs and control solutions. This pursuit tries to close the gap in locomotion agility in a wide range of terrains, between robots and the familiar mammal tetrapods, as cats, dogs, horses, cheetahs or gazelles.

Achieving such desired agility is no trivial task, as the main problems to solve involve the complexity of legs and body, stability and power consumption [197].

The versatility which legged locomotion allows is also one considerable challenge. On each leg, increasing the number of DOFs may allow for more versatile movements, but with the cost of more complex control and planning, and increasing energy expenditure. The dual role of legs in such a system is to provide propulsion while supporting the robot's weight, balancing the robot against gravity and accelerations from the walking itself. Maintaining a stable locomotion in the archetypal application of legged robots, walking on unstructured and uneven terrains, requires a good perception of the type of environment, acquisition of terrain properties, planning of ground contacts, and the subsequent motion generation for all the DOFs.

Robust locomotion under perturbations and on unperceived terrains is also a defining ability for obtaining an agile and stable locomotion. The ability to recover from perturbations is crucial for maintaining balance when the robot state gets out of scope of the initial planning, as in situations when slippage occurs or the robot encounters unperceived terrain features that might cause a fall. For instance, animals recover effortlessly and immediately after stumbling on unperceived obstacles, exhibiting what seems like innate stereotyped reflexes that counteract the perturbation, allowing it to balance itself and resume the walk.

Mechanical design of legged robots is also a major contributor for the success and achievement of agile legged locomotion. Biological energy storage, the muscle actuation systems employed in animal and insect locomotion, achieve torques, response times and conversion efficiencies much larger than similar scaled artificial made systems [197]. Many efforts have been made to increase energy efficiency [20], locomotion speeds, actuation power, flexibility and agility [87, 193, 222], while reducing weight and manufacturing costs of walking machines.

The proper design of the machine is a very important aspect to ease control requirements, and simultaneously allowing the exploitation of dynamical properties in order to perform energy-efficient, natural movements (i.e. regarding natural dynamics) and likely reaching the so desired versatility. Not only *intelligence requires a body* (here, motor intelligence), but there is a coupling between sensory-motor activity and body morphology, from which a better exploitation of the dynamics may result in simpler control [84]. However, current readily available commercial legged robots, such as those used in the present work, do not take such considerations into their design.

2.1.1 Characteristics of quadrupedal and bipedal walking

Terrestrial quadrupeds and bipeds adjust the locomotion's patterns of the limbs, the gait, to adequate the walking motions under different requirements, as changes in terrain, desired behavior or desired walking velocity [3]. The specific set of gaits of a given animal is limited by the structure and geometry of the body and the limbs. The execution of a given gait aims to reduce the energy expenditure while increasing walking velocity, increase maneuverability and to achieve different locomotor behaviors, as creeping behind a prey or running from a predator.

Gaits are grouped into three categories: walking gaits, running gaits and leaping gaits. These are differentiated according to their patterns of support sequence and walking velocity. Walking gaits are slow gaits where the animal keeps at least three feet on the ground at any given time in a step cycle. Running and leaping gaits are fast gaits that produce flight phases, with the body airborne and all the feet in the air at a given time during a step cycle.

A gait is characterized through its: stride frequency, the number of complete footfall sequences in a unit of time; the stride length, the covered distance during a single stride; the duty factor, the ratio of the duration of foot support relatively to the stride duration; and the interlimb relative phase, the relationship between the phase of the foot strike among the limbs as a fraction of the stride duration. A single stride can be described in simple terms, divided into two distinct phases, starting when the foot is lifted and placed in a more rostral position, the swing phase, followed by a supporting and propulsive motion that propels the body forward, the stance phase.

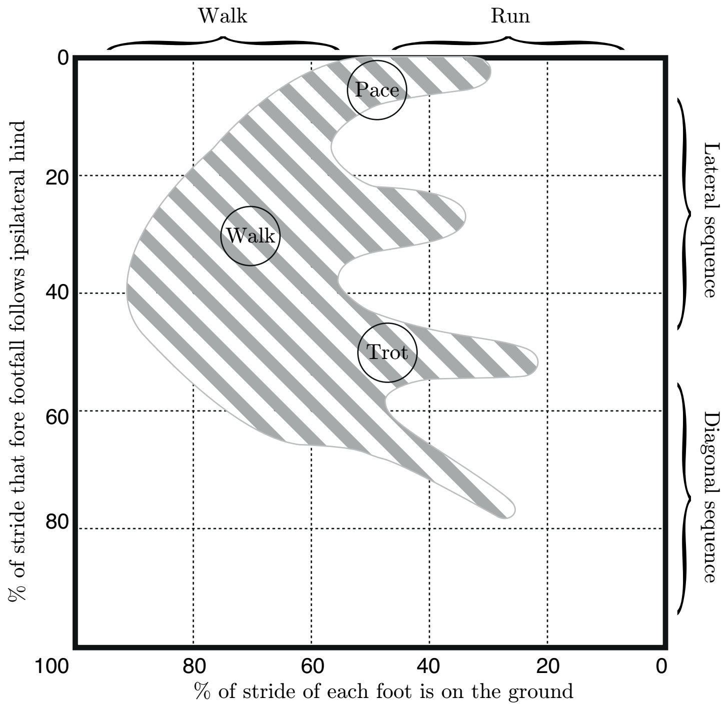

Figure 2.1: Figure adapted from [81], plotting the wide range of symmetric gaits exhibited by tetrapod animals. The regions of three common gaits are identified, which are easily generated by the quadruped CPG system proposed in the present work.

In quadrupeds the most common gaits are symmetrical gaits as the walk and trot gaits. The left and right limbs in a girdle perform the stride in strict alternation between swing and stance phases, having a relative phase of 0.5 between contralateral limbs. A wide range of possible symmetric gaits exhibited by tetrapods are depicted in fig. 2.1. The gait sequence of the lateral sequence walk and trot are presented in fig. 2.2.

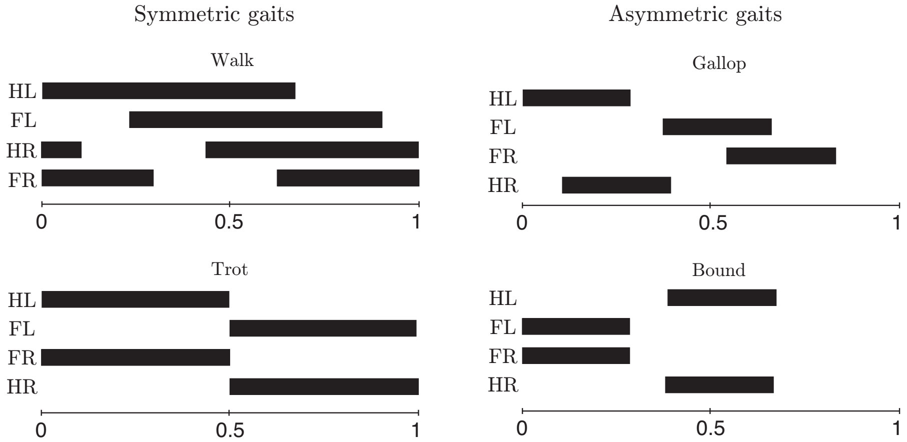

Figure 2.2: Gait diagrams with black bars representing foot contact and bottom axis the % of cycle time. It is depicted two symmetric gaits: lateral sequence walk and trot, and two asymmetric gaits: gallop and bound. FL: fore left, FR: fore right, HL: hind left, HR: hind right.

Asymmetrical gaits such as gallop and canter, or leaping gaits as bound and pronk, on the other hand, do not exhibit strict alternation between the limbs on the same girdle. Trot and bound gait sequences are depicted in fig. 2.2.

Humans and similar biped walking animals usually perform symmetrical gaits, maintaining strict contralateral alternation for walking and running. But they can also perform other symmetrical and asymmetrical gaits such hopping or child's skipping [144], usually not employed unless deliberately, since these gaits require much effort.

The distinction between walking and running gaits are based on the existence or not of flight phase, or in the number of feet in the ground at any time can be considered a simplistic method that does not consider mechanical dynamics [22]. Walking and running gaits exhibit distinct dynamics and center of mass motion.

Inverted pendulum models can be used to describe the motion and dynamics of bipedal walking, describing how kinetic energy of a stiff inverted pendulum is traded of into rise in potential energy and sequentially back to kinetic energy, how energy is expended during each of the steps, and the mechanical work required [118]. In running, a SLIP (spring loaded inverted pendulum) model is the simplest model used to describe the conversion between kinetic, potential and elastic energy, describing the motions and dynamics of running [24]. It was later demonstrated that the use of an inverted pendulum model is not sufficient to correctly reproduce the basic mechanics of walking, as well as the SLIP model reproduces for running. Geyer has shown that the same model used for biped running not only can be used for reproduce walking, but that also compliant legs are essential to obtain the basic walking mechanism [69].

2.1.2 Static balanced locomotion

A robot walk is basically successful if equilibrium is maintained and the robot does not fall over. Generally legged robot locomotion is divided into two balance conditions: static balance and dynamic balance. In static balance the robot moves completely stable at all instants, with small velocities and accelerations, with the only balance condition of the projection of the center of mass to be inside of the convex hull of the supporting points, the support polygon. A statically balanced walking robot can cease the movements at any instant and remain in equilibrium without falling. On the contrary, dynamically balanced robots can not cease the walking movements without a high risk of losing equilibrium and falling. Dynamic balanced locomotion is characterized by the continuous need to carry on proper motor actions to maintain equilibrium, even with the possibility of having the projection of the center of mass outside the support polygon.

Static and dynamic locomotion are quite distinct, meriting their own hardware and technological implementations, control architectures, mathematical frameworks and system analysis tools. The choice of performing static or dynamic locomotion is largely dependent on the actuation type, mechanical design of the robot, and the application of the robot. Static locomotion is ideal for slow and precise walking, when a slow terrain progression, careful transportation or external manipulation tasks are required. Dynamic locomotion on the other hand is much more adequate for higher velocities, as well as jumping and more reactive locomotion behaviors.

Early walking robots used static stable walking due to the weight, mechanical design and actuation technology of these early walking machines. It required slow, carefully planned movements of the legs, while producing a large enough support area where the COM would be maintained at all times [141, 199].

Static locomotion is an important method to robot locomotion, as some tasks and applications require important features offered by static mobility [16]. Slow, carefully planned support points, completely controlled positioning, leveling and heading of the robot's body, are features provided by static walking and it is typically used on multi-legged robots as they tend to have larger choice of foot placements.

Frequently used control schemes for static locomotion start with a definition of a set of 3D points for foot placements and COM progression, chosen to maintain the projection of the COM inside the support polygon at all times while guaranteeing a strong support point able to hold the weight. Foothold sequence planning algorithms may maximize static stability measures for even terrain [95], or focus on the minimum energy expenditure, movement agility by using a crab-walk gaits or free gaits in uneven terrain [59, 83, 90, 223].

Having the gait planned and the foothold sequence, the next step usually encompasses the application of classical control for the generation of trajectories and the proceeding execution and tracking [40], with the possibility of having dedicated online adaptation mechanisms for coping with terrain uncertainties, obstacles and disturbances [90].

Static locomotion controllers usually follow some variation of these methodologies, for hexapod, quadruped and biped robots.

2.1.3 Dynamic balanced locomotion

Static locomotion offers many important features for certain tasks, but can not achieve fast walking because dynamic effects are usually discounted from the stability criteria and from the control formulation. For faster walking or running, the consideration of dynamic effects is necessary. Dynamic locomotion is difficult to control due to the nominal unstable and nonlinear characteristics of the robot, their interaction with the environment, exhibiting time variant and intermittent dynamics.

In case of bipedal robot walking, static balance places tight constraints in the motions and velocity the robot can achieve in order to reduce the dynamics from accelerations of the body. The most popular method to produce walking motions while accounting and addressing these dynamic effects is the concept of Zero Moment Point (ZMP), firstly presented by Vukobratovic. The first practical demonstration was achieved in collaboration with Laboratory of Ichiro Kato's group on the WL-10RD robot [217].

ZMP is the point where the reaction force at the foot and the ground does not produce any moment, keeping vertical inertia and gravity forces equal to zero. Typically on a solution using the ZMP criterion, a sequence of foothold locations are chosen, the desired ZMP over the planned support areas are determined and the joint space vector is calculated using the inverse of the robot's model. In this solution a faster walking is achieved, tracking the COM reference trajectory, using for instance predictive control [220], and allowing it to take small excursions outside the support area while walking, stabilizing the robot by maintaining the ZMP inside the support area instead. Up to now, this method has been widely applied in commercial high-gain position controlled bipedal robots and improved upon, the *de facto* solution for full sized humanoid robots, used currently in most advanced humanoid robots [82, 104, 121] and also used for quadruped locomotion [35, 223].

Pioneering the theme of running, hopping robots and fast actuation, Raibert designed monopod, biped and quadruped robots actuated by hydraulic hips and pneumatic or mechanical springs to achieve the hopping. The hopping robots are controlled using simple decoupled control rules regarding hopping height, forward velocity and posture [166, 169, 170]. This seminal work not only demonstrated the possibility of achieving running locomotion with robots, previously limited to static and slow walks, but also suggested that stiffness in actuation is undesirable in running robots and passive dynamics should be exploited to increase their energy efficiency.

The early works by Raibert [169, 170] in hopping robots and McGeer [140] in passive walkers are the foundation and inspiration of many current works in dynamic locomotion, providing insight on the importance of designing robots with proper mechanical characteristics and underactuation, allowing to exploit the natural dynamics of walking and how to better control the interaction with the environment, fundamental for achieving better performances in legged robots.

Passive dynamic walking has been extended to the study of quadruped walking by Remy et al. [171]. The authors present a detailed simulation framework to study passive dynamic gaits of quadrupeds, achieving stable two-beat (e.g. trot and pace) and four-beat (e.g. walk gait) symmetric gaits through the use of a wobbling mass.

Research on legged robot locomotion has focused on how to get precise, but simultaneously compliant control, how to get robust and yet versatile behavior. Many works follow on the paradigm of force control and dynamical interaction control, by pursuing the design of better actuators and by designing appropriate control schemes. Some actuators mimic muscles from animals using antagonistic implementations with artificial pneumatic muscles [150, 180], cables and pulleys [161], or springs and electric motors [175]. The goal is to design robots and actuators with the relevant features for flexible locomotion, such as decreasing actuator impedances, provide controllable stiffness, and provide force control for active compliance [167].

Then by using a proper control framework, such as Virtual Model Control or inverse dynamics and force control [30, 168], one can achieve compliant and fast locomotion, including capability to handle some unplanned terrain impacts and unperceived disturbances. Other works investigate the resonant properties of the robot dynamics, with simple actuation and passive compliant elements paired with innovative simple control based on entrainment properties, in order to investigate the role of embodiment on locomotion [162].

Most of the works mentioned so far, for both static and dynamic locomotion, rely on model-based methods for the applied control algorithms. These algorithms typically use some form of forward and inverse models of the robot, models of the interaction with the environment and of the environment itself, for the planning and the generation of control policies, according to the desired task and under several constraints. However it may be hard to model more complex environments, compliant behavior in actuation and more dynamic interactions. These approaches may also not fare well on situations where the trajectories have to be adapted in real-time to unmodeled and unperceived perturbations.

In contrast, some model-free approaches, or which do not use explicit models, aim to tackle these limitations and generalize the control policies, such as approaches inspired by insights from biological research, as herein discussed briefly.

2.1.4 Bio-inspired robotic locomotion

Bio-inspiration in design is the application of knowledge from biological studies into real world engineering applications, as in biosensing, bioactuation and biomaterials, which may take the form of simple application of concepts to full biomimicry. In robotics, bio-inspiration has long been used to design robots which mimic animal's method of locomotion, from flying, snake and fish like, biped, quadruped and other multi-legged robots [74]. As presented in the previous section, researchers have reached important conclusions regarding the dynamic effects on the locomotion of legged robots, in part by generalizing the knowledge from animal locomotion studies. Not only this knowledge allowed for the design of new technologies in low impedance actuation and robot design, but also for the control of robots. In certain works the use of a bio-inspired motor control complements the bio-inspired structure and physical characteristics [17, 51].

For the presented work it is relevant to focus on the topic of motor control, specifically generation of walking and rhythmic movements. The broad field of computational motor control in neuroscience can provide useful inspiration to robot motor control, by drawing parallels between biological strategies and methods of control theory, studying the relationship between sensory signals and motor commands, identifying the methods employed in motor planning, motor control and the strategies by which the nervous systems overcomes the complexities of flexible and versatile movement generation [190].

Interesting insights from how movement may be modularly organized at spinal level could explain how nature simplifies the problem of motor generation. A promising perspective is that a set of stereotyped movements are flexibly combined to produce a variety of muscle tasks. The idea is that unit patterns of muscle activation, a synergy, are a specific output of simple functional units, and the motor movement is the result of a weighted combination of their output [23]. In the production of rhythmic motor patterns for walking, it has been suggested that these synergistic outputs are the product of Central Pattern Generators (CPGs).

The concept of CPGs has gained a widespread attention in robotics community as inspiration for the design of low level motor control, and is the central concept exploited in the presented work. The next section presents in more detail what is understood as a CPG, their role in motor producing, the CPG interaction with sensory information for adaptation and supraspinal motor commands.

2.2 Central Pattern Generators

It is generally accepted and defined the Central Pattern Generators as the functional ensembles of neural networks of the central nervous system which endogenously produce and govern the rhythmic motor processes in the body, such as respiration, swallowing, and locomotion [14].

Complex walking behavior is believed to be generated majorly by locomotor CPGs, which retain a repertoire of motor programs used in locomotion [72]. In complete absence of rhythmic inputs, the CPG produces the rhythmic motor patterns for locomotion, generating complex rhythmic movements which level of activity is solely commanded through tonic stimulation from supraspinal regions. Equally important, or even crucial, in the concept of CPGs, is the integration of sensory information and feedback mechanisms governing and shaping the generated patterns. This aspect is very important to provide the ability of adapting and correcting the walking behavior accordingly to the current environmental and behavioral context.

Evidence for Central Pattern Generators The initial finding of locomotor CPGs came from the first studies by Brown in 1911 [27], suggesting that locomotor behaviors are the result of central rhythmogenic mechanisms in the cat, followed by research in both invertebrate [128] and vertebrate animals [107, 154]. There is definite evidence on the existence of CPG for locomotion in lower vertebrates like the cat, dog, rabbit, but only indirect evidence has indicated the existence of CPG for locomotion in humans [52, 54]

Experiments in isolated preparations of the lamprey spinal cord have shown that it is possible to record patterns of activity similar to those of swimming [41]. These patterns of activity, or fictive locomotion, have been recorded in similar preparations of isolation of the spinal cord in several other animals [106].

One of the first significant experiments in the cat evidence the role of the supraspinal commands upon the CPGs and demonstrates its ability to generate coordinated movement for several gaits [195]. A decerebrate cat (removal of the fore and mid-brain) stands supported over a treadmill, as is made to progressively walk and run through an increasing constant electric stimulation of the mid-brain. Through the strength of the stimulation it was possible to control the walking rhythm, induce gait transition to running gaits and then back to walk. Despite the removal of the fore and mid-brain, the exhibited characteristics of walking and running were similar to the intact animal. Authors also demonstrated the existence of entrainment properties of the CPG through sensory integration, by moving the treadmill while providing no stimuli to the mid-brain, and observing walking behavior stimulated through mechanical action, and the respective velocity adjustment to varying speeds of the treadmill.

Organization and coordination Although not completely understood how vertebrate mammals' CPGs are neurally composed and organized, studies have strongly suggested the locomotor CPGs as distributed unit generators flexibly coordinated, able to generate a myriad of different coordinated locomotor patterns.

It is suggested that there is one CPG controlling each limb, and that vertebrate locomotor CPGs are located in the spinal cord, thought to be distributed rostrocaudally accordingly to its rhythmogenic ability. With the fore limbs' CPGs located in the cervical spinal cord, and the hind limbs' CPGs in the lumber spinal cord [107]. Each mammalian locomotor CPG is composed of multiple distributed rhythmic generating units, with one unit per articulation, exhibiting an excitability gradient in rhythmogenic capacity between rostral and caudal units. The highest rostral rhythmogenic capacity where hip motor neurons are located suggests that the units controlling hip movements may act as leading units in the CPG, entraining more caudal and less excitable units, for example, those controlling the knee and ankle [107].

Another interesting suggestion of CPG organization is the proposal that the mammalian CPG is divided in two layers: a rhythmic generation layer responsible for the rhythmic coordination within the CPG and between the coordination among the CPGs, and a pattern generation layer responsible for generating the patterns of locomotion [119, 139]. This proposed organization would allow for independent afferent influence onto each layer, with changes acting on motor pattern not directly influencing the rhythmic activity, or the rhythmic changes not influencing the motor pattern.

Both of these considerations on CPG organization may explain how motor complexity is addressed by nature and should be included in the formulation of robotic CPGs. It is a very interesting concept, a distributed organization of units within the CPG which provides for the production of several types of basic walking patterns and a myriad of complex locomotor behaviors, by simply modulating how these units interact with each other.

2.2.1 Sensory modulation and adaptation

Signals from supraspinal, spinal and peripheral structures are continuously integrated by the CPG for the proper expression and short-term adaptation of locomotion. Sensory mechanisms can select rhythmic patterns, modulate amplitude of muscle bursts and pattern frequency. It can also regulate the structure and transition between step phases, assist foot positioning and correct the movements when obstacles appear [176]. This short-term adaptation provides great versatility to an otherwise fixed set of motor patterns in the CPGs repertoire, dynamically adapting the movements to the environment.

Herein it is briefly mentioned a small selection of feedback mechanisms and observations from studies on the role of sensory feedback on locomotion. In the presented work the aim is not to discuss in detail how these mechanisms are organized and function at neuronal level, but the aim is rather to serve as reference of the possible roles of feedback in the adaptation of the CPG output. More detailed descriptions of the feedback mechanisms, behaviors and experiments are found in several reviews [138, 159, 160, 176].

The dynamic sensorimotor interactions between the central patterns and the feedback mechanisms are quite complex, relying on a multitude of sensory information, from cutaneous (skin afferents) and proprioceptive afferents (muscle spindles and Golgi organ), sensory inputs reaching supraspinal structures through ascending spinal pathways, descending supraspinal command signals, and through especial senses, such as: visual, vestibular, auditory.

Naturally, this multitude of information and feedback mechanisms translate into different kinds of influence on the adjustment of central patterns, from low-level, fast, stereotyped reflexes, to long-term adaptation of the locomotor movements. There are several closed loops of sensory information at different levels, depending on the recruited neural structures and the complexity of the feedback mechanism. Some are circumscribed to spinal structures due to the delays on the transmission of sensory information, because the locomotor movements may be faster than the time information takes to travel and be acted upon [145]. Others extend further and cover supraspinal structures, recruiting areas of the cortex to command and adjust locomotion.

These dynamic interactions have also been shown to include the influence of the CPG in the selection of feedback pathways or reflex reversals, depending on the locomotor behavior, step phase and type of stimulation [159]. This important organization and functionality of phase dependent sensory feedback would not exist without the operation of the CPGs [138].

Muscle Spindles

Muscle spindles are sensory receptors inside the muscles, parallel with muscle fibers, signaling the stretch (*II* afferents) and stretch velocity (*Ia* afferents) of the muscles.

It has been demonstrated that information from hip muscle afferents is used to signal the range of joint angular excursion, taking part on the adjustment on the duration of step phases [63, 143]. Hip extension contributes for the control of the transition from stance to swing, providing for resetting and entrainment by: prolonging ongoing phase of locomotion, or inducing a switch from one phase to the other [158]. Some experiments have shown that by preventing hip extension in a hind leg, stepping movements are stopped, and swing is initiated when the hip was slowly extended past an angle [158].

Golgi Tendon Organs (GTOs)

Group *Ib* afferents originate in the Golgi Tendon Organs, located in series with the muscle fibers and sensing the tension, transmitting information related with the exerted force at the muscle.

This sensory information has been shown to play a role in the regulation of the duration of step phases, the initiation of the swing and also reinforcing the activity of extensor muscle group during the stance. Activation of extensor group *Ib* afferents in the cat regulates the duration of the stance phase, inhibiting flexor burst generation and preventing the transition into swing while the ankle is under load [158,159]. *Ib* afferents also reinforce ongoing motor activity within a positive feedback loop during stance, increasing extensor muscle activity [80, 159, 176].

Cutaneous afferents

Cutaneous afferents are the cutaneous nerves projection onto the spinal cord, transmitting information relative to the sense of touch on the skin, spread all over the body, including the foot pads and dorsum.

These receptors serve several purposes in locomotion, as in corrective actions of the movements and in eliciting locomotion. It has been shown that the removal of cutaneous sensing from the pads do not prevent locomotion, but it does influence the swing duration, increases the double support phase, provide regulatory input to assess load on the limbs during up and down slopes, and mainly interferes with precise foot placement [63].

Cutaneous afferents and its role on stumbling corrective reactions is the best case in which it is observable the phase dependent feedback mechanisms. When a walking cat touches an obstacle while performing the swing phase, it elicits a prominent knee flexion and a simultaneous flexion of the ankle and hip to step over the obstacle and place the foot in front [137]. This mechanism is elicited depending on the step phase at when the foot touches the obstacle, whether the cat is walking forward or backward, and if the pads or dorsum collides with the obstacle. e.g. if walking forward, and the dorsum of the foot is stimulated during stance phase, no stumbling reaction is elicited.

Postural

One other type of adaptation and changes of the locomotor movements are related to posture and balance. Appropriate posture is essential for the coordinated control of motor behaviors, including locomotion. Postural activity can be divided into two modes of postural activity, feedback which compensates the deviation from a correct posture, and a feedforward mode, resulting from anticipatory postural adjustment to counteract voluntary movements. Analysis of different species has shown that there are individual central systems for posture and locomotion, that interact when required [48, 49]. Posture and balance tasks are achieved by adapting and correcting the locomotor movements, through innate reflexes ready to be elicited depending on context, and by sensory dependent responses that maintain the proper expression of locomotion in specific conditions. It requires concurrent processing of several sensory modalities, while the motor system simultaneously controls muscle actions [102].

It is suggested that in quadrupeds, the system stabilizing the trunk orientation in frontal plane consists of two relatively independent sub-systems, stabilizing the anterior and posterior parts of the trunk, and each sub-system is driven by somatosensory input from corresponding limbs [48]. These two subsystems are driven by input from limb proprioceptive information in addition to information from visual and vestibular centers, compensating postural disturbances by generating corrective motor responses. The mechanisms are also activated by tonic drive from some brain structures, which send commands to the spinal cord via descending pathways, contributing to corrections in posture.

Supraspinal centers

Supraspinal structures include all the brain regions above the spinal cord, the hindbrain, midbrain and forebrain. Each of these regions have a distinct role in the control of locomotion, with the voluntary motor control originating in the motor cortex, and the basic locomotor behaviors like food seeking and directed navigation mediated by the midbrain [71, 72, 103].

These descending signals from supraspinal regions exert powerful influences on locomotion, such as during precise visually guided walking, imitation and learning, necessary for the full expression of locomotion [53]. Various descending pathways from these regions are involved in activating, stopping and modulating the spinal locomotor CPG, as well as the excitability of transmission in the reflex pathways.

2.2.2 Interesting features for robot motor control

Interesting features can be taken from the concept of CPGs and vertebrate motor control, even if not completely understood the details of the CPG neural organization, how it integrates with other feedback and motor control mechanisms, and how descending commands influence voluntary changes in locomotion.

The current work aims to base the design of a robot locomotion controller on the interesting functional features of the CPG and organization of vertebrate locomotion control structures. The goal is not to use robotics to better understand biology by providing tools to test hypothesis or biological models. Herein only the concept of CPGs is considered, and mainly the functional features in a certain abstraction that allows an easier and more adequate transfer and implementation to legged robot control.

In a nutshell, the CPGs are structures with the capability of endogenously generate rhythmic activity without the need of an input driving signal. The CPG produces coordinated patterns of activation for several muscle groups, through a distributed organization of unit generators, which enables the production of different motor behaviors through their coordination and reorganization. This method of synergistic activity results in the reduction of the solution space, and tackles the problem of complexity in actuation of redundant limbs, the coordination of complex motor patterns and the interlimb coordination for several gaits.

The integration of the CPGs and feedback control loops is expected to provide the required adaptability to produce agile locomotion, organized in mechanisms covering different spinal and supraspinal levels, achieving fast reflexes, and long-term walking adaptations to varied types of terrains and entrainment to imposed rhythms.

Descending commands from supraspinal structures modulate the walking activity through simple tonic signals. The CPGs progressively change the gait as the tonic signal increases in strength, increasing locomotion velocity. This organization reduces the dimensionality of the descending control signals, reducing the complexity of commands from higher centers to the spinal cord.

Another interesting aspect is the developmental perspective of the CPGs and the vertebrate motor system, their ability to learn new motor tasks and adapt to the growing body. This is an important aspect in robotics, how can robot autonomy be increased by providing it with learning capacity.

All these features make the CPG concept a good candidate for the control design of legged robots, which can potentially generalize their ability in dynamic environments.

2.3 Central Pattern Generators in robotics

The Central Pattern Generator can be a powerful concept with interesting features to explore and apply in robotic motor control, as mentioned in the previous section. An extensive variety of implementations throughout the years reflects it, as surveyed by Auke Ijspeert [92].

In this section the author tries to expose the most relevant CPG works, trying to relate important aspects among them.

2.3.1 Robot locomotion and motor control

Before focusing in the application of CPGs for legged robots, it is worth mentioning briefly some works where CPGs have been applied to other types of robot locomotion and motor control.

The most relevant CPG works in non-legged robot locomotion are applied to anguilliform robots. Travelling undulating motions are produced for lamprey [12, 93], snake [210] and fish robots [86]. For the salamander robot from Crespi and Ijspeert [93], the CPGs produce solely undulating motions until the driving signal elicits a qualitative change in the rhythmic activity, recruiting the movement of the limbs for walking out of water.

CPGs can also be used for other rhythmic tasks besides locomotion. One curious example is the use of CPGs for the generation of an undulating motion of a flexible spine in a humanoid robot [153]. The humanoid robot walks while a ZMP monitor verifies at all times the performed ZMP, modulating the CPG activity which undulates an actuated spine. When the ZMP stability of the robot becomes at risk the undulation patterns are reduced. Another curious example is the CPG as a rhythmic manipulation generator for a simulated robot hand with 9 DOFs [39]. Using reinforcement-learning, the system searches parameter's sets for the CPGs, developing different manipulation skills, able to manipulate different objects.

2.3.2 Level of abstraction

Computational implementations and studies of CPGs are not only applied in the realm of robot locomotion, but also as a means of studying and further propose possible models for describing the spinal CPGs. These models were developed in several abstraction levels, as a means to explore several features, explain observed phenomena *in vivo* preparations and verify suggestions to the cellular organization of the CPG.

For instance, CPGs have been modeled as networks of simplified neuron models, as leaky integrators [55], integrate-and-fire neurons [177], continuous neuron models [133] and Hodgkin-Huxley model [75], with the objective of verifying the possible neuronal organizations of the CPG at the cellular level abstraction. At a higher abstraction, models intend to explain intersegmental coordination exhibited by the neural networks in the isolated spinal cord of the lamprey [41], explore entrainment of forcing frequencies in chains of oscillators, or synchronization for gait achievement in legged animals.

Some of the works only address the phenomena of coordination and synchronization between the CPGs for the expression of the correct gait phase relationships of legged gaits. Take as example the works by Golubitski, Buono and Pinto [33, 165], addressing only the problem of achieving quadrupedal and bipedal gaits in terms of gait phase relationships.

In other works, bio-mechanical simulations alongside with CPG model simulation complements the research, by answering if the proposed models and mechanisms are sufficient to explain the behavior observed at the complete systems. For instance, Ekerberg [55] in his work, simulates fish body mechanics, including the interaction with the water and stretch receptor feedback, demonstrating that the proposed cellular organization on the CPG model is sufficient for producing swimming and turning by asymmetric descending stimulation, requiring no especial circuitry. Maufroy [134] used a detailed CPG implementation using neuronal models, divided in three neural structures and testing it on detailed musculoskeletal simulations of cat's fore and hind girdles.

2.3.3 Locomotion in legged robots

The distributed characteristics of CPG based controllers allows it to be applied in multi legged robots. It can be applied in robots with as little as two legs, such as humanoid robots, up to robots with six, eight, or more legs. CPGs have been shown to be a simple method to control centipede like robots, with an indeterminate number of pair of legs, such in the modular robot presented by Shinya Aoi et al. [7]. However the most typical application, and the most extensive application of CPG based controllers are in hexapod, quadruped and biped robots.

Hexapod robots are good for applications where added stability is required, and where CPGs are able to easily produce the coordinated patterns of the different hexapod gaits [13, 60, 96, 97, 125, 127].

Quadruped robots are designed with distinct leg geometries, providing distinct stability characteristics to their walking, simplifying the control problem in some works. Some quadruped robots are designed with leg geometries similar to hexapod robots, with sprawling legs, providing a wider stance and greater stability [60, 208, 209]. Other quadruped designs have an erect posture, with a geometry closer to small mammals like the cat or dog [110, 115, 178], and even crawling toddlers [45, 174].

Bipedal robot walking is more challenging when compared to hexapod and quadruped walking. Having only two legs, the walking requires the alternate support of the body and constant adjustment of balancing for maintaining stability, with an higher chance of falling, unlike other multi legged robots. Even though biped walking presents an increased level of difficulty, CPGs have also been applied successfully to several kinds of biped robots. From servo actuated tethered bipeds constrained to the sagittal plane [114, 123, 149], to full sized humanoid robots [88, 147], including compliant actuated humanoids [89] and football playing robots [18].

An extensive number of works apply CPGs in simulated bipeds, many of which aim to demonstrate the feasibility of CPG based controllers and their integration with feedback mechanisms, or to achieve an easier system analysis [9, 187, 206, 207]. Although important the existence of extensive works demonstrating the capabilities of CPG based controllers on simulation, controlling a real robot can be considered in many aspects more challenging [57, 149]. Many dynamic effects are not considered correctly in simulation, either by using a simplified model, by the incomplete representation of mass distributions, the simplified actuator models, or even the choice of collision models.

2.3.4 CPG modeling and implementation

Many approaches to CPG based controllers have been tried throughout the years. Several mathematical tools and methodologies have been used to implement control solutions featuring the biological CPG characteristics.

Designing a solution for robot locomotion based on CPGs usually requires identifying the desired architecture of the system, how many DOFs will be controlled, identify the required motor patterns and how motor patterns are coordinated. One must decide the output of the system. Whether the CPG directly produces joint position, joint velocity, torque or simply a swing/stance step phase signal.

Neural Oscillators

One of the most applied tool in CPG based solutions is the Matsuoka oscillator/Neural oscillator [133]. Taga in 1991 presented a seminal work where walking and running was generated for a simplified biped model, resorting to a half-center approach to the CPG, using neural oscillators for producing torques to be applied at the joints [207]. The work was progressively improved and expanded to a more complex 7 DOFs biped model with feet and torso in 1995 [204, 205], to a 3D simulated biped in 1998 and expanded with the ability of anticipatory obstacle avoidance [206]. These works were so significant that many CPG based solutions have followed similar implementations.

Another significant work is the research conducted by Kimura and Fukuoka using neural oscillators in quadruped locomotion, first applying it in the Patrush quadruped robot [108]. Later, it was applied to the more capable quadruped robot Tekken [64, 109, 110], capable of achieving medium velocities in irregular and natural terrain. The CPG system produces the coordinated sequence of step phase sequences, defining swing and stance, for which PD controller gains and joints positions are selected.

These works in Tekken have shown that by integrating the CPG with sensory dependent responses and corrective reflexes, the robot can walk on natural and irregular environment.

Neural oscillators were extensively used in the solutions proposed for the Titan robots [100,196,208, 209], for the quadruped walking machine BISAM [19], for simulated biped [77, 99, 146] and bipedal robots [57, 58, 114, 132].

Phase oscillators

Another very popular approach to the implementation of CPG based solutions, is the division of the CPG into two functional layers. A distributed rhythmic generator layer is usually implemented as a phase oscillator with a unit for each leg, producing the coordinated base rhythmic signal that drives the pattern generation layer. The temporal reference generation layer and a spatial coordination layer can be controlled separately.

Tsujita and colleagues apply this approach with the phase oscillator driving a nominal end effector trajectory defined by key points on the task space, and temporally in swing and stance phases [216]. At each instant in time, the end effector position is returned by the nominal trajectory, and the leg joint positions are provided using the inverse kinematics of the robot. This became a popular approach that has been extensively used in subsequent works, by the authors and others, in biped [4, 5, 8, 151], quadruped robots [10, 11, 135, 136] and multi-legged robots [7].

A slight different approach was performed by Morimoto and colleagues, where the pattern generator consists on an ensemble of sinusoidal profiles for the joint trajectories rather than obtained from inverse kinematics [147, 148, 202]. Authors argue that since the nominal gait patterns are sinusoids, the approach does not need careful design of desired gait trajectories, as they are modulated through the detected phase and synchronization with the inverted pendulum the robot dynamics.

Dynamic movement primitives (DMP) is an imitation learning method for the representation of motor primitives, which also divides a motor primitive, rhythmic or discrete, into a temporal reference and a spatial reference. In the case of the rhythmic DMP, a temporal reference is also achieved by employing a phase oscillator, which drives the rhythmicity of the spatial reference. This imitation learning approach of rhythmic motor primitives was used to learn and generate bipedal walking patterns [88,149] and quadruped walking [61].

Limit cycle oscillators

CPG solutions implemented as nonlinear oscillators typically produce the temporal reference and coordination jointly with the spatial patterns. The characteristics of the nonlinear oscillators can be exploited to reproduce the features of the biological CPGs, as demonstrated by the extensive research by Ijspeert and his group.

Quadruped walking in simple compliant robots has been demonstrated to harness the characteristics of nonlinear oscillators to achieve global entrainment and resonant frequency tracking [26, 29]. This characteristic was also used to design an imitation framework using nonlinear oscillators, using the concept of Fourier decomposition. A given number of Adaptive Frequency Oscillators (AFO) is used on each joint to imitate a pre-defined trajectory, providing a system with the desired features of nonlinear oscillators. Its capabilities were demonstrated in a biped walking task [173]. The use of nonlinear oscillators was also explored to generate rhythmic and discrete motions, tackling the problem of hand-placement while walking for a crawling toddler robot [44, 45, 65]. Righetti [174] introduced a mechanism controlling the stance and swing phase on the solution produced by the Landau-Stuart oscillator, and feedback mechanisms for the control of phase transitions depending on the measured foot force. The Landau-Stuart oscillator is also the base of other works in biped robots [120].

Nonlinear oscillators such as Van der Pol and Rayleight have also been used to implement CPGs for simulated planar biped models, mimicking the trajectories of human hip, knee and ankle joints [163, 164].

Neural networks

Neural networks have also been used in the implementation of CPG based controllers. In [194] a small humanoid HOAP-1 robot walks resorting to three sub-controllers, implemented as recurrent neural networks (RNN). RNN were also used to reproduce the kinematical motions for a quadruped robot [213]. Using Cellular nonlinear networks (CNNs), Arena and colleagues implemented a hierarchical implementation for a hexapod robot [13], with high level commands translated into parameters through a motor map. Implementing a kind of pattern generation layer, a fuzzy neural network (FNN) controls the joints of the quadruped robot TIM-1 [203], and with a feed-forward neural network (FFNN) by Estevez et al. [60].

2.3.5 Feedback mechanisms in CPG based controllers

The possibility of feedback integration in CPG based controllers is one of the major arguments for the application of the CPG concept in robotics. It is intended that the integration of feedback mechanisms will provide a better framework for robot walking and running with increased flexibility and agility, through the desired features of motor adaptation and mutual entrainment.

Global and frequency entrainment

Taga's main contribution is the demonstration of the important role of global entrainment between the rhythmic activity of the nervous system and the rhythmic movements of the musculo-skeletal system, including interaction with the environment, for the generation of a more stable and flexible locomotion [207].

Typically when using CPGs implemented as neural oscillators, sensory information is input directly into the oscillator's dynamics, influencing directly its activity and achieving entrainment between the generated motions and the exhibited walking dynamics. Usual sensory information are the signals from proprioceptive information, such as joint position, joint velocity and exerted joint torques, and exteroceptive information as foot touch, foot ground reaction forces and body angle [19, 209].This mechanism is sufficient for these solutions to produce walking motions and in some cases to also walk on uneven terrains and reject small perturbations [58,108,205,225]. In [132] was demonstrated that the appropriate sensory information used in the CPGs could be learned using reinforcement learning.

Another method to achieve global entrainment is the exploitation of the natural dynamics, such as the pendulum dynamics of biped robots [88, 147, 148, 202], or taking advantage of the nonlinear oscillators' entrainment properties for tracking the resonant frequencies of a compliant system [26, 29].

Global entrainment has also been demonstrated to replace explicit interlimb coordination. Ishiguro and colleagues have demonstrated that interlimb coordination could be achieved through ground reaction force influence on the phase dynamics of the CPGs [105, 155], achieving good adaptability to changes in weight distribution and walking speed.

Phase resetting and step phase transition regulation

Another method that has been used on CPG based controller, for achieving entrainment between the system and the environment is phase resetting and phase transition mechanisms. These mechanisms take on the idea of regulating the timing of step phases, controlling the transition between swing and stance accordingly to external sensory events, such as foot placement. They are typically used on solutions which employ phase oscillators or limit cycle oscillators, from where the temporal reference is easily accessible in the system.

Phase resetting mechanisms change the current state of the phase oscillator to the nominal phase upon an external event, such as foot strike. It is used to provide robustness to small unperceived perturbations [149, 151, 173, 216], adapting the biped robot walking to split-belt treadmill with different speeds [4], and in some cases to adequate the motor patterns to the real robot, stopping it from falling [149].

It has been extensively used and studied by Aoi and colleagues [8, 10, 11], whom also analyzed the functional role of phase resetting in the walk [5, 6].

Slightly more complex are the transition regulations between the step phases, swing and stance. It can however, offer more control options and is probably closer in concept to the phase transition regulation in vertebrates. Righetti [174] proposed four transition mechanisms that regulate the transition from swing to stance, and the transition from stance to swing. The mechanisms halt the transition, or elicit the transition between the two step phases depending on foot load conditions. Maufroy used similar mechanisms in his quadruped controller [135, 136], with the phase modulations providing stability and robustness to unperceived slopes, steps and lateral perturbations.

Reflexes and rapid motor corrections

A reflex is here considered as a rapid corrective action triggered through sensory information or an event, internal or external. Reflexes are responsible for reacting quickly to unperceived disturbances, such as stumbling, crossed flexor reflex, lateral stepping and leg extension reflex.

Kimura, Fukuoka and colleagues have used reflexes within the CPG controller since the first work in quadruped robots [64, 108], initially applying stumbling, stretch, vestibulospinal, and extensor and flexor reflexes. In later works they extended and improved the used reflexes, including sideways stepping reflex to stabilize rolling motion, corrective stepping reflex to deal with loss of ground contact when walking down unperceived steps, and crossed flexor reflex [64, 110]. They argue that employing reflexes and responses is not sufficient, but necessary for stable walking on natural terrain.

Similar leg extension reflex is used by Lewis [122], along with postural control reflexes, adjusting bias of posture from foot pressure information.

A center of gravity (COG) adjustment is performed in the work by Fukuda [196], through the application of a soft terrain recognition reflex, making the robot move its own COG to a more stable position.

Long term motor adaptations and responses

Responses and long term adaptations modulate the motor patterns in a longer time frame than reflexes. These adaptations may adjust the rhythmic activity of walking to match the external conditions [101] or from repeating occurring reflexes [149].

Postural responses adjust and modulate motor patterns to slope conditions [225], changing leg height according to roll and pitch angles [64, 110]. Slippery terrain adaptation is achieved by Takemura et al. [208], through a mechanism which detects the slippage of the feet and chooses the appropriate strategy.

Lewis [123] proposed a visual adaptation of the motor patterns, learning in a long term context the required modulations of the step amplitude during obstacle approach, for a correct paw placement and obstacle step-over.

2.4 Dynamical systems approach

Dynamical systems approach to behavior generation and motor control has proven to be successful in many robotic applications, offering interesting characteristics based on the theory of dynamical systems, which apply well to robot motor control.

In this framework, behavior-based approaches to robotics link sensory events and perception to actions, through to the natural evolving solution of a dynamical system, defined as stable and unstable fixed points, modeling the task behavior relative to the goal and low-level sensory information [21,192].

Motor control is also achieved using this framework, encoding motor control policies into the dynamical system's landscapes, as defined by fixed points and limit cycles. Motor control policies are formulated recurring to systems with adequate attractor properties, resulting in a formulation which generates in real-time kinematic trajectories (e.g. position and velocities), resistant against transient perturbations and offering the ability for real-time modulations. Motor policies converge to goal states as defined by attractive fixed points, can converge to stable rhythmic motions by converging to a limit cycle (attractive closed orbit), while avoiding undesirable states or dealing with constraints which can be defined by repeller fixed points.

Dynamical systems present interesting properties for trajectory generation. It allows smooth real-time modulation of the trajectory with respect to the system's parameters, the location of the fixed points, amplitude and frequency of limit cycles. These systems also provide for robustness against small perturbations, converge to the original solution after transient perturbations because of existence of globally stable attractors. Also it is possible to integrate sensory feedback terms, by directly specifying the set of dynamical parameters as time-varying sensory-motor information, or by introducing external forces or new attractors to the system, changing the attractor landscape and adapting movements to external and dynamic conditions.

The motivation of the dynamical systems approach to motor control has been recently exposed [157] using ideas from optimal control.

All these properties were explored and applied in several works in robotics to achieve the generation of motor trajectories in multiple DOF robots. It has been applied to control of reaching movements in a robust way, adapting to sudden changes in the environment or external forces acting on limbs and generate collision free manipulation on redundant manipulators [78,98]; to represent motor actions used in learning through imitation [79, 91, 94]; and to control task execution time by exploiting the timing characteristics of nonlinear oscillators [198]. Also widely applied in tasks which involve rhythmic motions such as biped and quadruped autonomous adaptive locomotion over irregular terrain [110], juggling [191], drumming [46], and playing with a slinky toy [221].

CHAPTER 3

MODELING CENTRAL PATTERN GENERATORS

As presented in the previous chapter, many works achieve robot walking by successfully applying CPG based methods in a wide range of legged robots. However, there is no defined framework for applying CPGs, neither a fixed definition of what is understood as a CPG in robotics. The author herein considers that a robotic implementation of a CPG based controller should present the identified features from biological CPGs, as presented in section 2.2.2, regardless of the chosen methods for implementation. A summarized list of CPG desirable features is presented:

a) Endogenous generation of rhythmic patterns, independent of rhythmic inputs and external events.

b) Production of coordinated movements, addressing the redundancy problem by using a reduced set of synergistic motions.
c) Distributed implementation, allowing a flexible coordination to achieve different gaits.
d) Allow the modulation and control of locomotion through only a few high-level commands.
e) Allow the integration of feedback and reflex mechanisms for corrections based on sensory information.
f) Capable of performing different locomotor behaviors.
g) Permit the inclusion of mechanisms for anticipatory and voluntary action.
h) Having the potential for improving rhythmic patterns and learning motor abilities.

This chapter presents the pursuit of these identified features by harnessing the characteristics of dynamical systems and limit cycle oscillators, applied to the design of the proposed CPG on quadruped and biped robots.

The proposed solutions in this work, for quadruped and biped control are distinct on how the temporal and spatial references of motor activity are produced. For the quadruped walking problem, a CPG model based on a method of distributed unit generators was chosen. Uses a simple representation of the Landau-Stuart oscillator as its basic building block, producing the temporal and spatial references jointly. On the proposed CPG for the biped problem, the temporal and spatial reference is divided into two layers. The temporal reference is produced using phase oscillators, and the spatial reference using a pattern generator based on a set of forcing terms in attractor dynamical systems, which define motion primitives.

These systems offer interesting characteristics, which apply well to model the biological CPG features. Both the Landau-Stuart oscillator and phase oscillators produce endogenous rhythmic generation, addressing feature *a*). They also allow for an easy coupling and synchronization due to their entrainment abilities, allowing to accomplish feature *c*) straightforwardly.

Feature *b*) is the accomplished in the quadruped solution by the well-defined coupling between the unit generators. The biped solution addresses the coordinated set of motion primitives, which are dependent on the timing of the shared phase oscillator.

Both solutions allow for an easy modulation of the produced motor patterns by parameter manipulation, resulting in straightforward and meaningful changes in the produced motor behavior (feature *f*)). These changes result in smooth modulations for the produced trajectories, even if through abrupt parameter changes. Moreover, it is possible to map changes from the control parameters to higher-level command inputs, addressing feature *d*).

These systems produce stable rhythmic patterns in respect to their limit cycle behavior, returning to the normal stable state after small transient perturbations. This characteristic, the intrinsic robustness of the dynamical systems allows for an easy integration of sensory feedback mechanisms, by temporarily influencing the system's state (feature *e*)).

The proposed method also has been demonstrated to have the ability to produce rhythmic and superimposed discrete motions, allowing to tackle motor behaviors such as reaching movements while walking [44] (feature *g*)).

Lastly, due to its parameterizable and modular approach, it is possible to use optimization [152] and learning algorithms for extending the robot's motor abilities, addressing feature *h*).

3.1 CPG model of distributed unit generators

The key component on the proposed solution is the Landau-Stuart oscillator, as its versatility has allowed it to be used on several other motor generation contexts [44,46,186], and its properties are easily investigated analytically and numerically (presented in appendix A). The oscillator is here presented as a building block for motor generation, demonstrating its capabilities and the possible parameter modulations.

3.1.1 Landau-Stuart oscillator

Consider the nonlinear dynamical oscillator containing a supercritical Hopf bifurcation [201], given by the following differential equations:

$$\dot{x} = \alpha\left(\mu\nu - r^2\right)(x - O) - \omega\iota z, \tag{3.1}$$

$$\dot{z} = \alpha\left(\mu\nu - r^2\right)z + \omega\iota(x - O), \tag{3.2}$$

where $r = \sqrt{(x - O)^2 + z^2}$, and x, z are the state variables. The oscillator presents two extra parameters relatively to the simple Landau-Stuart oscillator usually used in previous works, ν and ι. This choice of introducing these two parameters was meant to decouple the role of the parameters that define the quantitative solution from the qualitative solution of the oscillator.

This nonlinear oscillator contains an Hopf bifurcation such that the solution bifurcates to either a stable fixed point at $(x, z) = (O, 0)$ for $\mu\nu < 0$, or to a structurally stable harmonic limit cycle around $(x, z) = (O, 0)$, for $\mu\nu > 0$. Herein, only parameter $\nu \in \{-1, 1\}$ is used to control these bifurcations, while $\mu > 0$ is maintained. Speed of convergence to the limit cycle or fixed point is given by $\left|\frac{1}{2\,\alpha\,\mu\nu}\right|$. These two qualitatively different solutions are depicted in figs. 3.1(a) and 3.1(b), respectively.

Oscillation frequency is specified through $\omega > 0\,(\mathrm{rad.s}^{-1})$. Amplitude of the oscillation (limit cycle radius) is given by $\sqrt{\mu}$. Variable O controls the oscillatory offset on the x solution when the oscillator bifurcates to a limit cycle, or the location of the point attractor in x when the oscillator bifurcates to the fixed point.

Fig. 3.2 demonstrates the role of these three parameters. In fig. 3.2(a) the frequency of the oscillatory solution is changed through the manipulation of the frequency parameter ω. The amplitude of the oscillatory solution is determined by parameter μ, which is set according to the desired amplitude: $\mu = A^2$ (fig. 3.2(b)). The tracking of the desired oscillatory offset is demonstrated in fig. 3.2(c) for $t < 5.5$ s ($\nu = 1$), and the tracking of the desired point attractor for $t > 5.5$ s ($\nu = -1$).

The oscillator can easily alternate the direction of the produced solution. As demonstrated in fig. 3.3, the limit cycle rotates clockwise or counterclockwise if $\iota = -1$ or $\iota = 1$, respectively. This change in the limit cycle's direction results in the inversion of the solutions in time.

Independent control of oscillator phase durations

The oscillator described by eq. (3.1,3.2) generates oscillatory solutions in which the ascending and descending portions have equal durations. However by manipulating the frequency parameter ω periodically, one can achieve durations with independent durations, as proposed by [174].

$$\omega = \frac{\omega_1}{\mathrm{e}^{-az} + 1} + \frac{\omega_2}{\mathrm{e}^{az} + 1}, \tag{3.3}$$

where frequency ω alternates between two different values, ω_1 and ω_2, depending on the value of z. For $\iota = 1$, on the positive portion of z ($z > 0$), the mechanism assigns ω_1 value to ω, and ω_2 during the

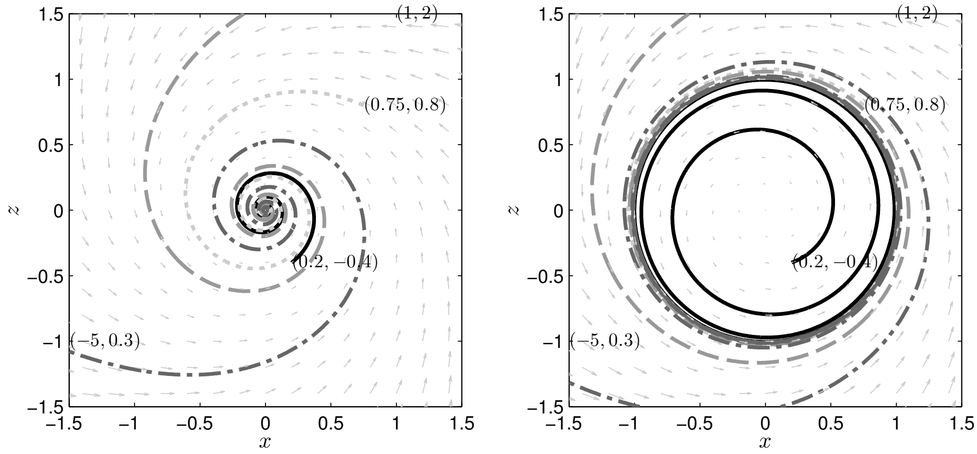

(a) Fixed point at $(0, 0)$

(b) Limit cycle with amplitude 1

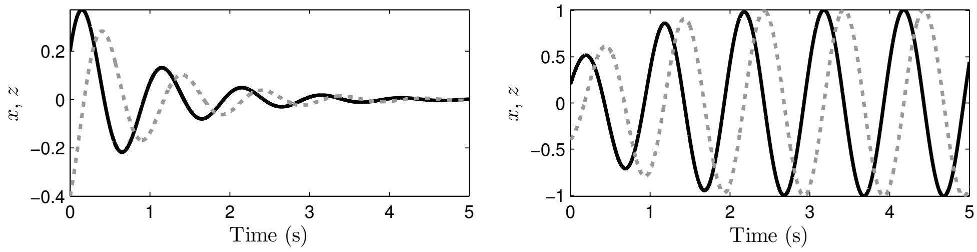

(c) Fixed point at $(0, 0)$

(d) Oscillatory solution with amplitude 1

Figure 3.1: Oscillator solutions for the system defined by eqs. (3.1, 3.2). When $\nu = -1$ an attractor fixed point solution is obtained ((a),(c)), and when $\nu = 1$ a limit cycle solution is exhibited ((b),(d)). Initial points: $(x_0, z_0) = (0.2, -0.4)$, $(x_1, z_1) = (0.75, 0.8)$, $(x_2, z_2) = (1.0, 2.0)$, $(x_3, z_3) = (-5.0, 0.3)$. The point attractor, and limit cycle center is $(0, 0)$ ($O = 0$), with $\mu = 1$ for a unitary amplitude. $\alpha = 1$, $\iota = 1$ and $\omega = 6.3 \text{ rad.s}^{-1}$. In (a) and (b) the vector field is presented in the background. In (c) and (d) x solution is the solid line and z is the dashed line.

negative portion of z ($z < 0$). For $\iota = -1$, the opposite is true. On the positive portion of z ($z > 0$), ω_2 is assigned to ω, and ω_1 for $z < 0$. By changing the frequency value in each portion of the x solution, it is possible to independently control the duration of each portion. The alternation swiftness between these two values is controlled by a.

Fig. 3.4 demonstrates this modulation mechanism, presenting the alternation in ω value and the resulting solution.

Summary

In summary, the discussed oscillator is able to produce solutions that can be summarized as follows:

- A discrete trajectory to a desired point O, if $\nu = -1$.
- Rhythmic trajectories with amplitude $\sqrt{\mu}$ and frequency ω around an offset O, if $\nu = 1$.
- The superimposition of both rhythmic and discrete solutions.
- Invertible solutions by setting parameter ι.

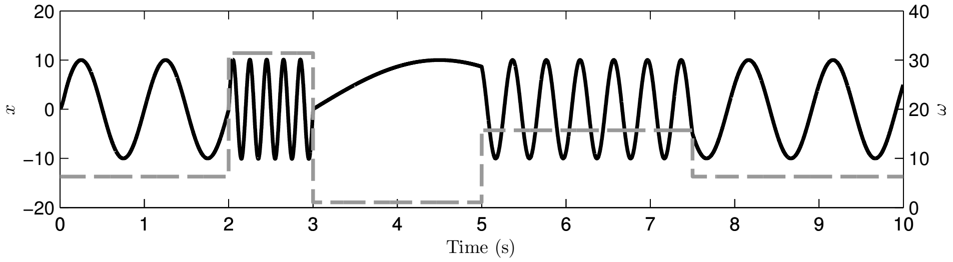

(a) Frequency modulation through ω parameter manipulation. $\omega = \{\frac{\pi}{3}, 2\pi, 5\pi, 10\pi\}$

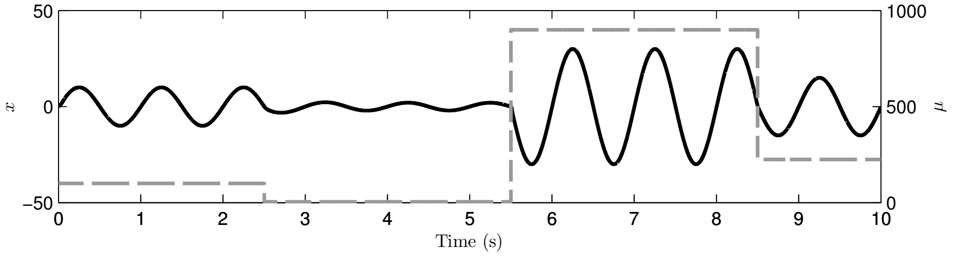

(b) Modulation of μ to obtain $\{2, 10, 15, 30\}$ amplitudes, by setting $\mu = \{4, 100, 225, 900\}$, respectively.

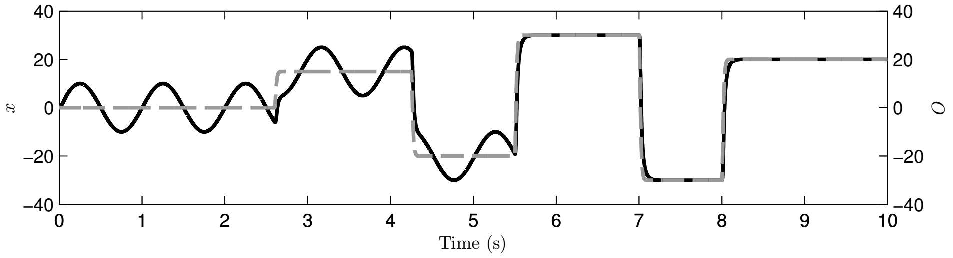

(c) Change of the offset $O = \{-30, -20, 015, 20, 30\}$, translating the limit cycle offset until $t < 5.5$ s, and producing discrete motions with a point-attractor from $t > 5.5$ s.

Figure 3.2: Demonstration of the quantitative changes on the solutions obtained when manipulating ω, μ and O.

- Rhythmic trajectories with independent durations of ascending and descending portions.

Fig. 3.5 demonstrates the parameters' roles in the generated trajectories and their modulation.

In panel (A) there is a discrete solution towards the offset O parameter (dashed line). Since $\nu = -1$, the rhythmic solution is off. Rhythmic solution is turned on at $t = 0.5$ s panel (B). The offset parameter O is also changed, altering the offset of the rhythmic solution. This superposition of discrete and rhythmic solution is verified both in panels (B) and (D).

In panel (C), small changes of the ω parameter modulate the generated trajectories in frequency. Note the fast but smooth amplitude modulation of the generated trajectories according to small changes in the μ parameter. The oscillator promptly changes the frequency and amplitude of the generated solutions, resulting in smooth and responsive trajectories. In (D) the oscillator is inverted.

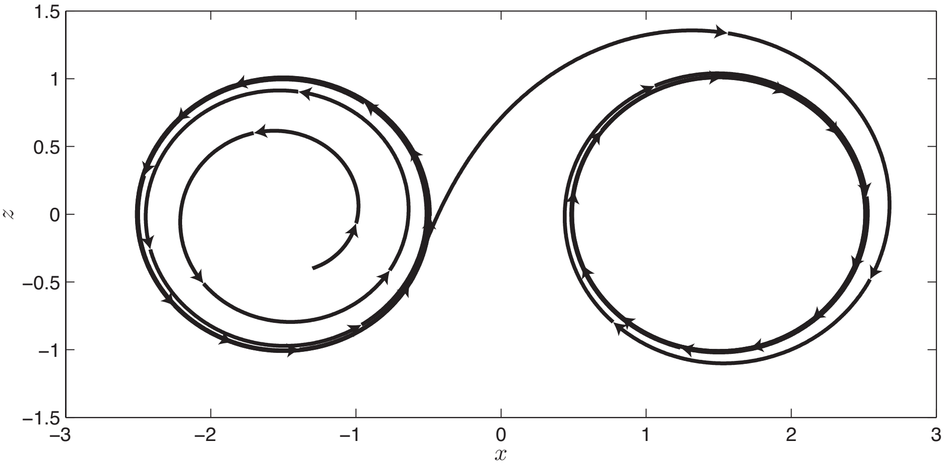

(a) Limit cycle exhibiting two oscillatory directions. The oscillator rotates counter-clockwise in the first seconds, as set by $\iota = 1$, and later rotates clockwise by changing the parameter to $\iota = -1$.

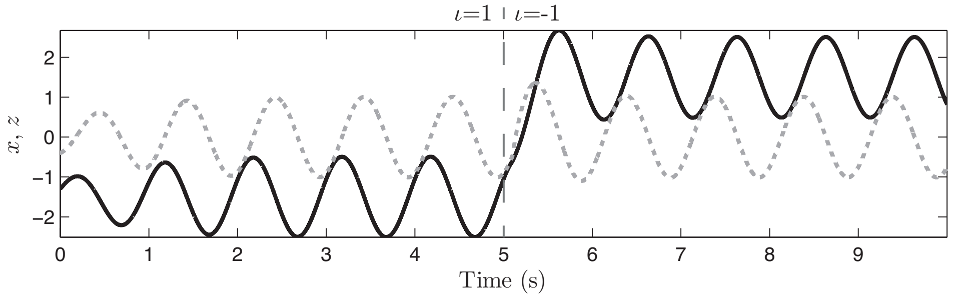

(b) The change in oscillatory direction is identified by the change in precedence between x (solid) and z (dashed) solutions. For $\iota = 1$, x is ahead of z, while for $\iota = -1$ x is trailing z.

Figure 3.3: Demonstration of the direction reversal ability of the oscillator. At 5 s parameter ι is changed from 1 to -1, changing the direction of the limit cycle. For a better visualization of this change, the limit cycle center point was changed from (-1.5,0) to (1.5,0) at 5 s.

These features enable the production of flexible trajectories within the solution space of the oscillator, encoded by the values of its set of parameters. It is therefore assumed that the presented oscillator presents advantageous characteristics for rhythmic motor control.

3.1.2 Oscillator coupling

The presented oscillator is also well suited for distributed use, as will be explored in the current section. This aspect will allow creating an organized network of oscillators resulting in a CPG, and after, a network of CPGs that result in the locomotor controller. Three different methods to achieve phase coordination among the oscillators are here presented, establishing arbitrary phase relationships, in-phase coupling and double frequency coupling, each with a distinct objective and application.

Besides the methods here presented, it would also be possible to use symmetry group techniques to achieve coordinated spatiotemporal periodic solutions in a coupled network, reflecting the temporal relationships existing in quadruped and biped gaits. However the method's simplest network requires a

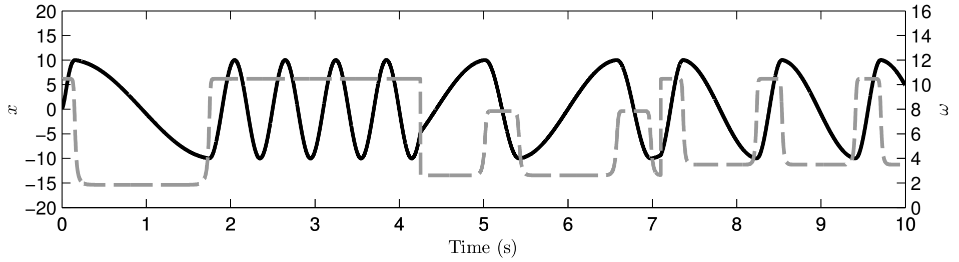

Figure 3.4: Frequency modulation mechanism as proposed by [174]. The frequency of the oscillator alternates periodically between two values, achieving independent control of the duration of the oscillation portions.

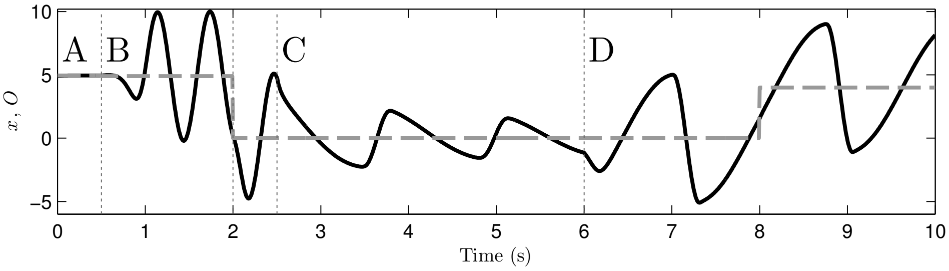

Figure 3.5: Evolution of the generated trajectory (black) through several changes of parameters. Dashed line depicts offset O throughout time. On (A), since $\nu = -1$ the oscillator relaxes to the value of O. The rhythmic activity is activated in (B),(C),(D). In (B) and (D) both discrete and rhythmic trajectories. Frequency is decreased from (B) to (C) and (D). In (D) the oscillator is inverted.

minimum of the double of cells to produce the possible gaits, eight cells in the case of quadruped gait and four cells in the case of biped gaits [33, 165]. Moreover, it is not clear to the author which kind of coupling terms should be used, and how to find the coupling values to achieve the desired spatiotemporal relationships. Besides, it is not evident if it is possible to switch in real-time and straightforwardly, among the possible spatiotemporal relationships.

Arbitrary phase relationship

Here it is considered that is desired to achieve an arbitrary phase relationship θ between two oscillators. This phase relationship may be obtained by the employment of a rotation matrix $\mathbf{R}(\theta)$, which rotates the linear terms onto each other, producing the correct influences on the oscillator to achieve the desired entrainment, as outlined by Buchli [26, 28].

The rotation matrix is added as a member to the oscillator, here represented in matrix notation.

$$\begin{bmatrix}\dot{x}_i\\ \dot{z}_i\end{bmatrix} = \begin{bmatrix} f_x(x_i - O_i, z_i)\\ f_z(x_i - O_i, z_i)\end{bmatrix} + \kappa\mathbf{R}(\iota_j\,\theta_i^j)\begin{bmatrix}\frac{(x_j - O_j)}{r_j}\\ \frac{z_j}{r_j}\end{bmatrix} \tag{3.4}$$

This coupling mechanisms maintains a desired phase relationship, θ_i^j, imposing a phase relationship from oscillator j onto oscillator i. Parameter κ specifies the coupling strength between the two oscillators, which can be useful when it is desired to decouple the specific oscillator, or increase the strength of the influence between two oscillators. The oscillator's influence is normalized, divided by the oscillator's radius r_j, minimizing the effects of the difference in amplitudes between the two oscillators. Parameter ι_i accomplishes a correct coupling between two oscillators, holding the information of the direction of the coupled oscillator.

In-phase coupling

In phase coupling is a particular case when the desired phase relationship $\theta = 0$, simplifying the terms to be added to the oscillator equations.

$$\dot{x}_i = f_x(x_i - O_i, z_i) \tag{3.5}$$

$$\dot{z}_i = f_z(x_i - O_i, z_i) + \kappa \frac{z_j}{r_j} \tag{3.6}$$

However, as shown in eqs. (3.5,3.6), the coupling term in x is ignored, to accommodate the possibility of oscillator with different limit cycle directions.

This mechanism allows for a very simple coupling method to achieve in-phase coupling between two of the presented oscillators.

Double frequency coupling

It may be desirable to achieve in-phase relationship maintenance between two oscillators, where the leading oscillator entrains a faster oscillator with double the frequency. By adding the coupling terms presented in eqs. (3.7,3.8), oscillator i can be coupled to a leading oscillator j.

$$\dot{x}_i = f_x(x_i - O_i, z_i) \tag{3.7}$$

$$\dot{z}_i = f_z(x_i - O_i, z_i) + \kappa \frac{z_j \, (x_j - O_j)}{r_j} \tag{3.8}$$

Fig. 3.6 demonstrates what is meant by coupling two oscillators with double the frequency. Leading oscillator (x_1, z_1) presents a period of 4 s, while oscillator (x_2, z_2) presents the double of this frequency. Notice that during one of the half portions of oscillator 1, a complete synchronized oscillation is performed by oscillator 2. The mechanism synchronizes the onset of oscillations between the two oscillators.

This coupling mechanism will be very useful in the achievement of periodic modulatory mechanisms on the proposed organization of the CPG, as will be presented in the next chapter.

3.1.3 Discrete dynamical system

On the proposed locomotor system, along with the production of rhythmic motions, it may also be required to produce solely discrete, point to point motions. This ability is accomplished by using a set

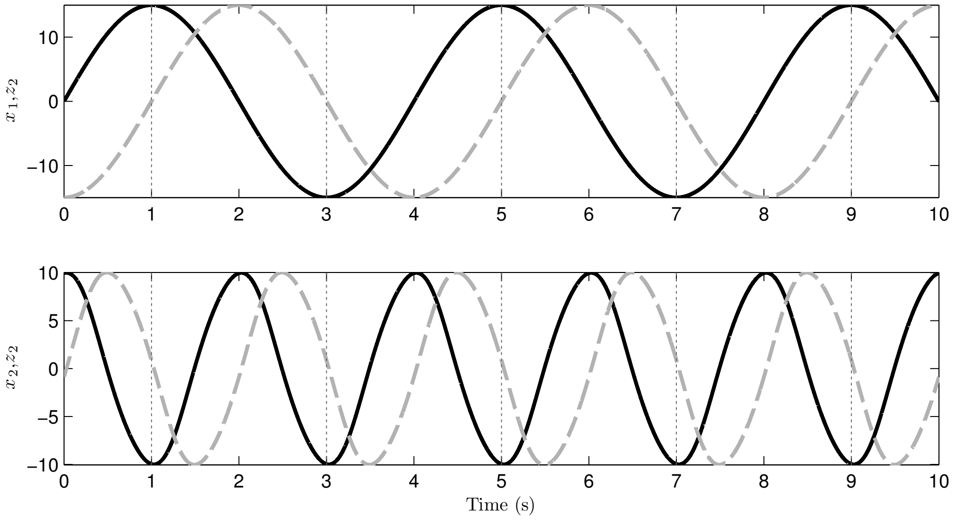

Figure 3.6: Leading oscillator 1 (top) performs a period of 4 s, and oscillator 2 (bottom) a period of 2 s. The coupling mechanism accomplishes a synchronized execution of oscillations between the oscillators, with coincident onsets.

of differential equations based on the VITE (Vector Integration To Endpoint) model [32], and based on the discrete system of [46].

A discrete motion is generated by:

$$\dot{y} = v, \tag{3.9}$$

$$\dot{v} = -\frac{b^2}{4}(y - y_{\mathrm{g}}) - bv. \tag{3.10}$$

The system produces stable, critically damped solutions that converge asymptotically and monotonically to target y_{g}, defined as an attractive fixed point, with a speed of convergence defined by parameter b.

The simplicity of the system is a very attractive characteristic for motor control, with one only tuneable parameter b and a control variable y_{g} for the goal of the motion. It also produces smooth and continuous trajectory accelerations, and its suited for the application along the proposed CPGs, or even into the CPG as control input.

3.2 Two layer CPG model

The proposed two layer CPG model is implemented by resorting to two dynamical systems tools into two distinct functional layers, a rhythm generation layer and a pattern generation layer. The division onto two layers addresses temporal and spatial generation independently, which allows to generate more complex spatial solutions than the previous Landau-Stuart oscillator.

For the rhythm generation layer, a phase oscillator is employed. The pattern generation layer is divided in several units of pattern generators, each including a set of forcing terms driven by the rhythmic phase produce periodic trajectories. The final periodic trajectory produced by a pattern generator is the overall result from the employment of these forcing terms. Forcing terms describe simple motions, meant to be employed as components for building and achieving more complex motions. Motor behaviors are achieved by performing complex motions, broken down into simpler constituent motions. It is a synergistic approach, considering that by weighting, modulating or sequencing the simpler motions, one can accomplish the generation of more complex trajectories.

This approach is based on the notion of *motor primitives*, which hypothesizes that the generated motor output from the vertebrate motor system is accomplished through a combination of a number of units of motor output [23, 62]. Small functional units in the spinal cord produce specific patterns of muscle activation, also named *synergies*, as discrete building blocks which combined result in the production of a variety of movements. This method for the problem of motor control allows the CNS to handle a large space of solutions, simplifying the low-level activation of the muscles, handling only the activation of synergies, instead of individual muscles involved in the movement [190]. It is an effective method to accomplish coordination among a large number of DOFs for a determined stereotypical behavior in low-level control. The problem of motor control comes down to a role in selecting, appropriately activating pre-existing motor primitives, or even transforming and deriving from an existing limited number of stored motor primitives.

This concept is applied in the presented approach as kinematic motor primitives, herein named *motion primitives*, proposed for the case of rhythmic motor behaviors in locomotion.

3.2.1 Rhythm generator

Similarly to other CPG implementations [10, 147, 216], a rhythm generator layer is implemented as a phase oscillator, producing the driving rhythmicity for the pattern generation.

The coupled phase oscillator is given by:

$$\dot{\phi}_i = \omega + k \sin(\phi_o - \phi_i + \pi), \tag{3.11}$$

where ϕ_i (rad) is the phase CPG i and ϕ_o (rad) is the phase of CPG o. The phase increases monotonically and linearly with rate of ω $(\mathrm{rad.s}^{-1})$, bounded in the range $[-\pi, \pi]$ (fig.3.7(a)). The goal is to have the phase of the oscillator set the pace for the generation of periodic trajectories, as a time keeping clock for the generation of the rhythmic motions for the CPG i.

The use of a phase oscillator provides for a simple mechanism for entrainment and phase locking, which has been extensively studied and applied to synchronization phenomena [1]. The included coupling term $k \sin(\phi_i - \phi_o + \pi)$ maintains a desired phase relationship of π between oscillator o and i, with a coupling strength of k. Analytical demonstration of the coupling is presented in appendix B

3.2.2 Motion pattern generator

In the proposed implementation, each pattern generator is based on a basic point attractive system, represented by a first order dynamics.

$$\dot{z} = \alpha(O - z) + \sum f_j(z, \phi_i, \dot{\phi}_i) \tag{3.12}$$

O specifies the goal attractor, or baseline for the final generated rhythmic motion, and α its time constant. Without any forcing terms f_j, the system converges asymptotically towards the goal O, and no rhythmic activity exists. The system must then be subject to periodic influences through the forcing terms and the phase oscillator output, producing the final rhythmic trajectory.

A single forcing function $f_j(z, \phi_i, \dot{\phi}_i)$ maps the current position and the phase of the step cycle to a force which influences the system's final output. Each forcing function is anchored into a specific phase value from $[-\pi, \pi]$ rad, resulting in a rhythmic pattern driven by ϕ_i. The final generated trajectory z results from the sum of all forcing functions.

Fig. 3.7(b) demonstrates the output of the pattern generator when employing a forcing term $f_1 = 10\dot{\phi}\sin(\phi)$ for z_1, and $f_2 = -10\dot{\phi}\frac{\phi}{0.274}\exp\left(-\frac{\phi^2}{0.548}\right)$ for z_2. The final pattern from z_3 is achieved by employing the two forcing terms, $f_1 + f_3$, resulting in a more complex rhythmic pattern.

In terms of stability, the system is guaranteed to converge to the attractor O in the absence of forcing terms if an appropriate α is chosen ($\alpha > 0$). Furthermore, the magnitudes of the forcing terms employed in eq.(3.12) are limited and bounded by design, thus the system is BIBO (Bounded-Input, Bounded-Output) stable, producing a solution around O given that the rhythmic forcing terms are limited in amplitude [94].

The system in eq. (3.12) could easily be substituted by a second-order system, like a linear spring-damper such as in forced velocity DMPs [91].

In this formulation, a single motion primitive is defined as a set of forcing functions assigned to the pattern generators among the required joints. The set of forcing functions defines a rhythmic motor behavior, coordinating all the recruited DOFs, used as a building block for the final motor behavior.

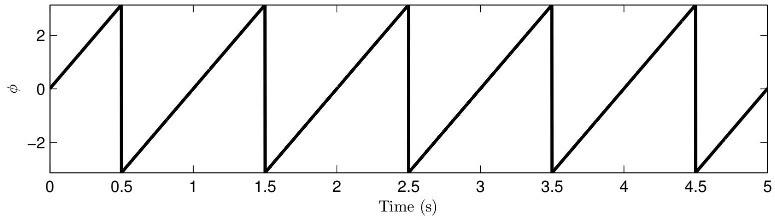

(a) Output from the phase oscillator in the rhythm generation layer.

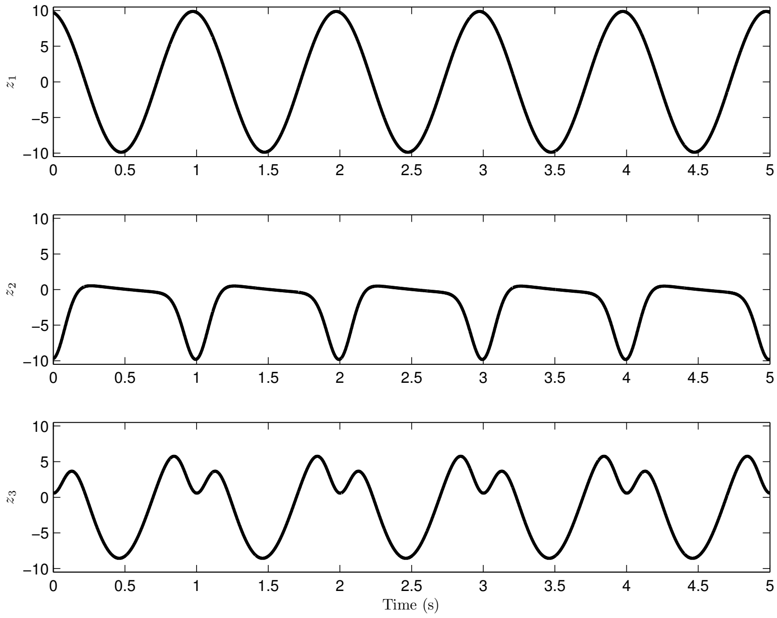

(b) Output from the pattern generation layer.

Figure 3.7: Demonstration of two distinct rhythmic patterns in z_1 and z_2 resulting from applying f_1 and f_2, respectively, as well as the combination in z_3, resulting from $f_1 + f_2$.

CHAPTER 4

QUADRUPED LOCOMOTION

Locomotion generation for legged robots is a complex problem that can be divided in several sub-problems such as: gait generation, posture control, adaptation to the environment, planning; too enumerate just a few. In order to tackle some of these problems in quadruped locomotion, a bio-inspired architecture is proposed, based on the functional model of biological motor systems, and on the use of dynamical systems to model Central Pattern Generators (CPGs), as presented in chapter 3.

The proposed architecture is able to produce a varied range of quadruped motors skills, having the ability to achieve goal-oriented locomotion and navigation as directed through high-level commands from local planning methods.

The chapter will start with the design of the proposed CPG controller, and explain how the tools presented in chapter 3 are used to produce the motor actions for quadruped locomotion. A series of experiments and simulations are subsequently presented to demonstrate the adequacy of the proposed CPG controller to produce purposeful, goal-oriented locomotion. The omnidirectional walking capabilities on the AIBO ERS-7 are presented, and a navigation application in simulation. Later on, a tentative approach to include a phase entrainment feedback mechanism is presented. Lastly a feedback mechanism for posture and balance maintenance for a standing quadruped is proposed, and tested on the AIBO ERS-7, subject to postural perturbations in a testing platform.

4.1 Related works

Quadruped omnidirectional locomotion Quadruped omnidirectional locomotion has been achieved through different methods in several works and applications. The most usual method for achieving omnidirectional walking is by employing model based methods, requiring the planning of footholds, resorting to a desired gait plan and the use of inverse kinematics and body dynamics [37, 59, 90, 224].

Parameterizable walking motions are also used and omnidirectional walks can also be found [76], where optimization was used to find the best parameters for the leg motions [38, 85].

There are some implementations of CPG based controllers where quadruped steering is achieved, but not omnidirectional locomotion. Tsujita and colleagues [215] proposed a dynamic turning control system for a quadruped robot with a body yaw joint, which is not is not suitable for the AIBO robot due to its configuration and rigid body. Hiroshi Kimura and colleagues [111] designed a locomotor controller based on neural systems and integrated it with a new navigation controller in order to achieve the turning motion, however their steering approach is specific for a quadruped robot with yaw joints on the legs. Omnidirectional locomotion by neural oscillator networks is presented and demonstrated in 6 and 8-legged robots in the work of Manoonpong [127], describing modular neural control structures consisting of three different functional modules, utilizing discrete-time neurodynamics, capable of performing omnidirectional walking as well as reactive behavior.

However, to the best of the author's knowledge, omnidirectional locomotion has not been addressed in the framework of dynamical systems and limit cycle oscillators. The proposed work tries to serve this purpose by presenting a general, model free controller using the framework of limit cycle oscillators and dynamical systems, that autonomously generate the required leg trajectories, modulated according high-level commands to achieve omnidirectional walking.

Entrainment in quadruped locomotion Many efforts have been taken to design methods for correcting and adequating the CPGs' nominal output in face of unexpected perturbations or unperceived changes in the environment. One typical approach is the adjustment of the nominal stepping frequency of the CPG, either by phase manipulation or frequency tracking.

In quadruped robots step phase manipulation has been achieved through phase resetting and through phase regulation. The former resets the phase of the step cycle upon an external event, typically foot strike [11, 216]. The other method for phase regulation controls the transition between step phases, delaying and eliciting the transition depending on external conditions, typically leg load [135,136,174].

Other methods exploit the entrainment properties of the oscillators employed in the CPGs. For instance, frequency tracking was demonstrated for the compliant quadruped robot Puppy [29].

The present chapter explores a phase feedback inspired in the work of Morimoto [88] and Fukuoka [64], aiming to entrain the CPG oscillators with the phase of the robot's periodic motions. The goal is to exploit the entrainment properties of the oscillator, while achieving phase manipulation for the adjustment of the nominal step frequency.

Posture control There are already a few works that apply CPGs and nonlinear dynamical systems to address locomotion and postural control. Hiroshi Kimura and colleagues [64] generate a dynamically stable gait on irregular terrains. They include a *vestibulospinal reflex* and a *tonic labyrinthine response* to adjust the pitch and rolling during locomotion.

Lewis et al. [122] apply CPGs to generate the movement for the hip and knee joints. Their goal is to equalize pressure on the feet by making suitable shifts in trunk position and trunk configuration, and therefore achieve postural control. However, it is required a twist joint in the robot trunk to apply the mechanism.

Ridderström and Ingvast [172] implemented a standing quadruped robot postural control to control the trunk's desired roll angle, pitch angle and height. They achieve posture control, maintaining the trunk's horizontal position by distributing the applied vertical forces of the body on the legs through hybrid control, relying on impedance and torque control from the WARP 1 robotic platform.

Maufroy [135,136] achieves postural control in the frontal plane of the quadruped robot, by applying phase resetting mechanisms, which extends the stance phase of the leg supporting the body's mass. However the proposed system does not explicitly deal with postural control, such as trunk attitude and height control. The postural corrections are an implicit result from the phase resetting mechanism.

Zhang and Zheng [225] present a control strategy biologically inspired that allows a quadruped robot to walk smoothly up and down hill. They present a CPG based control that uses the pitch angle of the trunk as feedback to adjust the body, argued by the authors as similar to the way that cats do.

The proposed work a places greater interest in exploiting the integration of different sensory modalities, creating a more robust response in posture. The proposed work strives only for standing posture control, as a precursor to locomotion integrated with posture control.

4.2 Quadruped CPG approach

The purpose of this section is to design a locomotor controller capable of generating and controlling the joints of the legs of a position controlled quadruped robot. The proposed architecture is bio-inspired in the vertebrate biological motor systems, and is structured in functional hierarchical levels according to their role on the motor control of locomotion, similarly to the motor control systems involved in goal-directed locomotion in vertebrates. The design of the architecture takes into account experimental knowledge about how the nervous system deals with the control problem in a robust and flexible way [47, 72, 189, 214]. Fig. 4.1 presents a schematic of the proposed architecture.

A generation level addresses the role of the spinal cord and generates the motor patterns by networks of CPGs [47, 107]. The concept of biological CPG includes the idea of hierarchical organized unitary oscillators: the unit-CPG. A single unit-CPG controls and activates the antagonistic muscle pairs, controlling the movements of a single joint. Movements of a leg are controlled by a limb-CPG, composed by a group of coordinated unit-CPGs within a leg. They are coordinated to provide flexible generation of motor patterns in a single leg, a synergy of movements from the joints that result in purposeful leg movements.

The regulation level models very basically the brainstem command centers for initiating, regulating and stopping CPGs activity and therefore initiate walking, switch among gaits, control the direction of movement and stop the locomotion, similarly to signals derived from the brainstem of biological systems [71]. It is assumed that despite the complexity of the desired motor behaviors, they should be built upon small blocks, which can be modulated according to parameter values that explicitly reflect on the desired final behaviors. Therefore, each motor behavior should have an associated set of parameters, selected, modulated and timed from high-level commands. This level receives the desired robot angular velocity, the robot walking orientation and a modulatory signal which encodes the desired duty factor and outputs the set of CPG parameters: frequency, amplitude and relative phases. By sending these at the right timing to the generation level, it results in the modulation of the generated trajectories and thus

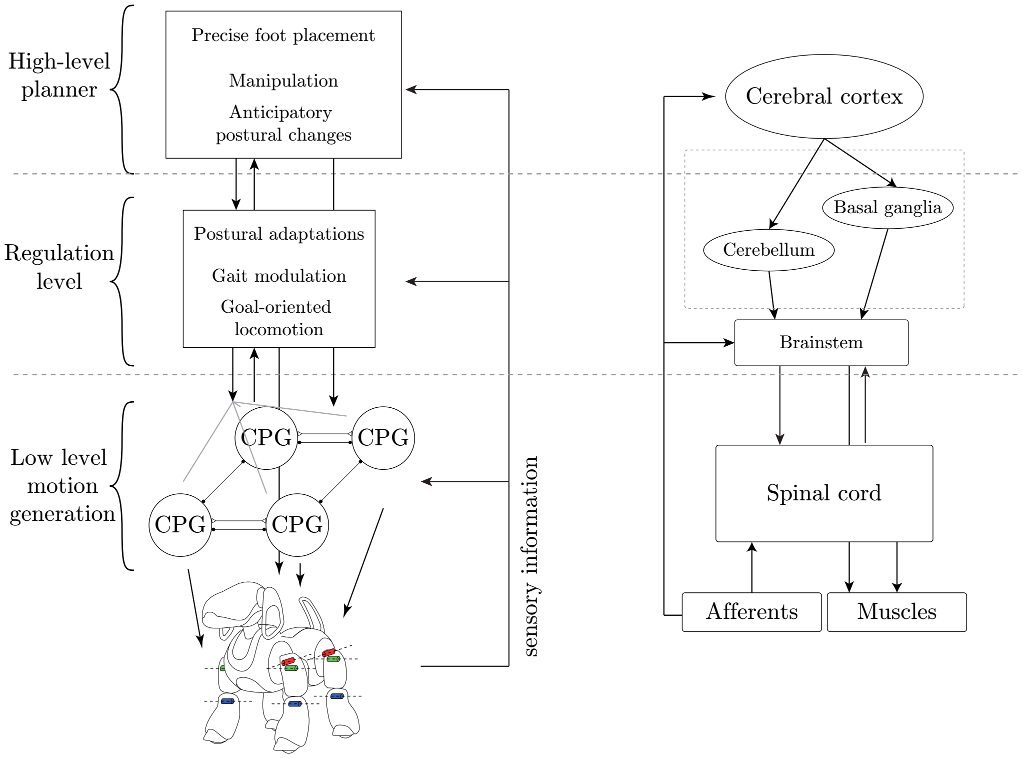
High-level planner
Precise foot placement
Manipulation
Anticipatory postural changes
Regulation level
Postural adaptations
Gait modulation
Goal-oriented locomotion
Low level motion generation
CPG
CPG
CPG
CPG
sensory information
Cerebral cortex
Basal ganglia
Cerebellum
Brainstem
Spinal cord
Afferents
Muscles

Figure 4.1: Proposed architecture based on a CPG network. Each CPG has a set of parameters that specify the leg movement.

in different motor behaviors. A smooth behavior switch and behavior modulation, which also can be elicited according to sensory information.

A third planning level would be responsible for the planning and execution of voluntary and anticipatory motor actions. It could use high-level sensory information, such as vision, and knowledge on the environmental context to elicit voluntary foot placement, or anticipatory balancing actions. In section 4.4, a simple local navigation controller will take the place of the planning level, as means of demonstrating the modularity of the architecture.

Similar architecture for accomplishing other behaviors is proposed by Degallier [44, 45], using simple dynamical systems that are able to generate discrete and rhythmic motor primitives, and more complex movements through their superposition.

Next, each of these levels is explained in more detail.

4.2.1 Generation level

This level generates the low-level motor activity that directly controls the joints of the robot. It is a coordinated network of four CPGs, able to produce quadruped walking motions, depending on the desired motor behavior specified by a set of parameter values. Each CPG controls the generation of the motor patterns within a leg, by employing coordinated unit-CPGs, one per joint. This scheme for the generation level addresses the problem of redundancy, through the tight coordination of the unit-CPGs, and the subsequent coordination among the four CPGs, reducing the solution space of possible motions to be generated.

Hip unit-CPG

The unit-CPG is the conceptual unitary constituent of the low-level movement generator and is considered to be implemented by the oscillator given in eqs. (4.1, 4.2, 4.3) (described in section 3.1) that generates movement for a single joint.

$$\begin{aligned} \dot{x} =& \alpha \left(\mu\nu - r^2\right)(x - O) - \omega\iota z, && (4.1)\\ \dot{z} =& \alpha \left(\mu\nu - r^2\right) z + \omega\iota(x - O), && (4.2)\\ \omega =& \frac{\omega_1}{\mathrm{e}^{-az}+1} + \frac{\omega_2}{\mathrm{e}^{az}+1}, && (4.3) \end{aligned}$$

The generated x solution from this oscillator is used as the control trajectory for both hip joints of the robot legs. These trajectories encode the values of the joint's angles (°) and are sent online to the lower level PID controllers of each hip joint.

It is assumed that the descending phase of the x trajectory, when $\iota = 1$, corresponds to the stance step phase, in which the foot moves backwards, and the hip-swing joint value is decreasing, thus propelling the robot forward. The ascending phase is the movement that places the foot in a more advanced position, ready for the next step, and corresponds to the swing step phase. This is depicted in fig. 4.2(a).

Changes in the limit cycle direction, through parameter ι, result in changing the step stance phase between descending ($\iota = 1$, counterclockwise limit cycle) and ascending ($\iota = -1$, clockwise limit cycle) phases of the x trajectory. In practice this change specifies the direction of the propulsive action on the stance phase, and the direction of the protraction on the swing phase.

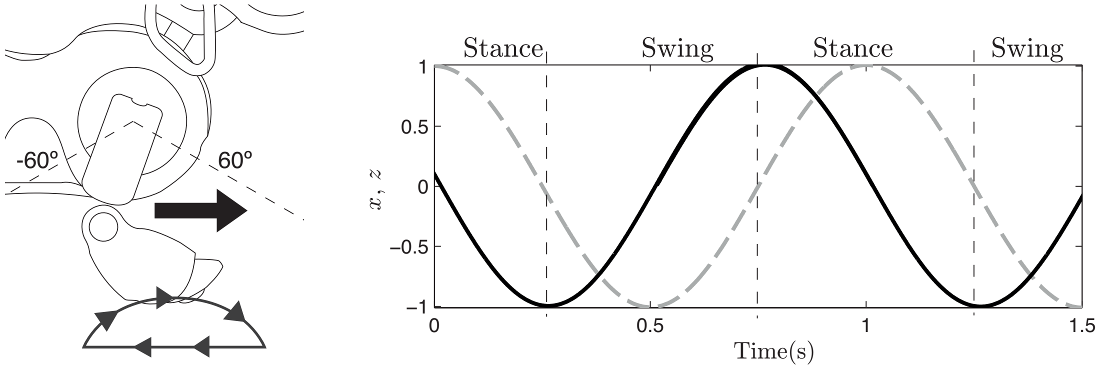

(a) (b)

Figure 4.2: Stance and swing phases for $\iota = 1$. **a)** The robot is pushed forward. The corresponding movement of the descending trajectory is the movement of pushing the robot forward. **b)** x (solid line) and z (dashed line) trajectories. x trajectory (solid line) is the control policy for the hip-swing joint of the robot. When $z < 0$, the robot is performing the swing phase. For $z > 0$ the robot is performing the stance phase.

The stance and swing phases are also easily identified by solution z, independently of the current limit cycle direction. Determined by the frequency modulation mechanism in eq. (3.3), when $z < 0$ the leg is executing the swing step phase. When $z > 0$ the leg is executing the stance step phase (fig. 4.2(b)).

Duty factor In quadruped locomotion, an animal changes its velocity by increasing or decreasing the number of steps per second [72, 81]. The two main phases of the movement are not equal in duration: the swing phase period (extension) keeps approximately constant, whereas the stance phase (flexion) varies in duration from a slow walk to fast running, a trot or a gallop [72, 81]. These two step phases are related through the duty factor $\beta \in]0, 1[$, given by:

$$\beta = \frac{T_{\text{st}}}{T_{\text{st}} + T_{\text{sw}}}, \tag{4.4}$$

where $T_{\text{st}}, T_{\text{sw}}$ are the stance and swing phase duration, respectively. By controlling the duration of the ascending and descending phases of the x trajectory with the frequency modulation mechanism from eq. 3.3, it is possible to control the durations of the swing and stance step phases independently, and thus the duty factor. To achieve a desired gait, a duty factor (β) is achieved by keeping the swing frequency constant $\left(\omega_{\text{sw}} = \frac{\pi}{T_{\text{sw}}}\right)$, and changing only the stance frequency for the different quadrupedal gaits (eq. 4.5).

$$\omega_{\text{st}} = \frac{1-\beta}{\beta}\omega_{\text{sw}} \tag{4.5}$$

Input parameters Each unit-CPG takes a set of parameters for the modulation of the generated trajectories for the specified joint. The set of input parameters are:

- $\nu \in \{-1, 1\}$, switches on/off the rhythmic activity
- $\mu > 0$, modulates the amplitude of oscillations ($\mu = A^2$)
- $\iota \in \{-1, 1\}$, modulates the direction of the trajectory
- $\beta \in]0, 1[$, changes the walking velocity since it controls the stance duration within the period of the step
- O, sets the value of the oscillation's offset or the goal-discrete movement

The goal is to have this set of parameters to serve as inputs, specified by the mechanism presented in the next sections, controlling the parameters for the different motor behaviors.

The parameters α, ω_{sw} and a are set *a priori*. Parameter ω_{sw} specifies the swing phase duration, which is kept constant. Its value depends on the desired speed of movements and on the robotic platform.

Notation It would be desirable to have a small clarification on the used notation from here onward.

The quadruped AIBO robot has four legs, each with three joints. Therefore, each instantiated unit-CPG for one joint will be identified using subscript notation, in the system variables and on the variable parameters. Subscript j denotes a joint, out of three possible joints within one leg, each one with their own subscript. i.e. hip-swing (flexion/extension): s; hip-flap (abduction-adduction): f and knee: k. Subscript i denotes a leg, out of the four: fore left - FL, fore left - FR, hind left - HL and hind right - HR.

Some examples:

- $x_{\mathrm{f},i}$ - x state from the hip-flap unit-CPG, on the general leg i.
- $\iota_{\mathrm{s,FL}}$ - control parameter for the hip-swing unit-CPG on the left foreleg.
- ω_{sw} - general frequency for the swing phase.
- $z_{j,i}$ - general representation for a z state from a unit-CPG, in joint j and leg i.

Knee unit-CPG

Two methods for the knee unit-CPG are here proposed. The first method accomplishes a simple mechanism to produce the flexion and extension of the knee. The second mechanism is a little more complex, as it must be able to produce a parameterizable double peak trajectory of the knee, mimicking the yield during the stance phase.

Simple flexion/extension The knee joint can also be controlled as simple as possible, by specifying a single angle value θ_{sw} for a flexed state of the leg during swing, and one other angle θ_{st} for an extended leg during stance. This simple motion can be achieved by employing the discrete system presented in chapter 3 by eqs. (4.6,4.7).

$$\dot{y} = v, \tag{4.6}$$

$$\dot{v} = -\frac{b^2}{4}(y - g) - bv \tag{4.7}$$

Goal attractor g is alternated between the two angle values $\theta_{\mathrm{st}}, \theta_{\mathrm{sw}}$, depending on the current step phase, as given by the hip unit-CPG:

$$g = \frac{\theta_{\mathrm{st}}}{\mathrm{e}^{-az_{\mathrm{s}}+1}} + \frac{\theta_{\mathrm{sw}}}{\mathrm{e}^{az_{\mathrm{s}}+1}} \tag{4.8}$$

If $z_{\mathrm{s}} < 0$, the leg is in the swing phase and the knee flexes to θ_{sw}. If $z_{\mathrm{s}} > 0$, the leg is in the stance phase and the knee joint extends to θ_{st}. Each time g is changed between these two values according to the current leg step phase, the system solution converges asymptotically towards the desired joint angle. A smooth and continuous joint acceleration is produced, as output from second order system generates the movements for the knee.

Double peak trajectory A parameterizable double peak trajectory is produced by employing the Landau-Stuart oscillator from eqs. (4.1),(4.2). For producing the double peak, the knee unit-CPG must have a general step period of half of the step cycle T, and produce two cycles during a step, one on swing and one on stance. Furthermore, for achieving a desired duty factor, it is required to have two frequencies for both cycles, one frequency for stance $\omega_{\mathrm{k,st}}$ and one frequency for swing $\omega_{\mathrm{k,sw}}$. By employing a similar frequency modulation mechanism as eq. (3.3), the frequency of the knee oscillator alternates between these two values, accordingly to the current leg step phase, as determined by the hip-swing unit-CPG (z_{s} in eq. (4.9)).

$$\omega_{\mathrm{k}} = \frac{\omega_{\mathrm{k,st}}}{\mathrm{e}^{-a\left(z_{\mathrm{s}}-z_{\mathrm{adj}}\right)}+1} + \frac{\omega_{\mathrm{k,sw}}}{\mathrm{e}^{a\left(z_{\mathrm{s}}-z_{\mathrm{adj}}\right)}+1}, \tag{4.9}$$

To provide a little more temporal flexibility in the specification of the flexion and extension trajectories of the knee, the z_{adj} is introduced. This parameter allows to widen the temporal duration of the swing phase, extending the duration of the swing cycle in the knee, by a fraction of the stance duration ($\delta_{\mathrm{adj}} \in]0,1[$). Parameter z_{adj} and knee frequencies are calculated from:

$$z_{\mathrm{adj}} = \sin\left(\frac{\delta_{\mathrm{adj}}\pi}{2}\right)A, \tag{4.10}$$

$$\omega_{\mathrm{k,st}} = \frac{2\pi}{T_{\mathrm{sw}} - T_{\mathrm{st}}\delta_{\mathrm{adj}}}, \tag{4.11}$$

$$\omega_{\mathrm{k,sw}} = \frac{2\pi}{T_{\mathrm{st}}(1-\delta_{\mathrm{adj}})}, \tag{4.12}$$

where ω_{st} is the employed stance frequency in the hip unit-CPG, and A its frequency. T_{sw} and T_{st} are the swing phase and stance phase duration of the step cycle, respectively.

The parametrization of the trajectory profile is performed by specifying three values: the amplitude during the stance phase, $A_{\mathrm{k,st}}$; the amplitude during the swing phase, $A_{\mathrm{k,sw}}$; and the offset during the stance phase, $O_{\mathrm{k,st}}$. Offset of the knee during the swing phase is determined according to the three values: $O_{\mathrm{k,sw}} = O_{\mathrm{k,st}} - A_{\mathrm{k,st}} + A_{\mathrm{k,sw}}$

The same mechanism used in frequency modulation is used for the periodic modulation of amplitude and offset.

$$\mu_{\mathrm{k}} = \frac{A^2_{\mathrm{k,st}}}{\mathrm{e}^{-a\left(z_{\mathrm{s}}-z_{\mathrm{adj}}\right)}+1} + \frac{A^2_{\mathrm{k,sw}}}{\mathrm{e}^{a\left(z_{\mathrm{s}}-z_{\mathrm{adj}}\right)}+1}, \tag{4.13}$$

$$O_{\mathrm{k}} = \frac{O_{\mathrm{k,st}}}{\mathrm{e}^{-a\left(z_{\mathrm{s}}-z_{\mathrm{adj}}\right)}+1} + \frac{O_{\mathrm{k,sw}}}{\mathrm{e}^{a\left(z_{\mathrm{s}}-z_{\mathrm{adj}}\right)}+1}, \tag{4.14}$$

$$\tag{4.15}$$

Fig. 4.3 demonstrates a knee unit-CPG (bottom) producing a double peak trajectory with a stance amplitude of $A_{\mathrm{st}} = 5$ around $O_{\mathrm{st}} = 0$, and a swing amplitude of $A_{\mathrm{sw}} = 25$ with and offset of $O_{\mathrm{sw}} = 20$. On the first example (left), the duration of the swing phase is exactly the same as the swing duration of the hip unit-CPG. On the second example (right), the swing phase of the knee is extended by half of the duration of the hip's stance phase.

In practical terms, this mechanism allows a more detailed production of knee trajectories, employing

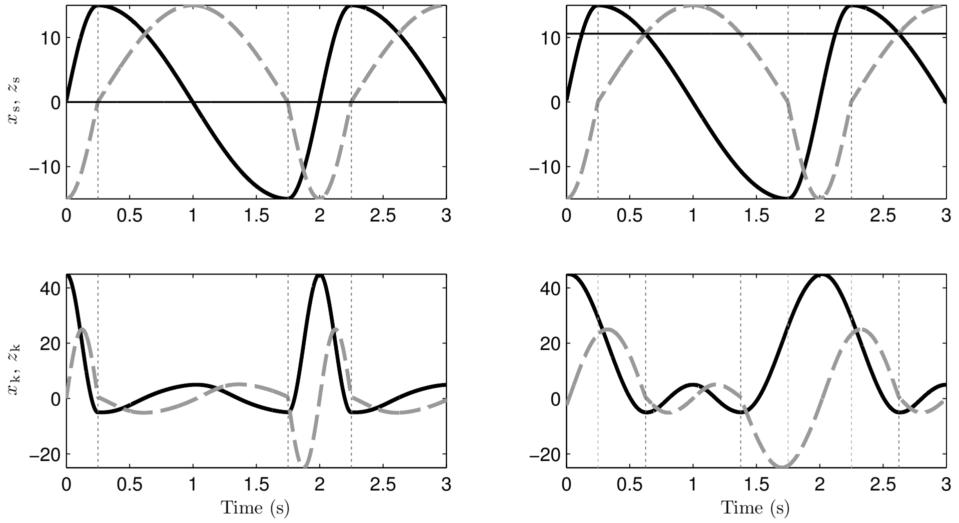

Figure 4.3: Double peak trajectory as produced by the knee unit-CPG (x_k, z_k). Both hip unit-CPG and knee unit-CPG are coordinated in the production of the stance and swing phases. The knee CPG is parameterized to produce an amplitude $A_{\text{sw}} = 25$ on swing, and an amplitude $A_{\text{st}} = 5$ on stance, around an offset of $O_{\text{st}} = 0$. On the left both unit-CPGs execute the same swing duration. On the right, the knee swing duration is increased in half the period of the stance phase.

the same oscillator, without increasing the dimensionality of the system.

Limb-CPG

For a correct expression of the movements within a single leg, a proper synergy of movements in all joints within a leg must be ensured. The generated rhythmic trajectories for the different leg joints must be therefore coordinated in time. The step phase in all leg's joints must be coordinated, accomplishing synchrony of step phases.

This kind of intralimb coordination is achieved within the limb-CPG[1]. The limb-CPG is composed by three unit-CPGs, one for each joint of a leg. i.e. hip-swing (s), hip-flap (f) and knee (k).

Coordination of the DOFs within a leg is achieved by coupling, in a specific manner, the unit-CPGs within the same leg. These couplings explore the entrainment and synchronization properties of the used oscillator. Specifically, when a swing joint is in the swing phase, also the corresponding flap joint should be in the swing phase; independently of their individual limit cycle directions, amplitude and offset.

Fig. 4.4 presents how the three unit-CPGs will be coordinated within a limb-CPG. It presents an hierarchical influence, with the hip-swing unit-CPG acting as a leading oscillator, entraining the other unit-CPGs. This coupling organization considers the ideas from the distribution of the spinal locomotor CPGs [107]. Each of the coupling mechanisms represented on the figure will be further detailed.

---

[1] In this work, CPG and limb-CPG are interchangeable terms.

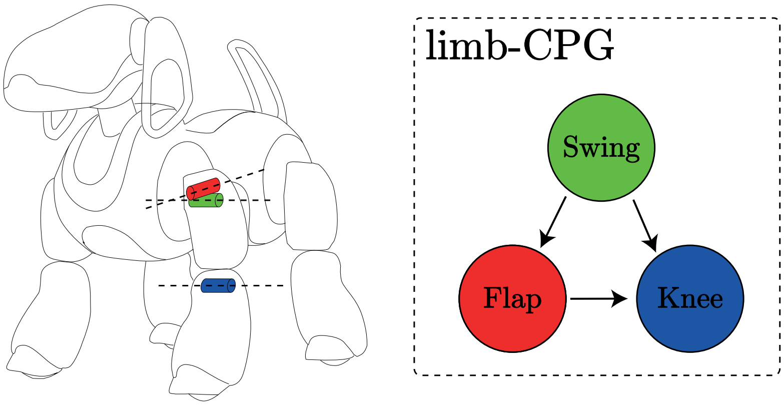

Figure 4.4: Schematic view of hierarchical coupling between the unit-CPGs. All the units are coordinated in order to generate the correct leg movement during locomotion.

Unidirectional coupling from hip-swing to hip-flap Each flap unit-CPG is unilaterally coupled to the corresponding hip-swing unit-CPG. This coupling is achieved by the mechanism presented in section 3.1.2. The unit-CPGs are coupled through z because it allows the simplest in-phase coupling method, where it is possible to independently control the directions of oscillations on both unit-CPGs.

Unidirectional coupling from hip to knee It is required to couple the knee unit-CPG to its leading oscillators when using double peak unit-CPG for the knee. Because the knee unit-CPG produces a faster rhythmic output, with double the frequency of the hip unit-CPGs, it is necessary to employ the coupling method presented in section 3.1.2.

The coupling accomplishes a correct synchrony of swing and stance phases between the hip unit-CPGs and the knee, even if the rhythmic activity in one of the hips is stopped.

CPG network

The four limb-CPGs are then coordinated among each other in order to generate the adequate stepping sequence of the desired gaits. This interlimb coordination is achieved by bilaterally coupling the swing and flap unit-CPGs among each other, ensuring a correct coordination between the legs.

Fig. 4.5 depicts how the coupling between the four limb-CPGs is achieved. Using the mechanism presented in section 3.1.2, two unit-CPGs are coupled together, maintaining a desired phase relationship θ. A layered approach is chosen: every hip-swing unit-CPG is coupled among each other, and all hip-flap unit-CPGs are coupled among each other. This approach is required to address the generation of decoupled trajectories for the hip-swing and hip-flap joints. e.g. in case of forward walking, hip-flap joints activity is stopped; in case of lateral walking, hip-swing activity is stopped.

Each unit-CPG has a parameter $\kappa_{j,i}$, which specifies the coupling strength upon itself, the unit-CPG for joint j in leg i. This aspect may be useful to detach a specific leg from the others, if ceasing rhythmic activity and performing tasks other than walking.

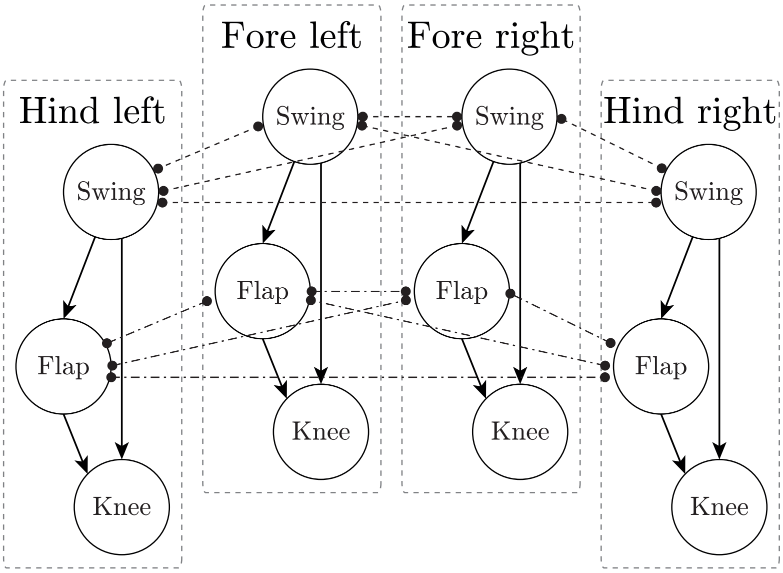

Figure 4.5: Structural view of the CPG network. The swing unit-CPGs are bilaterally coupled among each other, as well as the flap unit-CPGs (dashed arrows). The swing unit-CPGs are unilaterally coupled to the corresponding flap unit-CPGs (solid arrows). This level receives the required parameters from the upper level.

Quadruped phase relationships The relative phase relationships θ_i^o (rad) between the oscillators are calculated according to the gaits' relative phase. The gait relative phase of leg i, φ_i, is the time elapsed from the setting down of an arbitrary reference leg (herein chosen as the left foreleg), until the foot of leg i is set down, given as a fraction of the cycle time. The relative phase relationships between legs i and o are given by the difference of the gait relative phase of leg i and o in radians:

$$\theta_i^o = (\varphi_i - \varphi_o)\, 2\pi. \tag{4.16}$$

In this work are only addressed symmetric gaits, which always have $\varphi_{\text{FL}} = 0$, $\varphi_{\text{FR}} = 0.5$, and $\varphi_{\text{HR}} = \varphi_{\text{HL}} - 0.5$. Fig. 4.6 presents the gait sequence of the two gaits addressed in the presented work, walk gait and trot gait.

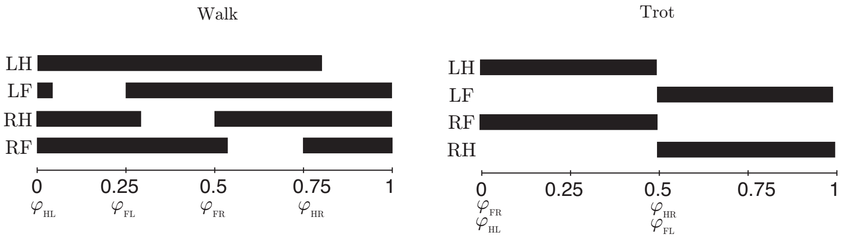

Figure 4.6: Gait diagrams for the walk and trot gaits, representing the phase relationships between the footfalls of the several legs.

By substituting the values onto eq. (4.16), it is possible to express the oscillators' relative phases θ_i^o

in terms of the gait phase φ_{HL}, as presented in table 4.1 ($\theta_i^o = -\theta_j^o$). Interlimb coordination can then be achieved by specifying only the gait phase φ_{HL}. Typically, $\varphi_{\mathrm{HL}} = 0.5$ and $\varphi_{\mathrm{HL}} = 0.75$, for trot and walk, respectively.

Table 4.1: Phase relationships between the oscillators.

i	o	θ_i^o
FL	FR	$-\pi$
FL	FL	$-\varphi_{\mathrm{HL}} 2\pi$
FL	HR	$(-\varphi_{\mathrm{HL}} + 0.5)\, 2\pi$
FR	HL	$(-\varphi_{\mathrm{HL}} + 0.5)\, 2\pi$
FR	HR	$(-\varphi_{\mathrm{HL}} + 1)\, 2\pi$
HL	HR	π

Overview of the generation level

The final CPG network (fig. 4.5) has controlled phase relationships and is able to generate complex, synchronized rhythmic patterns; discrete movements and a combination of both in a stable and flexible way. Due to the properties of this type of coupling among oscillators, the generated trajectories are smooth, stable and robust to perturbations; and thus ideally suited for trajectory generation in a robot.

This network constitutes the lower level of the proposed architecture (fig. 4.7). It receives from the upper level the required parameters that specify and modulate in a simple and straightforward manner the generated trajectories. Each limb-CPG receives two sets of ν, μ, ι and O parameters for the hip unit-CPG, and $O_{\mathrm{k,sw}}$, $O_{\mathrm{k,st}}$, $\mu_{\mathrm{k,st}}$ and $\mu_{\mathrm{k,sw}}$ parameters for the knee unit-CPG. For all the unit-CPGs a common set of parameters is specified. The coupling strength among limb-CPGs is specified by parameters κ_{s}, κ_{f} and κ_{k} for swing, flap and knee unit-CPGs, respectively. And the parameters that specified the desired gaits, β and φ_{HL}, and ω_{sw}.

The features of this network will allow for achieving omnidirectional locomotion. All the movements are performed allowing independent control of step movements of the different joints and still maintaining the intralimb and interlimb coordination.

4.2.2 Regulation level

The regulation level models very basically the brainstem command centers for initiating, regulating and stopping the CPGs activity of the generation level. It is responsible for selecting a motor behavior and for determining and sending the corresponding parameters for the generation level such that the desired task is achieved.

Bio-inspiration suggests that single tonic signals from supraspinal regions should somehow encode the required activity and/or modulation, providing a mapping from the tonic signals to the set of CPG parameters. Such mapping reduces the dimensionality of the control problem to just one excitatory signal. For instance, increasing activation of the brainstem locomotor center commands leads to an increase in quadruped locomotion speed, and to a gait switch from walk to trot.

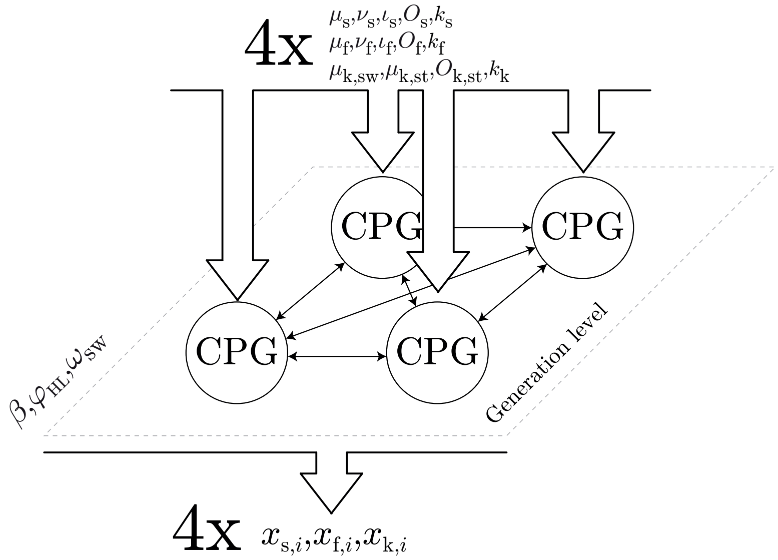
4x
μ_{s},ν_{s},ι_{s},O_{s},k_{s}
μ_{f},ν_{f},ι_{f},O_{f},k_{f}
$\mu_{\mathrm{k,sw}}$,$\mu_{\mathrm{k,st}}$,$O_{\mathrm{k,st}}$,k_{k}
CPG
CPG
CPG
CPG
β,φ_{HL},ω_{sw}
Generation level
4x
$x_{\mathrm{s},i}$,$x_{\mathrm{f},i}$,$x_{\mathrm{k},i}$

Figure 4.7: Representation of the generation level and its inputs and outputs. A global set of parameters for all CPGs: β, ω_{sw}, ϕ_{HL}. Each CPG receives a set of parameters, for each of the three unit-CPGs. All other parameters are calculated through a fixed set of relationships and rules.

The behaviors' parameters are the inputs of the four limb-CPGs, the control parameters required for generating movements. As they may be defined relatively to the environment, according to the time-varying sensory information, movements are adapted to the environment and allow for coordination and timing as well as behavior selection.

In order to perform omnidirectional locomotion, the robot must be able to move to any point of interest, with a given translation speed v, a turning rate $\dot{\phi}$ and walking orientation ϕ_{w} (fig. 4.9).

Gait Transition

In the presented model [131, 184], a given modulatory drive signal, m, models the mechanisms that underlie gait transitions induced by simple electrical stimulation of the brain stem, and regulates the activity of the CPG network. Different values of the drive lead to different walking behaviors, namely: locomotion initiation, speed change with adjustment of interlimb coordination and consequent gait transition, similarly to the biological counterparts [71]. In order to increase the robot stability the wave gait rule [95] is applied, meaning a gradually shift in interlimb coordination, from walk to trot.

These behaviors correspond to different specifications of the set of CPG parameters $\{\nu, \beta, \varphi_{\mathrm{HL}}\}$: ν parameter for stopping/initiating locomotion; duty factor β for adjusting frequency and gait phase φ_{HL} for adjusting interlimb coordination.

Herein an arbitrary mapping is suggested, from a modulatory drive signal m, to the desired walking activity. Below a low threshold, $m = 0.2$, the robot ceases stepping. Above this threshold, the robot starts with a slow walk (non-singular crawl), gradually increasing speed without adjusting the phase relationships. Above $m = 1$, locomotion speed is increased with adjustment of interlimb coordination. At $m = 2.5$, the robot is in trot.

Initiating/stopping locomotion The ν parameter controls whether or not there are oscillations generated by the unit-CPG and thus, locomotion generation.

Thus, the $\nu_{j,i}$ parameters are set according to the modulatory drive, m, as follows:

$$\nu_{j,i} = \begin{cases} -1, & m < 0.2 \\ 1, & m \geq 0.2 \end{cases}, \tag{4.17}$$

where $j \in \{\mathrm{s}, \mathrm{f}\}$, and i represents the leg $\in \{FL, FR, HL, HR\}$.

Robot velocity modulation As the modulatory drive increases in strength, the duty factor, β, linearly decreases from 0.89 (for the crawl gait) to $\beta = 0.5$ (for the trot gait). The duty factor is mathematically defined as a piecewise linear function of the modulatory drive:

$$\beta = \begin{cases} 0.89 & , m < 0.2 \\ -0.1667m + 0.9167 & , 0.2 \leq m < 2.5 \\ 0.5 & , m \geq 2.5 \end{cases} \tag{4.18}$$

This function presents a saturation for $\beta = 0.5$ because the robotic platform can not perform faster gaits.

Interlimb coordination modulation In this work, between $0.2 \leq m < 1$, the robot gradually increases its speed from a slow walk, but without adjusting the phase relationships. For a β ranging between 0.89 and 0.76, the robot presents a non-singular crawl gait with a constant gait phase $\varphi_{\mathrm{HL}} = 0.75$.

For $1 \leq m \leq 2.5$, the crawl gait slowly transfers into a trot gait while adjusting the phase relationship accordingly. For this purpose the wave gait rule for a quadruped is applied [95]: $\varphi_{\mathrm{HL}} = \beta$. In the resulting gait, subsequent legs are lifted closely after previous ones are set down, such that the time difference between the two events is equal to zero. Hence, m modulates the gait phases by specifying the gait phase φ_{HL} (eq. 4.19) as follows:

$$\varphi_{\mathrm{HL}} = \begin{cases} 0.75 & , m < 1 \\ -0.1667m + 0.9167 & , 1 \leq m < 2.5 \\ 0.5 & , m \geq 2.5 \end{cases} \tag{4.19}$$

The gait phase remains in $\varphi_{\mathrm{HL}} = 0.5$ for values of the modulatory drive greater than 2.5, that correspond to a $\beta = 0.5$. The robot performs then a trot gait.

Omnidirectional locomotion

The proposed omnidirectional implementation is based on the *wheel model* presented by Hengst et al. [76], applicable AIBO and other quadruped robots with similar configurations.

The *wheel model* basically assumes that each foot performs a step with a specified direction and length, and that the overall propulsion of the steps results in the desired robot motion. The feet move on a certain locus, creating an analogy of the leg as a small wheel, describing a circular movement during a step in a vertical plane with a specific direction. By controlling the orientation of this plane it is possible to control the step orientation and therefore the robot movement.

For performing a step with a specified orientation and length it is necessary to combine the feet movements on the sagittal and frontal plane. If feet movements are only in the robot's sagittal plane, the robot moves straight: forward or backward. When feet movements are only in the robot's frontal plane, it moves sideward: left or right. Movement in any direction is achieved by superimposing the movements of a foot on these two planes.

On the AIBO robot, it is assumed that the movements on the sagittal and transverse planes are controlled by the hip-swing and hip-flap joints, respectively. Fig. 4.8 shows some possible combinations of step directions and the resulting robot movement.

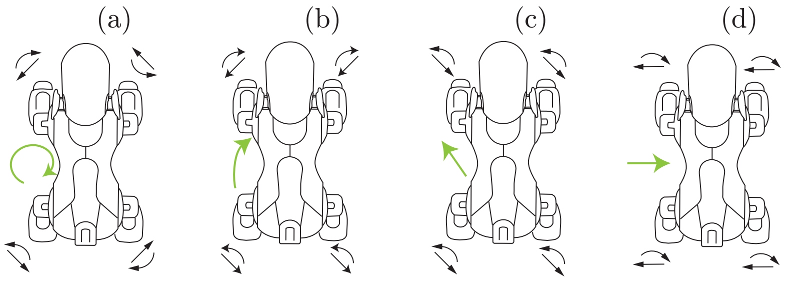

Figure 4.8: Some examples of possible robot movements. Resultant movement is indicated by light grey arrow. a) Rotation in spot; b) walk forward and turn; c) walk straight diagonally to the left; and d) walk straight sideways to the right. Swing and stance phase directions are indicated by curved and straight arrows near the legs, respectively.

The robot rotates in the spot in (a). All flap joints rotate the robot to the right, with fore and hind flaps moving in opposite directions, and the swing joints maintaining the robot in place. The robot steers right while walking forward in (b). The fore flap joints make the robot front move to the right, while the hind flap joints move the robot back to the left. All the swing joints propel the robot forward. This superposition of movements steers the robot right while walking forward.

When the flap joints make the robot move to the left and the swing joints propel it forward, the robot moves straight diagonally to the right (c).

The robot moves to the right in (d), because only the flap joints are employed to propel the robot.

By independently generating movements for the hip-swing and flap joints, it is possible to generate the desired movements in the sagittal and transversal planes, and thus a step with a certain direction and velocity.

Velocity of a step can be changed by either adjusting the stance phase duration or the step length. However, stance phase duration must be the same for all the legs for proper expression of the gait. The step length is then changed in the sagittal and transversal planes for each leg, enabling to achieve the desired step direction and velocity: All the legs perform a step with the same duration, but possibly with different amplitudes: steps with greater length propel the robot with greater velocity, and the opposite for smaller step lengths.

The *wheel model* is well suited for the proposed CPG network since both the step direction and length in the sagittal and frontal planes can be controlled independently for each leg, while maintaining the required intralimb and interlimb coordination. Modulating the CPGs requires finding the correct movement amplitudes, activations and directions of each step in the sagittal and in the transverse plane.

Because it is possible to describe the rotation of any point of the robot around a certain common point, where the translation speed is zero, i.e. the instantaneous center of rotation (ICR), it is possible to find the trajectory of any point of the robot when performing such rotation. For the robot to move around a certain ICR, each leg should perform a step of proportional size into a suitable direction, tangential to the circle with radius $r = \frac{v_{ref}}{\dot{\phi}}$, around the rotation center (fig. 4.9). When moving forward ($\dot{\phi} = 0$) the ICR is located at infinity.

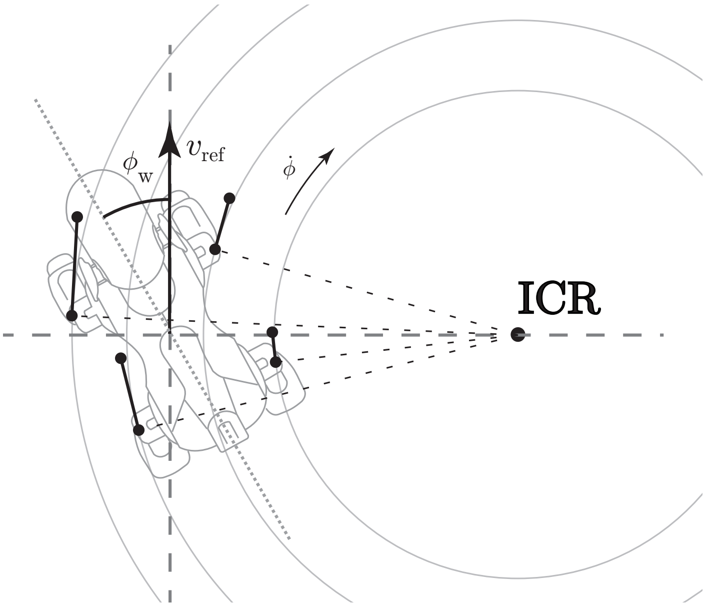

Figure 4.9: Robot motion for $\dot{\phi} \neq 0$, $v > 0$ and ϕ_{w}. The robot walks in a circle path centered on the instantaneous center of rotation (ICR). The figure also depicts the steps direction and length for achieving such walking motion.

From the ICR is possible to ascertain the movement for each leg. These trajectories will not describe ideal circles having the ICR as common centers, but instead approximate straight tangential trajectories.

By applying trigonometry, the amplitudes for hip-swing (s) and hip-flap joints (f) are given as follows, according to the walking velocity (v_{ref}), desired angular velocity ($\dot{\phi}$) and the desired walking orientation (ϕ_{w}):

$$A_{\mathrm{s},i} = A_{\mathrm{ref}} \frac{\dot{\phi} Y_i - v_{\mathrm{ref}} \cos(\phi_{\mathrm{w}})}{v_{\mathrm{ref}}}, \tag{4.20}$$

$$A_{\mathrm{f},i} = A_{\mathrm{ref}} \frac{-\dot{\phi} X_i + v_{\mathrm{ref}} \sin(\phi_{\mathrm{w}})}{v_{\mathrm{ref}}}, \tag{4.21}$$

where (X_i, Y_i) are the leg i coordinates in the robot reference frame. v_{ref} is an approximate obtained velocity when using a reference amplitude $A_{\rm ref}$ and the desired duty factor β (encoded in m). $v_{\rm ref}$ can be calculated from the duration of the propulsion phase ($T_{\rm st}$) and the length of the step ($l_{\rm st}$),

$$v_{\rm ref} = \frac{l_{\rm st}}{T_{\rm st}}. \tag{4.22}$$

The length of the step can be roughly deduced from the length of the leg ($l_{\rm leg}$) during the stance phase and the full amplitude of the locomotor movements ($2A_{\rm ref}(\rm deg)$), as $l_{\rm st} = 2l_{\rm leg}A_{\rm ref}$.

$A_{\rm ref}$ is an amplitude value set *a priori*, when tuning the parameters for locomotion. Since it is the value from where the calculated amplitudes will used as nominal reference, it must be suitable for the robotic platform, with the possibility to be increased and decreased without impairing locomotion.

CPG parameters have to be set such that small parameter changes modulate the generated trajectories. Therefore, for each of these unit-CPGs, a mechanism must determine their parameter values according to their roles in the final modulation.

$A_{{\rm s},i}$ and $A_{{\rm f},i}$ encode all the information needed to parameterize the CPGs, as demonstrated next.

Initiating/stopping locomotion To accommodate the calculated behaviors from the *wheel model*, the rules that modulate parameters ν are expanded. Now, $\nu_{j,i}$ parameters are set according to the modulatory drive, m, and also to calculated amplitudes $A_{j,i}$, as follows:

$$\nu_{j,i} = \begin{cases} -1, & m < 0.2 \;\vee\; |A_{j,i}| \leq 0.5 \\ 1, & m \geq 0.2 \;\wedge\; |A_{j,i}| > 0.5 \end{cases}, \tag{4.23}$$

where $j \in \{\rm s, f\}$, and i represents the leg $\in \{FL, FR, HL, HR\}$. An arbitrary dead zone is defined such that when the amplitude of the movement is negligible, the unit-CPG oscillatory behavior is turned off.

Amplitude Each unit-CPG amplitude is modulated such that the corresponding controlled foot describes a step with the correct step length, and thus the correct velocity. The μ parameter modulates the amplitude of each hip-swing and flap unit-CPG, according to the $A_{{\rm s},i}$ and $A_{{\rm f},i}$ values, as follows ($j = \{\rm s, f\}$):

$$\mu_{j,i} = A_{j,i}^2. \tag{4.24}$$

Step direction The signs of $A_{{\rm s},i}$ and $A_{{\rm f},i}$ hold the information on the direction for the step movements of each unit-CPG.

Limit cycle direction is specified by the value of ι. Basically, changing the limit cycle direction is changing whether the step stance phase is the ascending ($\iota = -1$) or descending phase ($\iota = 1$) of the x trajectory.

When the robot walks forward ($A_{\rm s} > 0$), all the swing unit-CPGs must have $\iota_{\rm s} = 1$, performing the stance phase during the descending trajectory of the movement. When the robot walks backwards

($A_{\mathrm{s}} < 0$), the opposite happens, and the unit-CPGs have $\iota_{\mathrm{s}} = -1$, performing the stance phase during the ascending trajectory.

For the hip-flap joints, another mapping is required. When walking right ($A_{\mathrm{f}} > 0$) and during the stance phase, the left joints perform the ascending trajectory and the right joints perform the descending trajectory. The opposite happens when walking left ($A_{\mathrm{f}} < 0$).

Table 4.2 shows the assigned values of ι according to this set of rules, depending on the swing and flap amplitudes.

Table 4.2: ι values for the hip-swing (s) and hip-flap (f) unit-CPGs.

	$\iota_{\mathrm{s,FL}}$	$\iota_{\mathrm{s,FR}}$	$\iota_{\mathrm{s,HL}}$	$\iota_{\mathrm{s,HR}}$
$A_{\mathrm{s},i} > 0$	1	1	1	1
$A_{\mathrm{s},i} < 0$	-1	-1	-1	-1
	$\iota_{\mathrm{f,FL}}$	$\iota_{\mathrm{f,FR}}$	$\iota_{\mathrm{f,HL}}$	$\iota_{\mathrm{f,HR}}$
$A_{\mathrm{f},i} > 0$	1	-1	-1	1
$A_{\mathrm{f},i} < 0$	-1	1	1	-1

In the following sections is demonstrated how the proposed controller achieves omnidirectional walking, and how it can be used in a navigation application.

4.3 Omnidirectional walking experiments

Several experiments were performed to verify the adequacy of the locomotor CPG network both to movement generation, velocity change, to achieve omnidirectional locomotion and to verify if the resulting robot motion matches the desired, specified high level commands, i.e. walking velocity, walking orientation and angular velocity.

Experiments were performed both on the Webots robotics simulator [219], a simulator based on the ODE physics engine for 3D rigid body dynamics, and on the real AIBO ERS-7 robotic platform. Four experimental results obtained with the real platform are depicted.

1. The robot walks forward and steers with a given angular velocity.
2. The robot walks diagonally with a given walking orientation.
3. The robot walks sideways.
4. The robot moves diagonally while steering with a given angular velocity.

The AIBO robot is a 18 DOFs robot made by Sony. Unlike its natural counterpart this robot has three joints per leg, with different configurations of a real dog legs. Besides, the robot body and legs are rigid with non-compliant servo joints. The joints are stiff, without any elasticity and position controlled with high feedback gains.

The CPG's swing frequency is set to $\omega_{\mathrm{sw}} = 6.28\ \mathrm{rad.s}^{-1}$ in regards with motor limitations, specifying a minimum swing period of 0.5 s for the step. Further, the dynamical parameters controlling the speed of convergence of unit-CPGs were set to $\frac{1}{2\,\alpha_\mathrm{i}\,\mu_\mathrm{i}} = 0.01$ s, in regards to stability during the integration process and to feasibility of the desired trajectories. At each motor and sensorial cycle, dynamic equations are calculated and numerically integrated using the Euler method with a fixed time step of 8 ms.

Experiments with the robot were carried on a flat environment with a grid of markers, spaced 20 cm apart. This grid enables to visually measure the performed path, comparing it with the expected path, to measure the achieved translational speeds, angular velocities and walking directions. A proper evaluation of performed the walking motions would require a proper motion capture system.

It is not expected precise and exact motions, since the CPG approach is not intended for such a goal. It is expected that the overall motion of the robot respects the specified motion commands, especially because in this work the CPG based controller is open-loop and disregards physical effects and other disturbances.

4.3.1 Steering

As a first step, it is verified if the steering behavior respects a specified angular velocity. In this experiment the robot walks forward, $\phi_\mathrm{w} = 0°$, with an angular velocity of $\dot{\phi} = -0.21$ rad.s^{-1}. The modulatory drive is set to $m = 2.5$, performing a trot gait ($\beta = 0.5$, $\varphi_\mathrm{FL} = 0.5$), where the diagonal legs are in-phase and the stance and swing phases have equal durations. For the given β, the robot velocity is approximately $v_\mathrm{ref} \approx 5.7\ \mathrm{cm.s}^{-1}$. The robot is expected to perform a circle with a radius of $r_\mathrm{ICR} \approx 27$ cm.

Fig. 4.10 presents an image composition of the experiment. It is possible to verify that the robot performs a circular path with an approximate radius of 30 cm, a marginal error when compared to the overall setup dimensions. This error is both due to the physical effects, error measurements and the open loop nature of the proposed controller.

Figure 4.11 depicts actual trajectories recorded from the joints encoders and planned trajectories $x_{j,i}$. Trajectories were generated as expected. Because the robot is steering right, amplitudes for the right hip-swing joints are smaller than those for the left hip-swing joints.

The knee joints flex and extend at the correct times, reducing the leg length while on swing and extending the leg during the stance phase employing the simple flexion/extension mechanism (right panels on fig. 4.11) .

The platform's weight and the resultant dynamics and forces on the legs influence the performed joint angles. For instance, fore right knee does not extend to the planned value. Considering forelegs' hip-swing joints, during the stance phase, the weight of the robot induces a further extension of the joint.

Highest discrepancies between generated and performed trajectories can be seen in flap joints. This difference is mainly due to the forces exerted over the legs and to the fact that flap joints torque limit is lower than swing joints.

Despite these discrepancies, the main features of the generated trajectories are still present on the performed joint trajectories and the desired robot motion was achieved.

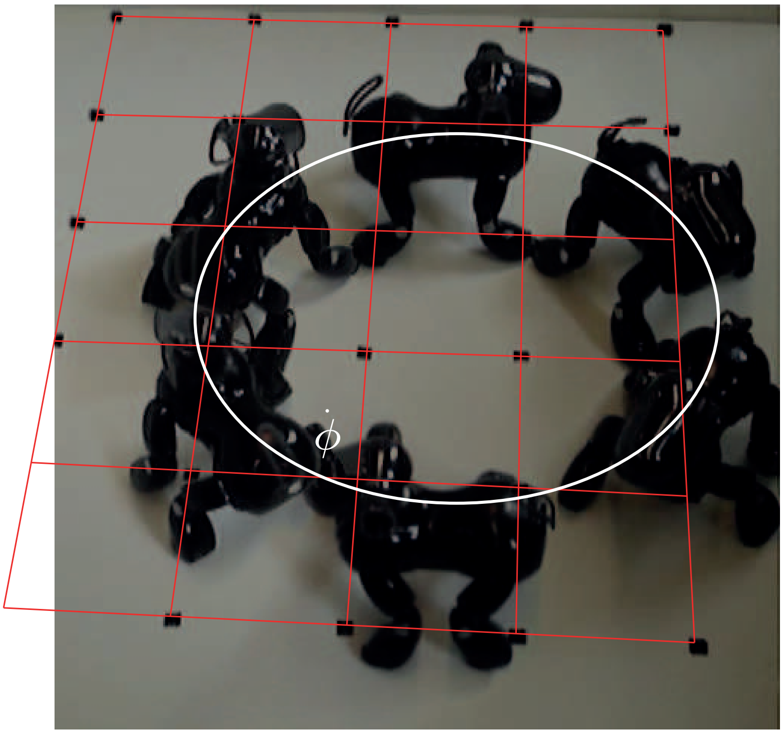

Figure 4.10: Image composition when the robot steers right when $\dot{\phi} = -0.21$ rad.s^{-1} and $\phi_\mathrm{w} = 0°$. The resulting radius is $\approx$ 30 cm.

4.3.2 Diagonal walk

In this experiment, the robot ability to walk with a given walking direction is verified. The robot performs a slow walking gait given by $m = 0.4$, yielding a $\beta = 0.8$ and $\varphi_{FL} = 0.75$, meaning an $v_\mathrm{ref} \approx 2.4\,\mathrm{cm.s}^{-1}$. An angular velocity $\dot{\phi} = 0°$ and a walking orientation $\phi_\mathrm{w} = -45°$ are specified, such that the robot is expected to walk diagonally, forward to the left, with equal forward and lateral velocities and no angular motion.

Resulting parameters are: $\nu_{\mathrm{s},i} = 1$ and $\nu_{\mathrm{f},i} = 1$, $i \in \{FL, FR, HL, HR\}$, such that both hip-swing and flap joints produce walking movements. Forward motion is achieved by obtaining the oscillators direction in the hip-swings, $\iota_{\mathrm{s},i} = 1$. Right lateral motion is achieved by obtaining the direction of the hip-flap oscillators to $\iota_{\mathrm{f},FL} = \iota_{\mathrm{f},HR} = -1$ and $\iota_{\mathrm{f},FR} = \iota_{\mathrm{f},HL} = 1$. Both swing and flap joints should perform stepping movements with the same amplitudes, propelling the robot equally forward and left.

Fig. 4.12 depicts the performed path on an image composition. The robot accomplished a forward displacement of about one grid forward, and two grid squares laterally, achieving a diagonal path of about $-63°$.

Fig. 4.13 depicts planned (dashed) and performed (solid) trajectories for hip-swing, hip-flap and knee joints. As expected, swing and flap trajectories have equal amplitudes. Further, intralimb and interlimb joints are coordinated as required. Hip-swings and hip-flaps are synchronized because swing and stance step phases are in phase. Directions in left fore and hind legs are inverted as specified in the parameters.

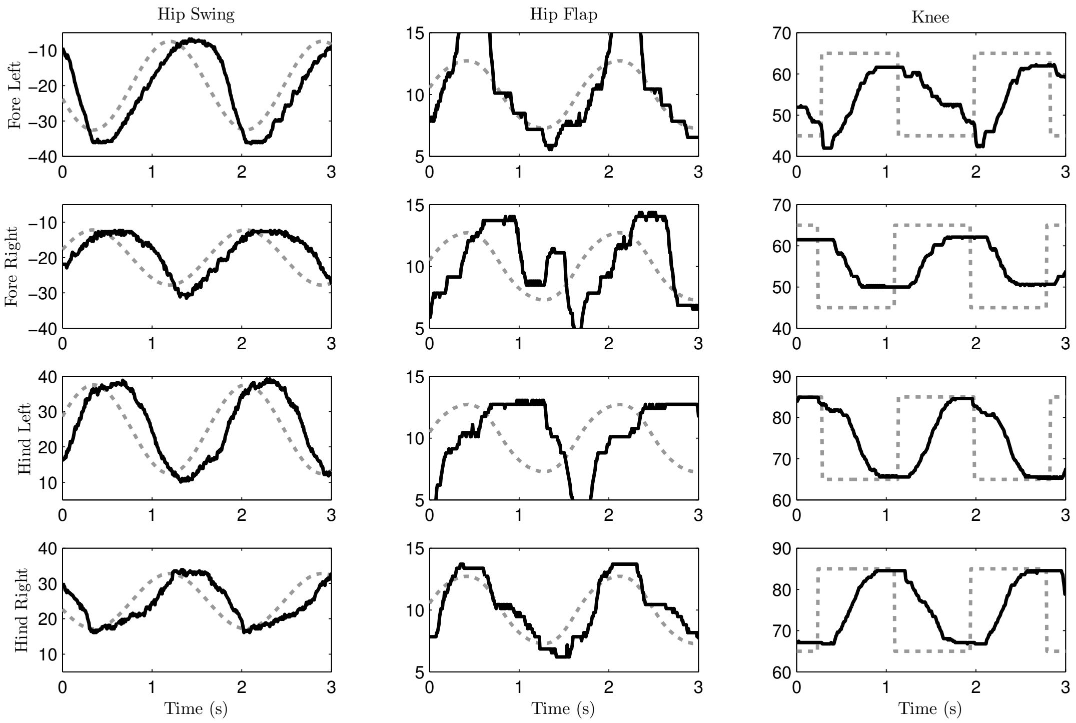

Figure 4.11: Planned trajectories (dashed) and actual performed movements (solid) for hip-swing, hip-flap and knee joints, for the steering motion depicted in fig. 4.10. All the generated trajectories respect the coordination constraints imposed by the couplings.

Generated and performed joint movements are much more similar than on the steering experiment because the frequency of movements is lower, and the used gait is much more stable, which results in walking dynamics that exert less force on the joints.

4.3.3 Walking laterally

This experiment is meant to demonstrate the robot capacity to walk laterally with a specified walking orientation $\phi_{\mathrm{w}} = 90°$. The robot performs a slow walking gait according to $m = 1$, yielding a $\beta = 0.75$ and $\varphi_{FL} = 0.75$, thus $v_{\mathrm{ref}} \approx 3.25\ \mathrm{cm.s}^{-1}$.

This requires the hip-swing joints to be at rest, $\nu_{\mathrm{s},i} = -1$, $i \in \{FL, FR, HL, HR\}$, while the hip-flap joints perform the rhythmic locomotor movement, $\nu_{\mathrm{f},i} = 1$. The robot to moves to the left and hip-flap joint directions are obtained as $\iota_{\mathrm{f,FR}} = \iota_{\mathrm{f,HR}} = 1$ and $\iota_{\mathrm{f,FL}} = \iota_{\mathrm{f,HL}} = -1$.

Fig. 4.14 shows snapshots of the robot walking laterally, achieving a straight path laterally, covering two grid squares in about 11 s, reaching a velocity of $\approx 3.6\ \mathrm{m.s}^{-1}$.

4.3.4 Steering diagonally

If the robot moves with a certain walking orientation and angular velocity, the robot will perform a circular path while not heading straight forward. i.e. the body orientation will not be tangential to the

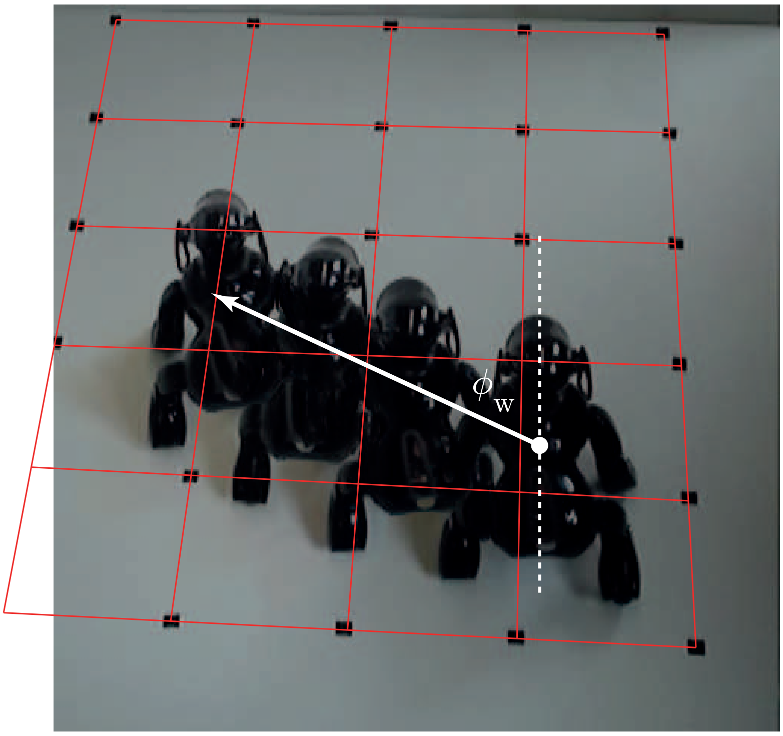

Figure 4.12: Image composition of four individual snapshots when the robot walks slowly ($m = 0.4$) forward diagonally to the left. It describes the path with $\dot{\phi} = 0$ rad.s^{-1} and $\phi_{\mathrm{w}} = -63°$.

circular path.

In this experiment the robot moves with a trot gait, specified by $\beta = 0.5$ and $\varphi_{\mathrm{FL}} = 0.5$ ($m = 2.5$), expecting a $v_{\mathrm{ref}} \approx 5.7\,\mathrm{cm.s}^{-1}$. The walking orientation is set to $\phi_{\mathrm{w}} = 65°$ and angular velocity to $\dot{\phi} = 0.27$ rad.s^{-1}. The robot is expected to walk while turning, heading about $\approx 65°$ to the center of its circular path with 22 cm radius. The obtained robot path is shown in fig. 4.15. It achieves a circular path of 2.5 grid squares in diameters, which indicates that the performed radius is close to 25 cm.

Similarly to previous experiments, flap joints have more difficulty in following the planned trajectories. However, the executed movements do present the features of the planned trajectories, even though the forces exerted on the legs influence greatly the angles of the joints (fig. 4.16).

Despite the discrepancies between generated and performed trajectories, the robot does perform the desired path with a heading orientation that approximates the desired one.

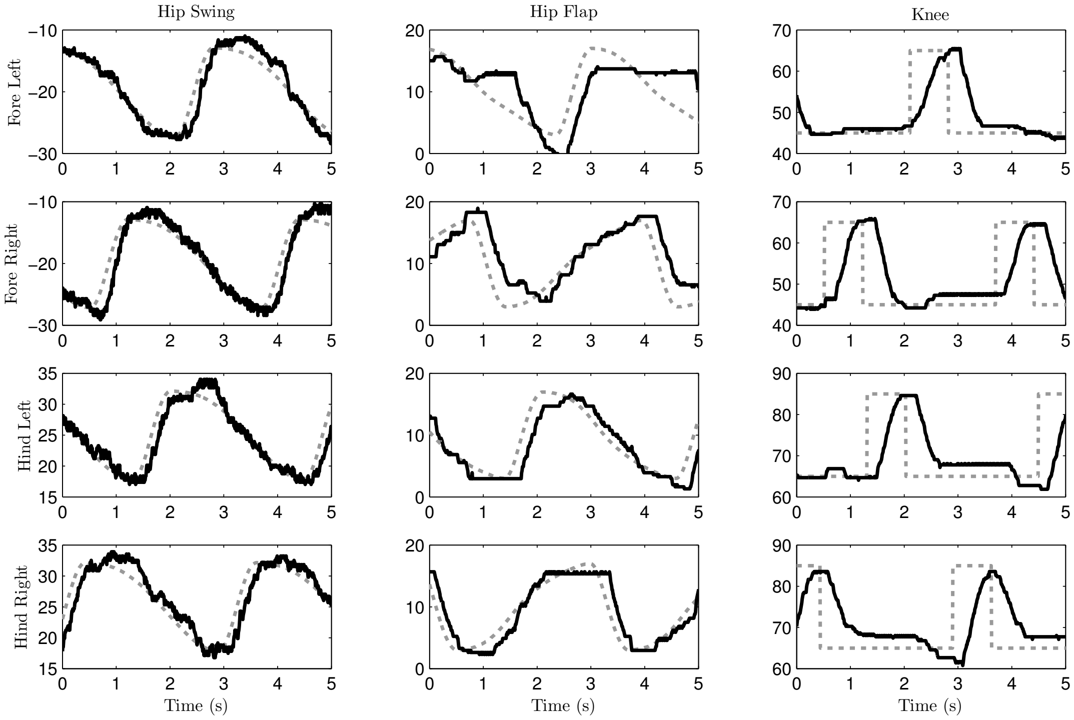

Figure 4.13: Planned trajectories (dashed) and actual performed movements (solid) for hip-swing, hip-flap and knee joints for the diagonal walk motion depicted in fig. 4.12. The robot generally performs the planned trajectories.

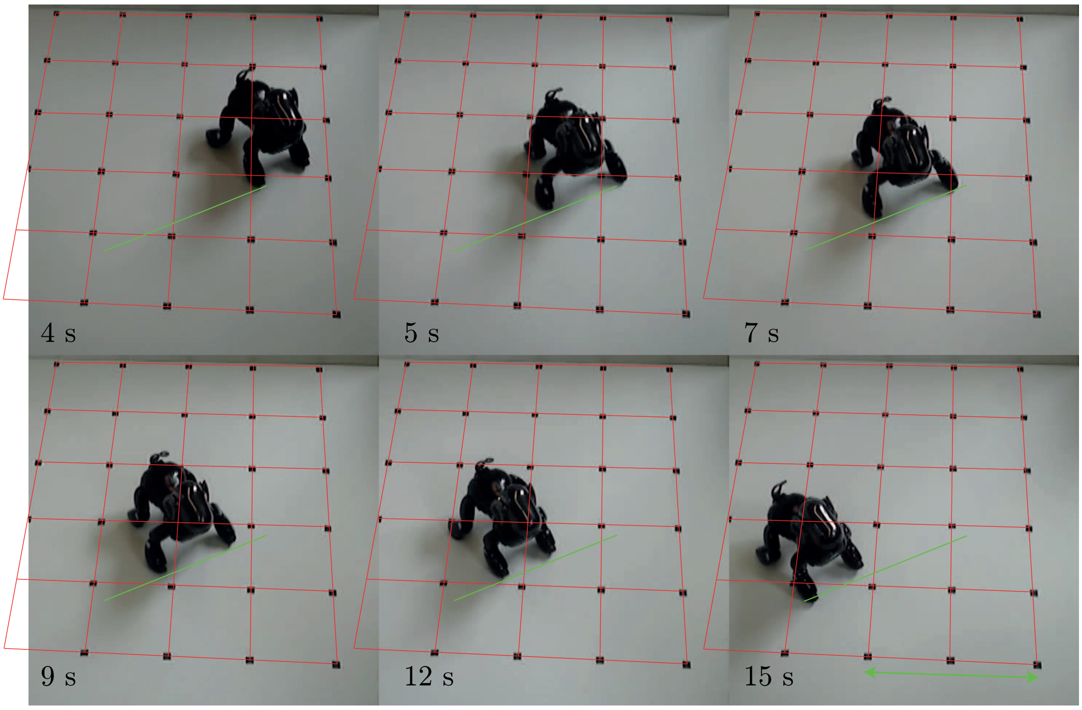

Figure 4.14: Snapshots depicting the robot trotting sideways to the right, with an reference velocity of 3.25 $\mathrm{cm.s}^{-1}$. A walking orientation of $\phi_\mathrm{w} = 90°$ was specified. The accomplished behavior is a lateral straight path, covering two grid squares in about 11 s, achieving an approximate velocity of $\approx 3.6\ \mathrm{m.s}^{-1}$.

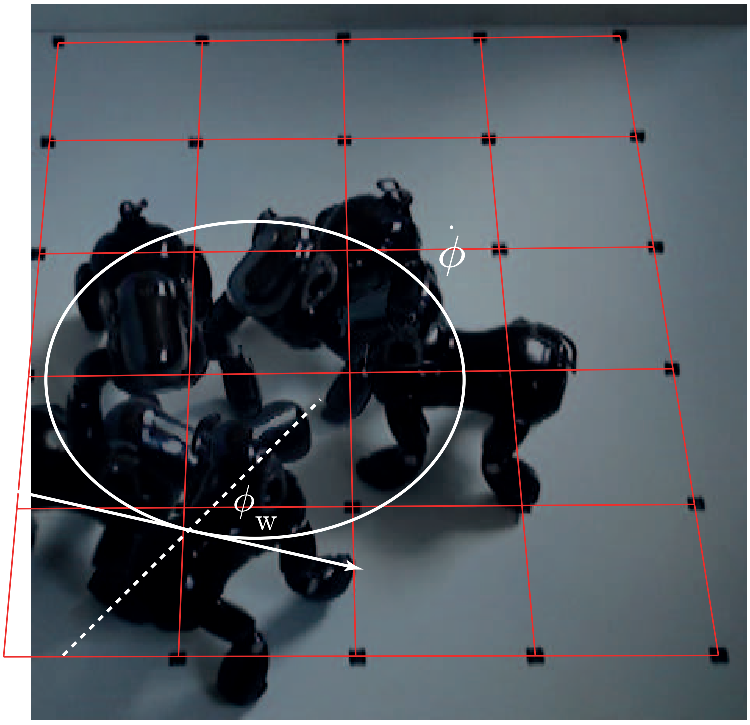

Figure 4.15: Image composition of four snapshots when the robot steers while heading to the center of the path, with $\dot{\phi} = 0.27$ rad.s^{-1} and $\phi_\mathrm{w} = -65°$. It walks diagonally to the right while steering right, in a path with a radius of ≈ 25 cm.

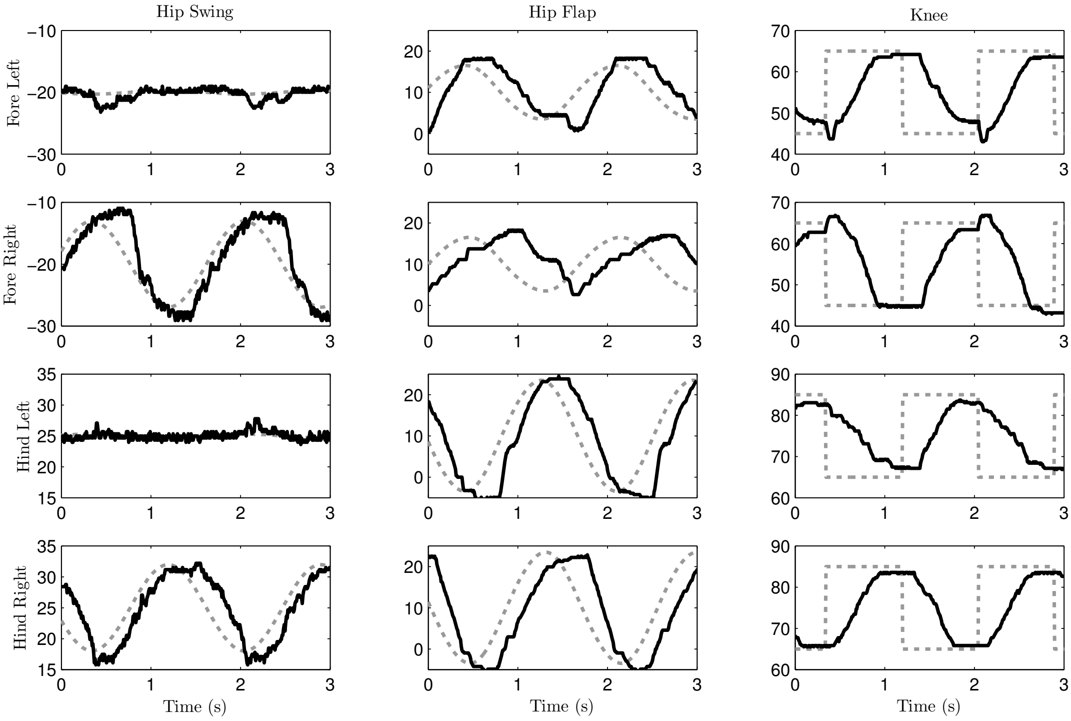

Figure 4.16: Planned trajectories (dashed) and actual performed movements (solid) for hip-swing, hip-flap and knee joints for the robot steering diagonally motion depicted in fig. 4.15. The joints do not correctly follow the planned trajectories.

4.3.5 Remarks on omnidirectional walking

These experiments have shown that by specifying m, the walking orientation ϕ_{w}, and the angular velocity $\dot{\phi}$, the CPG network produces the required leg movements in order for the robot perform omnidirectional locomotion. Results suggest that the procedure to calculate the movement's amplitudes and directions of each leg, despite being based on an approximate velocity value, can successfully be used to modulate the CPG parameters in terms of the desired translational speed, angular velocity and walking orientation.

As expected, the robot achieves successful omnidirectional locomotion and exhibits the desired general features, despite the model free and open-loop approach of the proposed CPG. However, the accomplished locomotion showed some inconsistencies in performance, exacerbated by the limitations of the approach and robotic platform. For instance, torque limits are not considered for the generation of the trajectories, which were reached in some experiments and resulted in the robot turning itself off.

The approach also does not produce the optimal trajectories for static walking, as in the walking gait, or for dynamic walking, such as in the trot gait. In many cases the simplified nature of the trajectories means that robot kinematics and dynamics are not considered for the maintenance of the static and dynamic stability. The maintenance of a stable walking is intrinsic to the parametrization of the CPGs, in terms of offsets, frequency and amplitudes.

In the walking gait, static stability is not always guaranteed, resulting sometimes in a foot that should be in the swinging phase touching the ground, or in a leg in stance phase not supporting the robot. In these cases the approach would benefit on a proper COM motion planning and more detailed trajectory planning based on kinematical specification of the robot. During the trot gait is also observed similar problems in guaranteeing a proper execution of the step phases and maintaining a dynamically stable walk.

In the next section, the capabilities of the proposed CPG approach are explored by addressing navigation in a cluttered environment.

4.4 Navigation application

If omnidirectional locomotion is expected to be useful in a behavioral context, a more complex form of sensory motor integration is required, for better adaptation to the environment. In this section, the ability of integrating the proposed CPG controller with a local navigation controller is tested. The robot is tested in a cluttered environment where it is expected to reach a target.

Visual information is acquired through a fixed camera mounted on the head of the robot. Target and obstacles are represented in a simulated world, by green and red colored, respectively. The location of the target and obstacles is continuously extracted from visual segmented information.

Steering is based on a dynamical system that determines the heading direction angle (steering angle), that enables the robot to circumnavigate obstacles and find their way to a target, while at all times the dynamical variable sits in a fixed point attractor. Extensive studies about this system can be found in other works [21, 183, 192].

The robot's angular velocity $\dot{\phi}$, one of the commands that specify the desired locomotion, is the output of another dynamical system based on the discrepancy of the robot's desired and current heading directions.

The desired tonic drive m is herein given by a very simple dynamical system, which assures that in the case of obstacle presence the robot's velocity is reduced as required.

The third and last command, the walking orientation (ϕ_w) is kept constant, with the robot always facing forward.

4.4.1 Heading direction dynamics

The robot's heading direction, ϕ_h, in angular space and in an allocentric coordinate frame, is controlled by a nonlinear vector field in which task constraints contribute independently. The task of reaching the target, $F_\mathrm{tar}(\phi_\mathrm{h})$, attracts ϕ_h towards the direction in which the target lies. The task of avoiding obstacles, $F_\mathrm{obs}(\phi_\mathrm{h})$, repels ϕ_h from the direction in which obstacles are perceived. These variables are depicted in fig. 4.17

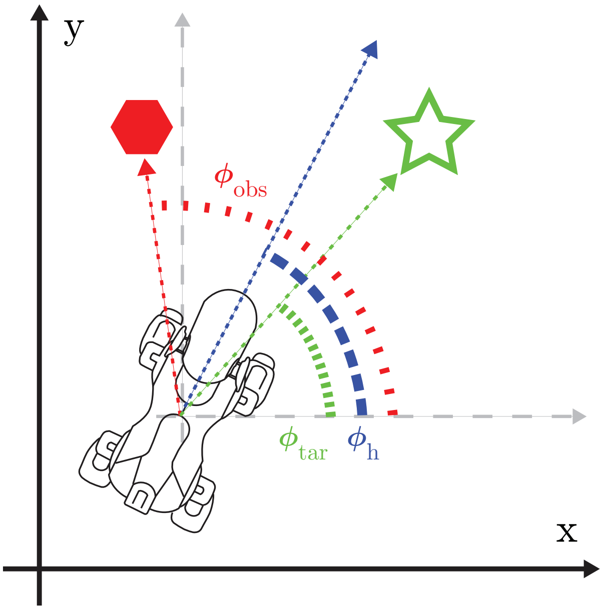

Figure 4.17: The angles ϕ_h, ϕ_tar and ϕ_obs are measured in the allocentric coordinate system (X, Y).

Integration of these tasks is achieved by adding each of them to the vector field that governs heading direction dynamics.

$$\dot{\phi}_\mathrm{h} = \quad F_\mathrm{obs}(\phi_\mathrm{h}) + F_\mathrm{tar}(\phi_\mathrm{h}) + F_\mathrm{stoch}. \tag{4.25}$$

A stochastic component, F_stoch, is added to ensure an escape from unstable states. For other examples and a full discussion see [21, 192].

Target reaching

The following dynamics are formulated for the task of target reaching

$$F_{\mathrm{tar}}(\phi_{\mathrm{h}}) \quad = \quad -\lambda_{\mathrm{tar}} \sin\left(\phi_{\mathrm{h}} - \phi_{\mathrm{tar}}\right). \tag{4.26}$$

This dynamical system erects an attractive force at the direction $\phi_{\mathrm{h}} = \phi_{\mathrm{tar}}$, specifying the position of an attractor in the heading direction dynamics.

The parameter λ_{tar} (> 0) controls speed of convergence of the target attractor in the heading direction dynamics.

Obstacle Avoidance

In order to avoid obstacles and make the robot steer away, a repulsive-force, $f_{\mathrm{obs},i}(\phi_{\mathrm{h}})$, centered at $\phi_{\mathrm{obs},i}$ is erected for each obstacle i detected, and summed up for the overall obstacle avoidance dynamics.

$$\begin{aligned} F_{\mathrm{obs}}(\phi_{\mathrm{h}}) \quad &= \quad \sum f_{\mathrm{obs},i}(\phi_{\mathrm{h}}) \\ &= \quad \sum \lambda_{\mathrm{obs},i} \left(\phi_{\mathrm{h}} - \phi_{\mathrm{obs},i}\right) e^{-\frac{\left(\phi_{\mathrm{h}} - \phi_{\mathrm{obs},i}\right)^2}{2\sigma_i^2}} \end{aligned} \tag{4.27}$$

Parameter $\lambda_{\mathrm{obs},i}$ controls the repulsive magnitude of each erected repulsive-force and decays exponentially with the distance between obstacles and the sensors.

Parameter σ_i defines the angular range over which each obstacle force exerts its repulsive effect.

Precedence of obstacle avoidance is accomplished making the strength of the obstacles contribution stronger than the target contribution.

Steering dynamics

The steering dynamics is given by:

$$\dot{\omega}_{\mathrm{h}} = -\alpha_{\mathrm{h}} \left(\omega_{\mathrm{h}} - \Delta_{\phi}\right) \left[1 + \left(\omega_{\mathrm{h}} - \Delta_{\phi}\right)^2\right], \tag{4.28}$$

that formulates a simple attractor ($\alpha_{\mathrm{h}} > 0$) at Δ_{ϕ}, specifying the robot's angular rate with the goal to steer towards the desired heading direction. $\Delta_{\phi} = \phi_{\mathrm{h}} - \phi_{\mathrm{r}}$, where ϕ_{h} is the reference heading as output from heading dynamics ϕ_{r} is the robot's actual heading direction.

The solution from the steering dynamics is assigned as reference to the angular velocity command: $\dot{\phi} = \omega_{\mathrm{h}}$

4.4.2 Velocity dynamics

The robot's gait, and its velocity, is controlled by the tonic drive command $m \in [0, 2.5]$, which is afterwards mapped onto the required limb-CPG parameters. The robot has to slow down when coming close to an obstacle, changing from the trot gait ($m = 2.5$), used when the path is clear, to a walk, or even crawl when it approaches an obstacle. The following dynamical system governs m:

$$\dot{m} = -\alpha_m \left(m - \left(\frac{2}{1 + \mathrm{e}^{-m_\mathrm{a}(\min(d_{\mathrm{c},i}) - m_\mathrm{c})}} \right) \right), \tag{4.29}$$

The fixed point is shifted depending on the current tonic drive and the distance to obstacles within a m_c range. By setting m_a and m_c parameters, the curve response for m is specified on the minimum distance over all the detected obstacles ($\min(d_{\mathrm{c},i})$). Parameter α_m sets the convergence of m to the solution.

4.4.3 Simulations

This section presents the simulation results in Webots, where the autonomous goal-direction locomotion is achieved with the presented navigation dynamical system.

Simulations in Webots are used to evaluate the architecture's ability to switch between motor behaviors, and are delineated such that the selection between the behaviors is triggered according to external stimuli. The robot walks in an environment towards a visually acquired target. During its path, obstacles may appear and force the robot to adjust its motion in order to successfully reach the target. The navigation system provides for the robot angular velocity and the required translational speed. These together with the robot walking direction, modulate the amplitudes of the flap and swing oscillators. The CPG parameters are modulated accordingly, and the joints' movements are generated such that the robot reaches the target, as required.

The built-in camera in the AIBO's head is used to online detect both obstacles and the goal. Since this work is focused on real-time visual control rather than scene understanding, image processing has been simplified by working with simple colors for the obstacles (red) and for the goal (green), balls with known dimensions, and in a structured environment, returning to the system the object distance and its angle to the robot. The target is always located higher, such that obstacles do not block its visibility.

Consider the experiment depicted in fig. 4.18, in which while the robot walks towards the target, two obstacles block its most direct route. Fig. 4.19 depicts the distance to obstacles (top) and the m tonic drive (bottom). ϕ_h, ϕ_tar, and two different ϕ_obs (top) and $\dot{\phi}$ (bottom) are shown in fig. 4.20.

Initially, at $t = 0$s, the robot is stopped ($m = 0$). It faces both the target and two obstacles. The tonic drive increases towards $m = 2.5$, to reach the nominal trot gait (fig. 4.19, left). As the robot approaches the obstacles ($d_\mathrm{c} < 1$m), it adjusts the gait in order to slow down and safely steer away (fig. 4.19, middle). The gait is only slightly adjusted, never reaching the walk gait ($m < 1$).

The robot walks towards the target, but steers away from the obstacle (snapshot at 12 s). Obstacles are to the right of the robot (grey dashed and dashed-dotted lines), so it steers left ($\dot{\phi} > 0$). However, while it steers away from the obstacles, it also steers away from the target (dotted black line) (fig. 4.20, left).

After clearing the obstacles, the robot steers back to the target's direction (fig. 4.20, middle). This situation can also be visualized at snapshots at $t = 18, 25$s in fig. 4.18.

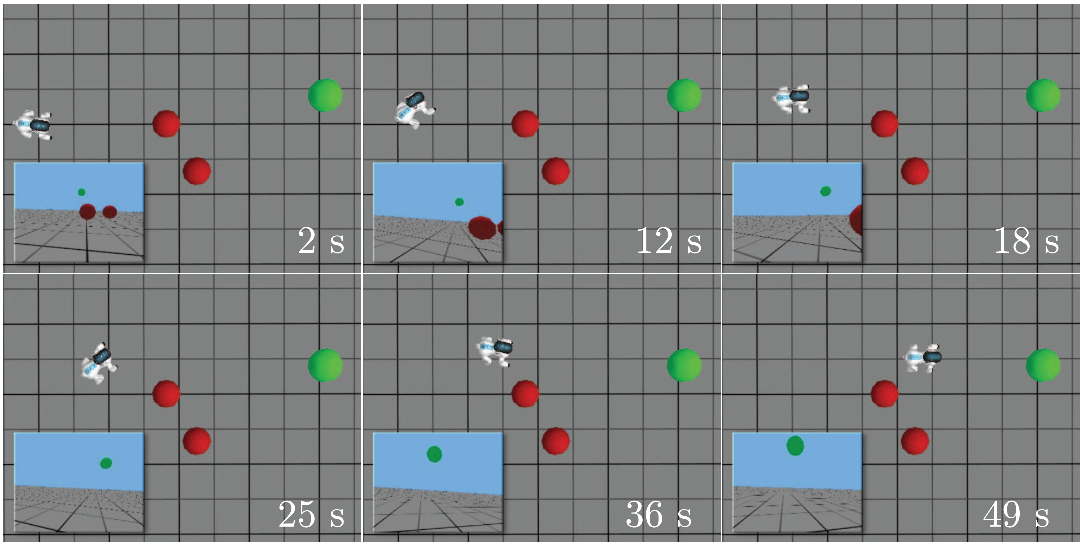

Figure 4.18: Six top-view relevant snapshots of the simulation. Time increases from left to right, top to bottom. The robot avoids the two red obstacles, and walks towards the green target. Snapshots of the camera view at those instances are presented at the left down corner of each snapshot.

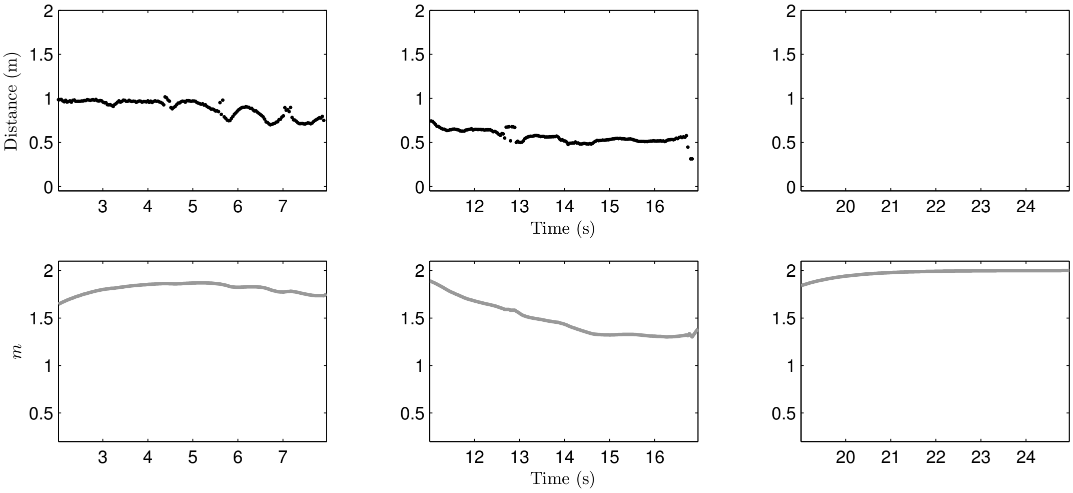

Figure 4.19: Distance to obstacles (top) and the m tonic drive (bottom) for the simulation depicted in fig. 4.18. Middle panels: As the robot approaches an obstacle, it adapts its gait to slow down the locomotion. Right panels: When no obstacle is detected, it walks with its nominal trot gait.

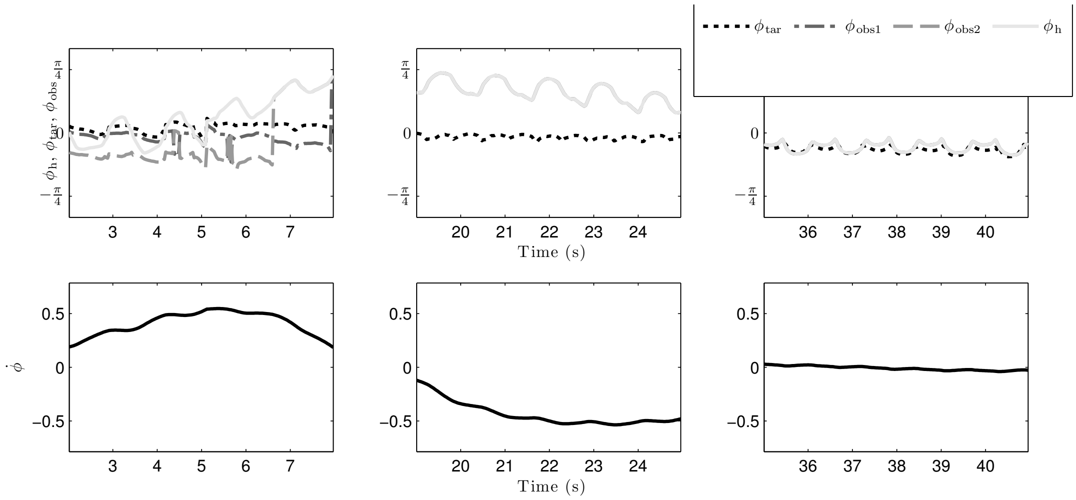

Figure 4.20: ϕ_{h}, ϕ_{tar}, and two different ϕ_{obs} (top) and $\dot{\phi}$ (bottom) variables for several intervals of time along the simulation depicted in fig. 4.18. Left panels: The robot steers left ($\dot{\phi} > 0$) to avoid the obstacles on its right. Middle panels: After clearing the obstacles, it steers back to the target. Right panes: When facing the target, it walks straight forward ($\dot{\phi} > 0$).

In the final moments of the simulation, $t \approx 49$s, there are no more obstacles, and the robot walks with $\dot{\phi} = 0$ (fig. 4.20, right) towards the target. The tonic drive is increased towards 2.5, performing the trot gait (fig. 4.19, right). Finally, at $t \approx 60$s, the robot reaches the target.

When the robot steers to the left ($\dot{\phi} > 0$) the amplitudes of hip-swing on the left side decrease, while on right side increase, and the hip-flaps start to move (fig. 4.21, left). All these coordinated movements of swing and flap joints steer the robot left.

When steering right ($\dot{\phi} > 0$), the robot increases the left hip-swing amplitudes, while the flap joints invert their step direction (fig. 4.21, middle).

After facing the target, the robot walks forward. Hip-swing movements have the same amplitudes on both sides, and the hip-flap joints stop their movement (fig. 4.21, right).

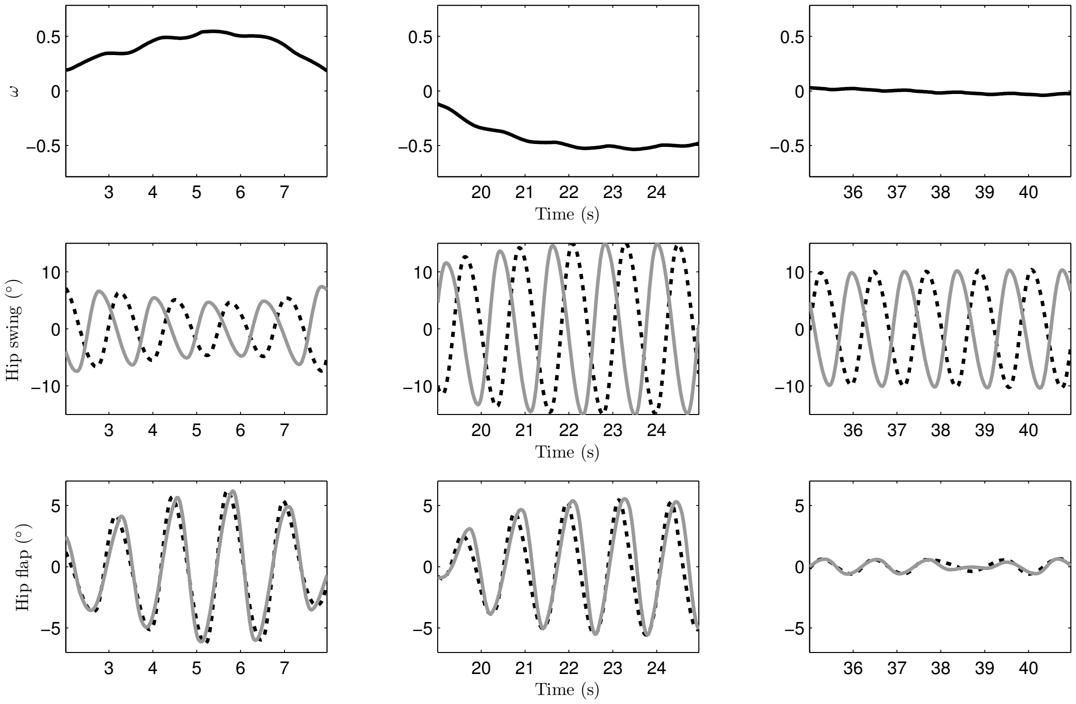

Figure 4.21: $\dot{\phi}$ (top) and trajectories of the hip-swing (middle) and flap joints (bottom) of the fore left (dotted grey) and hind left (solid grey) legs for several intervals of time along the simulation depicted in fig. 4.18. Left swing movements decrease when steering left ($\dot{\phi} > 0$), and increase when steering right ($\dot{\phi} < 0$). Flap rhythmic movements are performed when steering, with opposite step directions for steering left and right.

4.4.4 Remarks on quadruped navigation

This section demonstrated that the proposed CPG approach and architecture is able to achieve purposeful, goal-directed locomotion. A simple navigation task is accomplished by applying a local navigation controller based on the dynamical systems approach.

Results from this simplified navigation task shows the ability of the system to modulate in real-time the walking motions and to switch between locomotor behaviors, as deemed necessary by external behavioral context. The division in levels of abstraction in the control problem allows applying a local navigation controller which only deals with the problem of producing the high-level commands which specify the walking velocity and angular rate, and the low-level which continuously modulates the motion's amplitudes and the quadruped gait.

The important problem of selecting the best omnidirectional movement is not considered in this example. For instance, in order to walk diagonally the robot could either walk diagonally or instead rotate in spot and then walk forward in the desired direction. To fully exploit the capabilities of the system to produce omnidirectional locomotion, a more complex mechanism for action selection and navigation would have to be employed.

4.5 Entrainment of pendular effects

This section expands the previous quadruped locomotion controller, pursuing and exploring further contributions in the feedback process, ubiquitous for short and long-term adaptation of any kind of legged locomotion.

CPG systems can be designed starting from different conceptual approaches. They can be designed firstly from the CPG model as a feedforward generator, and only then the effect of feedback signals is included and the loop is closed; endorsing what kind of information should be considered and how will affect the final behavior [64, 174]. Or can be designed from the beginning with the closed-loop goal in mind, using feedback signals to tightly generate trajectories [29, 105, 135].

Systems of coupled oscillators are widely used for modeling CPGs, and while there exists extensive work and methods for analyzing these dynamical systems, less work has been carried out on methods and frameworks for synthesizing oscillators that have to exhibit a specific desired behavior. For instance, Buchli [31] presents a framework for characterizing and designing oscillators, as well as defining desired perturbations in order to achieve frequency-locking, phase-locking of any specific output signal shape.

Step phase feedback plays an important role in locomotion, allowing the adaptation of the onset of the swing and stance phases [158]. These were explored in legged robots, whether through phase resetting [9] or phase transitions depending on load/unloading of the legs [135, 174]

This section explores a different approach for phase feedback. A phase feedback inspired in the work of Morimoto [88] and Fukuoka [64] is devised, aiming to entrain the CPG oscillators with the phase of the robot's periodic motions. Here the effects of the addition of feedback on the rhythmogenic ability of the CPGs is discussed, and is proposed a methodology to explore the possibilities of physical entrainment with the system.

The proposed feedback couples the CPG system to the pendulum rolling motion of the projected Center of Gravity (pCOG). Robot's sensory information regarding body angle, joint position and foot touch sensors are used to calculate pCOG, which modulates the frequency of the leg oscillator through the feedback mechanism. The goal of this feedback is to avoid the swinging of a leg before the robot pCOG is transferred to the opposite support polygon, and this is achieved by synchronizing the oscillator's phase with the performed step phase.

The inclusion of feedback is expected to improve robot performance, herein measured by the Support Stability Margin (SSM), an adequate measure for a static stable walk. Besides, the proposed feedback should not affect the required duty factor and phase relationships of the nominal crawl gait.

Simulations are conducted with the model of an AIBO quadruped robot, and the robot's performance is studied, regarding velocity, SSM and the correct execution of the step phases. The influence of integrating this phase feedback along with the coupling network of CPGs is also explored.

4.5.1 Revisiting the locomotor system

The general locomotor system presented in section 4.2 is able to generate the complete leg motions for producing omnidirectional walking behaviors. However here, a simplified version of the controller is applied, as only forward locomotion is addressed with the inclusion of the proposed feedback.

The hip flap unit-CPGs are not employed, and therefore hip flaps are not actuated and kept fixed throughout all the tests. The knee is controlled using the simple flexion/extension mechanism as described in section 4.2.1. For simplicity, joint specification through notation j has been dropped, as only the hip swing unit-CPGs are employed.

The goal is to achieve a walk gait, by achieving a 0.75 duty factor and a 0.75 gait phase. Phase relationships for the walk gait are presented in table 4.3, note that $\phi_i^o = -\phi_o^i$. Coupling strength constant $\kappa_{j,i}$ from section 4.2.1 is here referred to k_{osc}. All the hip swing unit-CPGs are coupled with the same coupling strength specified by the value of k_{osc}.

Table 4.3: Phase relationships for the walk gait.

i	FL	FL	FL	FR	FR	HL
o	FR	HL	HR	HL	HR	HR
ϕ_i^o	$-\pi$	$-\frac{3\pi}{2}$	$-\frac{\pi}{2}$	$-\frac{\pi}{2}$	$\frac{\pi}{2}$	π

4.5.2 Robot phase coupling

The goal of using phase coupling in this CPG approach is to synchronize the phases of the CPG network to the dynamics' phase of the robot. The act of walking exhibits periodic motions, from which the phase of the robot's locomotion is extracted (robot phase). The periodic motion of the projected Center of Gravity (pCOG) is used to calculate the robot's phase, considering the body angle, joint positions and touch sensors. The proposed coupling tries to synchronize the generated swing phase of the

CPGs with the measured point in the step cycle in which the robot has its pCOG over the contralateral support polygon during the walk gait (fig. 4.22).

If this phase coupling is achieved correctly, the swing phase of each leg will be performed when the pCOG is over the contralateral support side, ensuring that the weight is not over the swinging leg, and thus the robot does not fall over it. This feedback mechanism by coordinating the swing phases with the correct support polygon presents the potential of improving the walk, by increasing the stability, forcing the pCOG to be over the side with most legs supporting the body. This improvement on stability is especially desired when the body COM goes from one side to the other, cases A to B, and C to D in fig. 4.22. Otherwise the normal tendency is to the COM make the robot fall over the swing leg.

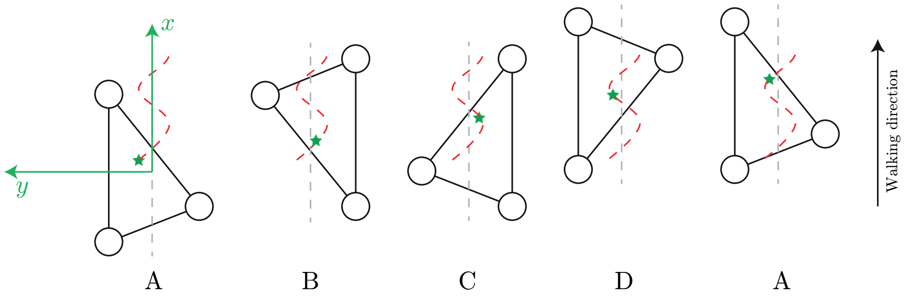

Figure 4.22: Depiction of oscillatory movement exhibited by the projected Center of Gravity during the walk gait (dashed trajectories). The pCOG (denoted by the star) moves between the contralateral triangular support polygons. Open circles denote feet ground contact.

To achieve this kind of entrainment between the oscillators and the robot dynamics, general guidelines from [31] are followed. The desired perturbation effect on the oscillator's phase is specified using its polar representation and transformed back to its cartesian representation.

Coupling mechanism

Consider the oscillator from eqs. (4.1),(4.2) in polar coordinates:

$$\dot{\phi}_i = \omega_i \tag{4.30}$$

$$\dot{r}_i = \alpha\left(\mu - r_i^2\right) r_i . \tag{4.31}$$

Consider the movement of pCOG in the frontal plane due to the robot's rolling motion as a simple oscillatory motion with its phase described by $\phi_{\mathrm{r}} = \arctan 2\left(\dot{\mathrm{pCOG}}_y, \mathrm{pCOG}_y\right)$. The robot's phase ($\phi_{\mathrm{r}}$) is coupled with the oscillator's phase (ϕ_i) with a desired phase difference of ϕ_{r}^i and coupling constant k_{r}, as follows:

$$\dot{\phi}_i = \omega_i + k_{\mathrm{r}} \sin\left(\phi_{\mathrm{r}} - \phi_i - \phi_{\mathrm{r}}^i\right) , \tag{4.32}$$

$$\dot{r}_i = \alpha\left(\mu - r_i^2\right) r_i . \tag{4.33}$$

In cartesian coordinates this phase coupling becomes:

$$\dot{x}_i = \alpha \left(\mu - r_i^2\right) (x_i - O_i) - z_i \overline{\omega}_i, \tag{4.34}$$

$$\dot{z}_i = \alpha \left(\mu - r_i^2\right) z_i - (x_i - O_i) \overline{\omega}_i, \tag{4.35}$$

$$\overline{\omega}_i = \omega_i + \frac{k_\mathrm{r}}{r_i} \left[x_i \sin\left(\phi_\mathrm{r} + \phi_\mathrm{r}^i\right) - z_i \cos\left(\phi_\mathrm{r} + \phi_\mathrm{r}^i\right)\right]. \tag{4.36}$$

Phase relationships

The desired phase differences are chosen to respect the following observations and assumptions (fig. 4.23):

a) When the robot leans left with its pCOG over the left support polygons, its obtained $\phi_\mathrm{r} = 0$, and the right legs should perform the swing phase, $-\pi < \phi_i < 0$;

b) When the robot leans right and the pCOG is on the right side, $\phi_\mathrm{r} = \pi$, the left legs should swing while the right legs perform the stance phase, $-\pi < \phi_i < 0$; and

c) The CPGs' oscillators should reflect the phase relationship and the sequence of the walk gait and exhibit a relative phase difference of $\frac{\pi}{2}$ among them.

Table 4.4: Robot phase relationships with the four limb-CPGs.

i	FL	FR	HL	HR
ϕ_i^r	$\frac{\pi}{4}$	$\frac{-3\pi}{4}$	$\frac{3\pi}{4}$	$\frac{-\pi}{4}$

Phase relationships are presented in table 4.4, and represented visually on fig. 4.23. Fig. 4.23 is a general representation of the limit cycles of the four coupled limb-CPGs (blue and red dots), and of the pCOG oscillation on the frontal plane. It depicts how the phase relationship between the phase ϕ_r and the four unit-CPGs should be maintained throughout the rhythmic motion. It shows which unit-CPGs should be performing the swing or stance phase, while pCOG moves between left and right positions.

4.5.3 Simulations

A series of simulations were performed in a simulated flat environment with the model of Sony AIBO quadruped robot in Webots.

First the coupling of interlimb coordination and robot phase is studied, by changing the values of the coupling weights $k_\mathrm{osc}, k_\mathrm{r}$. A systematic parameter exploration is performed on the parameter tuple $\langle k_\mathrm{osc}, k_\mathrm{r}\rangle$ in the range $[0, 9.5]$, in steps of 0.5. On each run the robot walks with a desired nominal gait, a statically stable walk gait ($\beta = 0.75$) for 10 s from where all the information on the robot's performance is recorded. Then the obtained average Support Stability Margin (SSM) and the achieved velocities are compared, followed by a discussion of the obtained results.

SSM is the smallest distance of the pCOG to the edge of the polygon defined by the supporting feet projection onto the plane with the gravitational acceleration as its normal. SSM is an indicator that tells

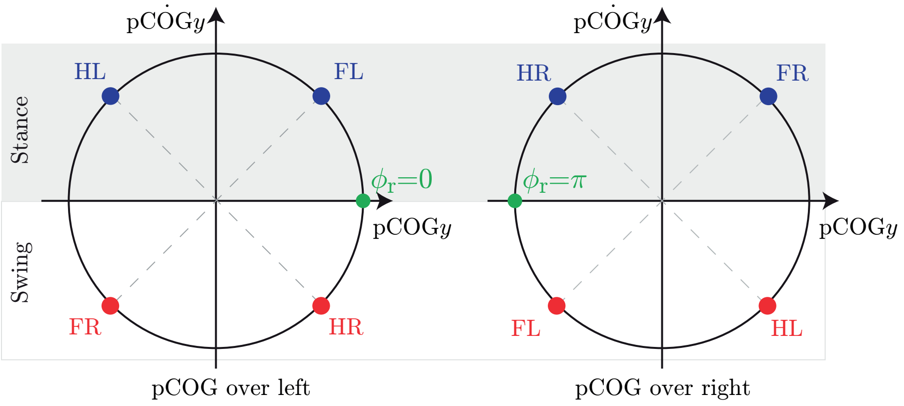
$\mathrm{p}\dot{\mathrm{C}}\mathrm{OG}y$
HL
FL
Stance
Swing
$\phi_{\mathrm{r}}=0$
$\mathrm{pCOG}y$
FR
HR
pCOG over left
$\mathrm{p}\dot{\mathrm{C}}\mathrm{OG}y$
HR
FR
$\phi_{\mathrm{r}}=\pi$
$\mathrm{pCOG}y$
FL
HL
pCOG over right

Figure 4.23: Limit cycle of the pCOG oscillation on the frontal plane (pCOG_y). When the pCOG is on the left side ($\mathrm{pCOG}_y > 0$) the robot's phase is $\phi_{\mathrm{r}} = 0$, and $\phi_{\mathrm{r}} = \pi$ when is on the right side $\mathrm{pCOG}_y < 0$. Each CPG performs the swing phase when $-\pi < \phi_i < 0$.

if the pCOG is inside the support polygon at all times, when considering statically stable gaits, like a walking gait. The greater the SSM value, the most centered is the pCOG on the support polygon, and the most stable is the robot. The placement of pCOG outside the support polygon is translated as a negative distance to the closest edge of the support polygon.

A set of $\langle k_{\mathrm{osc}}, k_{\mathrm{r}} \rangle$ values are chosen so that it results in the best walk in terms of trade-off between the average SSM and the achieved velocity, to compare and quantify the improvement of the walk without and with robot phase coupling. The robot's performance is analyzed regarding velocity, SSM and is used to discuss improvements over the execution of the step phases.

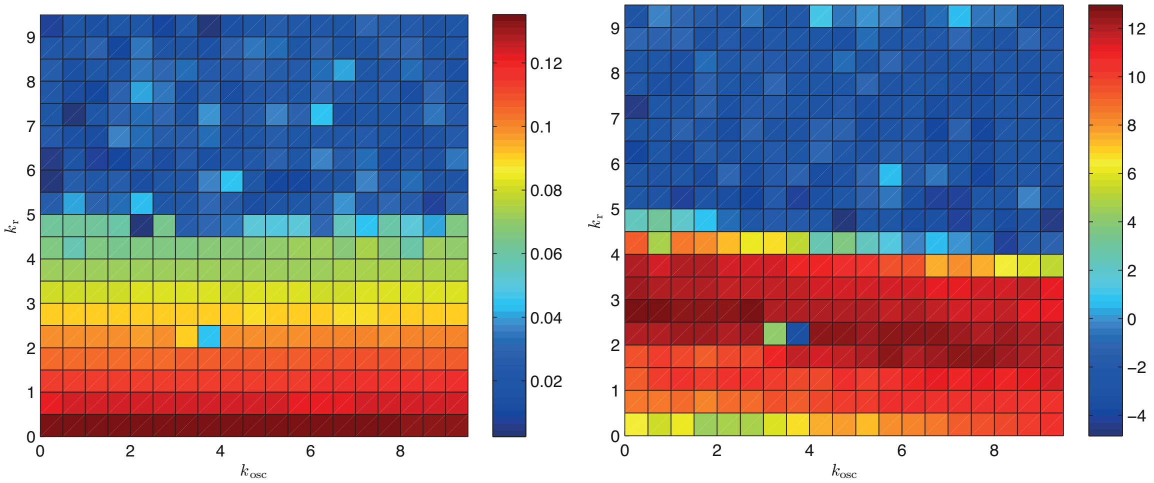

(a) Velocity achieved on each run.

(b) Mean support stability margin (SSM) on each run.

Figure 4.24: $k_{\mathrm{osc}}, k_{\mathrm{r}}$ parameter exploration, and its effects on velocity ($\mathrm{m.s}^{-1}$) and support stability margin (SSM). Velocity and SSM are mostly influenced by the value of k_{r}.

Parameter exploration

Interlimb coupling, k_{osc}, and robot phase coupling, k_{r} influence the walk in different ways. While interlimb coupling simply coordinates the phase relationships between the CPGs, robot phase coupling tries to coordinate the phase of each CPG to the phase of the robot motions.

From fig. 4.24(a) it is possible to observe that the achieved velocity does not change when the strength of interlimb coupling k_{osc} is increased or decreased. However, when changing the strength of phase coupling, k_{r}, the achieved velocity is influenced, decreasing when the coupling increases. This is a possible indicator that the oscillators are being adapted to respect the current step phase of the walk, being slowed down to match the robot dynamics. For $k_{\mathrm{r}} > 4.5$ the velocity decreases greatly, suggesting that beyond this point the influence and strength of this phase coupling is no longer adequate and tries to stop the robot.

Similarly, SSM shows no major variation for a changing interlimb coupling strength, k_{osc} (fig. 4.24(b)). The major determinant of the achieved SSM is the phase coupling strength, k_{r}. There is a range of k_{r} where the SSM shows higher values, $[1; 3.5]$. It suggests that the CPGs are being coordinated according to the robot dynamics, correcting the execution of the step phases. However, above 3.5 the SSM decreases to low values, similarly to the velocity.

The velocity achieved without phase coupling was $0.134\ \mathrm{m.s}^{-1}$ ($k_{\mathrm{osc}} = 1, k_{\mathrm{r}} = 0$) and the obtained SSM was $6.14\ \ \mathrm{mm}$. The highest obtained SSM was $12.97\ \mathrm{mm}$, when using $k_{\mathrm{osc}} = 2.5, k_{\mathrm{r}} = 2.5$, with achieved velocity $0.098\ \mathrm{m.s}^{-1}$. This result can be considered to be a fair trade-off between the achieved SSM and velocity for a walk gait.

Locomotion comparison

With phase coupling ($k_{\mathrm{osc}} = 2.5, k_{\mathrm{r}} = 2.5$) it is expected that the left legs' swing phases are performed when the pCOG is over to the right side of the support polygon. It is possible to verify this is true in fig. 4.25 (right) since the swing phase of both left legs (ascending trajectories) are performed when $\mathrm{pCOG}_y < 0$. These results show that the proposed phase coupling synchronizes the swing step phase of ipsilateral legs to the respective step phase of the cycle. The nominal step period is 0.8 s, specified from a swing period of 0.2 s and a duty factor of 0.75. When phase coupling is employed, the interaction of the CPGs with the robot's phase changes slightly the achieved average step period, from 0.8 s to 1.2 s, while maintaining the chosen duty factor, adapting the swing period to 0.3 s. This adaptation did not change the relative phases among the CPGs, maintaining the desired interlimb coordination of the nominal walk gait.

Fig. 4.26 shows the achieved SSM over the two runs. The dotted (solid) lines show the achieved SSM without (with) phase coupling. Positive values denote that the pCOG lies inside the support polygon, while negative values denote a position outside the support polygon, with a distance to the nearest edge correspondent to the absolute value.

In fig. 4.26 it is verifiable that the performed SSM increases when phase coupling is employed. Negative values of SSM indicate the robot may fall over the swinging leg. The moments of the step

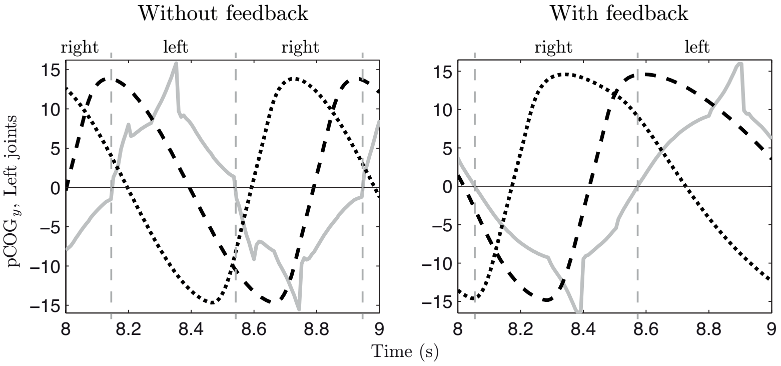

Figure 4.25: pCOG position in the frontal plane (grey) and left hip joints' trajectories (dashed:fore and dotted:hind). Swing phases correspond to the ascending parts of the trajectories. Without phase coupling the hind leg (dotted yellow) swing onset happens while the pCOG is in the ipsilateral side (left panel), meaning $\mathrm{pCOG}_y > 0$. With phase coupling (right panel) the swing phases on both left legs happen when the pCOG is in the contralateral side, $\mathrm{pCOG}_y < 0$.

where pCOG falls outside the support polygon (negative values) are reduced from 66% of the step phase without feedback (dotted), to 29% of step phase when feedback is employed (solid). The average value of SSM also increases due to the maintenance of the pCOG inside the support polygon.

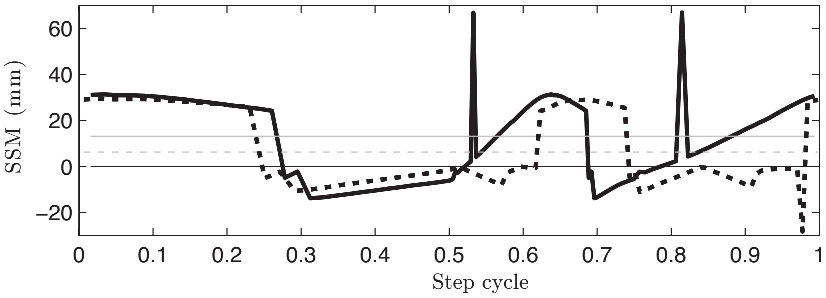

Figure 4.26: SMM without (dotted) and with (solid) robot phase coupling during a step cycle. The average SSM is 6.14 mm without phase coupling (dotted grey) and 12.97 mm with phase coupling (solid grey). Using phase coupling, increases the chance of brief four feet support (solid black).

The walk gait sequences from the two simulations are shown in fig. 4.27. Without phase coupling (top) the pCOG is generally closer to the edge of the support polygon than with phase coupling (bottom). pCOG also is in the same side in the onset of some swing phases when phase coupling is not employed, at 9.10 s and 9.50 s, which was solved when phase coupling is employed (bottom, at 9.10 s and 9.60 s). The concerning point of contralateral swing onset was dealt with by the proposed feedback mechanism and the result was to achieve brief four feet support between these contralateral phases (bottom, at 9.00 s and 9.50 s).

The differences between the nominal generated trajectories ($k_{\mathrm{osc}} = 1, k_{\mathrm{r}} = 0$, dotted lines) and the trajectories obtained when applying the phase feedback ($k_{\mathrm{osc}} = 2.5, k_{\mathrm{r}} = 2.5$, solid lines) are presented in fig. 4.28. The nominal step period is extended from 0.8 s to 1.2 s and the produced trajectories of the

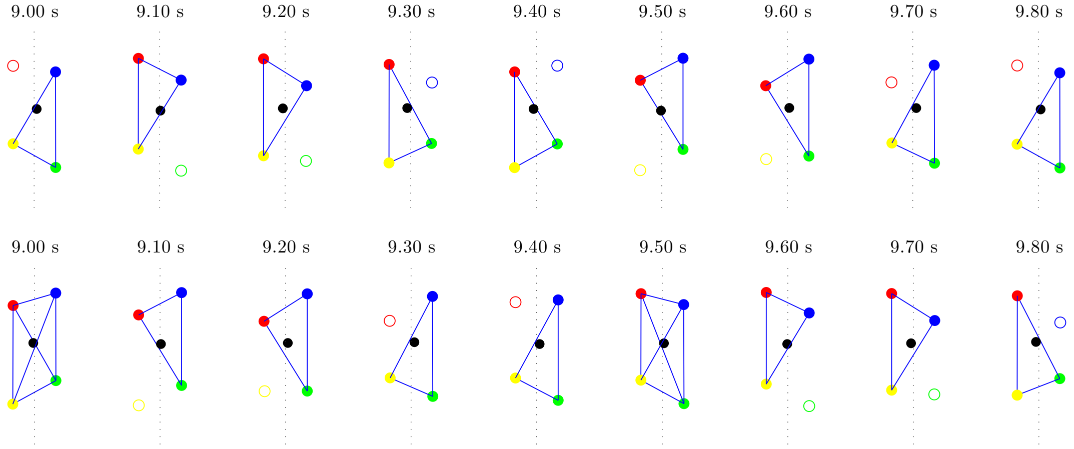

Figure 4.27: Performed gait sequence of the walk gait without (top) and with (bottom) phase coupling. Black dot is the position of the projected Center of Mass. Colored filled dots represent stance trajectories and empty dots swing trajectories. (red:left fore, blue: right fore, yellow:left hind, green: right hind) In this figure, the reference frame is centered on the robot.

fore legs present a slight shape change in the stance phase.

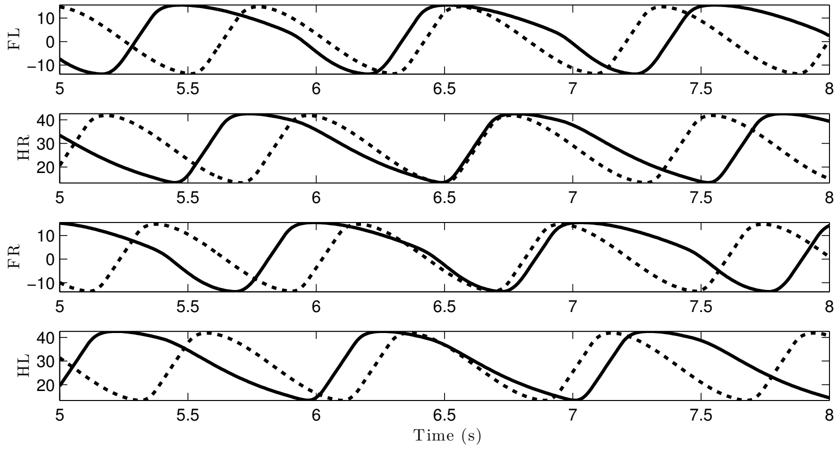

Figure 4.28: Generated trajectories from a nominal walk without phase feedback (dotted), and adjusted trajectories by the phase feedback (solid). It is observable the extension of the step period from 0.8 s to 1.2 s, and a slight shape change in the stance phase.

Results also show that unwanted touching during the swing, and lifting during stance has been slightly reduced in most cases (fig. 4.29). Front feet touching the ground incorrectly during the swing phase decreased from 12.60% to 11.90% of the swing phase period and from 1.30% to 0.07% on the hind feet (fig. 4.29(a)). The unwanted lifting of the feet occurring during stance phase decreased in the fore legs from 23.40% to 5.09% of the stance period, but increased for the hind legs, from 25% to 29% of the stance period (fig. 4.29(b)).

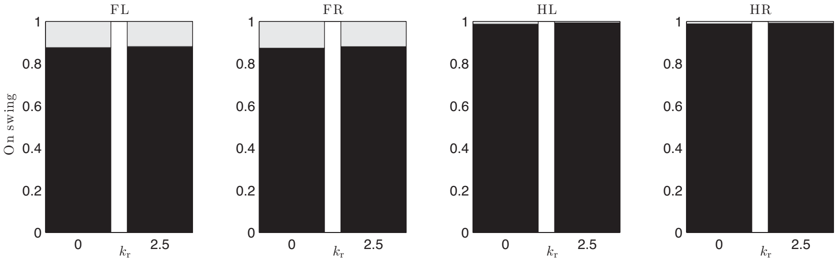

(a) Percentage of time the foot is on the air (black) and when is touching the ground (white) during the swing phase.

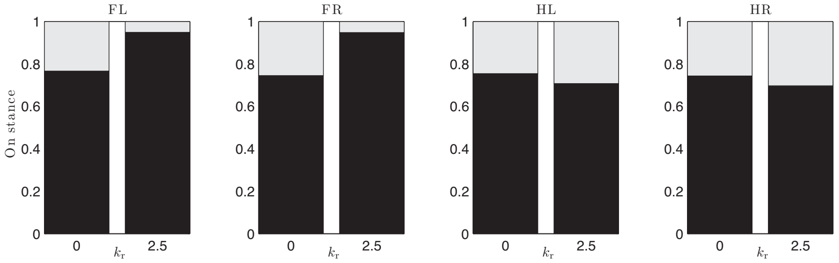

(b) Percentage of time the foot is on the ground (black) and when not on the ground (white) during the stance phase.

Figure 4.29: Average percentage of time of the swing and stance phases, on which unwanted touching and lifting occurs, respectively. Touching during swing decreased on the swing legs from 12.60% to 11.90%, and on the hind legs from 1.30% to 0.07%. Lifting on the stance phase decreased on the fore legs from 23.40% to 5.09%, but increased on the hind from 25% to 29%.

4.5.4 Remarks on entrainment of pendular effects

The feedback mechanism presented in this section investigates a simple phase coupling mechanism by exploring the properties of the oscillators used to model the CPGs, introducing a phase coupling term as given by the periodic motion of the projected COG. It is hypothesized that the inclusion of this coupling term could improve the stability of the walk gait and avoids the lifting of a foot which should be executing the stance phase.

Results from the simulations indicate an improvement of the stability on the walk gait, as measured by the SSM, maintaining the desired general features of the crawl gait such as duty factor and interlimb phase relationships. Simulations also demonstrated that the initial aim of the feedback is achieved in the forelegs, but not in the hindlegs. The inclusion of the phase feedback reduces the lifting of the fore feet during stance, but on the other hand increases slightly the lifting of the hind feet during stance. It also marginally reduces unwanted foot contact with the ground during the swing phase in the fore legs.

The application potential of the feedback seems however quite limited. It focuses mainly in the stability of the walk gait, as measured by the SSM, and it applies only on flat terrain. Further work could also investigate the integration with other kinds of feedback within the same framework, such as phase transition [174] and postural control [200], as well as on other legged robots, including robots with compliant actuators.

4.6 Standing postural control

Postural stability is one important requirement if the goal is achieving autonomous adaptive locomotion on irregular terrains. A robot should be able to maintain its orientation in respect to gravity, keep its equilibrium and adapt the body segments to the ongoing movement.

This chapter addresses postural control in quiet standing, considering it a first step for the design of a postural controller for locomotion. The CPG system proposed in section 4.2 is used to generate basic rhythmic motor patterns for locomotion, which assumes that complex movement is generated from the combination of discrete and rhythmic motions, modeled as dynamic systems. The independent nature of the rhythmic and discrete motor generation of the controller is the property which allows for the application of the presented approach and which is very interesting to be explored. While standing, the rhythmic movements are turned off, and the proposed postural system specifies discrete motions for the hip and knee joints [36, 44].

The system is validated through a few experiments in an AIBO ERS-7 robot. The robot is subjected to different posture perturbations ranging from roll and pitch variations to loss of feet support, reacting promptly and smoothly in a way to recover postural control.

4.6.1 Postural control

Neurobiological research has brought interesting concepts into the field of robotics, as the presented concept CPG that is used in legged robot locomotion. Researchers are also interested on how body posture during standing and walking is maintained, a ubiquitous and vital motor function, as most terrestrial, aquatic and flying animals maintain a defined global orientation in relation to the gravity force.

Mammal posture maintenance can be distinguished in two modes of control [49]. A feedback mode employs feedback loops to respond to perturbations of orientation and produces the postural actions to counteract the perturbations and bring the posture back to an equilibrium. The other is a feedforward mode, which entails the anticipatory postural changes in advance to expected external perturbations or voluntary destabilizing movements.

The motor responses of the legs are coordinated resulting in a final posture task, possibly from processed and integrated characteristics of the body posture, like the Center of Mass, body geometry and limb axes, or even orientation of the body [124, 129]. However under certain conditions, it seems that the postural system is divided in fore and hind mechanisms, controlling the stability of the anterior and posterior parts of the body independently, receiving information from the leg's mechanoreceptors [48, 49].

The postural system is suggested to be divided in two feedback loops, spreading between spinal and supraspinal levels (fig. 4.30). Mechanisms residing in the spinal cord are majorly driven by leg mechanoreceptors and contribute by generating corrective responses. These may be activated and modulated by higher structures, involving supraspinal centers that receive information from both girdles, and vestibular and visual information, outputting descending corrective commands. An interaction of fore and hind controllers seems to exist through supraspinal levels, to accurately coordinate the efforts of the individual legs [48, 50].

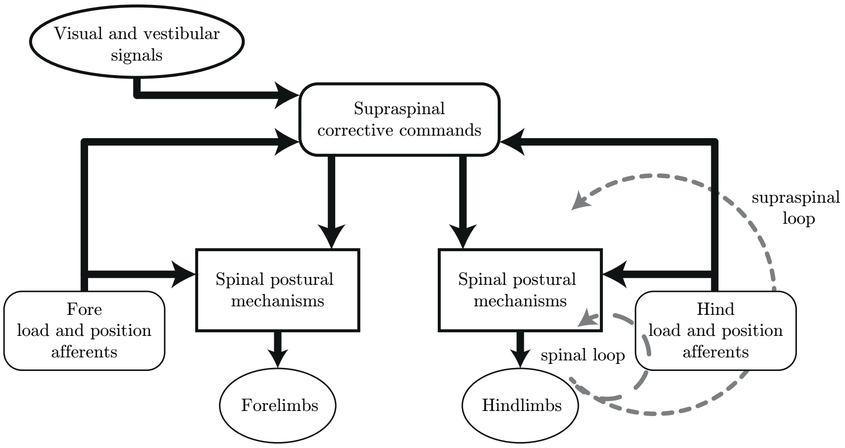
Visual and vestibular signals
Supraspinal corrective commands
supraspinal loop
Spinal postural mechanisms
Spinal postural mechanisms
Fore load and position afferents
Hind load and position afferents
spinal loop
Forelimbs
Hindlimbs

Figure 4.30: Representation of the feedback mode for posture control. Postural actions counteract through a two feedback loops. The spinal feedback loop receives input from leg mechanoreceptors and activation and modulation from supraspinal regions. Figure adapted from [49].

The proposed work concerns the feedback mode of postural system, loosely based on the concepts from studies on mammal's postural system. It shares the idea on the existence of postural mechanisms that respond to perturbations in body orientation supervised through different sensory modalities, closely interacting with the locomotor system and generating the movements for postural corrections. Herein is hypothesized that:

- The resulting leg corrective action is the overall output of parallel responses related to different sensory information modalities.
- Each response may be directly influenced by:
    1. Low level direct sensory signals, e.g. foot ground contact, joint position
    2. Processed regulated variables, e.g. center of mass

Thus, the integration of the parallel responses produces the final correct posture, and acts as the integration of somatosensory signals. Some of the responses that compose a leg controller have been designed based on existing reflexes observable in animals (e.g. tilt compensation), and others in requirements from a robotics point of view. Also, some responses are coordinated among the four legs, allowing joined efforts when corrective movements of full amplitude from one leg are required. Each of these responses will be detailed in the following sections.

4.6.2 Revisiting the CPG model

As presented in section 4.2, a network of four coordinated CPGs is responsible for generating the basic locomotor motions. All CPGs are composed by three unit-CPGs, controlling the hip-swing, hip-flap and knee joints, modeled using the oscillator in eqs. (4.1,4.2). In order to uniquely address the standing postural problem, the rhythmic activity is turned off by setting $\nu < 0$. Thus, the generated solution of the unit-CPGs (x) follows the input value O for the discrete component.

The proposed postural system outputs joint position into the three O inputs to the locomotor system, interconnecting both systems for the three joints of each leg: hip-swing, hip-flap and knee. The offset input $O_{\mathrm{s},i}$ for the hip-swing, $O_{\mathrm{f},i}$ for the hip-flap, and $O_{\mathrm{k},i}$ for the knee. Subscript i specifies one of the four legs, fore left, fore right, hind left or hind right.

4.6.3 Postural control system

The postural control system generates movements for posture correction. It enables integration of sensory feedback such that movements are robustly generated and adapted to the environment. Sensory information is noisy and changes as a result of the generated robot movement. The proposed postural control depends on a variety of sensory modalities through the integration of several responses, each based on its own sensory input. This integration of postural responses provides the system with some aspects of coordination, competition and redundancy.

Each response individually contributes to the posture of the robot with respect to its given sensory inputs. The different responses are then integrated to produce the final corrective motions.

The AIBO robot has a 3-axis accelerometer built into its body, enabling to calculate the sagittal and lateral tilt of the robot body. Each leg has a touch sensor in its foot, an encoder and PWM motor information for each joint. This work considers that information regarding the body angle, namely roll and pitch angles, foot touch information and a value relating to joint load are all available. The postural corrective responses and the respective sensory inputs are presented in fig. 4.31.

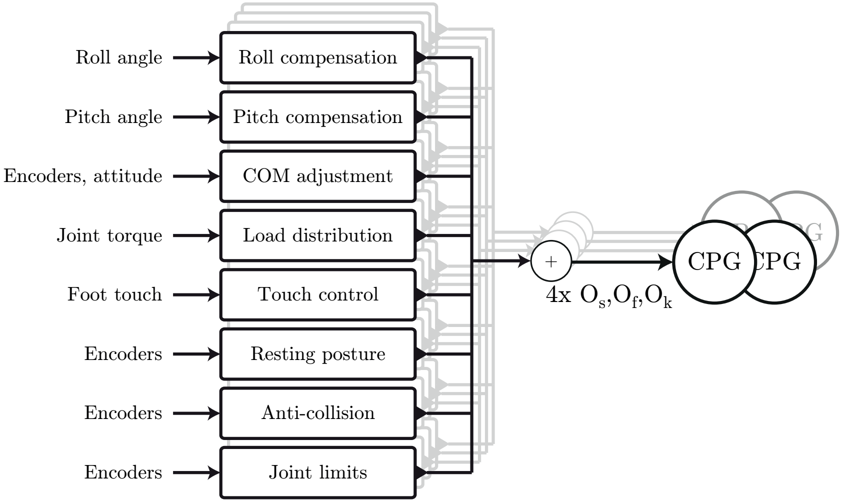

Figure 4.31: Parallel postural responses and the respective sensory modality. The overall solution of all postural responses is output and used as the offset for the unit-CPGs: hip-swing, hip-flap, and knee.

These responses are set for each leg, some of which work independently within the leg, while others are coordinated between the other legs. This coordination enables the assistance when the required corrective movements assigned to a leg are greater than the full amplitude.

Responses are designed as equilibrium forcing functions on a differential equation, and their combination is simply the sum of their dynamics.

$$\dot{y_{j,i}} = f_{j,i}^{\text{roll}} + f_{j,i}^{\text{pitch}} + f_{j,i}^{\text{COM}} + f_{j,i}^{\text{load}} + f_{j,i}^{\text{touch}} + f_{j,i}^{\text{disperser}} + f_{j,i}^{\text{reset}} + f_{j,i}^{\text{limits}} \tag{4.37}$$

The solution $y_{j,i}$ is the corrective movement for joint j on leg i, and is assigned to the unit-CPG's input $O_{j,i}$. Each response has one parameterizable gain, specifying the speed of converge to the equilibrium point. A careful parametrization of these gains allows to define the overall role of each response on the final postural correction, by weighting the responses. The parametrization of these static gains has been achieved empirically on the present work.

In order to prevent the system's solution to evolve out of allowable and desirable values, and at the same time limit the range of action of each joint, two system limits were added as repellers.

$$f_{j,i}^{\text{limits}} = k_{\text{jl}} \left(y_{j,i} - M_{j,i}\right) e^{\frac{(y_{j,i}-M_{j,i})^2}{2\sigma^2}} + k_{\text{jl}} \left(y_{j,i} - D_{j,i}\right) e^{\frac{(y_{j,i}-D_{j,i})^2}{2\sigma^2}}, \tag{4.38}$$

By having $f_{j,i}^{\text{limits}}$ (eq. (4.38)) in eq. (4.37), the range of solutions is limited to a range between $D_{j,i}$ and $M_{j,i}$. Parameter k_{jl} defines the amplitude and σ the width of the repellers.

Roll and pitch balance responses

The objective of these two responses is to adjust the body inclination, opposing to changes in terrain slope, so that the roll and pitch angles are reduced to a minimum. Slope compensation is achieved through extension and flexion of the legs, changing legs' height.

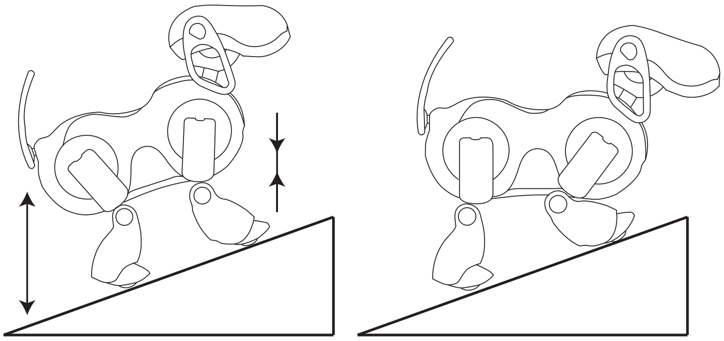

Figure 4.32: Robot's pitch angle is adjusted by extending/flexing the front/rear legs in coordination.

Pitch response uses the information about the robot's pitch angle and adjusts the body in the sagittal plane, changing the front and hind legs height by manipulating the joint position for the hip-swing and knee joints. When the robot is inclined backwards, it extends the hind legs and flexes the fore legs until it reaches a leveled position (fig. 4.32). Symmetrically, when the robot is inclined forwards, it flexes the hind legs and extends the fore legs.

The following function models the pitch response, for the hip-swing ($j = \text{s}$) and knee ($j = \text{k}$) of each leg:

$$f_{j,i}^{\text{pitch}} = k_{\text{pitch}}\, p_i \left(\phi_{\text{pitch}}\right), \tag{4.39}$$

where ϕ_{pitch} is the actual pitch angle, as measured by the robot's IMU. $p_i(\phi)$ is a piecewise linear function defining a dead-zone in order to deal with sensor noise. $p_i(\phi)$ also returns a positive or negative value, as required by the robot's joint configuration, in order to the solution result in the correct behavior. e.g. for ϕ_{pitch} it returns the symmetric value for the fore legs and positive for the hind legs. The static gain k_{pitch} defines the speed of convergence to equilibrium.

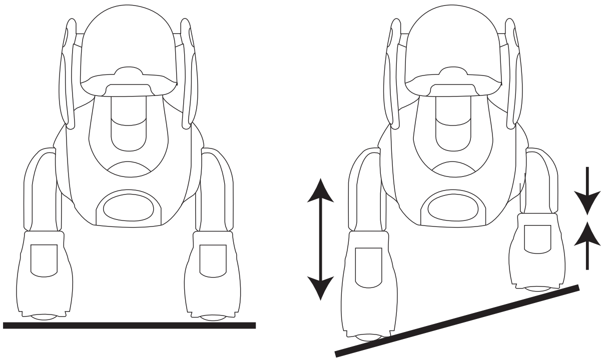

Figure 4.33: Robot's posture in the frontal plane is adjusted by extending/flexing the right/left legs in coordination accordingly to the current roll angle.

The same principle is applied to the frontal plane of the robot. Using the roll angle information ϕ_{roll}, the roll response changes the leg height on the left and right sides independently. If the robot is inclined to the left, it should extend the left legs and flex the right legs (fig. 4.33). Alternatively, if inclined to the right it should flex the left legs and extend the right legs.

The roll response also acts in the hip-swing ($j = \text{s}$) and knee ($j = \text{k}$) of each leg, as defined by:

$$f_{j,i}^{\text{roll}} = k_{\text{roll}} p_i \left(\phi_{\text{roll}}\right), \tag{4.40}$$

with ϕ_{roll} as the roll angle measured by the robot's IMU, and k_{roll} the speed of convergence. Similarly for the pitch response, the same $p_i(\phi)$ piecewise linear function defines a dead-zone, and returns a positive or negative value depending on the robot configuration. For the ϕ_{roll} it returns a negative value for the left legs and positive value for the right legs.

These two responses address the same joints, with possibly distinct behaviors as the resulting output, e.g. roll response tries to extend one leg while the pitch response flexes the leg. This is a clear case of possible coordination or competition between the output solutions of the different postural responses.

Roll and pitch coordination There are certain situations where the corrective movements of full amplitude are not sufficient to reduce the robot's inclination. On these situations, extending and flexing the legs to their limits does not yield a complete correction of the pitch and roll angles. The solution is a coordination of the previously presented responses, $f_{j,i}^{\text{roll}}$ and $f_{j,i}^{\text{pitch}}$, in order to work together on more difficult postural tasks.

In the situation where no action will produce a postural action, due to reaching an extension or flexion limit of a given leg, the other diagonal legs should change their height, taking the leg to within a workable range. The strategy is to flex or extend a current leg that has reached its equilibrium state in its own pitch and roll responses: $e^{\frac{-\left(p_i\left(\phi_{\text{pitch}}\right)+p_i\left(\phi_{\text{roll}}\right)\right)^2}{0.01}}$, and if one of the other diagonal legs still has not reached the equilibrium state: $p_i\left(\phi_{\text{pitch}}\right)+p_i\left(\phi_{\text{roll}}\right) \neq 0$.

The previously presented pitch and roll are then expanded by adding a member, reflecting this strategy:

$$\begin{aligned} f_{j,i}^{\text{roll}}+f_{j,i}^{\text{pitch}} = & k_{\text{pitch}} p_i\left(\phi_{\text{pitch}}\right)+k_{\text{roll}} p_i\left(\phi_{\text{roll}}\right) \\ & +k_{\text{C}}\left(\frac{\left|p_l\left(\phi_{\text{pitch}}\right)+p_l\left(\phi_{\text{roll}}\right)\right|}{2}\right) e^{\frac{-\left(p_i\left(\phi_{\text{pitch}}\right)+p_i\left(\phi_{\text{roll}}\right)\right)^2}{0.01}}, \end{aligned} \tag{4.41}$$

where k_{C} is a static gain, l denote the diagonal legs, and i the current leg. By choosing a smaller gain k_{C} than the gains k_{pitch}, k_{roll}, this mechanism is ensured to not overtake the role of the pitch and roll responses.

Center of Mass compensation

The center of mass (COM) compensation response is intended to position the robot's COM over the center of the support polygon, increasing the Static Stability Margin (SSM) of the actual robot's posture. By adjusting the hip-swing (s) and hip-flap (f) joints, the body is shifted, displacing the COM over the support polygon (fig. 4.34).

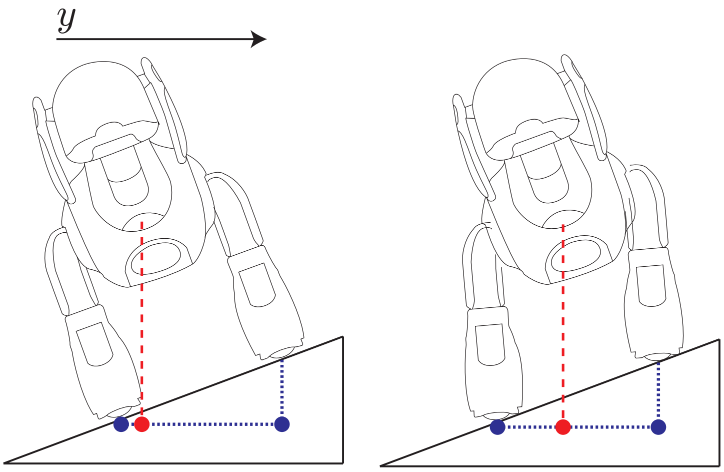

Figure 4.34: The projection of the robot's center of mass is displaced towards the support polygon's center, increasing the static stability margin.

A point attractor brings the hip joints to an equilibrium when the COM coordinates match the support polygon's center. The solution changes the offset of the hip-swing and hip-flap through the contributions defined in:

$$f_{\mathrm{s},i}^{\mathrm{COM}} = k_{\mathrm{COM,s}}(\mathrm{COM}_x - x_{\mathrm{center}}), \tag{4.42}$$

$$f_{\mathrm{f},i}^{\mathrm{COM}} = k_{\mathrm{COM,f}}(\mathrm{COM}_y - y_{\mathrm{center}}), \tag{4.43}$$

where COM_x and COM_y denote the center of mass projection position in the x and y axis, respectively, and x_{center} and y_{center} are the position of the support polygon's center. $k_{\mathrm{COM,s}}$ and $k_{\mathrm{COM,f}}$ are the static gains for the hip-swing and hip-flap compensation movements.

Load distribution

This response distributes the weight of the body equally over the four legs. Load information is estimated from joints by reading the motor PWM values and then a simple average $\overline{F}$ is calculated. Legs which are above this load average are being pushed harder than the others, bearing more load due to the gravitational force in this static setting. Load distribution is applied to hip-swing (s) and knees (k) joints, controlling leg height as follows:

$$f_{j,i}^{\mathrm{load}} = k_{\mathrm{load}}(F_i - \overline{F}), \tag{4.44}$$

where k_{load} is a static gain, F_i is the actual value read on the PWMs for leg i and $\overline{F}$ is the average force over the four legs.

Touch control

When the robot's feet lose ground contact, the robot loses support on that point. This response monitors the touch sensors in the foot and when it detects the loss of support, it searches for ground by extending the leg (fig. 4.35). Leg height is controlled by adjusting the hip-swing and knee joints.

The response is formulated as:

$$f_{j,i}^{\mathrm{touch}} = k_{\mathrm{t}}(1 - T_i)y_{j,i}, \tag{4.45}$$

where k_{t} is a static gain, T_i is the foot i touch sensor: 0 means that the foot is lifted and a 1 means that it has ground contact.

Touch coordination Sometimes the ground is too far and a fully stretched leg is still not able of regaining support. Therefore a method for coordinating the touch control response is proposed, enabling the other legs to lower at the same time that the lifted leg extends (fig. 4.35).

This mechanism uses the touch information from the other three feet touch sensors, which is used to act on the hip-swing and knee joints. This mechanism is added as a term to the touch response:

$$f_{j,i}^{\mathrm{touch}} = k_{\mathrm{t}}(1 - T_i)y_{j,i} + k_{\mathrm{C,t},i}[(1 - T_j) + (1 - T_k) + (1 - T_l)], \tag{4.46}$$

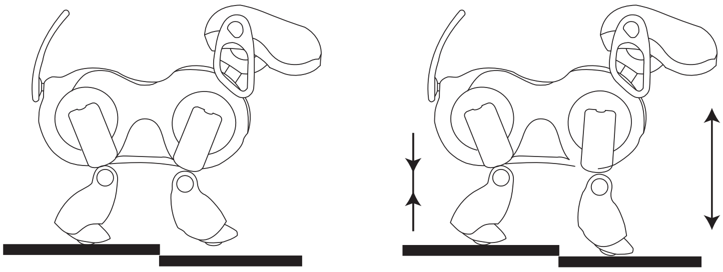

Figure 4.35: Foot touch sensors are used to monitor ground support loss, signaling the touch control response to extend the leg.

where T_j, T_k, T_l are the foot sensors from all the other legs. Similarly, $k_{\mathrm{C,t},i}$ is a static gain that controls the speed of convergence.

Leg disperser

It has been verified that in certain conditions the fore and hind knees would get very close or even collide, which caused a few stability problems since it made the robot become unbalanced and sometimes even provoked falls.

In order to avoid this undesired situation, a mechanism is proposed to prevent the knees from touching. The mechanism implements a leg disperser through an erected repeller, activated once the distance between the knees reaches a minimum undesired value. This response controls the hip-swings and is given as follows:

$$f_{j,i}^{\mathrm{disperser}} = k_{\mathrm{disperser}} \left(1 - \frac{1}{1 + e^{-k(d_i - d_{\mathrm{min}})}} \right), \tag{4.47}$$

where $k_{\mathrm{disperser}}$ is a static gain, d_i is the current distance between knees calculated using the robot kinematics, and d_{min} is the minimum value allowed for the distance between knees.

Posture reset

After a certain number of corrective movements the robot may lose its own initial posture. To force the quadruped to return to its initial position a weak attractor is implemented. The idea is to have a contribution weak enough so it does not disturb the other responses, but if allowed, it will slowly and surely return to the initial posture.

The response is given by:

$$f_{\mathrm{s},i}^{\mathrm{reset}} = k_{\mathrm{r}} \left(y_{\mathrm{s},i} - IP_{\mathrm{s},i} \right), \tag{4.48}$$

$$f_{\mathrm{f},i}^{\mathrm{reset}} = k_{\mathrm{r}} \left(y_{\mathrm{f},i} - IP_{\mathrm{f},i} \right), \tag{4.49}$$

$$f_{\mathrm{k},i}^{\mathrm{reset}} = k_{\mathrm{r}} \left(y_{\mathrm{k},i} - IP_{\mathrm{k},i} \right), \tag{4.50}$$

where k_{r} is the static gain and has a very low value. $IP_{\mathrm{s},i}$, $IP_{\mathrm{f},i}$ and $IP_{\mathrm{k},i}$ are initial positions for hip-swing (s), hip-flap (f) and knee (k) joints.

4.6.4 Experimental results

In this section are presented the results from experiments performed on the AIBO ERS-7 to demonstrate the feasibility of the proposed postural system to control the twelve DOFs for maintaining the robot's static stability.

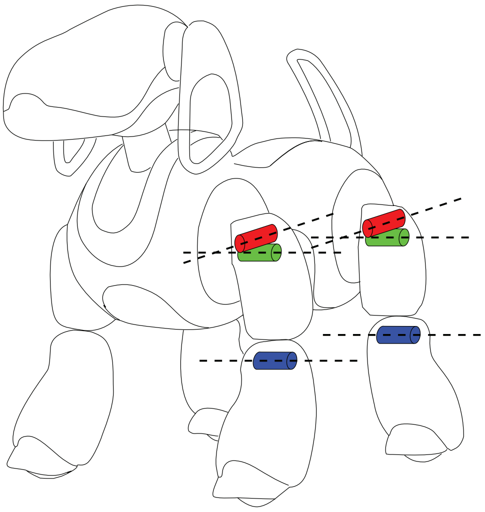

Figure 4.36: Schematic view of the ERS-7 AIBO model depicting the controlled DOFs for the left side.

The robot stands over four independent supports (fig. 4.37) which when operated together can mimic a stand-alone moveable plane, subjecting the robot to change in inclination, or can mimic the loss of foothold.

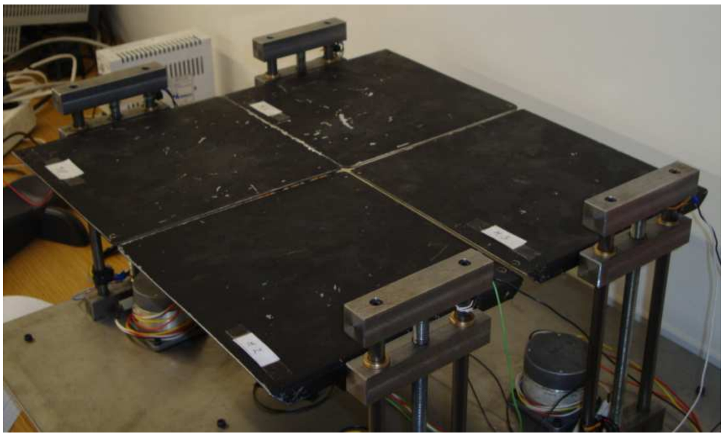

Figure 4.37: Platform used to perform the various and different experiments. This platform is composed by four independent moveable supports, where it is possible to raise or drop each of them.

The postural control system is validated through experiments, where the robot is subjected to different posture situations ranging from roll and pitch variations to loss of feet support.

The parameters used in the experiments are presented on table 4.5.

Table 4.5: Parameter values for the postural experiments.

k_{jl}	5000	k_{C}	4	k_{t}	2
σ	0.05	$k_{\text{COM,s}}$	1	$k_{\text{C,t}}$	2
k_{pitch}	4	$k_{\text{COM,f}}$	1	$k_{\text{disperser}}$	3
k_{roll}	4	k_{load}	0.5	k_{r}	0.5

Sagittal and frontal inclinations

This experiment intends to verify the robot's behavior when sagittal and lateral inclinations are applied. It is expected that the robot suppresses any inclination to values near zero. It is also expected that the COM position converges to the center of the support polygon.

The four platforms start moving at $t = 8\ s$, performing an inclination $-5°$ in the pitch plane (lowering the fore part of the body) and $-3°$ on the roll angle relatively to the ground (lowering the left side), during 20 s. At $t = 29$ s the platform started to return to its initial position ($0°$) taking 20 s.

From $t = 8$ s to $t = 28$ s the robot tries to oppose to the platform inclination (fig. 4.38), stretching the fore and left legs and folding the hind right leg doing a forward left move. It succeeds on suppressing it to values $|\phi| < 1°$ for the pitch and roll.

At $t = 28$ s the platform changed its movement, but despite the change, the robot continued suppressing the platform inclination, slowly folding the stretched legs and stretching the folded one, resulting in an opposite movement. At the end of the platform movement, at $t = 48$ s, the roll and pitch angles of the robot are near $0°$.

Based on these results it is possible to say that the inclination goals were attained.

On fig. 4.38 is possible to see that at the beginning of the experiment the robot does not have its COM centered on the support polygon. The first few seconds are used for the robot to position itself correctly. At $t = 8$ s the platform starts its movement and throughout the experiment, the COM position stays very close to the center of the support polygon. The COM response (fig. 4.39) normally opposes to the roll and pitch control, not letting it to do exaggerating moves in either direction. This competition resulted in a good performance since it was able to suppress the terrain inclination and center the robot's weight on the support polygon.

Fig. 4.39 shows each response for the fore left hip-swing. Note that the roll and pitch balance response ($f_{j,i}^{\text{roll}} + f_{j,i}^{\text{pitch}}$, blue solid line) is the dominant one, and the joint limiter and leg coordination were not activated since both are used at more demanding situations.

Touch and coordination

The purpose of this experiment is to demonstrate the implemented touch coordination. One of the four supports is dropped, forcing the foot to lose ground contact. Once ground contact is lost, the robot should stretch that leg in order to regain support. At the same time the other legs help out lowering the body to solve the problem as quickly as possible.

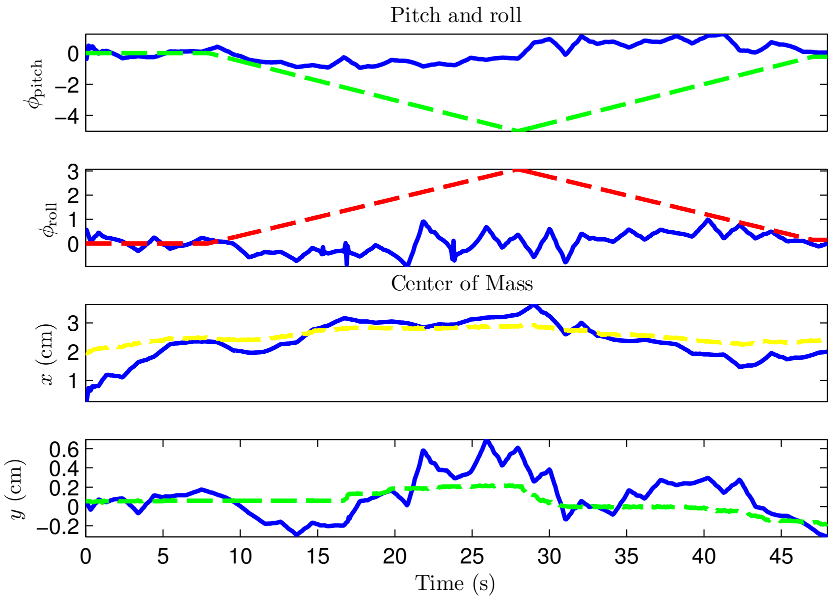

Figure 4.38: The first two plots show in degrees ϕ_{pitch} (1st panel) and ϕ_{roll} (2nd panel) variation of the platform (dashed) and of the robot (solid). The bottom two show the robot center of mass position (dashed) and the intersection point (solid) evolution.

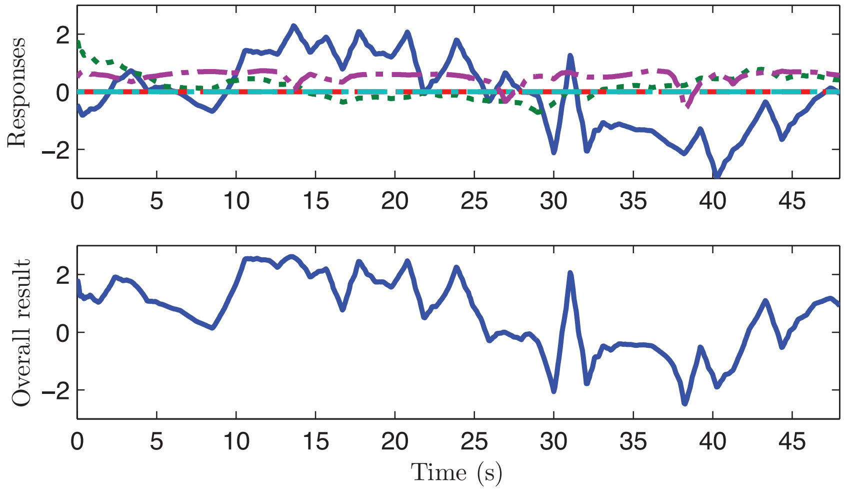

Figure 4.39: The top plot shows the response of the different responses for the fore left hip swing joint. The dotted line is the COM response, the solid line is the roll and pitch response, the dash dotted line represents the leg repeller, the dashed line is the joint limits control and the leg coordination is represented by the light blue dashed line. The bottom plot shows the sum of all responses.

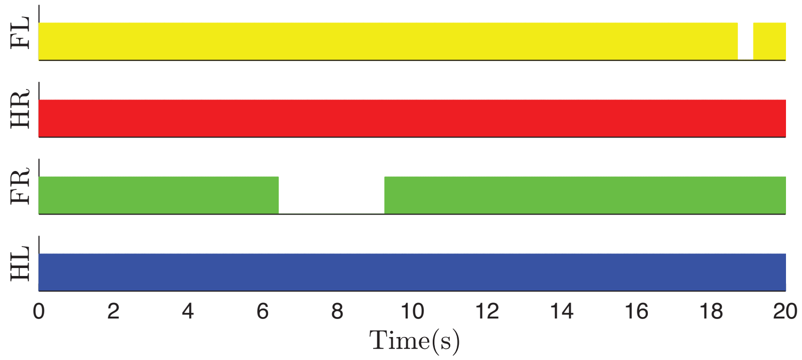

Figure 4.40: Fore left (FL), hind right (HR), fore right(FR) and hind left (HL) leg's touch. Filled area means that the respective foot is on the ground, otherwise is lifted.

At approximately 6 s the support beneath the fore right leg was lowered (fig. 4.40). On fig. 4.41 it is observable that to compensate the missing support the fore right leg was stretched as expected, since the swing and knee values of this leg are decreasing (dash dotted red line and dotted light blue line). In the same scale but in opposite direction was the fore left swing lowering the body of the robot to help the fore right leg. This lack of touch was soon eliminated showing a good coordination between the legs.

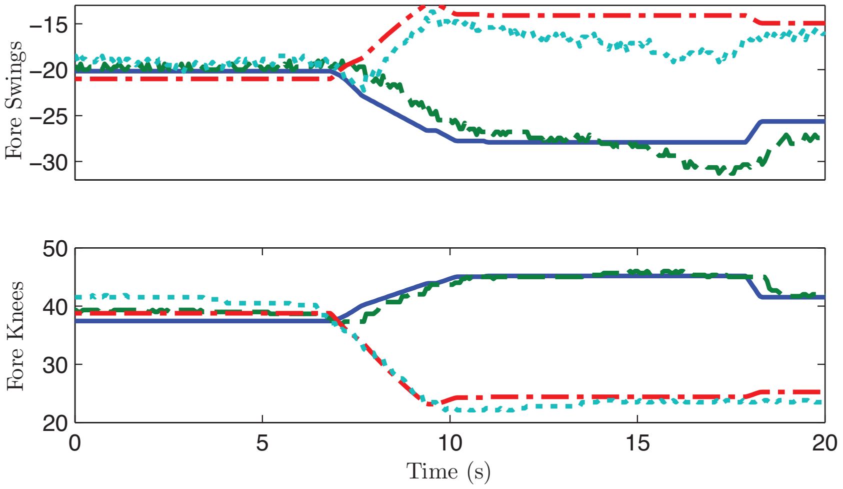

Figure 4.41: Top: Desired (solid line) and real (dashed line) trajectories for Fore Left Swing, desired (dash dot line) and real (dotted line) trajectories for the Fore Right Swing. Bottom: Desired (solid line) and real (dashed line) trajectories for Fore Left Knee, desired (dash dot line) and real (dotted line) trajectories for the Fore Right Knee.

Note that despite the noisy sensory information, the solution and resultant joint trajectories are smooth. Further, the joints are able to follow the planned trajectories correctly as expected.

All responses

The aim of this experiment is to verify the robot behavior when subjected to disturbances in posture that elicit the activation of all the postural responses, such as the experimented depicted in fig. 4.42.

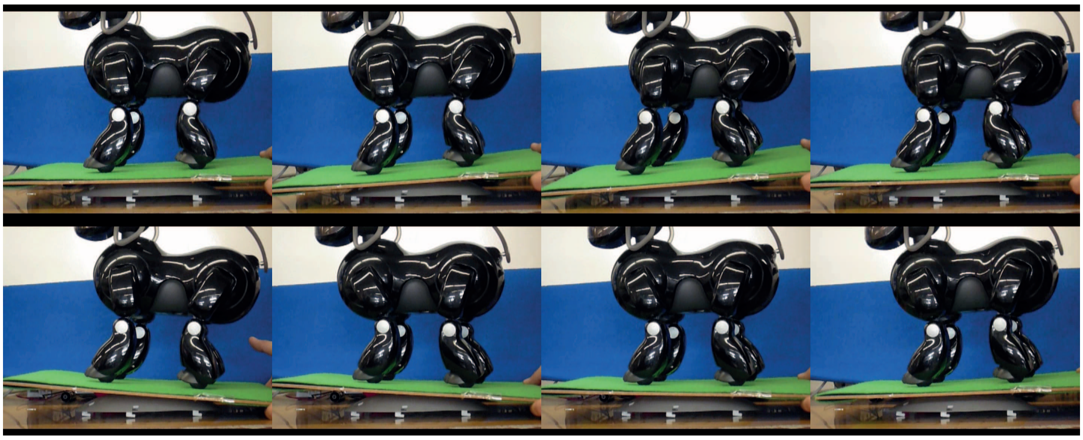

Figure 4.42: Video snapshots from an experiment where the robot is subject to faster and greater perturbations, and where most responses were elicited.

Fig. 4.43 depicts results from this experiment. At $t = 7$ s the four supports started moving such that during 15 s an inclination of $-6°$ was produced (lowering the fore part of the body) in the pitch plane and $-3°$ (lowering the left side) on the roll angle relatively to the ground. At $t = 22$ s, the platform starts returning slowly to the initial position ($0°$), taking 15 s to execute the task. When the platform reached the initial position (at $t = 46\ s$) it started moving again until reaching a pitch angle of $-3°$ and no roll angle. Finally, the platform is set back to $0°$.

Fig. 4.43 shows that the robot suppressed satisfactorily the provoked pitch and roll angles. The COM it follows closely the center of the support polygon throughout the experiment.

In fig. 4.44 is possible to observe that any loss of touch was regained as quickly as possible without compromising the overall posture of the quadruped.

On fig. 4.45 is possible to see each response for the overall solution. Each response has its importance as almost every single one of them contributed for the attained result.

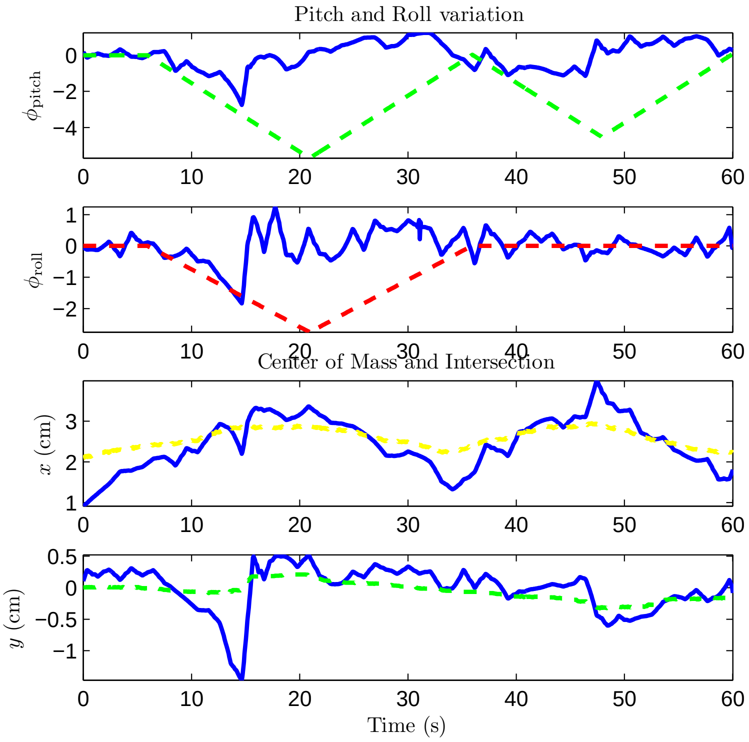

Figure 4.43: The first two plots show ϕ_{pitch}(1st panel) and ϕ_{roll}(2nd panel) variation of the platform (dashed) and of the robot (solid). The bottom two show the robot center of mass position (dashed) and the intersection point (solid) evolution.

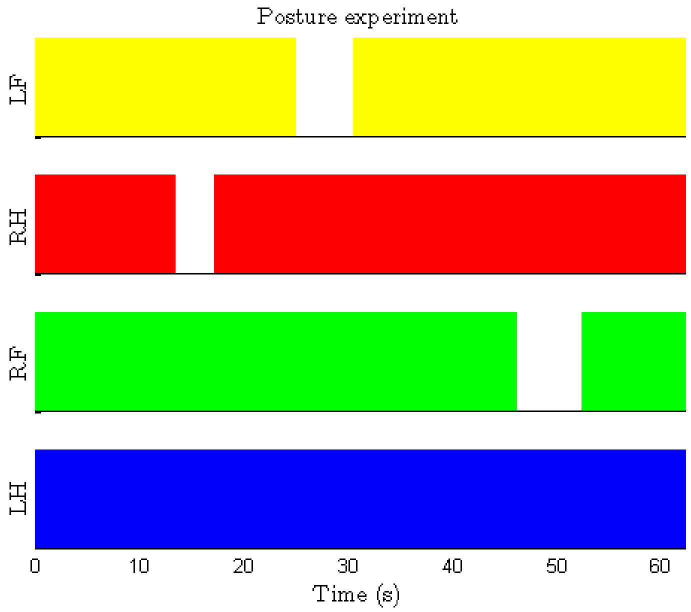

Figure 4.44: Fore left (LF), hind right (RH), fore right (RF) and hind left (LH) leg's touch. Where the filled area means that the respective foot is on the ground, otherwise is lifted.

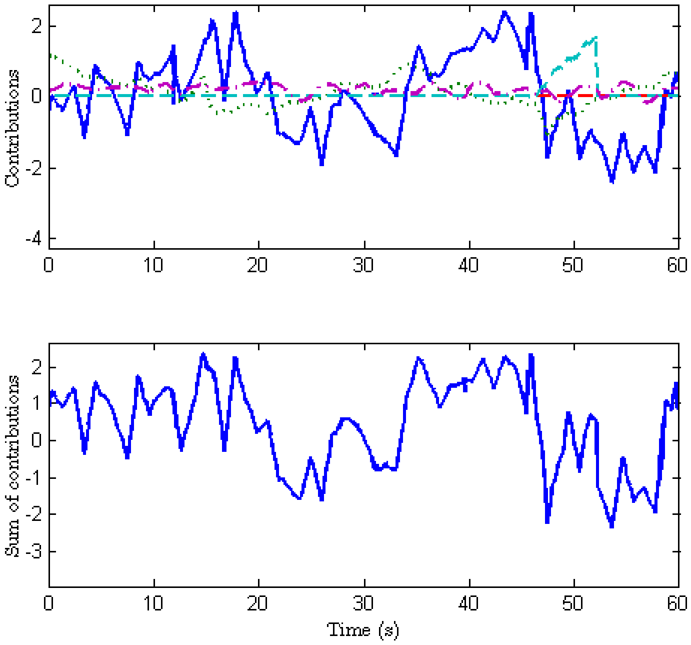

Figure 4.45: The top plot shows the response of the different responses. Where the dotted line is the center of mass response, the solid line is the roll and pitch response, the dash dotted line represents the leg repeller and with value zero is the joint limits control and leg coordination. The bottom plot shows the sum of all responses.)

4.6.5 Remarks on standing postural control

The proposed postural system presents an interesting and successful approach in accomplishing equilibrium maintenance in a standing postural task. The most interesting aspect of the approach is how the fusion of several responses based on different sensory modalities has been achieved. However, the system requires manual parametrization of each postural response, and is performed incrementally and individually.

Experimental results demonstrate that by having parallel postural responses, each defining a postural action according to a given sensory modality, the final behavior is achieved as a coordinated effort, even when the output of postural responses contradict each other. These aspects on coordination, redundancy and competition allow the system to tackle several postural disturbances, easily generalizing for different situations.

The major drawback of the proposed approach is that it does not consider dynamic effects. The proposed postural responses only tackle static conditions, disregarding dynamic effects, such as fast postural disturbances, or the self-imposed accelerations caused by postural actions. This drawback is the major detractor of applying the proposed postural system to the problem of locomotion.

4.7 Discussion

This chapter presents a contribution which strived to accomplish a step forward in the control of quadruped locomotion, with the goal to achieve efficient and adaptive, goal-directed locomotion. The goal of the presented solution is to build onto previous work using limit cycle oscillators to implement a CPG based approach. It presents an architecture functionally organized in separate levels of abstraction, dividing the role of high-level planning of locomotion, and regulation of locomotion and generation of motor patterns.

The generation level encompasses a flexible organization of Landau-Stuart oscillators, producing strictly coordinated motor patterns, yet flexible enough to produce a large range of movements which allows the quadruped robot to achieve omnidirectional locomotion. This level is modulated by the regulation level, receiving sets of parameters specifying the characteristics of the motor patterns to be executed. In this fashion, omnidirectional locomotion is specified by the planning level through high level locomotion descriptors, such as the walking velocity, walking orientation and angular velocity.

This approach greatly reduces the dimensionality of the control problem. All the motions are coordinated at the generation level, in two fronts: 1) the proper execution of a stepping pattern is guaranteed through a generation of coordinated motions for all the DOFs within a limb-CPG; 2) the maintenance of phase relationships among the four legs, through the coordination of the four limb-CPGs. Furthermore, the regulation level maps three high-level commands to the parameter values of all the four limb-CPGs, significantly reducing the parameters which are used to modulate the motor patterns.

A simple goal-oriented locomotion task was used to demonstrate the feasibility of the architecture and ability to continuously modulate the walking motions. The three high-level commands are output from local planning systems, reacting to real-time to visually acquired sensory information, making the robot walk towards a given target while avoiding obstacles, by steering and changing its velocity.

These characteristics and the simplicity of the solution are possible to attain mainly due to the properties presented by the Landau-Stuart oscillator. However, its simplicity also limits its application for a high gain position controlled quadruped robot, mainly because the oscillator produces sinusoidal shaped motions and the system does not make use of the robot's kinematical model. This fact limits the solution to not reach the performance of typical solutions for quadruped statically stable walking, and due to the platform characteristics, it is not possible to pursue dynamic walking. Nonetheless, the robot performs the desired locomotion and the obtained results have been quite satisfactory, especially considering the simplicity of the system.

The proposal of feedback mechanisms tries to address these issues to some extent, with the aim to include temporal and spatial adaptation terms onto the CPGs. However, it is not clear or yet established the best procedure on how to pursue the integration and design of feedback mechanism. One advantage on building upon the presented approach is the possibility of integrating sensory feedback mechanisms already presented in other works [45, 174].

This chapter investigates a method of coupling the CPG rhythmic activity to the step phase of the quadruped robot, trying to create a link between the robot dynamics and the walking motion of the locomotor controller. The phase coupling mechanism achieves slight improvements of the locomotion in flat terrain, slightly changing the shape and timing of the nominal trajectories and correcting some of the step phases. However, the usability of the proposed mechanism is largely dependent on the parametrization of the CPGs and limited to locomotion in flat terrains.

Postural stability of a standing quadruped was addressed with the goal of further expand the solution for locomotion. The proposed postural system produces online trajectory modulation, achieved through the inclusion of feedback loops through a set of integrated responses. The proposed responses are included in the dynamical system equations and generate the required joint trajectories that enable a coordinated and smooth movement towards an equilibrium condition. This coordination, competition and redundancy among the responses are a key element for the adaptive, flexible and fault tolerant postural actions observed from the system.

This solution for postural control relies on postural responses which specify static equilibrium conditions to be achieved, through reactive mechanisms. This choice was demonstrated to limit the application of the posture system to locomotion.

In the future, postural responses should include dynamic effects, taking in consideration accelerations and dynamic equilibrium conditions. The behavior of responses should also be augmented to include predictive action, not only reactive. For instance, the use of optic flow would be a good indicator of future postural conditions, depending on the observed terrain configuration. The hierarchization of the postural responses depending on the behavioral and postural context could also be explored, possible through weight manipulation of the postural responses.

Postural control should also be considered as a high-level complex skill, rather than only a combination of reflexes, because it requires estimation of the pose and mechanisms to address dynamic conditions, and to produce anticipatory postural corrections based on voluntary movements.

CHAPTER 5

BIPED LOCOMOTION

This chapter presents a CPG approach based on phase oscillators to bipedal locomotion where the designer with little *a priori* knowledge is able to incrementally add basic motion primitives, reaching bipedal walking and other locomotor behaviors as final result. The proposed CPG aims to be a model free solution for the generation of bipedal walking, not requiring the use of inverse kinematical models [8, 10] and previously defined joint trajectories [149, 173].

The incremental construction of bipedal walking allows an easier parametrization and performance evaluation throughout the design process. Furthermore, the approach provides for a developmental mechanism, which enables progressively building a motor repertoire. It would easily benefit from evolutionary robotics and machine learning to explore this aspect.

The proposed CPG system also offers a good substrate for the inclusion of feedback mechanisms for modulation and adaptation. Other studies have explored mechanisms for phase resetting [4, 5, 173], phase coupling [147], and frequency adaptation [149], entraining the walking dynamics with the controller. The current proposal explores phase regulation mechanisms using load sensory information, observable in vertebrate legged animals [158].

Results from simulations, on HOAP and DARwIn-OP in Webots software show the adequacy of the locomotor system to generate bipedal walk on different robots. Experiments on a DARwIn-OP demonstrates how it can accomplish locomotion and how the proposed work can generalize, achieving several distinct locomotor behaviors.

The last section explores the integration of the proposed CPG controller within a whole-body control framework formulated as a Linear Quadratic Program (LQP), to investigate how the proposed system fares in comparison with typically used approaches of ZMP based walking.

5.1 Bipedal CPG approach

On the proposed locomotion system each CPG produces the motions of a single leg, controlling all the leg's DOFs by outputting reference angle positions. In contrast with the quadruped CPG solution, the design of the biped CPG requires a different approach, as the simple sinusoidal patterns are not appropriate for achieving biped walking. The CPG is modeled on the suggested two layered organization, having one rhythmic generation layer producing the temporal reference and one other pattern generation layer receiving the temporal drive to produce the spatial reference. A group of motion pattern generators, each responsible for a single joint, are driven by a shared rhythmic generator [139] (fig. 5.1).

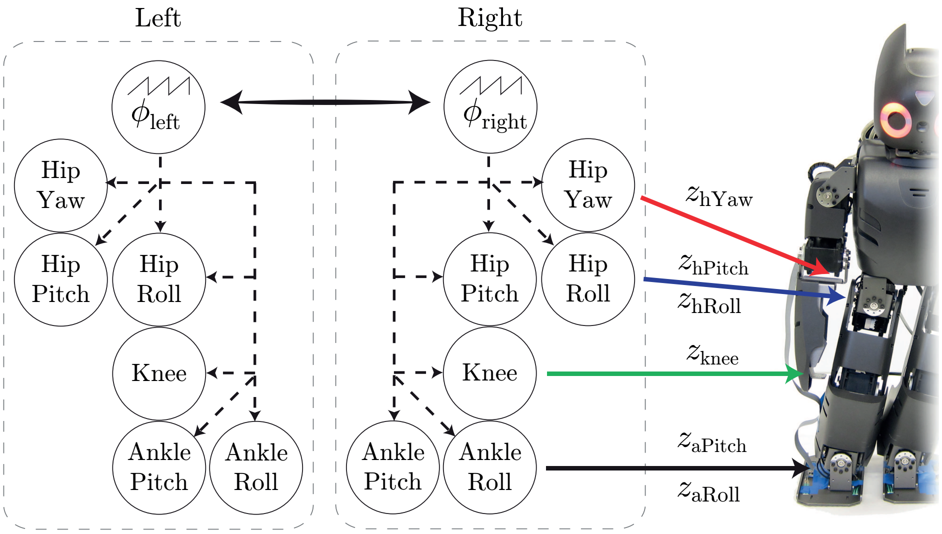

Figure 5.1: Representation of left and right CPGs. Each CPG is composed by a shared rhythmic generator and a group of motion pattern generators for the corresponding joints of the leg. Bilateral interaction between the rhythmic generators is represented by the bilateral arrow, providing for maintenance of interlimb relationships.

The rhythmic generator is implemented as a phase oscillator to generate the base rhythm of locomotion. The use of a phase oscillator presents appealing properties as straightforward maintenance of phase relationships and entrainment, which are used to achieve interlimb coordination and to serve as a substrate to feedback pathways, such as the later proposed phase regulation.

The motion pattern generators receive the rhythmic signal and generate joint trajectories through the sum of motion primitives. Similar to other approaches [91,142,149], motion primitives are encoded as a set of non-linear dynamical equations with well-defined attractor dynamics, and are smoothly and easily modulated regarding their amplitudes, frequencies, and pattern offsets.

A motion primitive describes a simple motion, meant to be employed as components for the achievement of more complex motions. This approach is based on the idea that certain biped locomotor behaviors are achieved by performing complex motions at the kinematic level, and these complex motions are best tackled when addressed separately. It is a synergistic approach, considering that by weighting or sequencing the motion primitives, it is possible to modulate the produced complex motions and alternate between the achieved locomotor behaviors. It also shares the idea that by weighting or sequencing the motion primitives, it is possible to modulate these complex motions and alternate between the achieved locomotor behaviors.

Motion generation in this approach is flexible in the sense that it allows for an easy addition and change of motion primitives, and provides for an easy integration with autonomous mechanisms for learning, optimization or evolution and exploration of locomotor behaviors. The expansion of the motor repertoire can be achieved through tuning of parameters for motions; creating new motion primitives; empirically, or even evolutionary methods; creation and reorganization of feedback pathways and its effects in motor patterns. Regardless, it is considered that as a starting point in the life of the robot, it should have a basic motor repertoire of motion primitives that achieve basic, but capable, walking behavior. It can also be regarded as a starting point for local policy search methods, which benefit from the existence of an initial solution, such as POWER [113, 211] and PI^2 [202, 212].

The creation of the basic motor repertoire for walking is presented in the next sections. The motor repertoire is created manually through a progressive increment of motion primitives, using sinusoidal and bell-shaped trajectories to describe general motions observable from biped walking.

Using only sinusoidal and bell-shaped profiles in the design of motion primitives is a conscious choice, reasoned on the designer's lack of knowledge and ability to describe any of the following: i) the complete joint trajectories for achieving biped locomotion; ii) changes in joint trajectories to achieve different locomotor behaviors; iii) modular motion primitives for achieving detailed biped locomotion. By using a reduced description through the superposition of only sinusoidal and bell-shaped motion primitives it is possible to overcome these limitations.

The proposed approach provides for an easy addition and change of motion primitives with the objective of performing a broad, flexible repertoire of locomotor behaviors.

5.1.1 Rhythm generator

A rhythm generator is implemented as a coupled phase oscillator, given by eq. (5.1) from section 3.2.

$$\dot{\phi}_i = \omega + k \sin\left(\phi_i - \phi_o + \pi\right), \tag{5.1}$$

It outputs a monotonically increasing periodic signal ϕ_i (rad), with rate ω $(\mathrm{rad.s}^{-1})$, which specifies the phase of the current leg i. The rhythmic output signal ϕ_i is employed as a time keeping clock, determining the state of the step. The signal drives the pattern generators, providing for a timely and coordinated generation of the motor trajectories.

To use the phase ϕ not only in $2k\pi$ periodic functions (e.g. sine and cosine), the output is bounded in the range $[-\pi, \pi]$. Each motion primitive is anchored into a specific phase value, where each period corresponds to the final step cycle period.

By having a single central rhythm generator for all the joints of a single leg, the coordination between all motions within that leg is guaranteed. Furthermore, the use of a phase oscillator provides for a simple mechanism for contralateral coordination, accomplished by simple bilateral coupling (eq. (3.11)) between the two legs, maintaining a strictly contralateral anti-phase relationship, between left and right legs.

5.1.2 Motion pattern generator

Each CPG is composed of six motion pattern generators driven by the shared phase oscillator, addressing all the joints in a leg for the DARwIn-OP and other robots with similar kinematical configuration. A single motion pattern generator produces the trajectories in real-time for each joint within a leg, and the final produced periodic motion is used as the reference angular position, input to the low level PID control. The produced periodic trajectory by each motion pattern generator is the overall result from the employment of several motion primitives.

In the proposed implementation, each motion pattern generator is based on a set of non-linear dynamical equations, defining the attractor dynamics. Joint position $z_{j,i}$ is generated according to the current phase ϕ_i of the CPG, in eq. (5.2) from section 3.2.2.

$$\dot{z}_{j,i} = \alpha(O_{j,i} - z_{j,i}) + \sum f(z_{j,i}, \phi_i, \dot{\phi}_i) \tag{5.2}$$

An offset attractor $O_{j,i}$ specifies the offset attractor, for the final generated rhythmic pattern. Subscript j defines the motion pattern generator of a single joint from DARwIn-OP's legs: hip roll (hRoll), hip yaw (hYaw), hip pitch (hPitch), knee (kPitch), ankle roll (aRoll) and ankle pitch (aPitch); and subscript i defines the left or right leg CPG. A single motion primitive is defined by a function $f_j^{\text{motion}}(z_{j,i}, \phi_i, \dot{\phi}_i)$, and the final generated trajectory $z_{j,i}$ results from the sum of all motion primitives for that joint.

Sinusoidal profile Sinusoidal motions are useful for recreating symmetrical motions which repeat a maximum excursion one or more times throughout the step cycle. A general sinusoidal profile is described by:

$$f_j^{\text{motion}} = -A_{j,\text{motion}} \dot{\phi}_i \sin\left(\phi_i + \psi_{\text{motion}}\right), \tag{5.3}$$

with amplitude A_{motion} and phase shift ψ_{motion} for joint j in leg i.

Bell-shaped profile Bell-shaped motions are more appropriate to describe motions which happen once in a step cycle, with a defined duration within the step period. A general bell-shaped profile is described as:

$$f_j^{\text{motion}} = -\frac{A_{j,\text{motion}} \dot{\phi}_i \left(\phi_i + \psi_{\text{motion}}\right)}{\sigma^2} \exp\left(-\frac{\left(\phi_i + \psi_{\text{motion}}\right)^2}{2\sigma^2}\right), \tag{5.4}$$

where A_{motion} defines the amplitude and σ the width of the bell curve, or the duration of the movement, and ψ_{motion} the phase shift.

Biped locomotion requires the same motions to be produced for both legs in alternate fashion, therefore, when a motion primitive is defined, it is used for both legs. Furthermore, for simplifying the design of motion primitives for the ankle joints, and to simplify the general walking behavior, it is assumed that the feet should be maintained parallel to the ground during the whole step cycle. To accomplish parallel movements of the feet, symmetric motion primitives from the hip pitch and ankle pitch are assigned to the joint ankles.

Each motion pattern generator is assigned a set of motion primitives, which can be enabled or disabled through own parameter manipulation. Modulation of each motion primitive is dependent on the final desired locomotor behavior, rendering locomotion a problem of modular motor programs.

5.2 Motion primitives

The proposed motion primitives for achieving basic goal-directed bipedal walking are herein presented in such an order, that by sequentially adding them, one can easily parameterize to achieve a correct and stable walking behavior. From own familiarity with human walking, observations and kinematical descriptions [188], one can put together a set of coarse motion primitives that compose a basic locomotion, resorting only to sinusoidal and bell-shaped profile trajectories.

A minimum of four motion primitives is required to achieve a capable biped locomotion. These four motion primitives are described next: the balancing motion; the flexion motion; the compass motion and the turning motion. Other motion primitives can be considered, either for expanding the locomotor abilities, e.g. turning motion, pelvis rotation motion, or to add detail to the walk, e.g. yielding motion.

In biped walking typically a duty factor of $\beta = 0.6$ is performed, achieving two types of support during a step cycle: single and double support. During single support the robot propels the body forward using one leg, while the other swings forward to be placed in the ground. At this point both legs support the robot simultaneously, describing a double support phase, transiting from one single support phase to the contralateral single support phase.

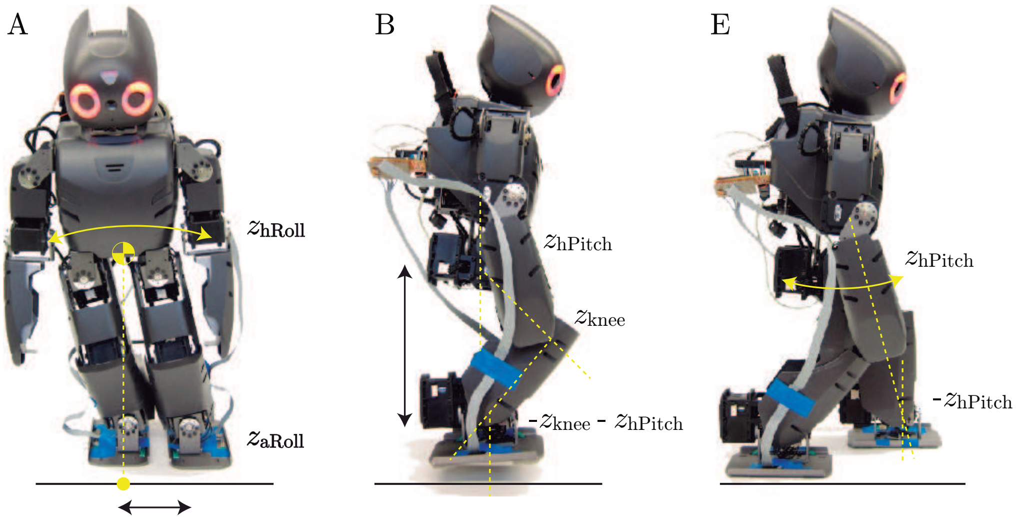

Figure 5.2: 3 motion primitives. A) Balancing motion; B) Flexion motion; E) Compass motion.

5.2.1 Balancing motion

The first motion primitive considered is the balancing motion (fig. 5.2, A), one of the crucial motions for bipedal walking. As the robot steps alternately, it exhibits moments of single foot support, requiring the displacement of the body over the supporting foot during a step cycle, unloading the swinging foot and allowing to execute the swing phase of the step, by lifting it from the ground and transferring it to a more forward position. Failing to achieve a correct displacement over the supporting foot at the correct timing for the next swinging foot, will certainly lead to a fall.

The balancing motion addresses the displacement of the body, transferring the body in the frontal plane from one foot to the other. It acts on the hip roll (hRoll) and ankle roll (aRoll) joints as a sinusoidal trajectory that makes the robot oscillate laterally. This motion is defined as:

$$f^{\text{balancing}}_{\text{hRoll},i} = -A_{\text{balancing}}\dot{\phi}_i \sin\left(\phi_i\right), \tag{5.5}$$

$$f^{\text{balancing}}_{\text{aRoll},i} = -f^{\text{balancing}}_{\text{hRoll},i}, \tag{5.6}$$

where i specifies the left or right leg, ϕ_i is the phase of left or right CPG, and parameter $A_{\text{balancing}}$ specifies the amplitude of the lateral displacement motion, disabling the motion when set to 0.

The phase shift of the balancing motion is 0, which means that when $\phi_{\text{L}} = 0$ (left CPG) and $\phi_{\text{R}} = \pi$ (right CPG), the balancing motion is at the maximum displacement, with the weight over the left foot. When $\phi_{\text{L}} = \pi$ and $\phi_{\text{R}} = 0$, the balancing motion is at the maximum displacement over the right foot. This phase difference of π is enforced by the contralateral coupling.

This choice effectively anchors the middle of the swing phase to be defined at $\phi_i = 0$, as the maximum excursion of the balancing motion in either leg.

The motion of the ankle roll joint is symmetrical to the hip roll joint, enforcing the assumption that the foot should always be parallel to the ground.

Fig. 5.3(a) shows the final trajectory when applying the balancing motion with $A_{\text{balancing}} = 11$ and joint offsets configured to $O_{\text{hRoll}} = -1.5$ and $O_{\text{aRoll}} = -1.5$. Snapshots of the executed balancing motion during half the step cycle are presented in fig. 5.3(b). A slight inward angling of the legs, specified by offset parameters $O_{i,\text{hRoll}}$, $O_{i,\text{aRoll}}$, reduces the required amount of lateral displacement [188].

5.2.2 Flexion motion

Flexion motion is the second essential motion, and is meant to achieve vertical clearance for the feet, effectively marking the swing phase of the step. After a correct displacement of the body weight through the employment of the balancing motion, the swinging foot is unloaded and the flexion motion changes leg length by actuating on the three pitch joints: hip, knee and ankle (fig. 5.2:B). This motion is described at joint level as having a bell shaped curve, resulting in a smooth profile for the trajectory

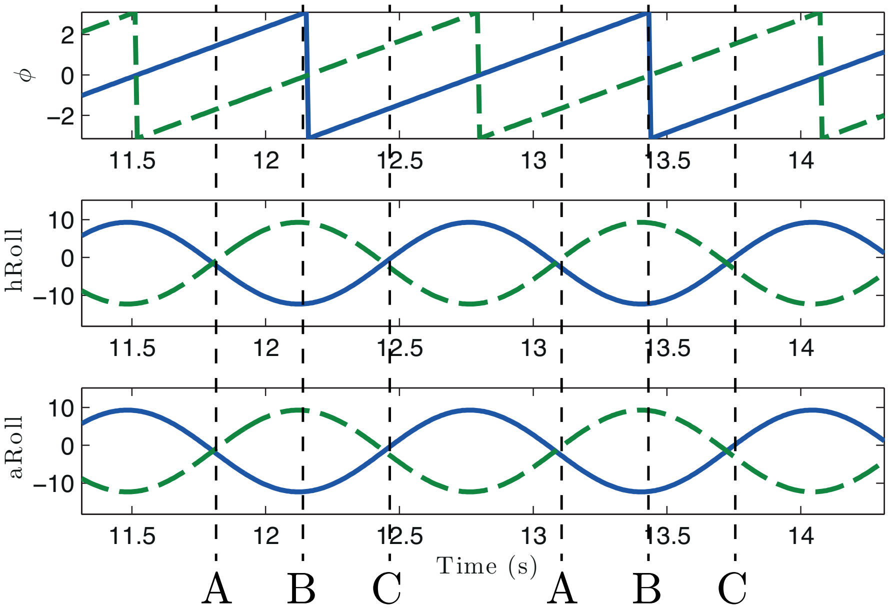

(a) Phase (top), hip (middle) and ankle roll (bottom) trajectories from the left (solid blue) and right (dashed green) CPGs.

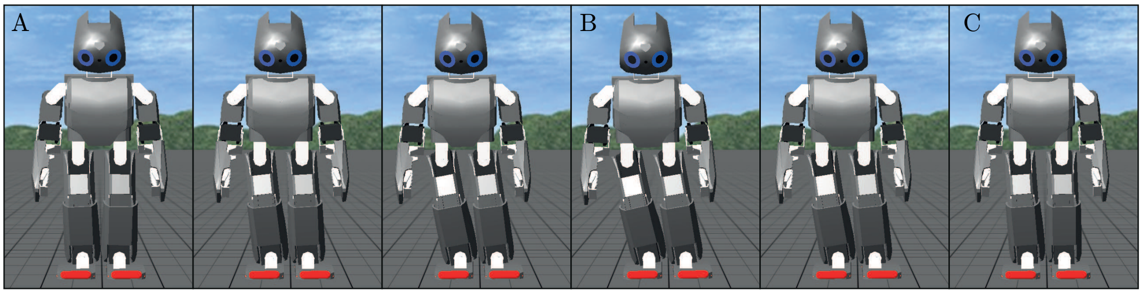

(b) Overall movement of the robot during half cycle of the balancing motion.

Figure 5.3: Balancing motion is applied to the hip roll (hRoll) and ankle roll joints (aRoll), displacing in the frontal plane the weight between the left and right feet. The balancing motion presented: $A_{\text{balancing}} = 11$, $O_{\text{hRoll}} = -1.5$, $O_{\text{aRoll}} = -1.5$.

of flexion. This is given in eq. (5.7) for hip, eq. (5.8) for knee, and eq. (5.9) for ankle.

$$f^{\text{flex}}_{\text{hPitch},i} = \frac{A_{\text{hip}}\dot{\phi}_i\phi_i}{\sigma^2} exp\left(-\frac{\phi_i^2}{2\sigma^2}\right) \tag{5.7}$$

$$f^{\text{flex}}_{\text{kPitch},i} = -\frac{A_{\text{knee}}\dot{\phi}_i\phi_i}{\sigma^2} exp\left(-\frac{\phi_i^2}{2\sigma^2}\right) \tag{5.8}$$

$$f^{\text{flex}}_{\text{aPitch},i} = -\left(f^{\text{flex}}_{\text{hPitch,i}} + f^{\text{flex}}_{\text{kPitch,i}}\right) \tag{5.9}$$

The amplitude of the flexion motion is specified by parameter A_{hip} for the hip and A_{knee} for the knee. This motion primitive in the ankle is the sum of the hip and knee flexion motions, imposing a parallel feet to the ground at all times.

The flexion motion is defined with phase shift of 0 rad, just as the balancing motion, centered at $\phi_i = 0$. It specifies the swing phase of the right leg when $\phi_{\text{L}} = 0$ and $\phi_{\text{R}} = \pi$, and the swing phase of the left leg when $\phi_{\text{L}} = \pi$ and $\phi_{\text{R}} = 0$.

Through the use of a bell-shaped profile, the joints perform a retracting movement only during a specified time frame, defining the swing phase. In order to achieve an overall swing phase of about 50% of the step cycle, the width of the flexion motion primitive should comprise the range $\left[-\frac{\pi}{2}, \frac{\pi}{2}\right]$, set by $\sigma = \frac{\pi}{6}$.

Fig. 5.4 demonstrates the final generated trajectories when applying the balancing motion to the roll joints and the flexion motion to all pitch joints, as well as the generated movement by the robot during the swing phase of the right leg.

5.2.3 Compass motion

The third essential motion is the compass motion, responsible for producing the propulsion of the body during locomotion. This motion moves the legs in the sagittal plane, alternately moving the contralateral legs forward and backward (fig. 5.2:E). It generates the forward steps in coordination with all the other motions, resulting in forward walking. This motion is described as sinusoidal profiles at the hip pitch and ankle pitch joints,

$$f^{\text{compass}}_{\text{hPitch},i} = -A_{\text{compass}}\dot{\phi}_i \sin\left(\phi_i + \frac{\pi}{2}\right) , \tag{5.10}$$

$$f^{\text{compass}}_{\text{aPitch},i} = -f^{\text{compass}}_{\text{hPitch},i} , \tag{5.11}$$

with amplitude A_{compass} and $\frac{\pi}{2}$ phase shift.

A phase shift of $\frac{\pi}{2}$ places the maximum excursion of the motion at the beginning and end of each swing phase. This results in the coordination between the transfer of the swing leg, and the propulsion of the stance leg, with the balancing and flexion motions.

The final trajectories that result when employing the compass motion, along with the balancing and flexion motions, are presented in fig. 5.5(a).

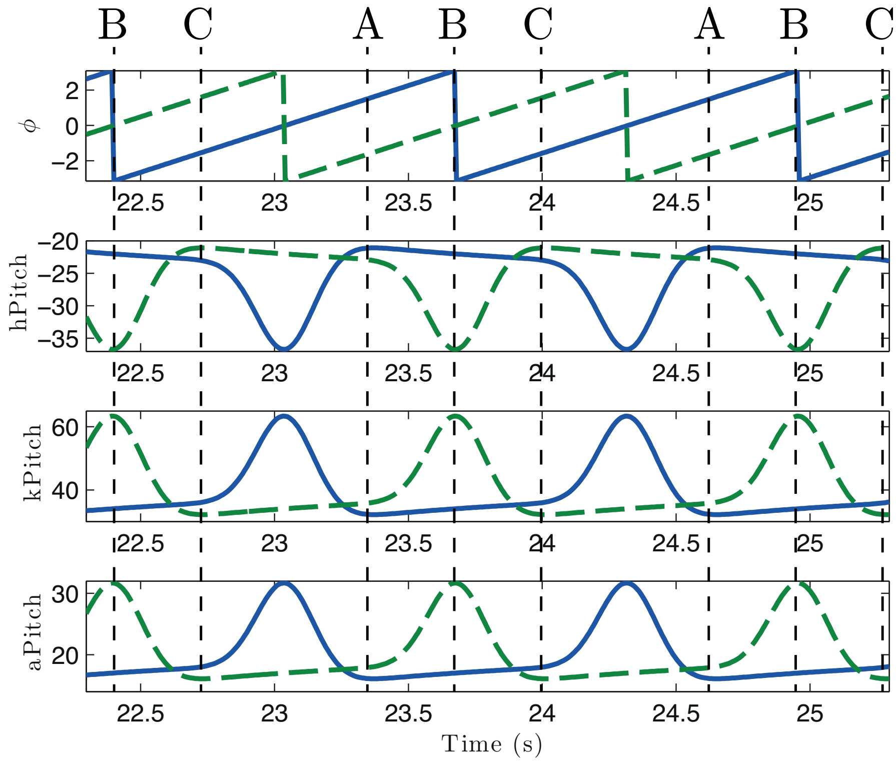

(a) Phase (top), hip pitch (2nd from top), knee pitch (3rd from top) and ankle roll (bottom) trajectories from the left (solid blue) and right (dashed green) CPGs.

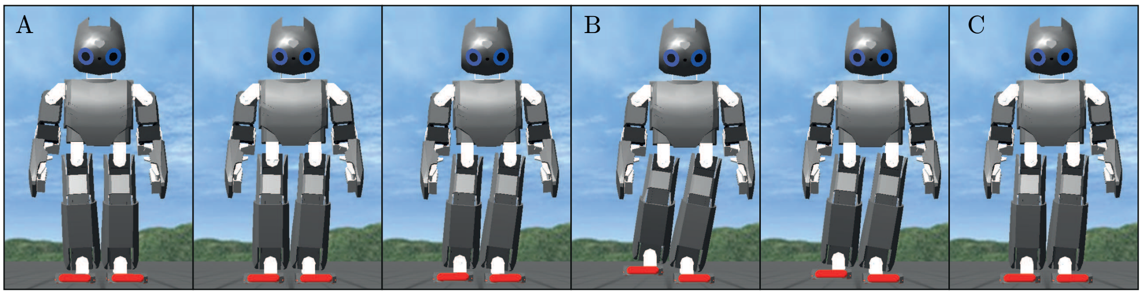

(b) Overall movement when applying the balancing and flexion motion during half the step cycle.

Figure 5.4: Flexion motion is applied to the hip pitch (hPitch), knee pitch (kPitch) and ankle pitch joints (aPitch), shortening the leg to increase foot clearance. The flexion motion presented: $A_{\text{hip}} = 15$, $A_{\text{knee}} = 30$, $O_{\text{hPitch}} = -25$, $O_{\text{kPitch}} = 40$ and $O_{\text{aPitch}} = 20$.

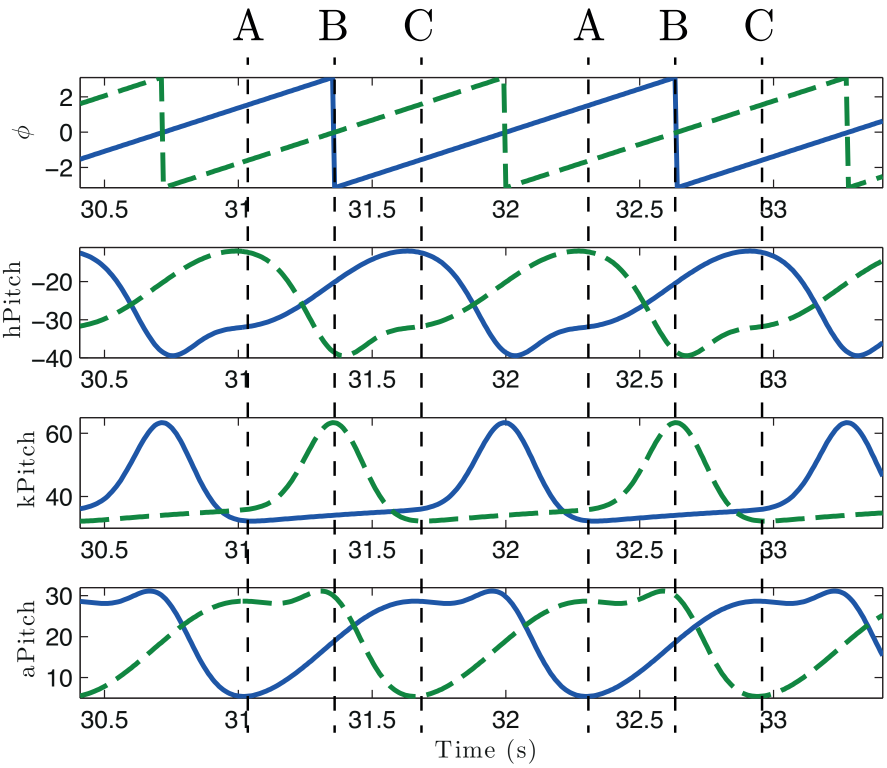

(a) Phase (top), hip pitch (2nd from top), knee pitch (3rd from top) and ankle roll (bottom) trajectories from the left (solid blue) and right (dashed green) CPGs.

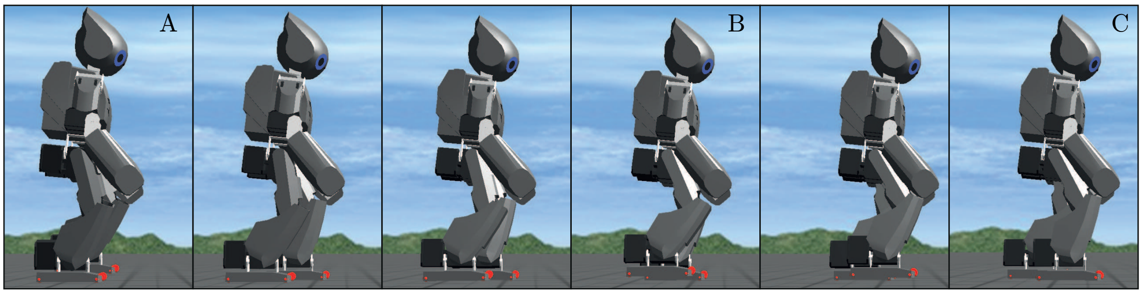

(b) Overall movement when applying the balancing, flexion and compass motions during half the step cycle.

Figure 5.5: Overall movement of the robot resulting from all the three motion primitives: balancing, flexion and compass motions. Compass motion is applied to the hip pitch (hPitch) and ankle pitch joints (aPitch). The compass motion presented: $A_{\text{compass}} = 11$, $O_{\text{hPitch}} = -25$, $O_{\text{kPitch}} = 40$ and $O_{\text{aPitch}} = 20$.

5.2.4 Turning motion

After having the robot able to walk forward, it is possible to achieve turning while walking. During the single support phase of the step cycle, if the robot twists by its vertical axis, the placement of the next stance foot will be pointing on the direction to turn. This turning can be achieved by employing a sinusoidal profile on the hip yaw joints of the robot, coordinated with the previous presented motions (fig. 5.6).

A single sinusoidal motion primitive,

$$f^{\text{turn}}_{\text{hYaw},i} = -A_{\text{turn}}\dot{\phi}_i \sin\left(\phi_i + \frac{\pi}{2}\right), \tag{5.12}$$

with a phase shift of $\frac{\pi}{2}$, acting on the robot's yaw joints can rotate the body by its vertical axis during the leg's support phase, proportionally to the modulated amplitude A_{turn}. Having the same phase shift as the compass motion, effectively synchronizes the turning motion with the compass motion.

5.2.5 Knee yielding motion

A characteristic of legged locomotion is the yield that occurs in the knee joint when the leg starts the stance phase and the body weight is passed onto it. As mentioned by Saunders [188] as the third determinant of walking, this flexion happens when the center of mass (COM) is passing its peak. Although shown to be more energy costly to maintain a flat COM during human walking [117], it may be beneficial in the used robotic platform to apply a small flexion on the knee joint during the stance phase, so the vertical trajectory of the COM of the walking robot is flattened.

This motion is added to the knee and ankle joints and is described by a sinusoidal profile of amplitude A_{yield} with π phase shift making the flexion occurring at middle of stance phase:

$$f^{\text{yield}}_{\text{kPitch},i} = A_{\text{yield}}\dot{\phi}_i \sin\left(\phi_i + \pi\right) \tag{5.13}$$

$$f^{\text{yield}}_{\text{kPitch},i} = -2A_{\text{yield}}\dot{\phi}_i \sin\left(\phi_i + \pi\right) \tag{5.14}$$

$$f^{\text{yield}}_{\text{aPitch},i} = -f^{\text{yield}}_{\text{hPitch},i} \tag{5.15}$$

5.2.6 Pelvis rotation motion

In level human walking the pelvis rotates alternately. Saunders et al. mention it as the first determinant of walking [188], flattening the vertical COM trajectory, as well as smoothing the inflections when changing the vertical direction of the COM.

Whether or not this motion will reduce vertical displacement of the COM, or will contribute to improve performance and stability, it has the ability of increasing the step length by twisting the body, placing the swinging foot further in front. This pelvic rotation is performed at the hip yaw joints, described as a sinusoidal trajectory

$$f^{\text{rotation}}_{\text{hYaw},i} = -A_{\text{rotation}}\dot{\phi}_i \sin\left(\phi_i + \frac{\pi}{2}\right), \tag{5.16}$$

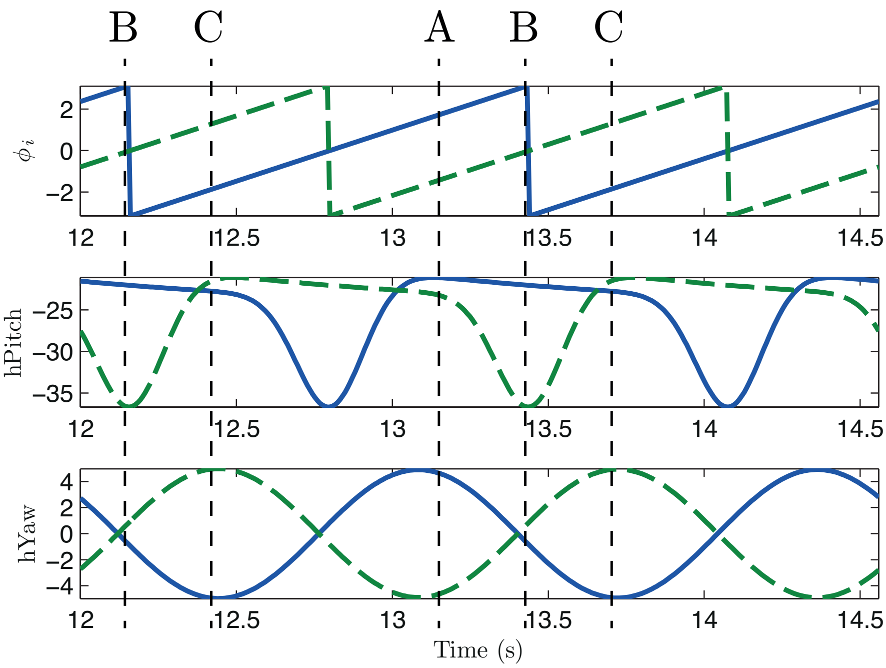

(a) Phase (top), hip pitch (middle) and hip yaw (bottom) trajectories from the left (solid blue) and right (dashed green) CPGs.

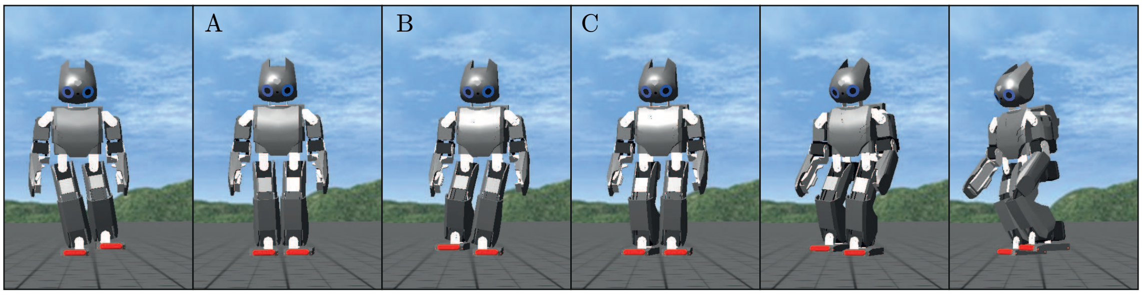

(b) Resulting robot movement when applying the balancing, flexion and turning motions.

Figure 5.6: Overall movement of the robot resulting from the three motion primitives: balancing, flexion and turning motions. The turning presented: $A_{\text{turning}} = -5$ and $O_{\text{hYaw}} = 0$. In panel (a) is observable in the generated trajectories the coordination between the joints. During the swing phase, here identified by the hip pitch flexion, the hip yaw rotates the robot in the vertical axis.

with amplitude A_{rotation} and $\frac{\pi}{2}$ phase shift.

A phase shift of $\frac{\pi}{2}$ anchors the maximum excursion of the rotation motion at the beginning and end of each swing phase, so the rotation motion happens only when one leg is on the ground, coordinated with the compass motion.

5.2.7 Motion summary

For the realization of goal-directed bipedal locomotion in flat terrain, only four motion primitives are strictly required: balancing motion, flexion motion, compass motion and turning motion. These four motion primitives can be considered the basic motor repertoire for bipedal locomotion, upon other motion primitives could be added. Other added motion primitives could be used to add new features to the walk or fine tune the performance, and toggling motion primitives can be used to alternate between locomotor behaviors.

A summary of the proposed CPG and motions primitives is presented:

$$\dot{\phi}_i = \omega + k \sin\left(\phi_i - \phi_o + \pi\right), \tag{5.17}$$

$$\dot{z}_{\text{hRoll},i} = -\alpha(z_{\text{hRoll},i} - O_{\text{hRoll}}) + f_{\text{hRoll}}^{\text{balancing}}, \tag{5.18}$$

$$\dot{z}_{\text{aRoll},i} = -\alpha(z_{\text{aRoll},i} - O_{\text{aRoll}}) + f_{\text{aRoll}}^{\text{balancing}}, \tag{5.19}$$

$$\dot{z}_{\text{hYaw},i} = -\alpha(z_{\text{hYaw},i} - O_{\text{hYaw}}) + f_{\text{hYaw}}^{\text{rotation}} + f_{\text{hYaw}}^{\text{turn}}, \tag{5.20}$$

$$\dot{z}_{\text{hPitch},i} = -\alpha(z_{\text{hPitch},i} - O_{\text{hPitch}}) + f_{\text{hPitch}}^{\text{flex}} + f_{\text{hPitch}}^{\text{yield}} + f_{\text{hPitch}}^{\text{compass}}, \tag{5.21}$$

$$\dot{z}_{\text{kPitch},i} = -\alpha(z_{\text{kPitch},i} - O_{\text{kPitch}}) + f_{\text{kPitch}}^{\text{flex}} + f_{\text{kPitch}}^{\text{yield}}, \tag{5.22}$$

$$\dot{z}_{\text{aPitch},i} = -\alpha(z_{\text{aPitch},i} - O_{\text{aPitch}}) + f_{\text{aPitch}}^{\text{flex}} + f_{\text{aPitch}}^{\text{yield}} + f_{\text{aPitch}}^{\text{compass}}. \tag{5.23}$$

A correct tuning of parameters is necessary for achieving bipedal walking in the robot. This parametrization is performed by sequentially and incrementally tuning and adding each motion primitive in sequence by trial-and-error, as detailed in the next section.

5.2.8 Other locomotor behaviors

The proposed system allows the achievement of other locomotor behaviors in a scalable manner through the manipulation of motion primitives. The method for addressing other locomotor behaviors and gait modulation in the proposed framework is to: 1) perform parameter modulation of already defined motion primitives; 2) toggling between primitives or defining new ones to fulfill the required locomotor ability.

Parameter modulation With parameter modulation, quantitative changes are imposed in the already established motions, which is quite useful for achieving a smooth continuous locomotor diversity. For instance, smooth variation of forward velocity can be achieved by adjusting the amplitude of the compass motion. The modulation of the same parameter, the amplitude of the compass motion, if set to a negative value will result in backwards walking.

Primitive selection Providing new locomotor abilities for the robot can be a matter of adding new motion primitives and toggling between the available set of motion primitives, selecting the appropriate ones to achieve the desired locomotor task. For instance, achieving goal directed walking is a matter of activating the correct primitives, toggling the activity of the turning motion.

In order to achieve other more complex behaviors, one could resort to mechanisms of developmental robotics, such as evolutionary or learning algorithms.

5.3 Bipedal walking demonstrations

In this section the adequacy of the system to produce walking behaviors for different robots in simulation is demonstrated, as well as the deployment on a real robot.

Initially is demonstrated the proceedings on how to tune the motion primitive's parameters, and how to sequentially pursue a basic walk. Then the results from the walking robot are presented, accomplishing several locomotor behaviors, such as walking forwards and backwards, and turning. After, a comparison of CPG walking and ZMP walking in simulation is presented, and results compared in matters of performance and stability.

The robot used in the demonstrations is the DARwIn-OP by ROBOTIS [73], a small open-platform humanoid with 20 DOFs, using digital position controlled servos, measuring 45.5 cm and weighting 2.9 kg. It includes a built-in computer equipped with 1.6 GHz Intel Atom Z530 (32 bit), 1GB RAM and on-board 4GB flash SSD. The robot's body is equipped with a 3-axis gyro, a 3-axis accelerometer and each foot is equipped with four force sensing resistors (FSR) distributed through the four corners. The DARwIn-OP humanoid presents a common configuration for the DOF to other humanoid robots.

A simulated model of the robot is used in the Webots, using ODE physics simulator, to perform preliminary tests and validations before transferring the solution to the real robot.

5.3.1 Motion primitive parametrization

A few simple steps are taken to find adequate amplitude parameters for the motion primitives, following a sequential procedure by trial-and-error in a short number of tries.

The robot starts upright, stopped on its feet, with all motion primitives disabled (amplitudes zeroed). First, joint offsets are chosen to find a correct posture for the robot. Usually for this type of biped robots, legs are maintained flexed, in a posture that allows for feet placement at the onset of swing and onset of stance, without reaching singularities. Offsets for the hip, knee and ankle pitch joints are assigned in a fashion to achieve this posture and a pre-determined leg length. Table 5.1 presents the chosen offsets that specify the general posture of the robot. Legs are pointing inward in the frontal plane by setting symmetrical offset values for the hip and ankle roll joints. Offsets for the hip, knee and ankle joints are assigned to achieve a flexed leg posture, with a slight forward body tilt.

After achieving an acceptable body posture, the balancing motion is parameterized by choosing an adequate amplitude that results in a movement transferring the COM over the two feet alternately. Having the correct alternate displacement of the COM, the stepping movements can be executed by

Table 5.1: Joint's offsets to maintain upright posture.

Offset	$(^\circ)$
O_{hYaw}	0
O_{hRoll}	1.5
O_{hPitch}	-25
O_{kPitch}	40
O_{aPitch}	20
O_{aRoll}	-1.5

choosing the amplitudes for the flexing motion primitives. Now, the forward progression resulting from the walk depends only on the step length, which is dependent on the compass motion amplitude.

Parametrization of the motion primitives is not critical, nor necessarily detailed. Due to the nature of the synergistic approach, the influences to the final trajectory from the preceding parameterized motion primitives are not clear. The used motion primitives are coarse kinematic descriptors, and especially when combined, the final achieved kinematic and dynamic behavior is difficult to anticipate. It is therefore difficult to pursue more detailed locomotion and a better performance. Following the described steps ensures that the resulting movements from the overall motion primitives will produce a successful walk.

Balancing motion parameters

The role of this motion is to displace the COM away from the swing foot. Finding a suitable amplitude value for the balancing is a matter of increasing the amplitude until the displacement of the body weight is directly above the support feet, which can be visual inspected and further tuned by the readings from the COP measured at the robot's feet.

Fig. 5.7 shows the trajectories produced for the hip and ankle roll joints, and the resulting ground reaction force on each foot. For different amplitudes of balancing, different degrees of displacement are achieved. The greater the $A_{\text{balancing}}$ value the greater the displacement and the weight transfer, as shown in fig. 5.7(a) for $A_{\text{balancing}} = 11$ and fig. 5.7(b) for $A_{\text{balancing}} = 14$. At maximum excursion it is possible to observe a greater weight release from one foot to the other. With $A_{\text{balancing}} = 11$ the maximum supported weight in the stance leg is 23.4 N and in the swing leg is 6.7 N, and for $A_{\text{balancing}} = 14$ is 26.7 N in the stance leg and 3.6 N in the swing leg.

This effect is better observed from the COP readings in fig. 5.8, showing the COP is transferred to the center of the foot when $A_{\text{balancing}} = 14$, while when $A_{\text{balancing}} = 11$ the COP does not reach the center of the foot. Also, if balancing amplitude is too large, the weight will be displaced beyond the foot's outer edge and the COP will leave a valid support region.

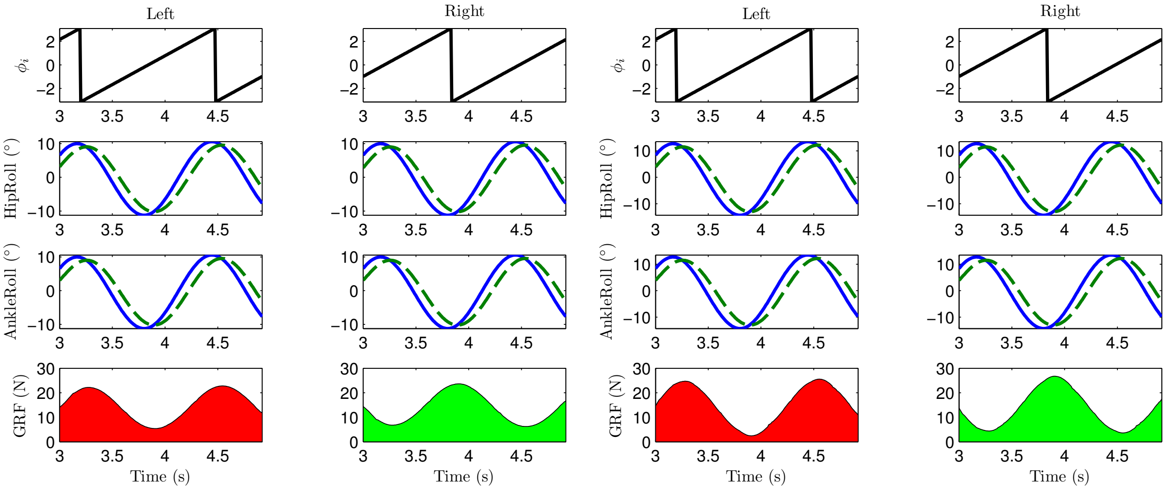

(a) $A_{\text{balancing}} = 11$ (b) $A_{\text{balancing}} = 14$

Figure 5.7: Trajectories generated (solid blue), performed joint position (dashed green) and the resulting ground reaction forces (GRF) for the left and right legs. The balancing motion with $A_{\text{balancing}} = 14$ achieves a greater release of the weight at the maximum excursion.

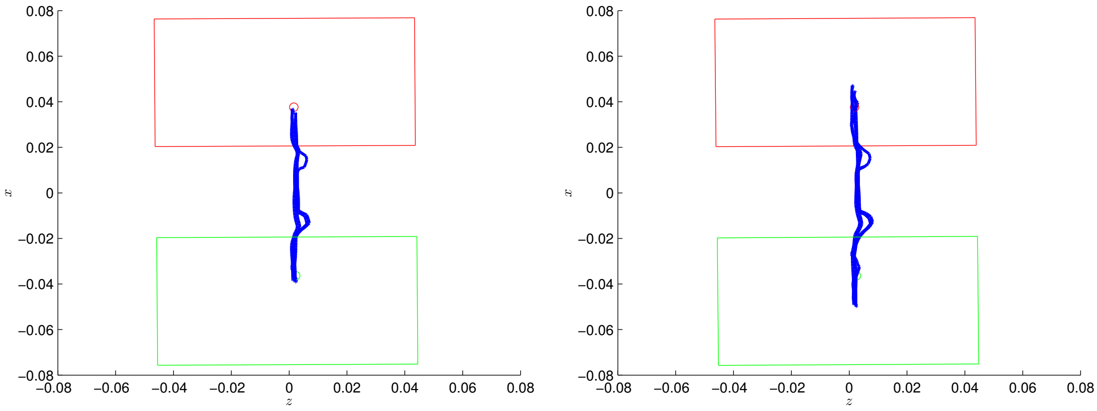

(a) $A_{\text{balancing}} = 11$ (b) $A_{\text{balancing}} = 14$

Figure 5.8: Progression of the COP during the balancing motion. Red rectangle represents the left foot, and the green rectangle the right foot as seen from the top. The balancing motion with $A_{\text{balancing}} = 14$ achieves a closer displacement of the COP to the center of the feet.

Flexion motion parameters

The shortening of the leg, preparing for the execution of the swing phase, is achieved by the flexion motion primitive. Fig. 5.4(b) shows the resulting movement of the robot when the balancing and flexion motion primitives are employed. The robot displaces the weight over the supporting foot, allowing for flexion of the contralateral leg.

The generated trajectories from the application of this flexion motion are presented in fig. 5.9, as well as the resulting foot vertical clearance achieved by the robot's feet. This achieved vertical clearance can be controlled by the amplitudes used in the motion, A_{hip} and A_{knee}. In this example amplitudes are set to $A_{\text{hip}} = 15$ and $A_{\text{knee}} = 30$. From the force sensor readings in the feet it is possible to conclude that the weight is successfully supported alternately (bottom in fig. 5.9).

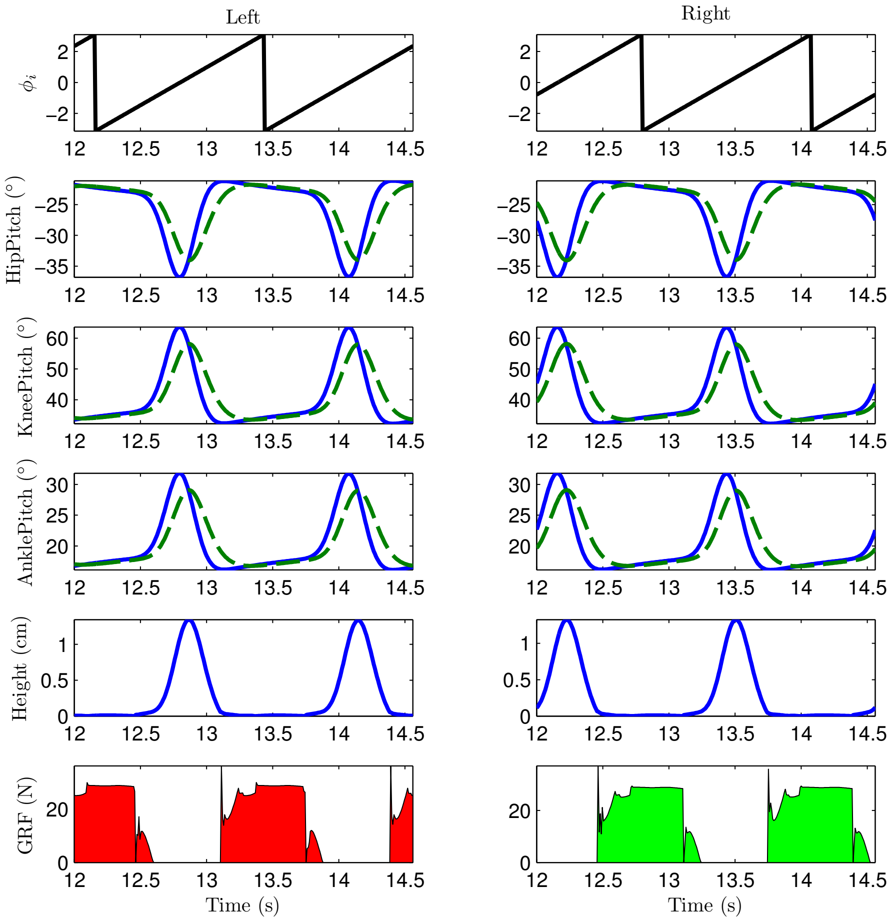

Figure 5.9: Trajectories generated (solid blue), performed joint position (dashed green), the resulting foot height and ground reaction forces (GRF) for the left and right legs. The flexion motion with $A_{\text{hip}} = 15$, $A_{\text{knee}} = 30$ achieves a ground clearance around 1.5 cm.

Compass motion parameters

The final motion required for a complete walk is the compass motion. The robot is already able to step in place, missing only the propulsive action to walk. Compass motion achieves this propulsive action, parameterized in amplitude by A_{compass}, which directly influences the step length. The greater the amplitude, the greater the step length and therefore the achieved velocity. This motion accepts a range of values for the amplitude, starting from deactivation by setting $A_{\text{compass}} = 0$, to a upper limit value that the robot no longer can perform the walk without falling. In the current configuration using the previously defined offsets and motion's amplitudes (tables 5.1 and 5.2), the upper limit was found to be $A_{\text{compass}} = 13.7$ when applying the previously chosen parameters.

Table 5.2: Motion's amplitudes.

Amplitude	$(^\circ)$
$A_{\text{balancing}}$	11
A_{hip}	15
A_{knee}	30
A_{compass}	$[0, 13.7]$
$\omega(\text{rad.s}^{-1})$	4.9087

The different step lengths performed by the robot when using different values are evident in fig. 5.10. When walking with $A_{\text{compass}} = 6$ the robot achieves a step length of 3.26 cm, and when walking with $A_{\text{compass}} = 11$ achieves a step length of 6.0 cm.

An almost linear relationship between the compass motion amplitude and the achieved walking velocity was found on the current configuration, as shown in fig. 5.11. The robot was made to walk forward with different A_{compass} values, with increments of 0.1 for each eight steps, and the velocity achieved at each step was recorded. Fig. 5.11(a) presents the mean achieved velocity for all steps for a given A_{compass} value, and fig. 5.11(b) presents the performed step length. In the bottom panels is possible to take a closer look at the mean values and the standard deviation at the higher values of A_{compass}. As the robot approaches the upper limit of A_{compass}, the measured velocity and step length present a greater variation, evidencing an increase in instability, just before falling for $A_{\text{compass}} > 13.7$.

Turning motion parameters

The robot would be able to navigate its environment if a controller changed the motion primitives' parameters. It was shown that the forward walking velocity has a relationship with the compass motion amplitude. Here it is evidenced that the turning velocity of the robot also has a relationship with the turning motion amplitude.

A set of simulations are performed, where the robot walks with the offsets from tab. 5.1, the amplitudes from tab. 5.2 with $A_{\text{compass}} = 8$, and a set of A_{turn} values: $\{0, 1, 2, 3, 4, 5, 6, 7\}$. Fig. 5.12

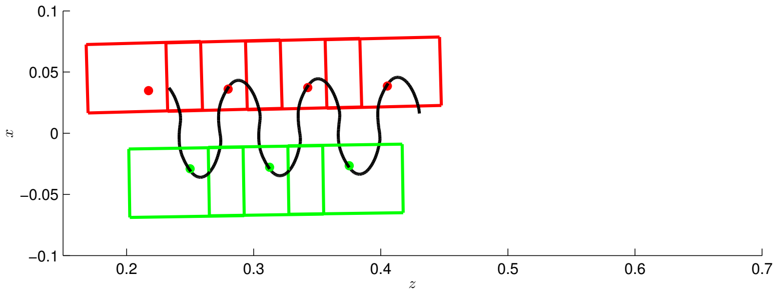

(a) $A_{\mathrm{compass}} = 6$

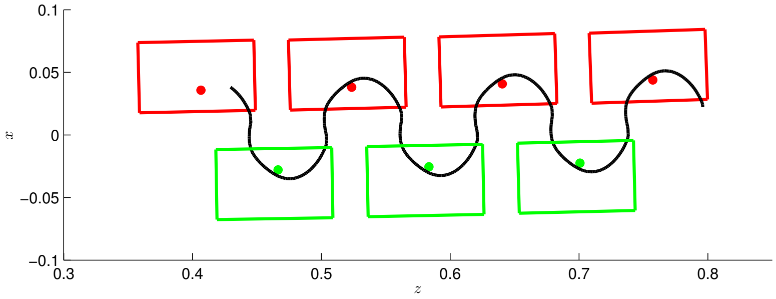

(b) $A_{\mathrm{compass}} = 11$

Figure 5.10: Feet placements when walking with two distinct values, left foot is red and right foot green, as seen from above. The trajectory of the COM (black line) throughout the walk. The achieved step lengths are influenced by A_{compass} value. Walking with $A_{\mathrm{compass}} = 6$ it achieves a step length of 3.26 cm, and achieves a step length of 6.0 cm when using $A_{\mathrm{compass}} = 11$.

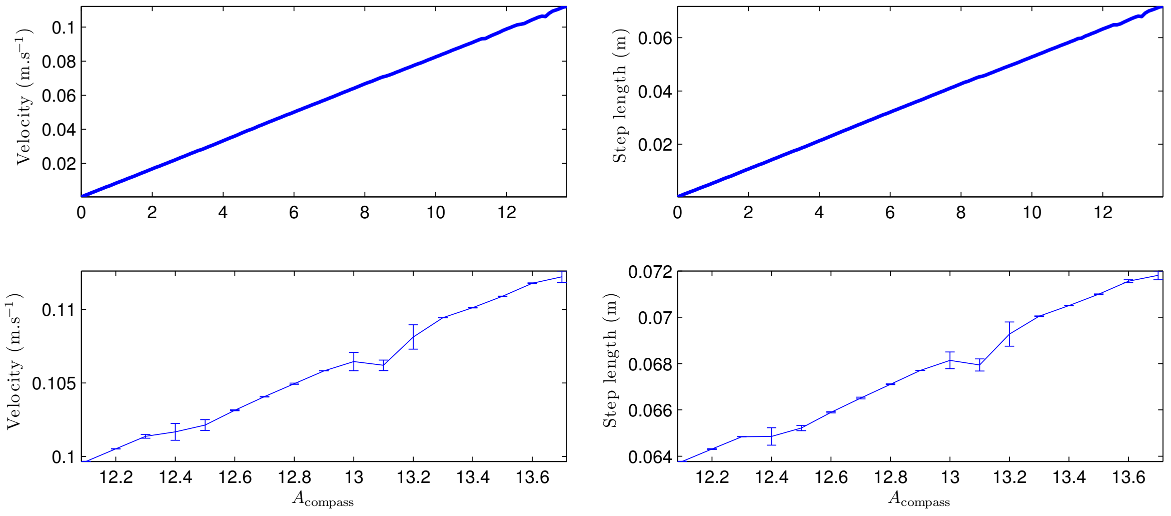

(a) Achieved velocity.

(b) Performed step length.

Figure 5.11: In the presented posture and parametrization, the achieved velocity and the performed step length can be approximated by a linear relationship with A_{compass}. The velocity is calculated for each performed step, and the mean is presented. In the bottom panels is observable the deviation from a linear relationship as the value of A_{compass} reaches the upper limit. Evidence of the robot reaching instability.

illustrate the paths taken by the robot using these eight amplitude values. It demonstrates that there is a relationship between A_{turn} and the achieved angular velocity, and that there is an upper limit for the A_{turn}. In the right panels is observable the increase in instability when changing from $A_{\text{turn}} = 6$ to $A_{\text{turn}} = 7$, suggesting either that the chosen motion primitives are not adequate for performing tighter curves, or the value of A_{turn} is not adequate for the current CPG configuration, i.e. the chosen offsets and other motion primitives.

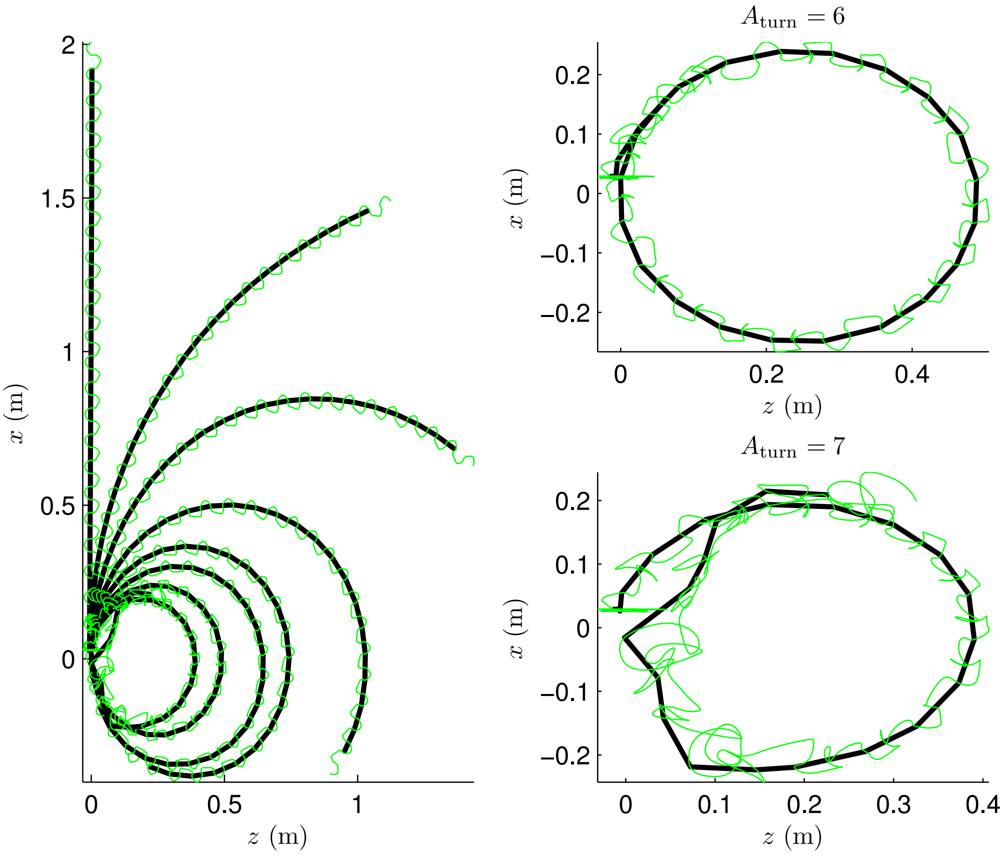

Figure 5.12: Top-down view of world and the paths (black line) performed by the robot while walking with the previously defined configuration, using 8 values for A_{turn}, $\{0, 1, 2, 3, 4, 5, 6, 7\}$ (left panel), and isolated views for $A_{\text{turn}} = 6$ (top right) and $A_{\text{turn}} = 7$ (bottom right). The green line represents the path of the COM. The bottom right panel shows that the combination of $A_{\text{compass}} = 8$ and $A_{\text{turn}} = 7$ is on the limit of stability.

The mean angular velocities for twenty steps are presented in fig. 5.13, along with the standard deviation between steps. For $A_{\text{turn}} > 6$ there is an increase on the variance of the achieved angular velocity at each step, caused by a decrease in walking stability.

In these demonstrations was shown that by controlling the motion primitive's parameters, certain characteristics of biped walking can be controlled. The magnitude of lateral displacement of the body is controlled by the $A_{\text{balancing}}$ parameter, which in turn influences the displacement of the COP in the frontal plane. Foot clearance during the swing phase depends on the leg flexion, which is mainly

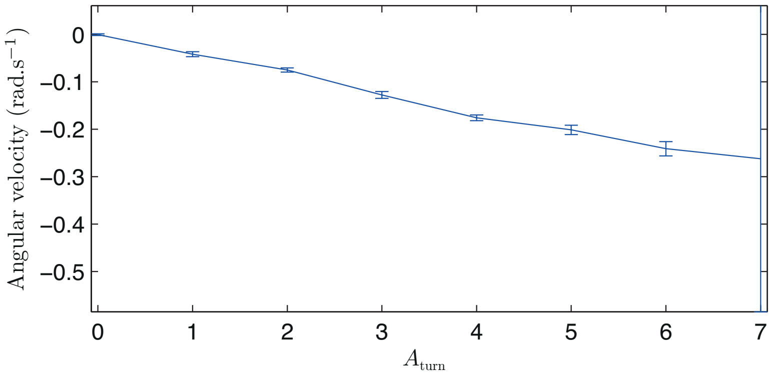

Figure 5.13: Achieved angular velocity when applying different A_{turn}. The applicable range values for A_{turn} is highly dependent on the chosen offsets, on the employed motion primitives and on the chosen motion's parameters. In the presented tests, applying $A_{\text{turn}} > 6$ exhibits a greater variation in the achieved angular velocity at each step, and also an increase in instability.

generated by the flexion motion, parameterized by A_{hip} and A_{knee}. The compass motion parameter, A_{compass} influences directly the performed step length while walking, as well as walking direction accordingly to $\text{sign}\left(A_{\text{compass}}\right)$. The angular velocity of the robot is directly controlled by A_{turn} from the turning motion.

5.3.2 Forward walking

As in simulations, the real DARwIn-OP robot walks successfully in flat terrain after a short parametrization of motions. Parameters for forward walking are presented in tab. 5.3.

Table 5.3: Parameters for the real DARwIn-OP

Amplitude	(°)	Offset	(°)
$A_{\text{balancing}}$	10	O_{hYaw}	0
A_{hip}	20	O_{hRoll}	1
A_{knee}	40	O_{hPitch}	-30
A_{yield}	2	O_{kPitch}	40
A_{rotation}	10	O_{aRoll}	-1
A_{compass}	9	O_{aPitch}	20
ω(rad.s^{-1})	5.236	k	1

Fig. 5.14 depicts the forward walking behavior of the robot through snapshots from the video recording[1].

Recorded joint trajectories and resulting ground reaction forces are presented in fig. 5.15. The robot walks forward successfully. However it should be noted that despite the strict symmetry in the

---

[1] Available at `http://asbg.dei.uminho.pt/user/1`.

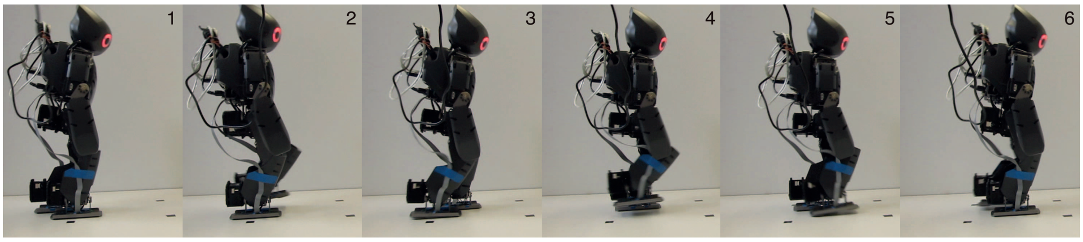

Figure 5.14: Snapshots of video recording of the DARwIn-OP robot walking forward.

generation of walking motions, the resulting walking behavior is not entirely symmetric, as seen from the foot force readings, and the performed joint trajectories (green).

The resultant foot force profiles are dissimilar between the left and right leg. Despite the striking on the ground with the outside first, the weight distribution is different throughout the step cycle, and presents different duty factors, 0.8 for the left leg and 0.72 for the right leg.

Joint trajectories are generally tracked by the servo's low-level PD controllers with a slight delay. However, in the hPitch joint at the foot strike instant it is observed the highest deviation from the reference trajectory.

5.3.3 Turning

Achieving turning is just a matter of modulating the amplitude of the turning motion, independently of what other motions the robot is performing. If the robot is stepping in place, the robot turns in place. If it is walking forward, the robot turns while walking, performing a circular path. Fig. 5.16 presents snapshots from the robot walking and steering left[1].

The performed trajectories are alike the trajectories for forward walking, excepting the trajectories produced for the hYaw joints, due to the employed turning motion primitive of $A_{\mathrm{turn}} = 5$. The resulting ground reaction forces are also similar to the ones recorded during forward walking (fig. 5.17).

5.3.4 Ball following

A simple ball following scenario was devised to demonstrate the ability of the system to produce goal-directed walking through simple parameter modulation (fig. 5.18)[1]. This scenario serves only as a demonstration of the accomplishment of locomotor behaviors, and does not strive for an accurate tracking or a robust solution. The robot detects a colored ball using its built-in head camera, maintaining its gaze directed at the ball, using a simple PID control loop to keep the detected ball in the center of the image. Goal-oriented walking is then controlled through the gaze of the robot, through simple parameter modulation:

- A_{compass} is kept proportional to the vertical angle of the head, controlling the forward velocity of the robot. If the gaze at horizon level, $A_{\mathrm{compass}} = 12$, if its located down at the feet, $A_{\mathrm{compass}} = 0$.

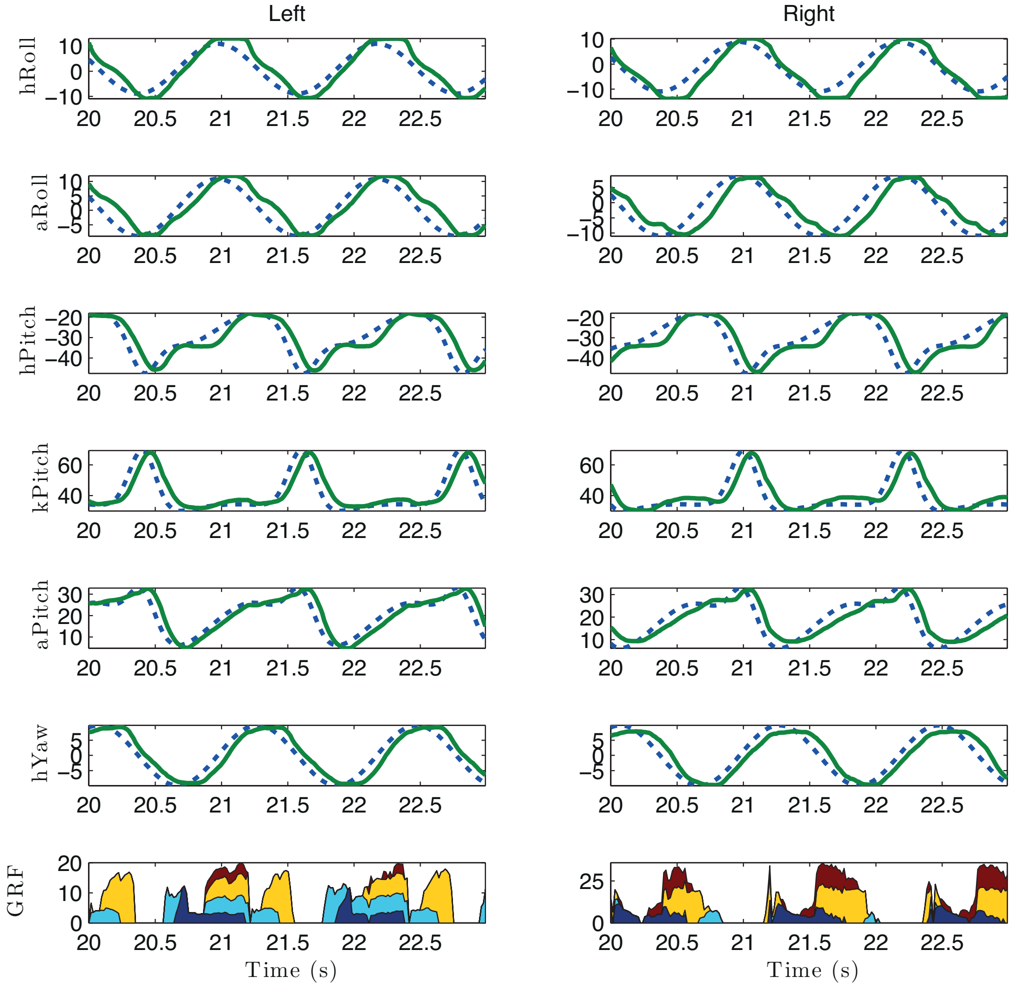

Figure 5.15: Reference trajectories for forward walking as output from the proposed CPG (dashed blue) and the performed joint motions (solid green). Ground reaction forces as read from foot force sensors. Blue: front left; red: front right; yellow: back left; cyan: back right.

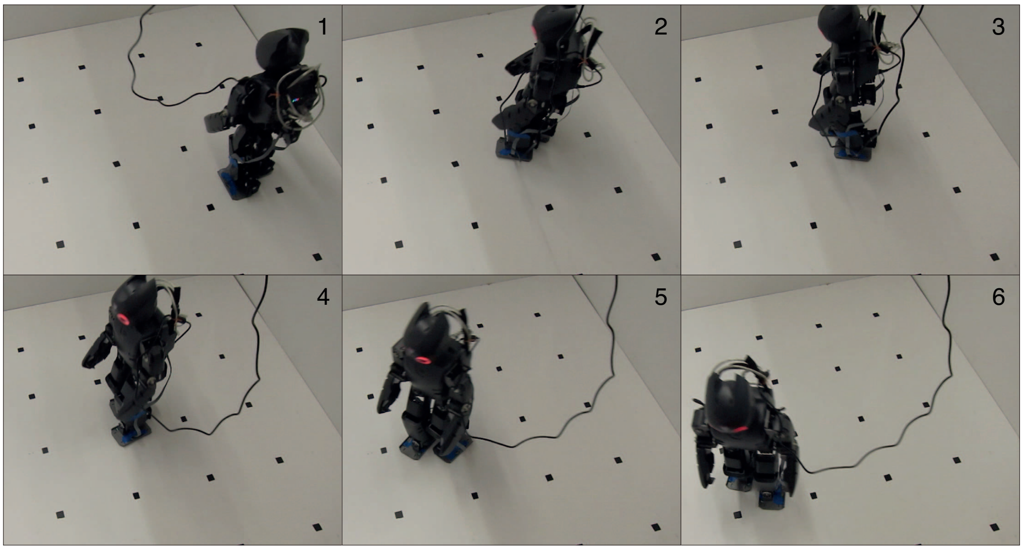

Figure 5.16: DARwIn-OP steering left. Walking behavior defined by parameters in table 5.3 and $A_{\text{turn}} = 5$.

- A_{turn} is modulated in proportion to the lateral gaze, controlling turning velocity. If the robot looks $\frac{\pi}{2}$ to the left or to the right, $A_{\text{turn}} = [-15, 15]$.

In fig. 5.19 are depicted the joint motions during three time intervals, where is possible to observe the role of the modulation of the motion primitives. The leftmost time interval is depicted in snapshots 1 and 2 (fig. 5.18), when the robot walks right almost in a 90° turn. It is observable in the hYaw joint that the turning motion has increased its amplitude (A_{turn}) to perform the turn. A slight turn to the left happens depicted in snapshots 3 and 4, resulting in an opposite amplitude of A_{turn}, as presented in hYaw trajectory, in the middle time interval. The rightmost time interval is depicted in snapshot 7, where the robot is close to the ball and therefore it reduces its walking velocity by reducing A_{compass} close to zero. The influence of the compass motion primitive in the whole trajectory is observable on the hPitch and aPitch joints.

5.3.5 Comparison with ZMP walking

From an engineering perspective it makes sense to directly compare different solutions which aim to solve the same problem in the same application platform, as a means to choose the most cost effective and the best performer. In the case of robot biped locomotion, the typical approach is to employ a ZMP based method for the generation of walking motions. Both ZMP and CPG solutions aim to solve the problem of generating the reference joint trajectories to achieve biped locomotion, applicable to the generation of a stable walk for a high-gain position controlled biped robot, allowing a direct comparison in terms of performance and cost of implementation. Both solutions produce the position for the joint space vector in real-time, open-loop implementations, with the only difference being how these two implementations reach the value for the joint space vector at a given time.

The ZMP is a popular and widely used method in humanoid robotics for the design of walking

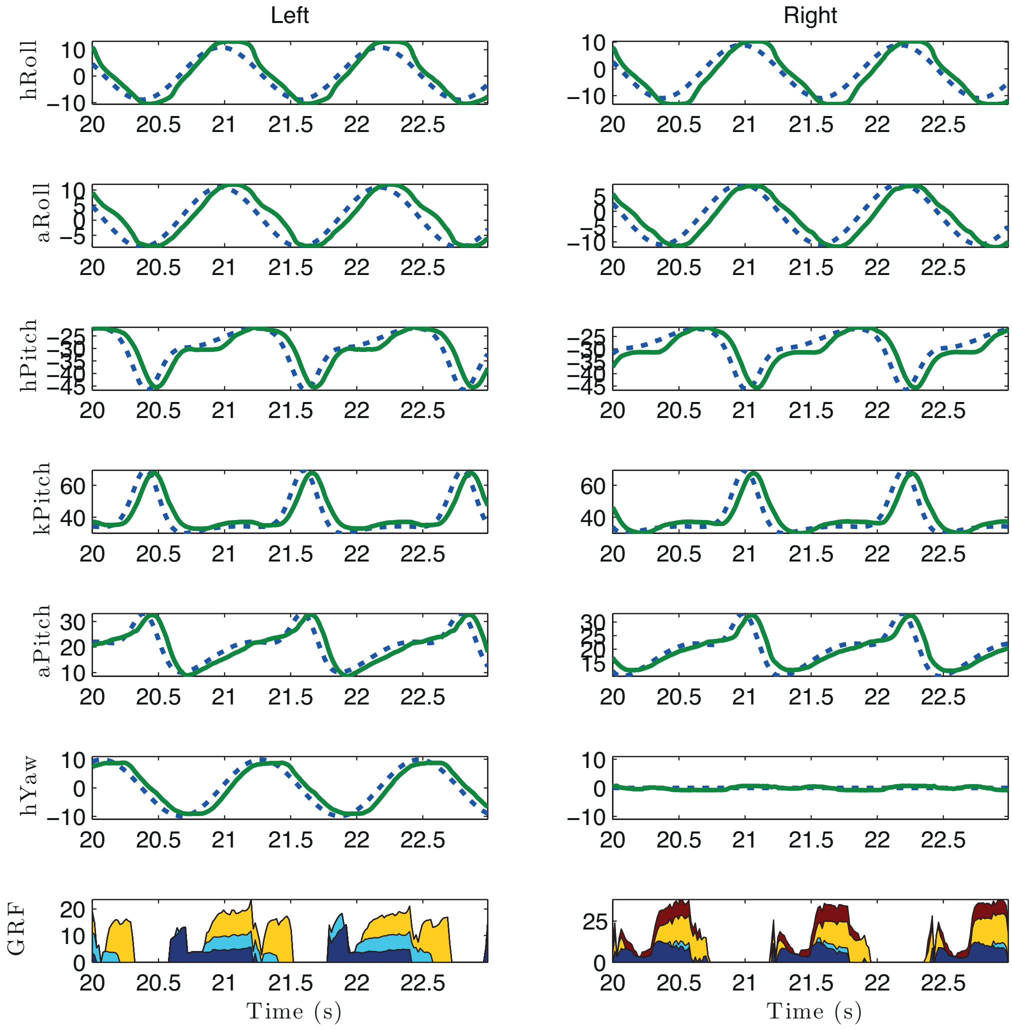

Figure 5.17: Reference trajectories for walking left (dashed blue) and the performed joint motions (solid green). Ground reaction forces as read from foot force sensors. Blue: front left; red: front right; yellow: back left; cyan: back right.

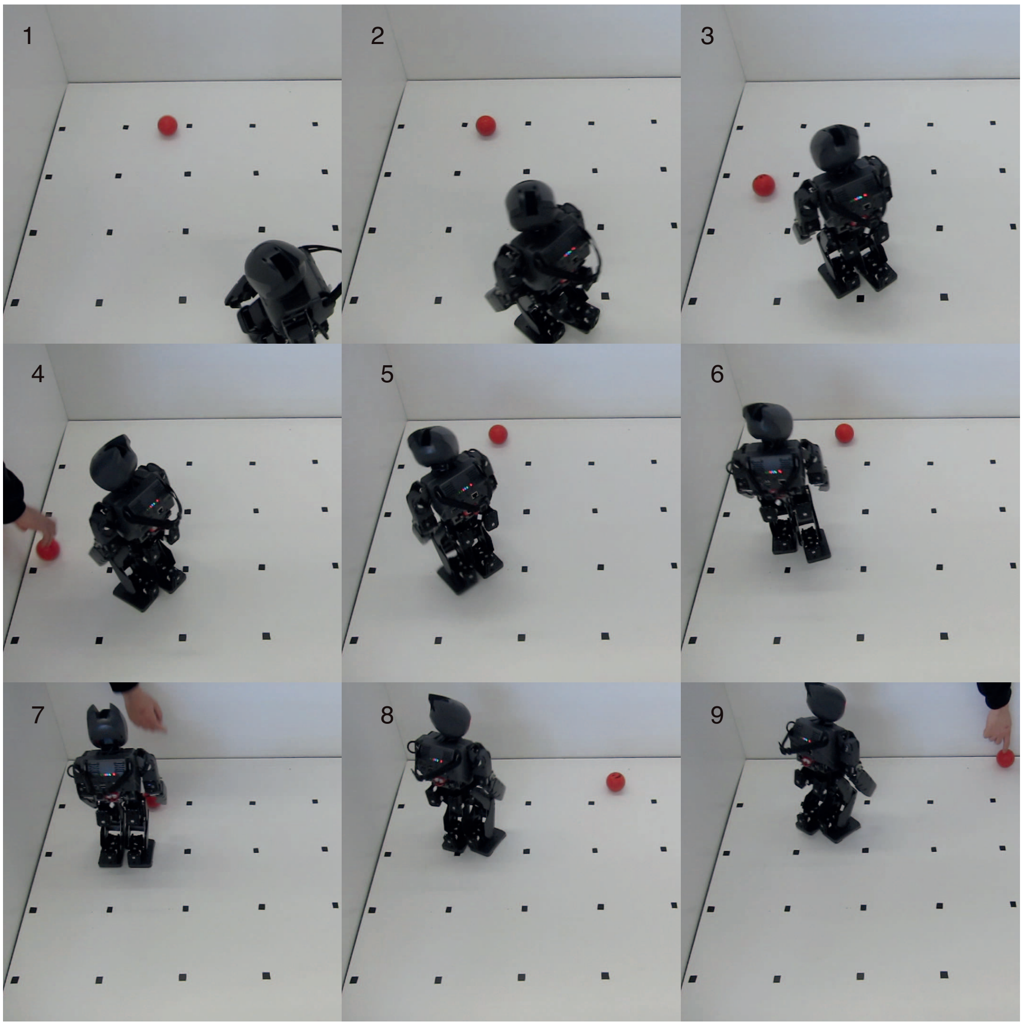

Figure 5.18: Snapshots from ball following scenario. The robot’s gaze towards the ball directs the walking, through simple parameter modulation.

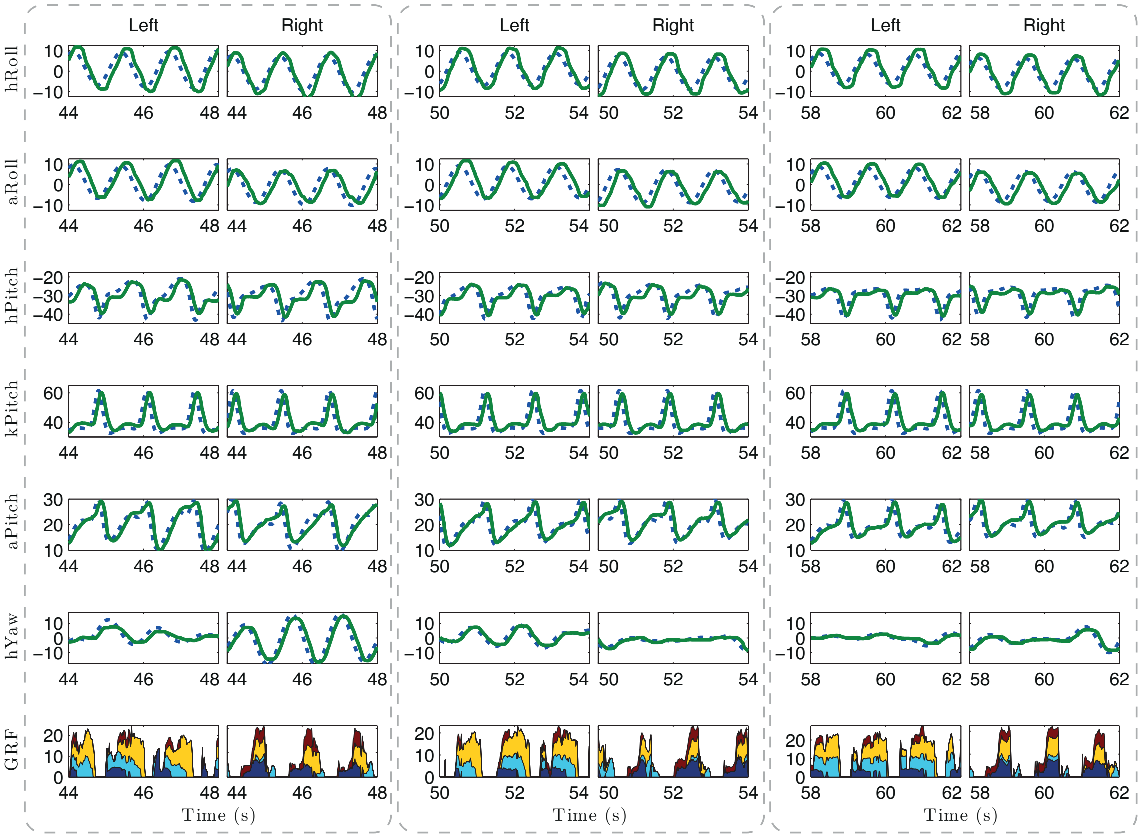

Figure 5.19: Three time intervals from the ball following scenario (fig. 5.18) and the resulting joint trajectories and ground reaction forces. Leftmost: 1 and 2, the robot turns right. Middle: 3 and 4, the robot turns slightly to the left. Rightmost: 7, the robot walks forward towards the ball and reduces greatly the velocity.

generators, with many contributions that furthered its study and resulted in subsequent improved locomotion abilities [226], such as omnidirectional walking, walking on ramps, climbing stairs and obstacle negotiation.

In this comparison the implemented walking generator is based on ZMP method and on the work for a NAO robot [70]. This walking generator relies on 1) desired body motion, 2) a stepping planner, 3) ZMP criterion, 4) inverse kinematical model. Given a desired translational and rotational velocity for the body, a planner computes the foot placement before each step, which will achieve the desired motion. The motion of the body is adjusted to satisfy the ZMP criterion on the planned foot placements, using a dynamical representation of a biped simplified model. The final step is the computation of the joint positions, using the inverse kinematic model of the robot, to perform the footsteps and the correct ZMP body motion.

For the comparison, the tests were performed in the Webots simulator and the same assumptions are made in regards to the two solutions: the ground is flat, the robot walks unperturbed and both solutions achieve very similar locomotion characteristics:

- Step period, 1.28 s
- Duty factor, ≈ 0.6
- Sagittal step size, ≈ 0.057 m
- Lateral foot placement, ≈ 0.032 m
- Walk velocity, $\approx 0.085\ \mathrm{m.s^{-1}}$
- Body height and posture, 0.29 m and 7° forward pitch

To achieve these similar characteristics for both solutions, the CPG approach was first parameterized to achieve the upper limit in walk velocity. The footstep planner used in the ZMP solution was parameterized in order to exhibit the same achieved locomotion characteristics as the CPG approach. The parameters used in the CPGs are presented in table 5.4.

Table 5.4: Parameters for straight walking.

Amplitude	(°)	Offset	(°)
$A_{\text{balancing}}$	14	O_{hYaw}	0
A_{hip}	15	O_{hRoll}	1.5
A_{knee}	30	O_{hPitch}	-25
A_{yield}	0	O_{kPitch}	40
A_{rotation}	0	O_{aRoll}	-1.5
A_{compass}	11	O_{aPitch}	20
$\omega(\mathrm{rad.s^{-1}})$	4.9087	k	1

Visually inspecting both solutions yields the conclusion that both walks are successful, and the achieved walking characteristics are very similar, only a more detailed analysis can shed some information on the difference in performance between both solutions. It will be analyzed and compared the difference in the generated trajectories, the resulting COP throughout the walk, the ground reaction forces and the body oscillations.

Computational time The first difference between the two approaches is the computation time required for calculating a solution at each computation cycle of the robot. The difference in the required time to compute the solutions, in a modern laptop equipped with an Intel Core i7-2620M@2.7GHz and 6GByte RAM, is tenfold, the ZMP solution takes 0.0233 ms (0.00702 ms std) while the CPG approach takes 0.0023 ms (0.00043 ms std). These results are expected, as the CPG approach only requires the numerical integration of the used dynamical equations in the CPG, while for the ZMP solution it requires a sequence of procedures to reach the desired body motions and foot placements, and the computation of the inverse kinematics to find the respective joint positions.

Energy consumption It is assumed that for comparison purposes, the energy consumption on the leg's servo joints can be inferred by the produced torques (τ), as recorded from the simulator's dynamics engine.

$$E = \int_{t=0}^{t=20} \tau^{\top} \tau dt \tag{5.24}$$

For this comparison, both CPG and ZMP solutions walk straight for 20 s. The produced torques and respective trajectories were recorded, relaying an energy consumption of 8698 $(\mathrm{N.m})^2$ for the ZMP solution, and 10867 $(\mathrm{N.m})^2$ for the CPG solution.

Produced trajectories Similar walks are achieved for both solutions in terms of general characteristics, but are distinct in some aspects when analyzed carefully, such as the produced trajectories. In fig. 5.20 are presented all the outputs to the joints of ZMP (dashed green) and CPG (solid blue) solutions. It is possible to observe that both solutions produce trajectories with similar coarse features, but the ZMP solution produces more detailed trajectories and with sharper inflections.

One can infer that the differences in the trajectories between both solutions will cause divergent walking performances, despite producing similar general walking characteristics.

Ground reaction forces A look at the ground reaction forces of each solution provides some insight on how the weight is distributed throughout the walk and how it is transferred from single support to double support. In fig. 5.21 is presented the force sensor resistor readings (FSR) from the left (top) and right (bottom) feet, from the CPG (solid blue) and ZMP (dashed green) solutions.

As stated previously, the produced weight distribution throughout the walk is similar for both solutions, exhibiting a strict alternate foot placement and the same duty factor. Observing the instant of foot strike in the right foot (bottom), it is clear that the CPG solution suffers higher impact forces than the ZMP solution. Otherwise both solutions exhibit generally the same ground reaction forces.

The ZMP solution produces slightly smoother weight transfers between support phases than the CPG solution, as expected from a solution which uses ample knowledge of the robot kinematical model.

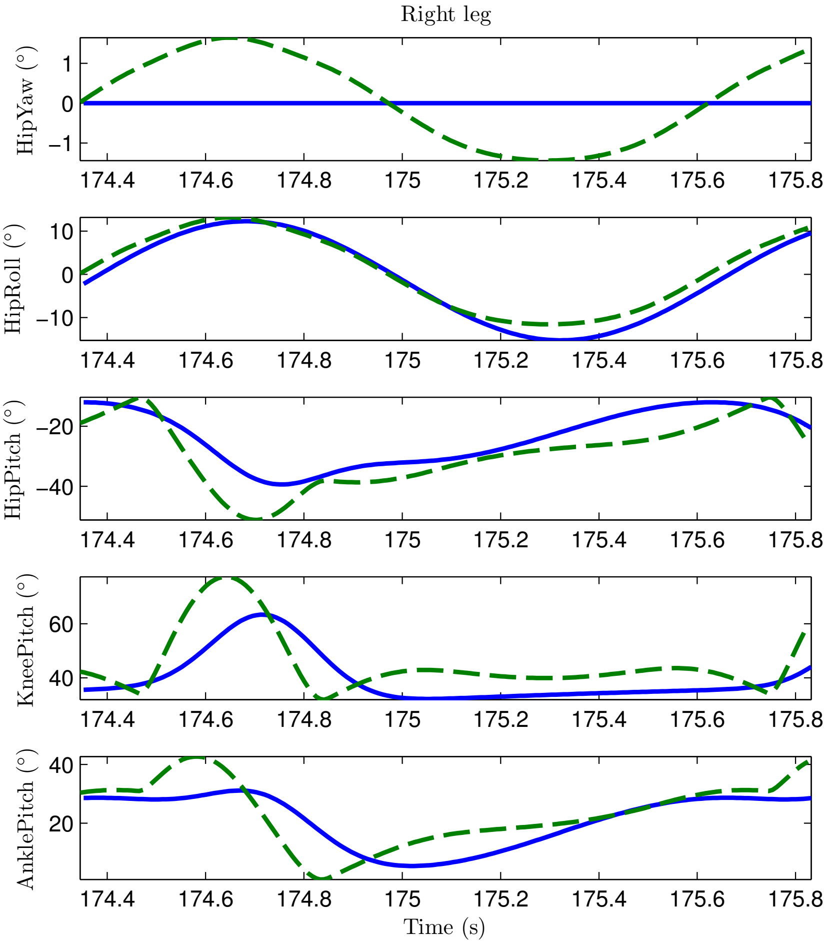

Figure 5.20: Joint trajectories generated by the CPG (blue solid lines) and ZMP (dashed green lines) solutions. These periodic trajectories with a period of 1.28 s share the same coarse features. However, the ZMP generated trajectories are more detailed because the approach uses the robot's inverse kinematics model.

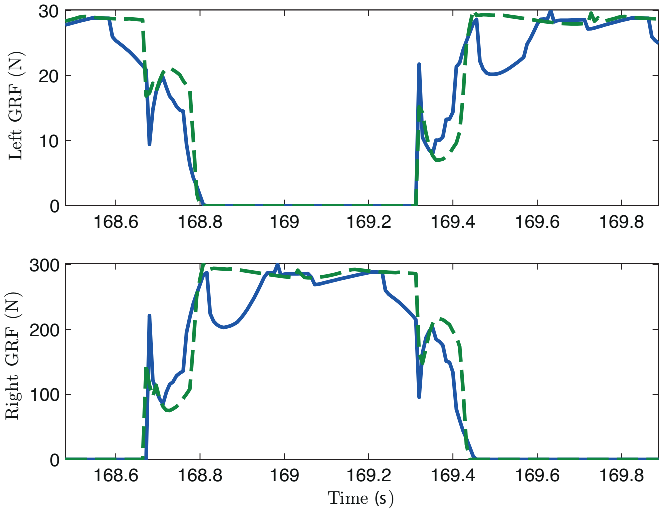

Figure 5.21: Ground reaction forces (GRF) measured from force sensing resistors (FSR) in the robot's feet. Blue solid lines are the values read from the CPG solution, and green dashed lines from the ZMP solution.

Foot placements and center of pressure It should be given closer attention to the progression of the COP in order to perform a more detailed analysis in the differences in the weight transfer between support phase throughout the walk, and the respective walking stability. The measured COP is considered to correctly represent the performed ZMP when the robot is dynamically balanced, as is well explained by Vukobratovic [217].

In fig. 5.22 the foot support throughout the step cycles can be observed, in the top for the CPG solution and bottom for the ZMP solution. Comparing the feet placements (red for left foot, green for right foot) it is possible to observe that both walks are very similar in step size in the sagittal and frontal planes.

The described trajectories of the COM (fig.5.22(a)) and COP (fig.5.22(b)) for both walks are strikingly different however. For the ZMP solution, the COM follows a straight, direct progression between support areas as planned through the ZMP planner. In contrast, for the CPG solution, the resulting COM progression is not directed, presenting wider curves and brief backward motions during double support phases. The lack of COM planning in the CPG solution, means that the COM progression over the support areas in detail is uncertain, but the resulting broad characteristics are expected from the overall motion primitives employed.

The progression of the COP in the CPG solution is quite difficult to follow in the figure, due to the transition from single support to double support phase and then back to single support. The full weight of the robot starts at the center of the left foot, where it lies throughout the entire single support of the left foot. At the time of ground strike the center of pressure shifts instantly from the left foot to the right front corner of the right foot. It then progresses through the front edge of the support defined by the two feet, returning to the left foot. The COP then progresses from the middle of the left foot to the back of the right foot, and then to the middle at the onset of the right single support phase.

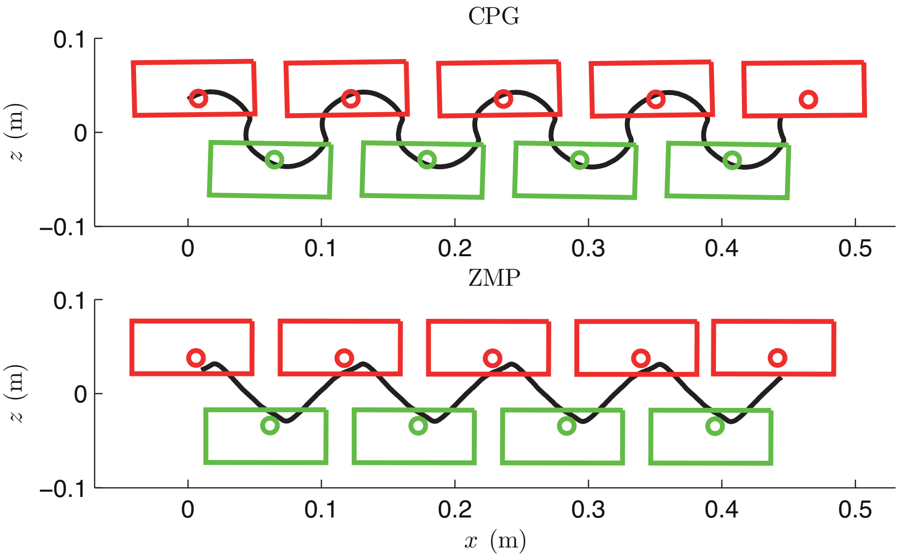

(a) Recorded COM progression.

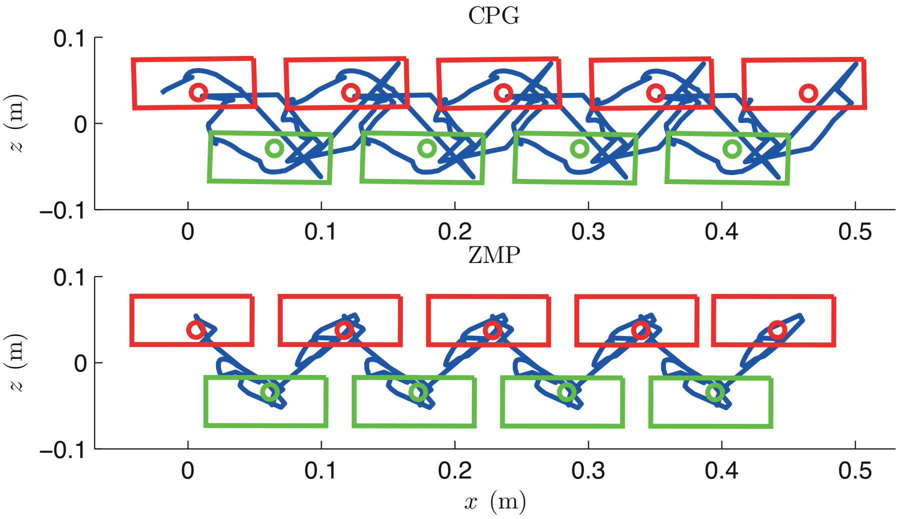

(b) Recorded COP progression.

Figure 5.22: Feet placement sequence for CPG (top) and ZMP (bottom) solutions, as viewed from top to bottom. Robot walks forward in the x axis (left to right). Red rectangles represent the placement of the left foot and green rectangles represent the placement of the right foot. Black lines represent the COM progression projected in ground plane, as viewed from the top, and the blue lines represent the COP throughout the walk.

In the ZMP solution the COP follows a close progression on the planned points, taking a direct route between support areas, despite a small oscillation around the center of the end effector (small circle in the foot). This oscillation of the COP, back and forward between the two feet, reveals a slight oscillation in the robot during the transition between single support and double support phases.

Body oscillations The greater oscillations in weight transfer exhibited by the COP on the CPG solution, compared to the ZMP solution, can be corroborated by the body angle oscillations measured through the robot's IMU.

The robot's body pitch and roll angles are depicted in fig. 5.23, with the measurements from the CPG solution in solid blue and from the ZMP in dashed green.

Roll angle oscillations (bottom) are close in amplitude, $\approx 10°$, and shape for both solutions, which is expected from analysis of the produced trajectories in the roll joints that govern the movements in the frontal plane (fig. 5.20), and from the frontal displacement of the COM and exhibited trajectory of the COP, as seen in fig. 5.22.

Oscillations in pitch angle (top) present an amplitude of $\approx 4°$ in the ZMP solution, while for the CPG solution the amplitude is $\approx 10°$. The difference in detail produced by the CPG solution in the movements that govern the sagittal plane, the three pitch joints in fig. 5.20, may be the cause of this greater oscillation in the pitch angle. This greater oscillation in the sagittal plane was also observed in the COM displacement and COP path in fig. 5.22. Curiously, the resulting oscillations in the pitch angle from both solutions are in anti-phase.

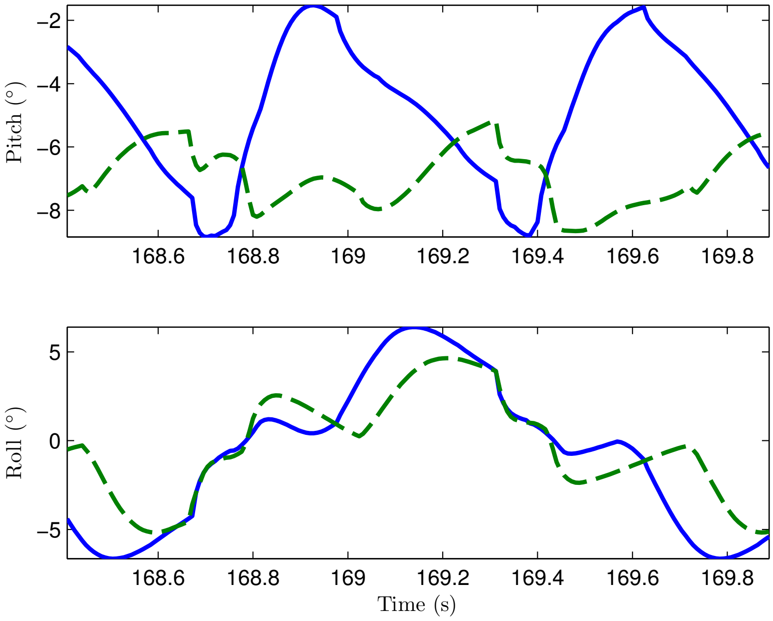

Figure 5.23: Pitch and roll angles measured from the robot's IMU for the CPG (blue solid lines) and ZMP (green dashed lines) solutions.

5.3.6 Remarks on bipedal walking

The proposed CPG solution for biped walking successfully produces the required motion patterns for purposeful, goal-oriented biped walking. The procedure to attain the manual parametrization of the motion primitives has been demonstrated, revealing a brief and straightforward sequence of intuitive tuning steps. Each motion primitive produces an intuitive motor action, rendering the tuning of the motion primitive's amplitudes a matter of observing the robot's walking behavior, and adjusting the amplitudes accordingly.

The performance achieved by the robot using the proposed CPG solution is similar to the performance achieved by a typical ZMP solution.

The major difference in performance is observed during the double support phase of the step, with the CPG solution presenting greater oscillations in the weight transfer on the support area. This effect is the result of a lack of kinematical planning of the end effector pose at the instants of the double support phase. The absence of kinematical planning in the generated motions also reflects onto the maximum attainable step length, with the ZMP solution being able to perform larger steps, almost the double length of the CPG solution.

Despite these slight differences in performance, the CPG solution is capable of accomplishing almost all the locomotor behaviors as the ZMP solution in flat terrain, except side stepping and choosing the position of feet placement to achieve precise walking.

The proposed solution is able to produce stable, goal-oriented walking with real-time modulation of walking, as shown in the ball following demonstration. Head gaze towards the ball is sufficient for modulating the amplitude parameters of the significant motion primitives, resulting in a ball following behavior.

5.4 Phase regulation

Feedback pathways play an important role in the generation of legged locomotion. Sensory information originating from tactile information; from muscle position, velocity and strain; as well as other more complex senses like vestibular and vision; are used to dynamically adapt the centrally generated pattern of locomotion to the requirements of the environment.

Step phase transition is a well discussed feedback in vertebrate walking, with many studies evidencing feedback mechanisms which control the transition from swing-to-stance and stance-to-swing, dependent on afferent signals [56, 143, 156, 160]. Direct evidence from observations in walking decerebrate and intact cats indicate that two types of sensory afferents are involved in eliciting transitions between step phases, relating to ankle loading and hip extension.

For example, it has been observed that chronic spinal and decerebrate cats adapt the rate of hind stepping to the speed of the treadmill, by adjusting the duration of the stance phase through holding or initiating the transition to swing [160]. Manipulation of the hip extension can hold the stepping action, by holding the hip in place, or elicit the transition from stance to swing by bringing the hip backwards [143]. Also, swing-to-stance transitions can be initiated by taking the leg and bringing it towards the front.

These observations were the subject of investigation in research works on animal locomotion and CPG modeling simulations, including phase transition rules based on the sensory information related to hip position and leg load [56, 68, 218]. In robotics, some works have explored feedback mechanisms which use the ideas from these observations to some extent.

Phase resetting mechanisms have been used quite frequently in CPG based controllers [4, 6, 149, 173]. Phase resetting updates the nominal temporal state of the rhythmic generator based on some external sensory event, usually a foot strike. It aims to synchronize the temporal reference with the external state through a specific, well timed event, usually the contact of the foot with the ground which indicates the initiation of the stance phase.

However the mechanisms at play in regulating the transition of step phases also address the transition from stance-to-swing, and more importantly they regulate the duration of the step phases by advancing and delaying the transitions. This kind of phase regulation has been explored for quadruped robots usually only relying on foot load sensory information. It has been discussed as a method for achieving physical entrainment [174], interlimb coordination and to increase robustness to unperceived slopes, steps and lateral perturbations [135, 136].

5.4.1 Phase regulation mechanism

The proposal for the phase transition mechanisms are designed on the assumption that by delaying and advancing between phase transitions, it provides for adaptation and adequation of the executed motions to the robot state and environment. The transitions between swing and stance phases are regulated using four mechanisms, divided in two roles for each temporally defined transition, swing to stance and stance to swing. For each transition there are two mechanisms with the ability to delay or elicit the advance to the next step phase, triggered when certain events occur or certain conditions are met.

A phase transition is delayed with the aim to hold the transition to the next step phase, until a correct expression of the walk is observed, or the fulfillment of certain events. If some expression of the walk is observed earlier than expected or certain events have already occurred, an early phase transition can then be elicited, promoting for the execution of the next step phase.

Swing to stance

At the transition from swing to stance, the leg comes from executing the transfer of the foot towards the front, up to the point when the foot is placed on the ground, at the same instant the motions of stance phase start to be performed. If the sequence of these events is not followed, the phase transition mechanism should regulate the performed motions. In this sequence the easily identifiable event is the placement of the foot, which happens at the same instant as the transition from swing to stance.

Therefore, the foot placement event is used as an indicator for whether or not the executed step phase matches the exhibited step phase, performed by the robot.

Two circumstances in the transition from swing to stance are considered, when the foot has touched the ground before swing phase has finished, and when the stance phase has already initiated even before the foot being securely placed and able to support the body. Herein it is assumed that a corrective action should take place accordingly to these two circumstances by applying delay or advance mechanisms.

Advance If the foot touches the ground before the end of the swing phase, an early and fast transition from swing to stance should be elicited.

Delay Just before the initiation of the stance phase, if the foot has yet to touch the ground, the transition from swing to stance should be delayed.

The designed mechanisms need to detect the transition between the step phases, and it should act accordingly with the described adjustments in case sensory events are not occurring correctly.

Detecting the transition between step phases is a matter of verifying the value of each CPG's phase ϕ_i. The transition from swing to stance happens around $\phi_i = \frac{\pi}{2}$. This value is used to temporally activate the advance mechanism before the transition (eq. (5.25)), and activate the delay mechanism at the boundary region between the two step phases (eq. (5.26)).

$$a_{i,\text{adv}} = \begin{cases} 1, & 0 \leq \phi_i < \frac{\pi}{2} \\ 0, & \text{otherwise} \end{cases} \tag{5.25}$$

$$a_{i,\text{del}} = \begin{cases} 1, & \phi_i \approx \frac{\pi}{2} \\ 0, & \text{otherwise} \end{cases} \tag{5.26}$$

The mechanism, if activated within the correct temporal region, is able to be triggered through the loading and unloading of the feet. Feet force sensors are used to detect the loaded and unloaded status, returned by a boolean function δ_i for the foot i and defined by a pre-determined threshold (eq. (5.27)).

$$\delta_i = \begin{cases} 1, & \text{load is higher than threshold} \\ 0, & \text{load is lower than threshold} \end{cases} \tag{5.27}$$

Advance from swing to stance Triggering of the advance mechanism for the swing to stance transition happens when the foot comes in contact with the ground, $\delta_i = 1$, before the transition to the stance phase, $a_{i,\text{adv}} = 1$, meaning the CPG is in swing phase, contrarily to the real robot. Eliciting an early and fast phase transition is a matter of influencing the dynamic state of the i leg's CPG: phase ϕ_i and the motion trajectories $z_{j,i}$.

The presented mechanism in eq. (5.28) advances the phase by increasing $\dot{\phi}_i$ to a very high value, much higher than the value of the stepping frequency ω and the effects from the coupling term. After the triggering of the mechanism, the phase of the oscillator ϕ_i rises abruptly until it reaches the stance step phase ($\phi_i > \frac{\pi}{2}$), resuming the normal behavior dictated by ω and the coupling terms. Function

$a_{i,\mathrm{adv}}$ deactivates the mechanism just after reaching stance phase.

It is unclear what should be the ideal behavior of the generated motion when a phase transition is elicited. Therefore it is proposed that the generated motions should resume from the same trajectories exhibited just before the transition was elicited. This choice is justified by the need to maintain the joint positions at the moment the foot touches the ground, not allowing the trajectories to change abruptly by the sudden change in the phase ϕ_i. To block the change in $z_{j,i}$ during the transition, $\dot{z}_{j,i}$ is set to 0 by the mechanisms in eq. (5.29), activated on the region before the stance phase ($a_{i,\mathrm{adv}}$) and triggered by the foot touching the ground (δ_i).

$$\dot{\phi}_i = \omega + k \sin\left(\phi_i - \phi_o + \pi\right) + \tau_{\mathrm{adv}} a_{i,\mathrm{adv}} \delta_i \tag{5.28}$$

$$\dot{z}_{j,i} = \frac{-\alpha\left(z_{j,i} - O_{j,i}\right) + \sum f_j\left(z_{j,i}, \phi_i, \dot{\phi}_i\right)}{1 + \tau_{\mathrm{adv}} a_{i,\mathrm{adv}} \delta_i} \tag{5.29}$$

By setting a very large value for τ_{adv}, it is ensured that the transition on the phase from swing to stance will happen in a very short time, and the trajectory will be brought to an halt by means of $\dot{z}_{j,i} \approx 0$.

Delay transition from swing to stance Similarly to the fast transition from swing to stance, the triggering of the delay mechanism is carried out by the activation of the mechanism within the range of the boundary between swing and stance, $a_{i,\mathrm{del}} = 1$, and the lack of foot contact with the ground, $\delta_i = 0$. Changes in phase oscillator are presented in eq. (5.30). Holding the transition is a matter of not allowing ϕ_i to change at its normal rate, which is achieved by setting $\dot{\phi}_i \approx 0$ when the mechanism is triggered. The motion patterns are also stopped while the mechanisms are delaying the transition. The resulting $\dot{z}_{j,i} \approx 0$ from having $\dot{\phi}_i \approx 0$ will hold the trajectories at the positions just before as the transition from swing to stance had occurred.

$$\dot{\phi}_i = \frac{\omega + k \sin\left(\phi_i - \phi_o + \pi\right)}{1 + \tau_{\mathrm{del}} a_{i,\mathrm{del}} \left(1 - \delta_i\right)} \tag{5.30}$$

A large value of τ_{del} easily achieves the desired effect of holding the transition in terms of phase ϕ_i. The CPG resumes nominal behavior after the triggering of the delaying mechanism, as soon as the foot touches the ground.

Stance to swing

The transition from stance to swing marks the point when the leg ends the execution of the stance phase, reaching the maximum leg extension, followed by the initiation of the swing phase by lifting the foot.

Again, the lifting of the foot is a good indicator of whether or not the stance phase has finished, and the swing phase has been initiated, compared to the currently generated motions. Discrepancies between the executed motions and the requirements for a proper expression of a walk may result in problematic situations. For instance, initiating the swing phase, and the lifting motion, of a loaded foot may leave the robot unsupported. It is assumed that delay and advance mechanisms for the step phase transition should address these situations and correct the discrepancies.

Advance If the foot is unloaded before the end of the stance phase, an early transition from stance to swing is elicited.

Delay At the limit of the transition between stance and swing, if the foot remains loaded, the transition should be delayed.

The detection of the transition from stance to swing is performed by verifying the value of ϕ_i, which is carried out by functions $b_{i,\text{adv}}$ and $b_{i,\text{del}}$. These functions are used to activate the advance and delay mechanisms at well-defined temporal zones. The advance mechanism is activated in the later half of the stance phase, allowing for the mechanism to elicit an early fast transition into the swing phase (eq. (5.31)). The delay mechanism is activated by detecting the transition region between stance and swing of the currently executed phase ϕ_i (eq. (5.31)).

$$b_{i,\text{adv}} = \begin{cases} 1, & -\pi \leq \phi_i < -\frac{\pi}{2} \\ 0, & \text{otherwise} \end{cases} \tag{5.31}$$

$$b_{i,\text{del}} = \begin{cases} 1, & \phi_i \approx -\frac{\pi}{2} \\ 0, & \text{otherwise} \end{cases} \tag{5.32}$$

Within the activation zones of the step phase, which concerns the transition from stance to swing, the mechanisms are able to be triggered by events regarding the readings from the feet sensors. These events are detected by function δ_i defined in eq. (5.27), detecting the loading of the feet ($\delta_i = 1$) and unloading of the feet ($\delta_i = 0$).

Advance from stance to swing A fast transition from stance to swing is triggered when the foot is unloaded before reaching the swing phase, enabled by $a_{i,\text{adv}} = 1$ and triggered by $\delta_i = 0$. Similarly to the advance from swing to stance, a fast transition is achieved by manipulating the phase ϕ_i and the motion trajectories $z_{j,i}$ dynamics. Increasing $\dot{\phi}_i$ to a value much higher than $\omega + k \sin(\phi_i - \phi_o + \pi)$ and stopping the motion generation by holding $\dot{z}_{j,i} \approx 0$, as given by:

$$\dot{\phi}_i = \omega + k \sin(\phi_i - \phi_o + \pi) + \tau_{\text{adv}} b_{i,\text{adv}} (1 - \delta_i) \tag{5.33}$$

$$\dot{z}_{j,i} = \frac{-\alpha (z_{j,i} - O_{j,i}) + \sum f_j \left(z_{j,i}, \phi_i, \dot{\phi}_i\right)}{1 + \tau_{\text{adv}} b_{i,\text{adv}} (1 - \delta_i)} \tag{5.34}$$

The phase of the oscillator rises abruptly after triggering, until just reaching the swing step phase, where the function $b_{i,\text{adv}}$ deactivates the mechanism. A very large value for τ_{adv} is chosen, ensuring a fast transition on the phase, and a stop on the generated motions.

Delay transition from stance to swing Just like the delay on the transition from swing to stance, the delay mechanism is enabled at the boundary region of the transition ($b_{i,\text{del}} = 1$) and triggered by a continued load of the foot ($\delta_i = 1$). The manipulation of the phase dynamics is presented in eq. (5.35), delaying the transition for the next step phase by making $\dot{\phi}_i \approx 0$, for a large τ_{del}.

$$\dot{\phi}_i = \frac{\omega + k \sin\left(\phi_i - \phi_o + \pi\right)}{1 + \tau_{\text{del}} b_{i,\text{del}} \delta_i} \tag{5.35}$$

The nominal behavior of the CPG is resumed after the unload of the foot is detected, releasing the delaying mechanism.

Phase regulation summary

In summary, it is considered that the transition advancing mechanism is enabled during the latter half of the step phase, defining $a_{i,\text{adv}}$ from swing to stance and $b_{i,\text{adv}}$ from stance to swing. Delaying mechanisms are enabled on the boundary region between two step phases, which defines $a_{i,\text{del}}$ from swing to stance and $b_{i,\text{del}}$ from stance to swing. A phase transition mechanism is triggered if a determined loading or unloading condition is verified in the respective leg i through the function δ_i.

The four mechanisms are implemented as term added to the phase oscillator eq. (3.11) and motion pattern generators eqs. (3.12) for all leg joints:

$$\dot{\phi}_i = \frac{\omega + k \sin\left(\phi_i - \phi_o + \pi\right)}{1 + \tau_{\text{del}}\left(a_{i,\text{del}}\left(1 - \delta_i\right) + b_{i,\text{del}} \delta_i\right)} + \tau_{\text{adv}}\left(a_{i,\text{adv}} \delta_i + b_{i,\text{adv}}\left(1 - \delta_i\right)\right) \tag{5.36}$$

$$\dot{z}_{j,i} = \frac{-\alpha\left(z_{j,i} - O_{j,i}\right) + \sum f_j\left(z_{j,i}, \phi_i, \dot{\phi}_i\right)}{1 + \tau_{\text{adv}}\left(a_{i,\text{adv}} \delta_i + b_{i,\text{adv}}\left(1 - \delta_i\right)\right)} \tag{5.37}$$

where τ_{adv} and τ_{del} are positive constants that adjust the strength of delay and advance effects.

The objective of adding members in eq. (5.36,5.37) is to increase or decrease the rate of change of the CPG phase ϕ_i and stop joint motion $z_{j,i}$ during phase regulation. Making $\dot{\phi} \approx 0$ delays phase transition, while increasing $\dot{\phi}$ above the nominal frequency achieves an earlier transition. For stopping the joint motion, $\dot{z}_{j,i}$ is set to ≈ 0.

This interplay, between phasic dependent feedback and triggering conditions from physical exhibitions of the walking dynamics, is expected to adjust the nominal walking trajectories according to the robot and environment needs.

5.4.2 Simulations with HOAP-2

Simulations are used to demonstrate the proposed phase regulation mechanisms work as designed and to compare the effects of phase regulation in the walk. Herein are presented the results from simulations in the Webots robotics simulator, using the model of the HOAP-2 humanoid robot. HOAP-2 is a small biped robot with 48 cm, weighting 6.8kg, with 28 DOFs, presenting a very similar kinematical configuration as the DARwIn-OP.

Fig. 5.24 shows the phase regulation mechanism elicited at the designed conditions in a straight walk in flat ground. An early transition from swing to stance is triggered at (A), after the foot touching the ground earlier than expected. At this instance the phase of the CPG advances to the next step phase, the stance phase, and the trajectories are held until the transition is complete, resuming from this point throughout the stance phase. At the end of the stance phase, noted by (B), the foot measures a sudden unload, which triggers an early transition from stance to swing. However this transition is not completed because the foot remains loaded in the subsequent instants, which is deemed a false positive on the triggering of the mechanism. At (C) the delay mechanism from stance to swing is triggered due to the remaining load at the foot. The phase of the CPG and the trajectories are held until the foot is unloaded below the threshold, resuming after the swing step phase.

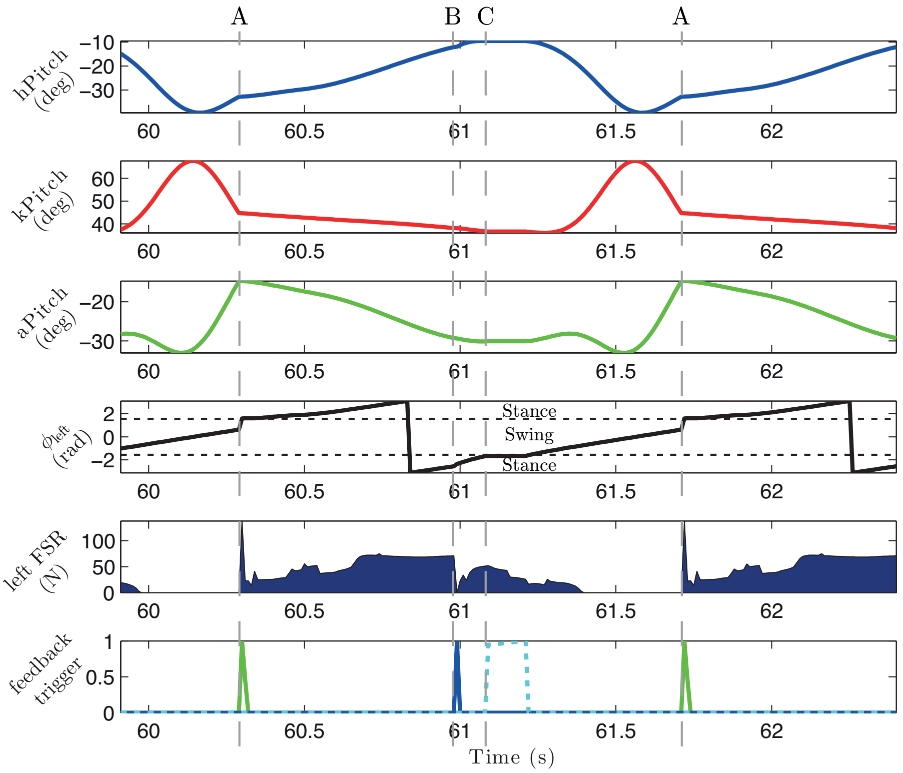

Figure 5.24: Left leg trajectories and phase regulation mechanism triggering during one step cycle. A transition was elicited from swing to stance due to early foot touchdown (A). When the load decreased under the threshold a transition from stance to swing is elicited (B). However, the foot was not fully unloaded before entering the swing phase, so the oscillator was delayed until reaching below the force threshold (C).

Several simulations were performed with the aim to test a range of values for the compass motion amplitude A_{compass}, ranging from 1 to 16, affecting the nominal step length. In fig. 5.25 is observable the achieved step period, velocity and step length with (cross) and without (circle) the feedback for each value of applied A_{compass}. The inclusion of phase regulation allowed to increase A_{compass} further than 8 without the robot falling. Globally, the effective achieved velocity was lower at the same amplitudes when the feedback was active (cross). This is due to the effect of the delay mechanism in the transition from stance to swing. The step period is similar in both situations. However for $A_{\text{compass}} > 9$ the period is reduced due to the effect of elicited early transitions between swing and stance (cross). When phase regulation is active (cross), the achieved step length is slightly smaller than when it's disabled (circle), mostly due to the early transitions.

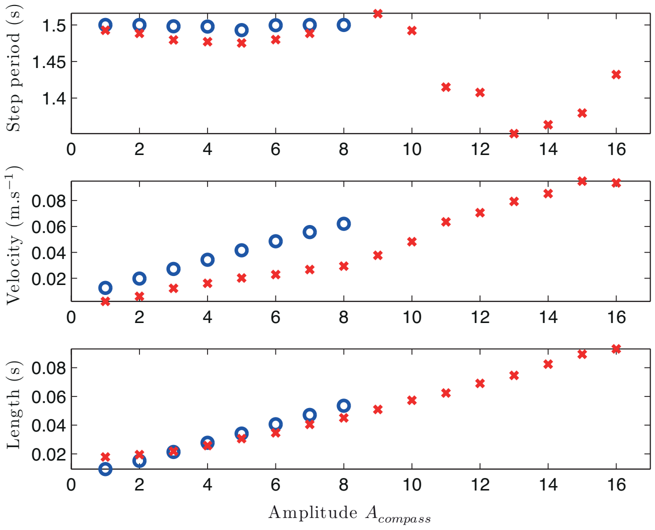

Figure 5.25: A smaller velocity is achieved overall, when phase regulation is active (cross). However the inclusion of phase regulation feedback allows for greater A_{compass} values, compared to when the feedback is not used (circle). The range of useable values increased 100% for a successful walk with phase regulation.

Simulations suggest that with phase regulation feedback the designer has more room in parametrization of walking motions. It is not necessary to find the perfect parameters for slight variations in environment and is possible to use a greater range of values. An adaptation to slight environment changes was also verified, where nominal motions are adjusted and the robot is able to walk up and down modest slopes.

Simulations in up and down modest slopes have also been performed (fig. 5.26). The aim was to ascertain if the application of phase regulation mechanisms enable any adaptation in the walk, which would enable it to cope with perturbations such as tilted ground. A range of slope inclinations was tested, from $0°$ to $4.5°$ upslopes and from $0°$ to $-3.4°$ in downslopes.

Without phase regulation the robot is not able to walk, either, up-slope or down-slope, falling in the very first steps.

5.4.3 DARwIn-OP experiments

The real robot walks successfully in flat terrain after a short parametrization of motions, and when phase regulation is active it adjusts slightly the nominal gait. Walking slight sloped terrains (up: $\approx 4°$, down: $\approx 2.5°$) is not possible without the activation of phase regulation, reinforcing the obtained results from simulations. Videos of the experiments are available at `http://asbg.dei.uminho.pt/user/1`.

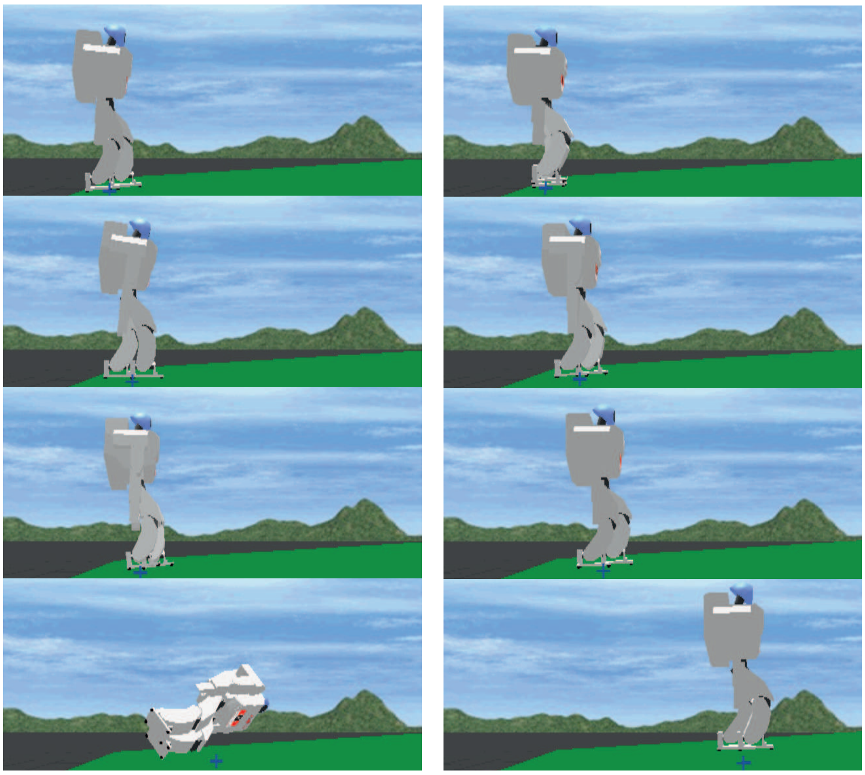

(a) Up-slope walking without phase regulation.

(b) Up-slope walking with phase regulation.

Figure 5.26: Simulations' snapshots from up-slope walking with an inclination of $4.5°$.

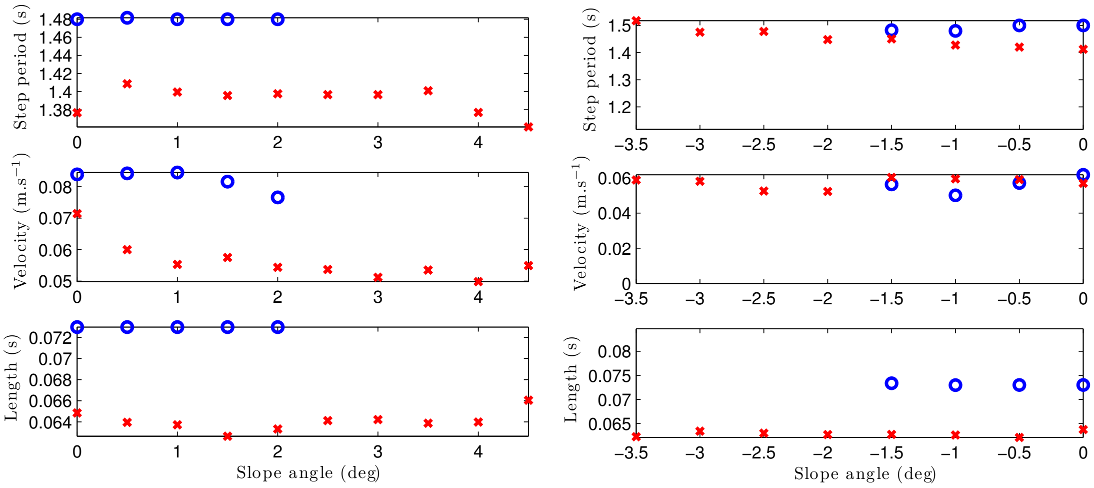

(a) Up-slope results.

(b) Down-slope results.

Figure 5.27: Results from the simulations testing up and down-slope walking with different angles, in terms of step length, step period and achieved velocity. The simulations with phase regulation allowed the robot to walk in steeper slopes.

The robot walks a down-slope of $\approx 2.5°$ with the phase regulation activated until 36.8 s in the experiment. At this instant of time, phase regulation is deactivated, just about when the next step takes place, the robot loses balance and falls (fig. 5.28). Fig. 5.28 depicts joint trajectories for the right leg, ground reaction forces from the right foot, right phase and triggered phase regulations. Only advance transition from swing to stance is triggered at ≈ 35 s and ≈ 36 s, when the foot touches early the ground because of the inclination. Clearly visible is the difference between the adjusted joint trajectories when phase regulation is employed ($t < 36.8$ s) and the nominal trajectories when phase regulation is not employed ($t > 36.8$ s).

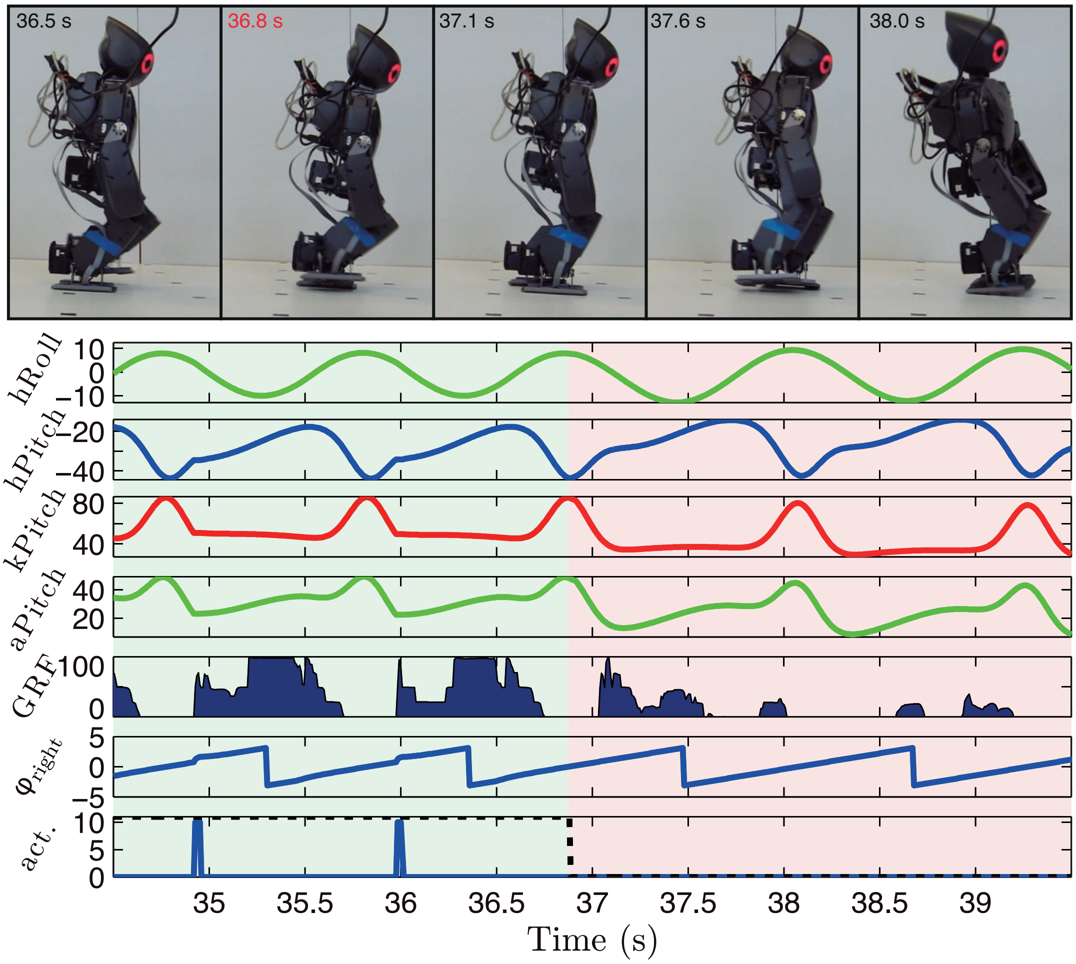

Figure 5.28: DARwIn-OP walking down a slope up until phase regulation is deactivated and falls. After deactivating phase regulation ($t > 36.8$) nominal trajectories are no longer adjusted according the sensed ground reaction forces (GRF). Just about the next step ($t = 37$ s) no phase advance is elicited due to an early touchdown, making the robot lose balance and fall.

These achieved adjustments changed the overall step period in up-slope walk from 1.20 s to 1.04 s and also reduced the performed step length from the nominal 0.0505 m to 0.0424 m.

5.4.4 Remarks on phase regulation

In this section a phase regulation mechanisms is proposed, using foot load information for controlling the transition between the step phases, and investigated the potential improvements on biped walking. Although not necessary for obtaining a stable walk in flat terrain, results have suggested that the application of the regulation mechanisms does introduce some level of adaptation to the walk.

The inclusion of the phase regulation mechanisms has increased the range of admissible values for the amplitude parameters of certain motion primitives, such as the compass motion. Besides the ability to perform larger motions, the feedback mechanisms correct out of range motions resulting from parameters with values greater than it would be admissible.

Experiments have demonstrated that without the adaptation of the nominal walking motions produced by the proposed motion primitives, the robot falls when walking up and down slopes. The inclusion of the phase regulation mechanisms allows the robot to walk up slopes up to 4° and walk down up to 2.5°, eliciting especially the transition from swing to stance upon earlier contact with the ground.

The proposed phase regulation mechanisms requires, nonetheless, a very careful choice of parameter values and magnitude of the regulation effects, otherwise it the effect of the mechanisms risk to hinder the walk. The region of activation on the rhythmic phase signal controls for how long the mechanisms are listening to the signals from sensory information, having an important role of defining a temporal window of the step which the feedback is able to affect the walk. A careful choice of the load thresholds used for each transition mechanism is also required, as a less adequate value can result in intermittent walking behavior. For instance, choosing a low load threshold for the transition delay from stance phase to swing phase may cease stepping, completely halting the walking robot.

The robot was subject to other disturbances for purposes of evaluating the role of the phase regulation feedback, such as small pushes in the sagittal and frontal plane and stepping on unperceived small steps. However, the inclusion of the regulation mechanisms was not fruitful, as the robot was not able to recover from such disturbances.

5.5 Open-loop CPG within LQP whole-body control

The current section demonstrates the integration of a CPG based walking controller within a model-based paradigm for whole-body control [181,182]. The goal is to have the CPG to control the locomotor task, in a framework which can pursue several tasks simultaneously. The CPG approach presented in section 5.1 will be used to substitute the ZMP walking generator that has been previously applied in the framework. It will explore the advantages of general purpose, model-based, control framework allowing for the combination of tasks of different nature, and the CPG's ability to produce periodic and stereotypical behavior such as locomotion. However, the CPG should provide the same abilities as the ZMP based solution, in terms of generating proper walking behavior, to allow change in walking velocity, have the ability to navigate the environment and to work well within the whole-body framework.

Here the proposed CPG is integrated in the framework as a task which produces reference positions and how it is combined with other tasks. Then the performance of the resulting walk is compared to the produced ZMP walk, in energy consumption, computational time, stability and walking abilities. Finally it is demonstrated how the CPG has the ability to produce goal-directed walking within the whole-body control framework, in a scenario where the robot has to perform several tasks. Videos of all simulations are available at `http://asbg.dei.uminho.pt/user/1`.

The LQP whole-body control framework will be next summarized.

5.5.1 Whole-body control

The control problem formulation for whole-body control presented is based on [182]:

1. A description of the constraints acting on the system;
2. An objective function to minimize.

At each time step the control algorithm computes the actuators' input torque that minimizes the objective function without violating the constraints.

Constraints

The constraints of motion of a floating-base robot, as biped or other legged robots, can be described using the Euler-Lagrange formalism for the equations of motion:

$$M(\boldsymbol{q})\ddot{\boldsymbol{q}} + \boldsymbol{n}(\boldsymbol{q},\dot{\boldsymbol{q}}) + \boldsymbol{g}(\boldsymbol{q}) = S\boldsymbol{\tau} + J_c(\boldsymbol{q})^t\boldsymbol{w}_c. \tag{5.38}$$

For a given state $(\boldsymbol{q},\dot{\boldsymbol{q}})$, this first constraint relates the generalized acceleration $\ddot{\boldsymbol{q}}$ to the generalized forces acting on the system. These forces are due to the inertial (M), Coriolis, centrifugal/non-linear ($\boldsymbol{n}$) and gravitational ($\boldsymbol{g}$) effects as well as to the actuation and the interactions of the robot with the environment. On the left hand side, S and $\boldsymbol{\tau}$ are respectively the actuation matrix and the input torque vector whereas $J_c, \boldsymbol{w}_c$ are the contact points Jacobian and the contact wrench. S allows to account for the fact that some DOFs are not actuated (typically the free-floating base).

Other constraints considered are: joint position, velocity and actuation torque limits as well as the ones related to the contact of the robot's feet on the ground. These constraints are written as equality and inequality functions of $\ddot{\boldsymbol{q}}$, $\boldsymbol{\tau}$ and $\boldsymbol{w}_c$ and their general expression is given by:

$$A(\boldsymbol{q})\mathbb{X} \quad \leqq \quad \boldsymbol{b}(\boldsymbol{q},\dot{\boldsymbol{q}}) \tag{5.39}$$

where $\mathbb{X} = \begin{bmatrix} \ddot{\boldsymbol{q}}^T & \boldsymbol{w}_c^T & \boldsymbol{\tau}^T \end{bmatrix}^T$ is defined as the dynamic variable of the system.

Tasks

Redundant robots, like humanoid robots, with a large number of DOFs and several end-effectors can pursue several objectives simultaneously. For example, walking and holding an object, in a transporting task, or in a more challenging example, holding an object with the left arm, opening a door with the right arm while balancing in one leg and kicking a ball.

The objectives are described in terms of *operational* tasks, i.e. tasks associated to controllable parts of the robot. More specifically, an operational task can be defined as:

- a frame on some part of the body of the robot and which is to be controlled;
- the target value for this frame;
- the desired error dynamics.

Using this kind of control, depending on the task to pursue, the target can be expressed in terms of desired frame pose (frame position + frame orientation), frame acceleration or using screw theory by means of a target twist or wrench. For the error dynamics, a local controller is used, as the commonly applied PID, or an impedance controller structures. In cases where pure reactive control is not sufficient, model predictive control can be used.

Task i outputs $\boldsymbol{v}_i^{des}$ at each control instant, related to the dynamic variable $\mathbb{X}$ through models of the system and the task is written as a weighted-euclidean norm to minimize:

$$T_i(\boldsymbol{q}, \dot{\boldsymbol{q}}, \mathbb{X}) = \| E_i\left(\boldsymbol{q}\right) \mathbb{X} - \boldsymbol{f}_i\left(\boldsymbol{q}, \dot{\boldsymbol{q}}, \boldsymbol{v}_i^{des}\right) \|_{W_i}^2 \tag{5.40}$$

where $E_i\left(\boldsymbol{q}\right)$ and $\boldsymbol{f}_i\left(\boldsymbol{q}, \dot{\boldsymbol{q}}, \boldsymbol{v}_i^{des}\right)$ encapsulate model related information. W_i is the weight used for computation of the weighted-euclidean norm.

Considering a task consisting in controlling the operational acceleration of the right hand of the robot, $E_i\left(\boldsymbol{q}\right) = \begin{bmatrix} J_{RH}(\boldsymbol{q}) & 0 & 0 \end{bmatrix}$ and $\boldsymbol{f}_i\left(\boldsymbol{q}, \dot{\boldsymbol{q}}, \boldsymbol{v}_i^{des}\right) = -\dot{J}_{RH}(\boldsymbol{q}, \dot{\boldsymbol{q}})\dot{\boldsymbol{q}} + \boldsymbol{v}_i^{des}$ where $\boldsymbol{v}_i^{des}$ is the desired acceleration at control time t and $J_{RH}(\boldsymbol{q})$ is the Jacobian associated to the right hand of the robot.

Solver

Given the generic task formulation (5.40), convex optimization theory [25] is employed through the use of a LQP solver which, at each time step, minimizes the combined task errors while ensuring strict compliance to the constraints. Such solvers do not require the explicit inversion of any model of the system, they are implicitly done through the constrained optimization process. Moreover, physical constraints are, for most of them, naturally described as inequalities which can naturally be handled by this type of solver.

For combining incompatible or conflicting tasks there are two options. Either tasks are organized in hierarchical fashion, which strictly decouples the tasks, or tasks are weighted. Both strategies are valid and more adequate depending on the applications. A comparison and further detailed analysis are presented by Salini et al. [182]. The presented work uses weighted tasks.

The retained n-tasks solver can be summarized by

$$\begin{aligned} \min_{(\mathbb{X})} \quad & \frac{1}{2}\left(\sum_{i=1}^{n}\left(\beta_i^2.T_i(\boldsymbol{q},\dot{\boldsymbol{q}},\mathbb{X})\right)+\beta_0^2.T_0(\boldsymbol{q},\dot{\boldsymbol{q}},\mathbb{X})\right) \\ s.t.: \quad & A\mathbb{X} \leqq \boldsymbol{b}(\boldsymbol{q},\dot{\boldsymbol{q}}) \end{aligned} \tag{5.41}$$

where β_i is the weight of task i, T_0 is a regularization task and $\beta_0 \ll \beta_i$.

5.5.2 CPG based walking on Whole-body control

Considering the previously summarized whole-body control framework, a minimum of four tasks are necessary to achieve a bipedal locomotion in a humanoid robot:

T_1 Task enforcing body posture;
T_2 Task enforcing body height;
T_3 Task enforcing the tracking of feet placement;
T_4 Task maintaining and tracking the COM on a reference trajectory from ZMP.

Task T_3 controls the feet frames' pose, tracking the placement positions computed through a parameterized walking pattern generation. To maintain stability throughout the walk, T_4 controls the COM of the robot using linear model predictive control, maintaining the robot's ZMP coincident with the reference ZMP, from the feet placements.

While task T_3 controls the legs' DOFs and T_4 controls the COM, the pose of upper body's DOFs, back joints, arm joints and neck joints, are not provided a reference value. These other DOFs would be left adrift and their pose would result solely from the COM tracker in task T_4 and feet placement from T_3. It is important to remember that the solver will find the most efficient solution in terms of energy and use minimum effort to fulfill the tasks. To maintain an upright body posture, T_1 provides for the tracking of reference positions in all the body joints to result in a upright stance. Legs are maintained stretched and back straight, holding the robot upright under its own weight. Neck and arm joints are set in a pose to complete the overall upright posture of the robot. Task T_2 aims to reduce the body oscillations and height variation from the walk, maintaining a prescribed height and upright orientation on the *root* frame.

Besides of the typical constrains regarding robot's configuration and actuators' limitations, feet collision constraints are added to the control problem formulation in this walking application.

In this section the aim is to demonstrate how the biped CPGs proposed in this chapter can take the role of the two later tasks in the generation of locomotion. Here is hypothesized that a CPG task $T_{3'}$ could generate lower body joint reference trajectories, replacing tasks T_2, T_3 and T_4. The CPG task $T_{3'}$ is expressed in terms of a desired joint position $q_{j,i}(t)$, input to a local PID controller. It implements the integration of the differential equations, outputting the solutions $z_{j,i}(t)$, in the proposed abstraction used as leg joint trajectories $q_{j,i}(t) = z_{j,i}(t)$.

The implementation from the presented biped CPG solution in section 5.1 is retained, each CPG is constituted by a rhythm generator and six motion generators, one for each joint. Motion generators rely on the specified motion primitives and on the phase output from the coordinated rhythm generator to generate the respective joint trajectories. In the following demonstrations five motion primitives are used:

- Balancing motion - lateral displacement of the body;
- Flexion motion - achieves vertical clearance;
- Knee yielding - perform small flexion of knee on stance;
- Compass motion - generates propulsive movements;
- Turn motion - allows the robot to turn while walking.

In the CPG demonstrations, two tasks are sufficient to address the walking problem. Task $T_{1'}$ is similar to task T_1 and maintains upright posture by maintaining reference positions in the back, arms and neck joints. Task $T_{3'}$, the CPG task, produces the reference positions on the leg joints to maintain the upright posture, configured as rhythmic offset on the rhythmic motions, and the necessary walking patterns to achieve a successful walk.

However, the achieved performance in terms of step length or velocity achieved, and the occasional loss of balance in certain situations brings to attention the limitations of the simple and limited nature of the selected motion primitives and the effect of open-loop trajectory generation. To quickly address these issues a task T_5 to control the COM was devised. Task T_5 was designed to take a reactive role to maintain a projection of the COM of the robot over a reference COM, calculated from the center of the current convex hull of the support polygon.

5.5.3 Simulations

To validate the proposed CPG application in the whole-body control framework and to quantitatively compare it to the ZMP implementation within the same framework, two scenarios are simulated. Simulations are performed in Arboris-Python [179], an open-source dynamic simulator developed at ISIR in Python programming language. The implementation of LQP relies on CVXOPT/CVXMOD, two Python packages for convex optimization [43]. The simulated robot is a model of iCub present at ISIR, with 38 DOFs (32 joints + 6 floating joints to locate the root in space) and four contact points at each foot.

To fully demonstrate how the CPG controller can successfully substitute the walking algorithm based on the ZMP point, two simulation scenarios are addressed. In the first scenario the robot walks forward, freely in a flat environment. The goal is to demonstrate the ability of the CPG controller to produce and fulfill the walking task and then further compare the performance between the walking implementations. The second scenario demonstrates the ability of the whole-body control framework to sequence tasks, and the ability of the CPG controller to produce different locomotor behaviors, accordingly to external commands.

Parameter values used in these two simulation scenarios are presented in table 5.5.

Table 5.5: Parameters used in both simulation settings.

$A_{\text{balancing}}$	6	O_{hYaw}	0
$A_{\text{flex,knee}}$	35	O_{hRoll}	-1.5
$A_{\text{flex,hip}}$	18	O_{hPitch}	15
A_{yield}	2	O_{knee}	-25
A_{compass}	$[0, 7]$	O_{aRoll}	1.5
A_{turn}	$[-10, 10]$	O_{aPitch}	-16
$\omega(\text{rad.s}^{-1})$	4.18	k	1

Walking simulation

On this simulation scenario, the robot is made to walk forward, freely in a flat terrain (fig. 5.29), to demonstrate the ability of the CPG controller to produce the leg's walking motions and substitute the typical ZMP based implementations in this whole-body control scheme.

Three walking implementations are simulated and presented, aiming to provide results for comparing the performance of each approach. A summarized view of the three implementations:

I_1 CPG walking, tasks:

- $T_{1'}$ - upper body pose,
- $T_{3'}$ - CPG task;

I_2 CPG and COM task walking, tasks:

- $T_{1'}$ - upper body pose,
- $T_{3'}$ - CPG task,
- T_5 - COM task;

I_3 ZMP walking, tasks:

- T_1 - body posture,
- T_2 - root frame height and pose,
- T_3 - feet placement,
- T_4 - ZMP tracking.

In implementation I_1 only two operational tasks are used to control the complete walking of the robot. Task $T_{1'}$ goal is to maintain an upright posture of the robot, controlling all the joints, except leg joints, by maintaining fixed reference positions. The CPG task $T_{3'}$ is assigned to control the 12 leg joints, achieving two goals: supporting the robot and generating the movements that will produce the actual walking.

It has been verified that in certain cases when using I_1, the whole-body control scheme would not always follow the reference trajectories produced by the CPG task. To quickly address these cases, in I_2 an additional task T_5 was introduced. Task T_5 tries to maintain the robot's COM over the center of

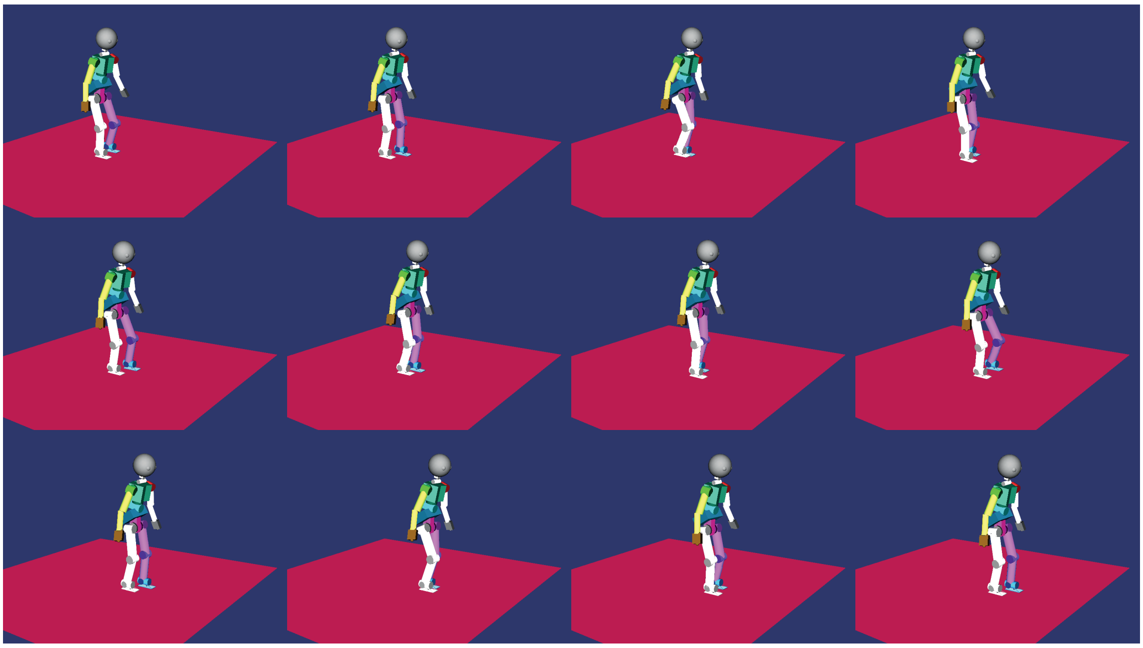

Figure 5.29: Snapshots from straight walking using implementation I_2.

the support polygon, defined at the different step phases as the center of the foot and ground contact points, aiming to provide increased robustness while walking.

The I_3 implementation is similar to the walking implementation by Salini [182]. Body posture, orientation and altitude are controlled by tasks T_1 and T_2. Task T_3 and T_4 produce the actual walking.

The task weights used in the three implementations are presented in table 5.6, based on previous works [182] and heuristically.

Table 5.6: Weights for active tasks.

	T_1	T_2	T_3	T_4
β_i	1	0.1	0.1	0.1

	$T_{1'}$	$T_{3'}$	T_5	
β_i	1	0.1	0.1	

These implementations achieve straight, forward walking, and present very similar walking characteristics in terms of step period, step length and progression. Parametrization for the stepping planner in I_3 was performed to reflect these similarities from the CPG based walking in I_1 and I_2 that use the parameters in table 5.5, $A_{\text{compass}} = 5$ and $A_{\text{turn}} = 0$, the longest step length able to be performed when not using the COM task T_5. Using COM task T_5 allows for a slightly larger range of values for the CPG parameters, e.g. maximum $A_{\text{compass}} = 7$ when using COM task.

Fig. 5.30 shows the CPG produced joint trajectories (dotted) and the performed joint trajectories (solid). For the two CPG implementations I_1 and I_2, the output joint trajectories from the CPG task are the same, since the only difference is the existence of task T_5. Even the performed joint trajectories are almost indistinguishable, despite the inclusion of task T_5.

In fig. 5.30, in both implementations during swing phase at around 13.5 s, it is evident the role of the LQP in producing the final joint positions. The reference trajectories from the CPGs are not followed by the LQP as to produce the final solution. Because the whole-body framework is kind of black box, it is very difficult to have an idea on why the final joint trajectory does not result from a perfect tracking of the CPG output. It results in a lack of information on the causes of the tracking error demonstrated in the ankle roll (fig. 5.30).

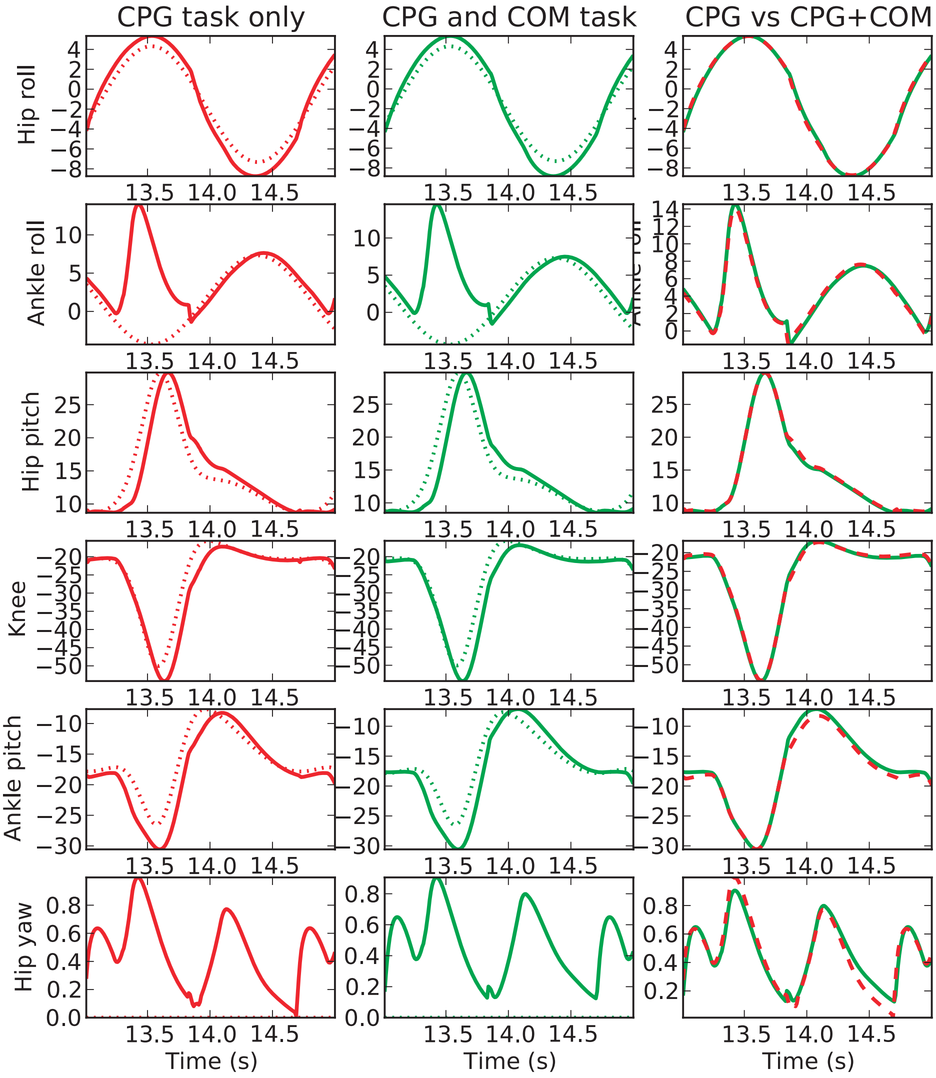

Figure 5.30: Joint trajectories output from the CPG task (dotted lines) and the performed joint trajectories (solid lines). In the first vertical panels are presented I_1 solutions (red) and in the second panels I_2 solutions (green). The third vertical panels superimposes the performed joint trajectories for better visualization and comparison.

Fig. 5.31 brings more insights in the small differences between the simulations. It presents the feet placement sequence for I_1 (top), I_2 (middle) and I_3 (bottom), as well as the COM path during the walk (solid).

Foot placements can be clearly visualized and an idea of the achieved step length in the three implementations can be obtained. In implementation I_1 the step length achieved is slightly smaller than the step length achieved in implementation I_2. Both implementations use the same CPG parameters, with the sole difference on the additional COM task T_5 in I_2.

The COM path progression on the frontal plane (y axis in the figure) is similar in both all implementations. However, in the sagittal plane (x axis) the COM exhibits a backward motion during double support phase in the first implementation (I_1). Fig. 5.31(b) shows a detailed area where this effect is visible. With the addition of T_5 in I_2, the backward motion during double support phase is practically suppressed. Therefore it can be deduced that task T_5 affects the progression of the COM, resulting in a monotonically increasing progression during the walk and an increased step length.

Comparing both I_1 and I_2 CPG implementations to the ZMP implementation I_3 in fig. 5.31(b), it is observable that the sagittal progression of the COM (x axis) in the ZMP linearly increases at a constant rate, while for the CPG it presents periodic halt in progression, happening during the double support phase.

To investigate the energy efficiency between the CPG and the ZMP based solutions, energy consumption was approximated by:

$$E = \int_0^{t_\mathrm{f}} \tau^\top \tau \,\mathrm{d}t, \tag{5.42}$$

The energy values are presented in table 5.7, which suggests that CPG based locomotion is more costly energy wise. A direct correlation appears between energy consumption and the efficiency of the control of the COM. Minimum energy expenditure is obtained when explicitly controlling the COM in I_3 by using a dynamical criterion. A reduced energy consumption in I_2 in comparison to I_1 is suggested by the use of a static balancing criteria in T_5. Also, most of the energy consumption in the three strategies is dedicated to walking.

Table 5.7: Energy consumption and average computation time per control iteration for the three walking implementations.

Consumption ($N^2.m^2$)	I_1	I_2	I_3
Whole-body	811669	771504	512931
Legs	776711	752606	499215

Computation time (ms)	I_1	I_2	I_3
Total time	72.13 (9.08)	83.45 (8.57)	125.68 (s.d.=11.83)
Constraints and tasks update	12.42 (0.61)	25.54 (0.75)	57.4 (6.28)
Solver	59.71 (9.28)	57.90 (8.70)	62.28 (8.88)

In terms of computation time presented in tab. 5.7, the results are as expected and rather logical: the more model reliant the approach is, the longer is the computation time. This time difference is one of the argued benefits of using a CPG based approach for performing cyclic tasks, such as walking. Other computational task unrelated to the generation of walking movements, take a similar amount of time for the three implementations.

Task sequencing simulation

In the second scenario is demonstrated the ability of the whole-body controller to achieve sequential and simultaneous task execution, where walking is produced by the CPG control.

The sequence of executed tasks is depicted in fig. 5.32: the robot initiates walking (1), walks forward towards a table (2,3). It then stops and reaches for a box on the table, picking it up (5). While holding the box, it turns right in place (6-9) and then resumes walking while transporting the box (10-12). On this simulated scenario the tasks defined previously in implementation I_2 used , and two new tasks are added:

T_5 Left hand contact point with the box, $\beta_5 = 0.02$;
T_6 Right hand contact point with the box, $\beta_6 = 0.02$.

Task sequencing is achieved by altering the weights of relevant tasks at certain triggering events [182]. For instance, when the robot reaches a certain distance from the table and stops, the tasks that maintain the contact between the hands and the box are activated. Events also trigger the change and modulation of CPG parameters, producing different locomotor behaviors. Such events:

- start locomotion at the beginning of the simulation;
- modulate the compass amplitude in proportion to the distance of the table;
- stop the robot at the table;
- initiates walking after holding the box and turns right in place, by changing motion amplitude values;
- resumes forward walking after finishing a $90°$ turn, transporting the box.

The used CPG parameters are presented in tab. 5.5 and are maintained constant throughout the simulation, except parameters in tab. 5.8 for the values used in the triggered events and walking modulation, such as A_{compass} and A_{turn}.

Table 5.8: Parameters used while turning and walking while holding the box.

Walking forward:	(°)	Turning:	(°)	Walking and holding box:	(°)
A_{compass}	7	A_{compass}	0	A_{compass}	5
A_{turn}	0	A_{turn}	-10	A_{turn}	0

Fig. 5.33 shows the footsteps of the robot throughout the simulations as well as the optimal (dotted) and actual COM path (dashed). When walking with the box, the robot performs smaller steps as the

mass of the box increases. The measured step length after grabbing the box are 0.163 m, 0.161 m and 0.158 m for the simulations with 0.1kg, 0.5kg and 1.0kg boxes respectively. However, one can not draw a definite conclusion on what is causing the difference in step length in the obtained results. The only changing factor is the box's mass. Results suggest that the extra mass from the box is weighting down the robot, and therefore it produces smaller steps, or it could be the result of the application of the task T_5 which adapts the walk to the change of the robot's global mass.

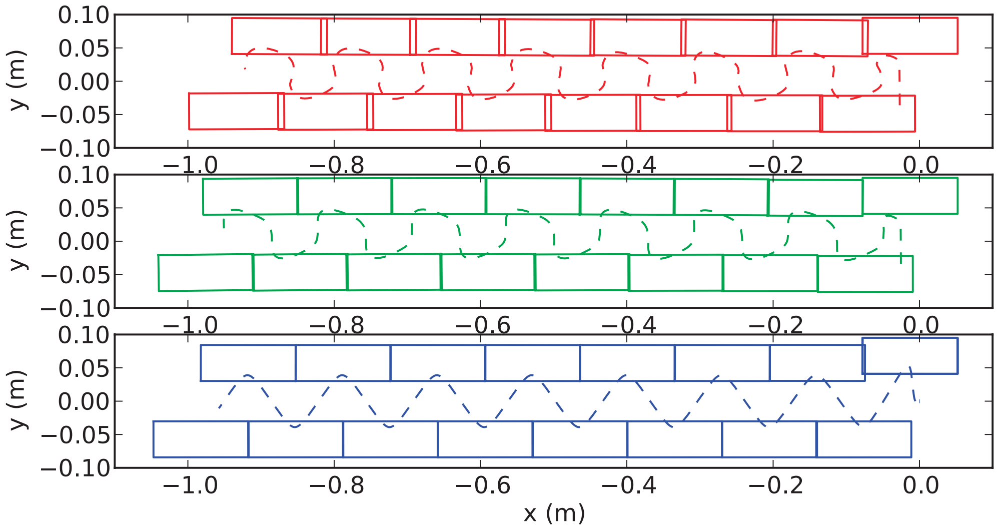

(a) I_1 - top, I_2 - middle, I_3 - bottom

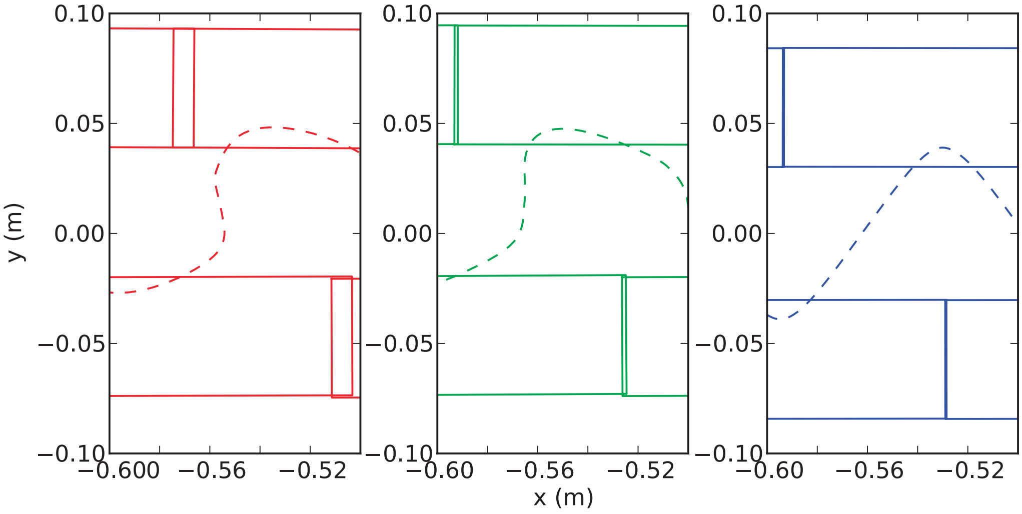

(b) I_1 - left, I_2 - middle, I_3 - right

Figure 5.31: Feet placement sequence and COM path when walking forward.

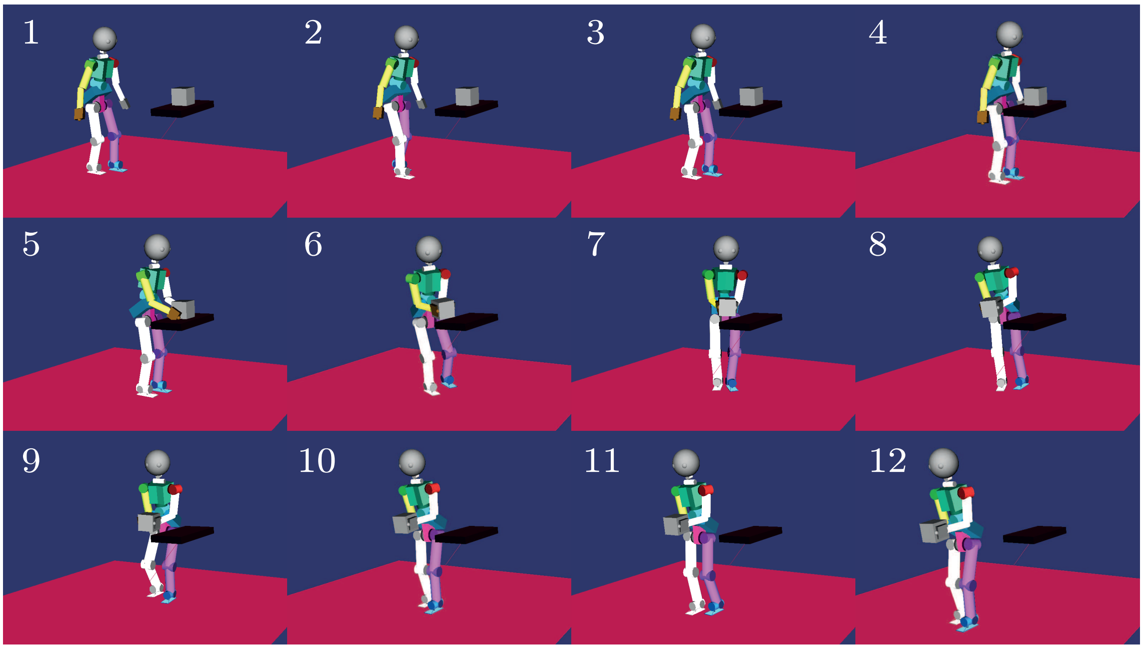

Figure 5.32: In the depicted scenario, the robot initiates walking towards the table, until it stops when reaches a minimum distance to the box. The box picking task is activated, and the robot resumes walking while holding the box. The robot turns right and then walks forward while transporting the box.

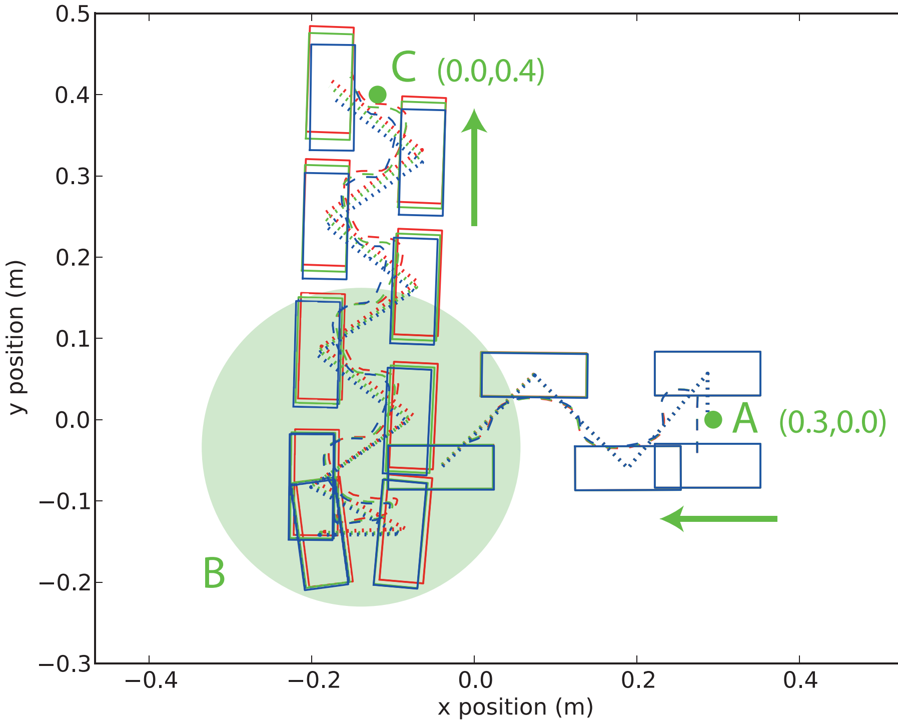

Figure 5.33: Second scenario: Feet placement throughout the simulation and resulting CoM ground projections when A) walking towards the table, B) grabbing the box and turning in place and C) holding the box while walking. Results are shown for different weights of the box: 0.1kg (red), 0.5kg (green) and 1.0kg (blue).

5.5.4 Remarks on CPG within whole-body control framework

The proposed CPG is included in the whole-body controller, as a task which produces joint reference trajectories, substituting the ZMP controller which produces reference end-effector positions.

Simulations demonstrate how the CPG task is able to achieve basic goal-oriented walking, and goal-oriented walking while the whole-body controller pursues several tasks simultaneously. The walking task is achieved as well as the ZMP's task, with only slight change in the obtained performance. However, the employment of the CPG task instead of the original ZMP task does not seem to yield many advantages.

Effectively, the robot is able to walk and perform goal-directed locomotion which is modulated in real-time, and the total time of a computing cycle decreases almost twofold when using only the CPG task to govern the walk. Besides these advantages, the employment of ZMP task seems more favorable. It achieves lower energy expenditure by a third in comparison the CPG walk, it performs a smoother progression of the robot, it is possible to achieve precise foot placement and easily include placement planning methods for navigation in cluttered environments, climb stairs and slopes. Moreover, stability cannot be guaranteed with the same confidence as the ZMP implementation.

5.6 Discussion

In this chapter is proposed a CPG based solution for the generation of biped locomotion for a small humanoid robot. In contrast with the CPG solution presented in chapter 4 for a quadruped robot, the design of a CPG for a bipedal robot requires a different approach, as the sinusoidal patterns from the CPG are not appropriate for achieving biped walking. The CPG solution proposed in this chapter addresses this problem by tackling the generation of a temporal and spatial reference in two separate layers, allowing to accomplish more complex motions, and to accomplish the required temporal coordination for a walk.

An initial repertoire of motion primitives is proposed as a starting point in the locomotor abilities of the robot, presented as a set of simple motions which are able to produce goal-oriented walking. The main idea is that the motion primitives can be combined, sequenced and scaled, depending on the desired locomotor behavior. Despite the simple representation of the motion primitives and the possible final motor patterns, the approach has been demonstrated to be applicable to goal-oriented locomotion in a ball following scenario, and in more complex scenarios which also required the simultaneous execution of other tasks.

The idea of having motion primitives which can be generalized, scaled and modulated depending on the desired locomotor behavior has been demonstrated to be practical, but within a limited scope. For instance, one could think that by increasing the amplitude of the stepping motion, the robot would produce enough vertical clearance to step on stairs, generalizing in this fashion the ability of walking forward, to the ability of climbing stairs. In this case, the robot is indeed capable of clearing the stairs' height by increasing the flexion motion, but the act of climbing the stairs requires careful displacement of the body's weight, which is not considered in flat forward walking.

Performing all biped locomotor behaviors is not possible solely by generalizing the basic motor repertoire here proposed. To perform other locomotor behaviors, such as stair climbing or walking on slopes, the improvement and expansion of the motion primitives repertoire is required, as initially intended when the approach was proposed. The aim is having a robot performing a basic walk, facilitating the task of policy exploration methods such as recent reinforcement learning methods, PoWER [113] and PI^2 [212]. The question is: to what extent can these methods explore the policy space through interaction with the environment and learn new, and very distinct motor behaviors? This question has been preliminarily addressed by Teixeira et al. [211], with the goal of improving the robot's walking velocity by adding DMPs on the compass motion primitive, and using PoWER to explore the DMP policy, rewarding the trials with greater performed velocity.

A phase regulation mechanism is proposed with the goal of exploring feedback mechanisms which influence and adapt the centrally generated motor patterns, with the aim to reject disturbances while walking. Phase regulation and phase resetting are popular feedback mechanisms in CPG based solutions, adding robustness to the walking behaviors. Simulations of simple planar bipeds have employed phase resetting, providing robustness against small pushes, increase in mass and small slopes [5, 6]. In real biped robots it increased the robustness against limited external forces pushing on the robot and adapted the walk for different friction surfaces [149].

The experimental results obtained with the employment of the proposed phase regulation feedback indicate an adaptation of the walking behavior, the regulation of the temporal reference and shaping of the final motor patterns. This adaptation allowed the robot to tackle slight unperceived perturbations in terrain inclination, preventing the tumble of the robot when walking in up and down slopes.

It is unclear, however, if it should be expected to have a broader scope on the abilities of disturbance rejection by employing the phase regulation mechanisms, or if the obtained robustness is limited by the nature of the high gain position control of the robot, or other characteristics of the platform, such as the big flat feet.

The usefulness of the proposed CPG, on producing walking behaviors in more realistic scenarios, was investigated within a whole-body control framework. Simulated scenarios demonstrate the feasibility of using the CPG as a walking generator task, successfully substituting typical model based methods, as the ZMP based walking generator. Results have demonstrated that the CPG is able to produce goal-oriented walking controlled in real-time, even when used simultaneously with other working tasks. After a more careful and objective evaluation of the attained performance by the CPG and motion primitives, the lesser performance in stability and the exhibited oscillatory progression is apparent, due to the lack of accurate control of the COM, even with the use of the COM task. The use of the ZMP method with predictive control achieves a smoother progression of the robot, especially when performing tight walking maneuvers and performing simultaneous tasks which alters the dynamics of the robot.

CHAPTER 6

REFLEX-BASED QUADRUPED WALKING

The organization of the neural mechanisms for the generation of rhythmic motions, fundamental to locomotion, had two prospective explanations in the beginning of the 20th century [27]. One idea, by Charles S. Sherrington [34], defended that rhythms could be the result of a chain of reflexes triggered and governed by external sensorial events, producing the final rhythmic locomotor activity. The other explanation, by T.G. Brown proposed the generation of rhythmic activity as a central neural process [27], not relying on external sensory events to generate the rhythmic activity for locomotion, bringing the conceptual idea of a CPG, granted by further research and evidence as discussed in section 2.2.

Even though locomotion is a centrally generated process, the important role that sensory feedback plays in the adaptation and correction of legged locomotion is unarguable. It has been shown that the CPG and locomotion generation is highly integrated and dependent on feedback pathways. For instance, it has been demonstrated [176] that stimulation of sensory afferents can elicit locomotion, sensory events can adjust the duration of the rhythmic activity and sensory removal deteriorates locomotor abilities, such as precise foot placement.

Also studied in the last decades, is the importance of the mechanical characteristics on the achievement of locomotion. Passive mechanisms have been made to walk and run, only pushed forward by gravitational or elastic energy, exploiting concepts of mechanical self-stability [140]. Without a walking controller, these mechanisms are able to walk relying solely on their characteristics and their interaction with the environment. Furthermore, locomotion has also been achieved by the application of simple sensory driven reflexes rules, both in simulations and in robotic platforms [42, 67, 68].

All these aspects evidence the fact that locomotion generation is much more complex than a simple feedforward process of muscle activations. Despite much research on the topic, it is still not clear how CPGs and spinal mechanisms are neurally organized and how they are integrated with feedback pathways. The relative roles in the interplay between the CPG feedforward generation are also largely unknown, the feedback pathways and the mechanical stabilization for control of locomotion.

Arthur Kuo [116] discusses the relative importance of feedforward and feedback, and their prospective roles on the control of rhythmic movements. He hypothesizes that the primary advantage from the existence of a central rhythmic generator is in the processing of sensory information for use in feedback, instead of timing control. This hypothesis suggests that the CPG has a role as a spinal processor within the feedback loop, correcting imperfect sensory feedback and adapting peripheral inputs and feedback pathways. Kuo argues that the relative role of feedforward and feedback components depends on the relative significance between unexpected disturbances and imperfect sensors.

In this chapter are presented the tentative steps in exploring this idea of the CPG as a regulator for a reflex chain network. The goal is not to propose or study a biological plausible model of the CPG or of the reflex network. The goal is to explore the idea of the CPG as a possible endogenous rhythmic internal model which governs the reflex network, either by modulating the reflexes, determining the activated feedback pathways, or serving as an internal model of the expected sensory information.

In the following sections is presented a survey on works which achieve walking through the reflex based control, and the respective applied reflex mechanisms. These mechanisms are summarized and implemented in a sensory driven reflex controller which aims to control the walk of a quadruped robot. The goal is to accomplish a parsimonious controller, resorting to a minimum number of reflexes to produce a successful walking behavior. How the CPG could be integrated with the reflexes and improve the walking behavior is discussed after demonstrating the ability of the proposed reflex network to produce quadruped walking.

6.1 Related works

In this section are surveyed some works in computational simulations and robot locomotion which use purely rule based or reflex based generation of locomotion, or use CPG generated locomotion and apply reflexes to tightly regulate the rhythmic activity. To compare, some works which use CPG generated locomotion augmented with corrective reflexes are also mentioned.

One of the earliest works accomplishing rule based locomotion stemmed from the research on the locomotion of the stick insect, by Cruse et al. [42]. Several models have been proposed with the goal of understanding the biological control of locomotion in insects, to the building of low computational demanding locomotion control for walking machines. Cruse took a set of six rules defining the interactions between legs, based on the observation of locomotion on the stick-insect, and designed a locomotion controller that later was used to control a hexapod robot [42]. A leg controller consists of three parts: the swing net, the stance net, and the selector net which determines whether the swing or the stance net can control the motor output, and it uses sensory inputs from joint position and velocity and four sensory inputs signaling obstructions during the swing. The designed controller is considered as a distributed controller of six leg controllers, coordinated through the six rules:

In work of Wörgötter et al. in 2005 [66] a purely reflexive controller generates the walking of a planar biped robot. The simple reflex network is divided into a top level and a bottom level, encoding the locomotor reflexes in the connections between the sensory events and motor interneurons. These

Table 6.1: The six rules based on stick insect locomotion in the work of Cruse et al.

Action	Description	Goal
Suppress lift-off	caudal leg swing inhibition while rostral leg is performing swing	avoid static instability
Elicit earlier protraction	rostral excitation of swing when caudal leg begins retraction	favours temporal coherence
Enforce late protraction	caudally influence depending on position of the leg	maintain temporal coherence
Aim touchdown location	legs to be placed in similar locations	exploit prior foothold location of the fore legs
Distribute propulsive force	increase in leg load causes other legs to prolong stance	share the load efficiently
Enforce correction step	becomes active if one leg step of the neighbour leg	avoids stepping in the rostral leg

connections are summarized in table 6.2. The top level implements the network which encompasses hip stretch receptors, ground receptor and interneurons responsible for integrating these receptors. On the bottom level are implemented the motor neurons and joint angle sensor neurons. The interneurons are implemented as leaky integrators, and sensory receptors as sigmoid functions with parameterizable gain and bias.

Table 6.2: Reflexes encoded in the network in the work of Wörgötter et al. [66].

Sensory event	Action
Ground contact	contralateral knee flexor and hip extensor excitation
Ground contact	ipsilateral knee extensor and hip flexor excitation
Anterior extreme position (AEP)	ipsilateral knee extension excitation
AEP	ipsilateral knee flexion inhibition

The work was later extended [67]. A very similar controller is applied, but two parameters defining the AEP at the hip joints and the gain of the motor-neurons in hip joints are learned on-line to reach faster velocities. Besides the reflex network, Manoonpong [126] proposed a body control mechanism that moves a mass to control the balance during the walk, relying on an infrared sensor to detect a white ramp, while the postural response is learned on-line.

Geyer demonstrated that it is possible to accomplish locomotion in a biped musculoskeletal simulation [68], by having a set of reflexes which exploit the principles of legged mechanics. Simple reflexive positive and negative feedback loops control muscle activity, specific for each step phase, swing and stance, identified by the existence of ground contact. For instance, in the stance phase, a positive force feedback loop is used to achieve compliant behavior of the leg. Although very relevant and interesting, it is possible that most reflexes would not translate well to the presented abstraction.

Ekeberg in 1998 [218] developed a single leg walking simulation, using a Neural Phase Generation (NPG) and a system of fast feedback pathways, adapted from a model used for the simulation of swimming lamprey [55]. The NPG is implemented using neurons as leaky integrators, divided into four phases: touchdown, propulsion, lift-off and swing. Each of the phases activates the respective excitatory and inhibitory interneurons that activate the extensor and flexor muscles. This description of the state of the leg sets the appropriate feedback pathways, which benefits the ability to correct any inconsistencies in the afferent input. Sensory feedback influence directly the transition in the activity of the NPG, it influences the activity of the motor interneurons and the respective motor activity, and also entrains the NPG. A summarized description of the reflexes and their effects are presented in table. 6.3.

Table 6.3: Feedback mechanisms employed by Ekeberg [218]

Sensory event	Action
Reaching AEP (anterior extreme position)	excites transition to touchdown
Reaching PEP (posterior extreme position)	excites lift-off
Ground contact on touchdown	excites the transition from touchdown to propulsion
Ground contact on lift-off	excites the transition from lift-off to swing

Using a similar NPG, Ekeberg and Pearson studied the role of the sensory information in the regulation of the transition from stance and swing. Their goal was to investigate the relative role of the two sensory inputs in the regulation of the transition: the hip angle and the ankle loading. In a simulation of the cat hind legs, muscle activation is controlled in a sequence of four states, lift-off, swing, touchdown and stance. The transition between the four states is governed by sensory information related to leg:

- Swing - transits to touchdown after hip and knee reach a certain angle value.
- Touchdown - transits into stance after the leg establishes ground contact.
- Stance - transits into lift-off after reaching a certain hip angle, and/or the unload of the ankle tendon.
- Lift-off - transits into swing after loss of ground contact.

Authors conclude that coordination of the stepping depends on load information of each leg, and that the mechanical connection between the hind legs mediated by the transition mechanisms, play a significant role in establishing the alternating gait.

The same ideas presented in these works are used by Maufroy et al. [134] to implement a walking controller for quadruped musculoskeletal model of the fore and hind legs. The four NPGs previously employed are reduced to only two in this work, one *Extensor module* and one *Flexor module*. In this work they extend the controller, subdividing the different parts and improving the adaptive stepping motion. By having only two NPG states, four synergies are used to produce muscle activation, *lift-off*, *swing*, *touchdown* and *stance*, activated and timed in relationship to one of the NPG states, or combined with sensory events such as foot placement. Similarly as the other exposed works, the controller relies on sensory information related to hip angle, AEP and PEP, as well as leg loading, to regulate the transition between the step states of the NPG. This sensory information is input into the NPGs, inhibing/exciting the transition between Flexor and Extensor modules, and into the synergies, serving to regulate the stretch reflex and load compensation feedback. For receiving a tonic input and drive rhythm of the NPG, a mechanism is employed in the proposed controller, the *propulsive force control module*.

Lewis et al. [112] study a neural architecture of the CPG with reflexes, employed in a model of the human lower body, as a planar biped robot implemented with motors and straps mimicking the human leg muscles. The proposed CPG has four central neurons controlling hip extension and hip flexion, receiving sensory information from ground contact, load sensor, and hip position. The lower limb is controlled by the phase of the step cycle and the hip angular position. The CPG produces the rhythmic activity for the hip, and simultaneously modulates the activity of the reflexes which govern the muscles in the knee and ankle. The interaction between the reflex system, CPG and body dynamics produces an entrained walking cycle. Authors argue that the CPG helps to stabilize the gait against perturbations, when comparing to a purely reflexive system.

In other works, reflexes are used as fast, involuntary actions triggered by sensory events during a certain state of the step. For instance, in the work of Kimura and Fukuoka [110], CPGs implemented as a Neural Oscillators produce the step rhythm which is divided into three states: *lift-off*, *swing* and *stance*. For each of these states, a reference joint position and PD gains are obtained from a lookup table. Then, several reflexes were proposed to correct the stepping motions in case of disturbances. The proposed reflexes are presented in table 6.4.

Table 6.4: Corrective reflexes from Kimura and Fukuoka [110]

Reflex	Trigger	Step phase	Description
Flexor reflex	collision with obstacle	swing	Enhance flexion during swing upon touching an obstacle, to prevent stumbling
Stepping reflex	forward speed	swing	adjustment of touchdown angle of a swinging leg
Vestibulospinal	body pitch	stance	shortens/extends the legs in the sagittal plane to control the pitch angle
Tonic response	roll	stance and swing	shortens/extends the legs in the frontal plane to control the roll angle
Sideways stepping	roll	swing	Yaw joint proportional to roll
Corrective stepping	loss of ground contact	swing	at the end of swing, extends the leg further if it does not touch the ground as expected
Crossed flexor	ground contact of contralateral leg	swing	higher swing in contralateral leg due to excessive yield

6.1.1 Summary of reflexes

Most of the presented works on reflex based locomotion are implemented in simulation, using models of musculoskeletal fore and hind legs, with the solution producing muscle activations, or the torques to be applied at the joints calculated from the musculoskeletal models. Only the work by H. Cruse and the work by Wörgötter are applied to rotational controlled DOFs in robots. In the case of H. Cruse the generator outputs the joint velocities for the hexapod robot, and in Wörgötter's work, the locomotion generator outputs motor voltages for the biped robot.

However, in all these works three sensory events are used to trigger locomotor actions (reflex based walking) or regulate the rhythm activity of the CPGs. In common is the use of the angle of the hip joint, indicated by the AEP and PEP signals, regulating the timing of the stance and swing phases. The signals indicating ground contact from foot sensors are also used, or even leg load, used to inhibit the transition from the stance phase to the swing phase. Here a summary of the reflexes is presented, which tries to abstract from the implementation details and how they are integrated in the controller, concerning only to a general description of the sensory-action effect.

- Hip reaching the Anterior Extreme Position (AEP) initiates the stance phase by eliciting the extension of the leg.
- Hip reaching the Posterior Extreme Position (PEP) initiates the swing phase by flexing the leg.
- Unload of the leg elicits, or allows, the swing phase.
- Ground contact promotes the stance, or reinforces stance behavior
- Contralateral ground contact promotes swing, or lack of contralateral ground contact inhibits swing/lift-off phases.

6.2 Modeling and implementation

The proposed reflex system controls a quadruped robot with position controlled hips and retractable, passive compliant knees. Some assumptions on how to bring the biological reflexes' to the current abstraction are here clarified.

It is assumed that the final trajectories are not previously known, and should result from the interplay between the motor actions and the sensory information. The walking behavior should be an emergent realization of motor actions reflecting the general rules as encoded in the reflexes, and not a result from strict tracking of a predefined desired behavior.

Some of these reflexes express motor activities as a continuous activity depending on sensory information. e.g. ground contact promoting/reinforcing the stance phase of the step. It is therefore assumed that joint velocity is the best abstraction for the output of the system based on the reflexes described in section 6.1.1. Reflexes reflect a set rate of change dependent on sensory information, producing motor actions while a determinate sensory condition is maintained, or mimic positive feedback mechanisms found in the motor control of animals. This assumption accepts that joint positions change while necessary, and sensory events determine the final output trajectory.

It is considered that one step cycle is divided into four motor actions:

1. Lift-off - reduction of the leg length by flexing the knee.
2. Swing - bring the leg forward by acting on the hip.
3. Touchdown - having the leg in the rostral (to the front) position, increase the leg length to support the foot on the ground, by extending the knee.
4. Stance - propulsion of the robot by acting on the hip.

These motor actions are not mutually exclusive in time, for example, the swing action could be executed just after lift-off has started.

The position controlled joints track the position as integrated from the reflex system output in joint velocity, $\dot{\theta}$:

- Hip joint: θ_h joint position, $\dot{\theta}_\mathrm{h}$ joint velocity
  - By specifying a positive velocity for the hip joint, the leg produces the motion of propulsion, reflecting the hip action in the **stance**.
  - A negative velocity for the hip joint transfers the leg to the front, reflecting what happens in the **swing**.
- Knee joint: θ_k joint position, $\dot{\theta}_\mathrm{k}$ joint velocity
  - A positive velocity in the knee flexes the leg and decreases the leg length, achieving **lift-off**.
  - And a negative velocity in the knee releases the spring, extending the leg, achieving **touchdown.**

These motor actions are implemented by assigning fixed rates of change, activated by discrete neuron activations from a reflexive network dependent on sensory information. The joint output is given by:

$$\dot{\theta}_\mathrm{h} = \alpha_\mathrm{h} u_\mathrm{stance} - \gamma_\mathrm{h} u_\mathrm{swing} \tag{6.1}$$

$$\begin{aligned} \dot{\theta}_\mathrm{k} &= -\left(\alpha_\mathrm{k} u_\mathrm{touchdown} - \gamma_\mathrm{k} u_\mathrm{liftoff}\right) \\ &\quad + g_\mathrm{lim}(\theta_\mathrm{k} - \Theta_\mathrm{k,max}) \exp^{-\frac{\left(\theta_\mathrm{k} - \Theta_\mathrm{k,max}\right)^2}{2\sigma^2}} \\ &\quad + g_\mathrm{lim}(\theta_\mathrm{k} - \Theta_\mathrm{k,min}) \exp^{-\frac{\left(\theta_\mathrm{k} - \Theta_\mathrm{k,min}\right)^2}{2\sigma^2}} \end{aligned} \tag{6.2}$$

where u are the neuron activations of the described actions ($u \in [0, 1]$), and α and γ are the fixed rates of change for hip and knee joints. To limit the range of activity on the knee, due to its limited range of action, two additional joint limiting terms are included. Parameter g_lim defines the strength of the repeller, σ the width of the repeller, and $\Theta_\mathrm{k,max}$ and $\Theta_\mathrm{k,min}$ the maximum and minimum joint limits of the knee, respectively.

6.2.1 Neuron model

The reflex network is based on the neuron model used by Ekeberg [55], representing a population of functionally similar neurons and outputting a mean firing frequency.

$$\dot{\xi}_+ = \frac{1}{\tau}\left(\sum_{i\in\Upsilon_+} u_i w_i - \xi_+\right) \tag{6.3}$$

$$\dot{\xi}_- = \frac{1}{\tau}\left(\sum_{i\in\Upsilon_-} u_i w_i - \xi_-\right) \tag{6.4}$$

Eq. (6.3) and eq. (6.4) are simple leaky integrators which model a single neuron, with a time constant τ, and a set of excitatory (Υ_+) and one set of inhibitory (Υ_-) connections, weighted by the parameter w. The output of the neuron is given by eq. (6.5), reflecting a mean firing rate, between 0 and 1. The activity of the neuron is characterized by its gain Γ and the activation threshold Θ.

$$u = \begin{cases} 1 - \exp\left(\left(\Theta - \xi_+\right)\Gamma\right) - \xi_-, & \text{if positive} \\ 0, & \text{otherwise} \end{cases} \tag{6.5}$$

6.2.2 Sensory inputs

The sensory inputs to the reflex network translate sensory events based on the leg's proprioceptive information, such as leg joint position and foot force:

- Anterior extreme position - sensory signal becomes active if hip exceeds AEP angle Θ_{AEP}
- Posterior extreme position - sensory signal becomes active if hip exceeds PEP angle Θ_{PEP}
- Ground contact - sensory signal becomes active if touch force sensor exceeds a small threshold

These sensory events are detected through the logistic function in eqs. (6.6)(6.7)(6.8), activated ($= 1$) when the sensory value crosses the defined threshold. For each leg there is a set of sensory inputs:

$$u_{\mathrm{AEP}} = \frac{1}{1 + e^{-b(\theta_{\mathrm{h}} - \Theta_{\mathrm{AEP}})}} \tag{6.6}$$

$$u_{\mathrm{PEP}} = \frac{1}{1 + e^{b(\theta_{\mathrm{h}} - \Theta_{\mathrm{PEP}})}} \tag{6.7}$$

$$u_{\mathrm{GC}} = \frac{1}{1 + e^{b(F_{\mathrm{threshold}} - F_{\mathrm{touch}})}} \tag{6.8}$$

6.2.3 Reflex network

The three sensory events are assigned to the neuron inputs which govern the motor actions.

A single leg is controlled by four neurons, which determine the activation of the four motor actions. Two motor actions are assigned to the hip joint, each governed by one neuron, **swing** and **stance**. The other two motor actions, **lift-off** and **touch-down** are assigned to the knee joint.

Based on the description of the reflexes in section 6.1.1 and the three sensory events, the following behaviors are encoded in the reflex network as excitatory and inhibitory connections:

- Hip reaching AEP elicits the touchdown action on the knee: $\Upsilon_{+,\text{touchdown},i} \supset \{u_{\text{AEP},i}\}$ and $w_{\text{AEP},\text{touchdown},i} = 1$
- Hip reaching AEP inhibits the continuation of hip protraction: $\Upsilon_{-,\text{swing},i} \supset \{u_{\text{AEP},i}\}$ and $w_{\text{AEP},\text{swing},i} = 1$
- Hip reaching PEP elicits lift-off, making the knee flex: $\Upsilon_{+,\text{liftoff},i} \supset \{u_{\text{PEP},i}\}$ and $w_{\text{PEP},\text{liftoff},i} = 1$
- Ground contact elicits and reinforces the stance: $\Upsilon_{+,\text{stance},i} \supset \{u_{\text{GC},i}\}$ and $w_{\text{GC},\text{stance},i} = 1$
- Lack of ground contact elicits the protraction of the hip: $\Upsilon_{+,\text{swing},i} \supset \{(1 - u_{\text{GC},i})\}$ and $w_{\text{GC},\text{swing},i} = 1$

These connections are depicted in fig. 6.1. This simple reflex network is enough to produce stepping motions in a single leg.

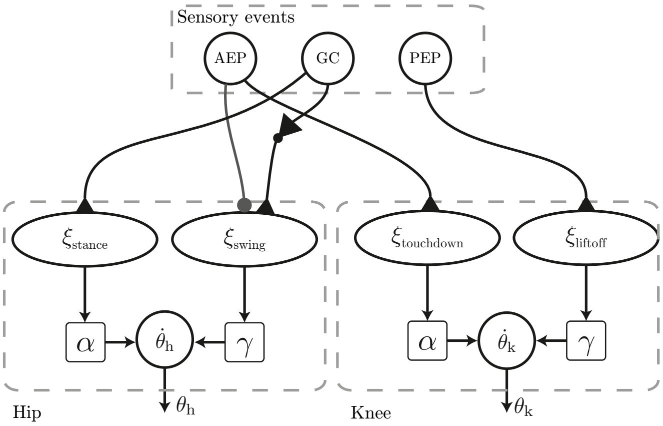

Figure 6.1: Reflex network governing a single limb. Ground contact (GC) excites the stance and the lack of ground contact excites the swing of the hip. The hip reaching AEP inhibits the swing on the hip and excites the liftoff on the knee. Reaching PEP excites the lift-off of the knee.

Contralateral coordination

Although independent leg reflex networks produce alternated stepping in a girdle, the addition of an inhibitory contralateral connection imposes strict alternation of step phases, preventing the execution of simultaneous swing motor action on contralateral legs.

The inhibitory contralateral connection comes from the contralateral ground contact sensor input, to the lift-off motor action in the knee (fig. 6.2):

- Lack of ground contact in the contralateral leg (j), inhibits the initiation of the lift-off (in leg i): $\Upsilon_{-,\mathrm{liftoff},i} \supset \{(1 - u_{\mathrm{GC},j})\}$ and $w_{\mathrm{GC},\mathrm{liftoff},j} = 1$

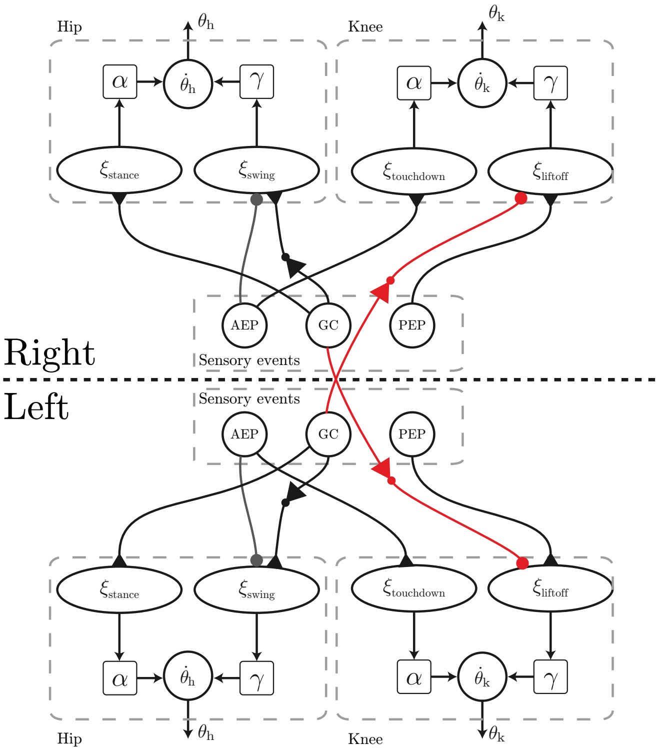
Hip
θ_h
Knee
θ_k
α
$\dot{\theta}_\mathrm{h}$
γ
α
$\dot{\theta}_\mathrm{k}$
γ
ξ_stance
ξ_swing
$\xi_\mathrm{touchdown}$
ξ_liftoff
AEP
GC
PEP
Right
Sensory events
Left
Sensory events
AEP
GC
PEP
ξ_stance
ξ_swing
$\xi_\mathrm{touchdown}$
ξ_liftoff
α
$\dot{\theta}_\mathrm{h}$
γ
α
$\dot{\theta}_\mathrm{k}$
γ
Hip
θ_h
Knee
θ_k

Figure 6.2: Added contralateral connection meant to accomplish strict contralateral coordination. The lack of ground contact inhibits contralateral touchdown on the knee.

Ipsilateral coordination

Ipsilateral coordination can be achieved by applying an inhibitory connection when a strict alternation of ipsilateral legs is desired.

- Lack of ground contact in the ipsilateral leg (o), inhibits the initiation of the lift-off (in leg i): $\Upsilon_{-,\mathrm{liftoff},i} \supset \{(1 - u_{\mathrm{GC},o})\}$ and $w_{\mathrm{GC},\mathrm{liftoff},o} = 1$

This inhibitory connection (fig. 6.3) is applied with the goal of preventing the execution of the swing motor action in ipsilateral legs, as in a pace gait, and impose some phase relationship in ipsilateral legs to achieve walk or trot gaits.

6.3 Simulations

In this section are presented the results from simulations on the reflex network applied to the compliant quadruped robot Oncilla. The Oncilla is a small quadruped robot, with pantograph, three-segment leg design, providing passive compliant behavior to the cable driven retractable knees. The movements

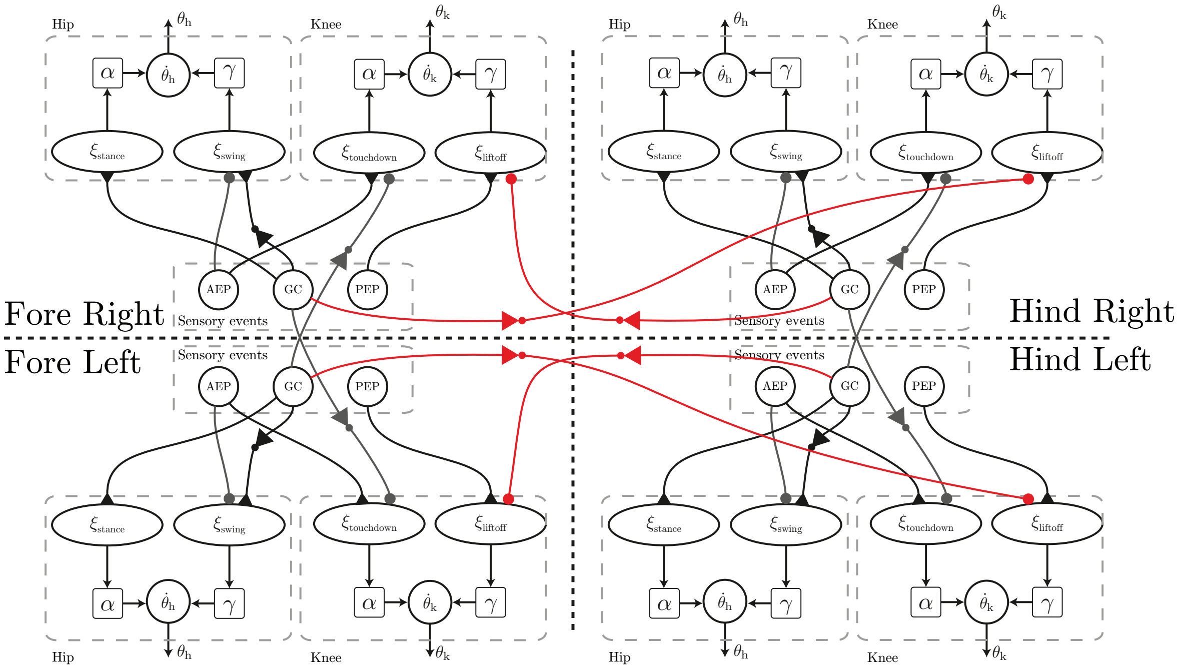

Figure 6.3: Meant to prevent the execution of the pace gait, an ipsilateral inhibition is added, relating to the lack of ground contact.

of the leg on the sagittal and frontal plane are actuated by position controlled servos. Pertaining videos are available at `http://asbg.dei.uminho.pt/user/1`.

The reflex network is parameterized empirically and based on other works [134, 218]. The experiments are divided into three experimental setups, for an easier study and parametrisation of the reflex network. The first two experiments only concern the employment of the reflex network on a single girdle. On the first experiment it is only considered the employment of the reflex network on the hind legs, with the robot supported on the front by two fixed wheels with the same width as the fore legs, such that only the hind legs propel the robot and slightly constraining rolling motions (fig. 6.4). The second experiment presents a similar setup as the first, but applied only to the fore legs, while the back of the robot is supported (fig. 6.8). On the third experiment it is intended to accomplish the full quadruped walking, by using the empirical insight from the previous two simulation scenarios on the full quadruped reflex network (fig. 6.12).

As far as startup conditions are concerned, the joint positions are established such that the contralateral limbs are at the AEP and PEP positions, and initial neuron activities are set to the respective step phase.

6.3.1 Hind legs

Here the simulation results from the reflex network applied only to the hind girdle are demonstrated. First it is explained how the sensory events trigger the sequence of reflexes which produce the motor actions, followed by a short comparison between the results obtained from the two sets of parameters

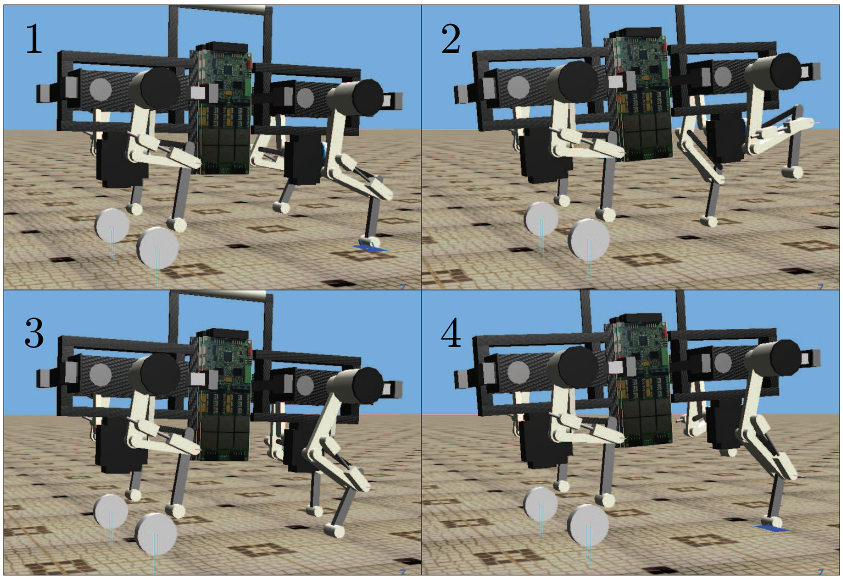

Figure 6.4: Snapshots from simulation depicting the four actions of stepping. Left leg: 1- stance, 2- lift-off and swing, 3- swing and touchdown, 4- stance.

values presented in table 6.5. This simulation aims to verify if the reflex network is able to produce stepping behaviors, and gain insight for the application of the reflex network to the quadruped robot.

Table 6.5: Neuron parameters and joint output parameters for hind leg simulation.

	τ	Γ	Θ
liftoff	0.01	0.1	1
stance	0.01	0.1	1
touchdown	0.01	0.1	1
swing	0.01	0.1	1

	Θ_{AEP}	Θ_{PEP}	$F_{\mathrm{threshold}}$	α_{h}	γ_{h}	α_{k}	γ_{h}
set 1	10	0	1	50	300	300	500
set 2	10	0	1	100	300	300	500

Fig. 6.5 and fig. 6.6 depict the activity of the neurons and the respective motor output in the two hind legs simulations. It is possible to analyze in these figures how the chain of reflexes produces the motor actions.

Consider the left panels on fig. 6.5 and fig. 6.6, depicting the hind girdle simulation with $\alpha_{\mathrm{h}} = 50$. Initially the *stance* neuron is active ($u_{\mathrm{stance,HL}} = 1$, dashed line in fig. 6.5) due to the existence of ground contact $u_{\mathrm{GC,HL}}$, producing a constant propulsive motion in the hip. After the hip angle reaches the PEP value ($u_{\mathrm{PEP,HL}} = 1$), the *lift-off* neuron is activated ($u_{\mathrm{liftoff,HL}}$, solid line in fig. 6.6), producing a flexion motion of the knee, shortening the leg's length and lifting the foot from the ground. The lack of ground contact ($u_{\mathrm{GC,HL}} = 0$) activates the *swing* neuron $u_{\mathrm{swing,HL}}$ (dashed line in fig. 6.5) which produces a flexion motion of the hip, transferring the leg to a rostral position. After reaching the AEP value ($u_{\mathrm{AEP,HL}} = 1$), the *swing* neuron $u_{\mathrm{swing,HL}}$ (solid line in fig. 6.5) is deactivated halting the motion of the hip, and the touchdown neuron $u_{\text{touchdown,HL}}$ (dashed line in fig. 6.6) becomes active, producing the extension of the knee and the consequent foot placement. Just as the foot regains contact with the ground ($u_{\text{swing,HL}}$), the *stance* neuron becomes active and produces the propulsive motion of stance. The sequence repeats onwards, producing the stereotyped motions of walking.

The neuron activations and motor output of the second hind girdle simulation with $\alpha_{\text{h}} = 100$ are depicted on the right panels of figs. 6.5 and 6.6. Despite the same sequence of reflexes and motor actions, it is possible to observe a distinct motor output solely by changing one motor gain parameter. In terms of reflex neuron activity, one striking difference is the delay on the activation of the *liftoff* neuron ($u_{\text{liftoff,HL}}$, solid line in fig. 6.6) with respect to the ipsilateral excitation of $u_{\text{PEP,HL}}$, due to the lack of contralateral ground contact ($u_{\text{GC,HR}} = 0$).

The motor output is also quite distinct. By using a larger α_{h} in set 2, the motor action of the stance phase is executed with an increased angular rate of change, resulting in faster stance movements and greater amplitude of motions in the hip and knee joints, and a larger step length. Notice that the hip extension well exceeds the defined PEP value.

Despite only changing one parameter relative to the angular rate of the stance phase, the obtained walking pattern has changed considerably. Fig. 6.7 presents the obtained stepping sequence in the two simulations, presenting an alternating walking pattern. It is observable an increase on the performed velocity, and a decrease on the duty factor. However, the increase of the velocity results from the increase of the step length, and not from the decrease of duty factor or step period like typical animal locomotion. The step period increased, due to the increase of the swing duration, maintaining the stance duration.

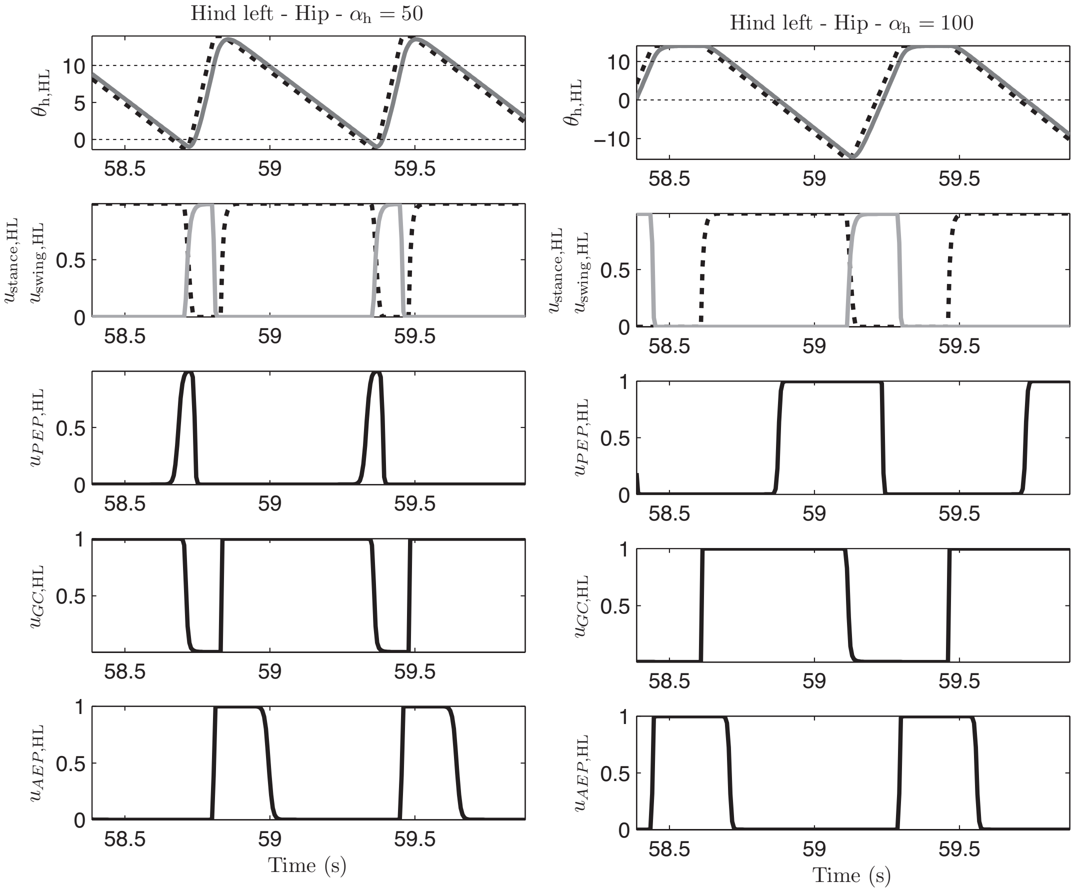

Figure 6.5: Neuron activity and motor output for the hip joint. Results from parameter set with $\alpha_{\text{h}} = 50$ are on the left, and with $\alpha_{\text{h}} = 100$ on the right. The first row presents the resulting motor output for the hip joint, dashed lines are the reference values, the solid lines the produced joint values, and dotted lines represent the AEP and PEP values. In the second row, solid lines represent $u_{\text{stance,HL}}$ and dashed lines $u_{\text{swing,HL}}$. $u_{\text{stance,HL}}$ is active as long the sensory neuron $u_{\text{GC,HL}}$ is active. $u_{\text{swing,HL}}$ is active until when the hip hasn't reach AEP and there is not ground contact.

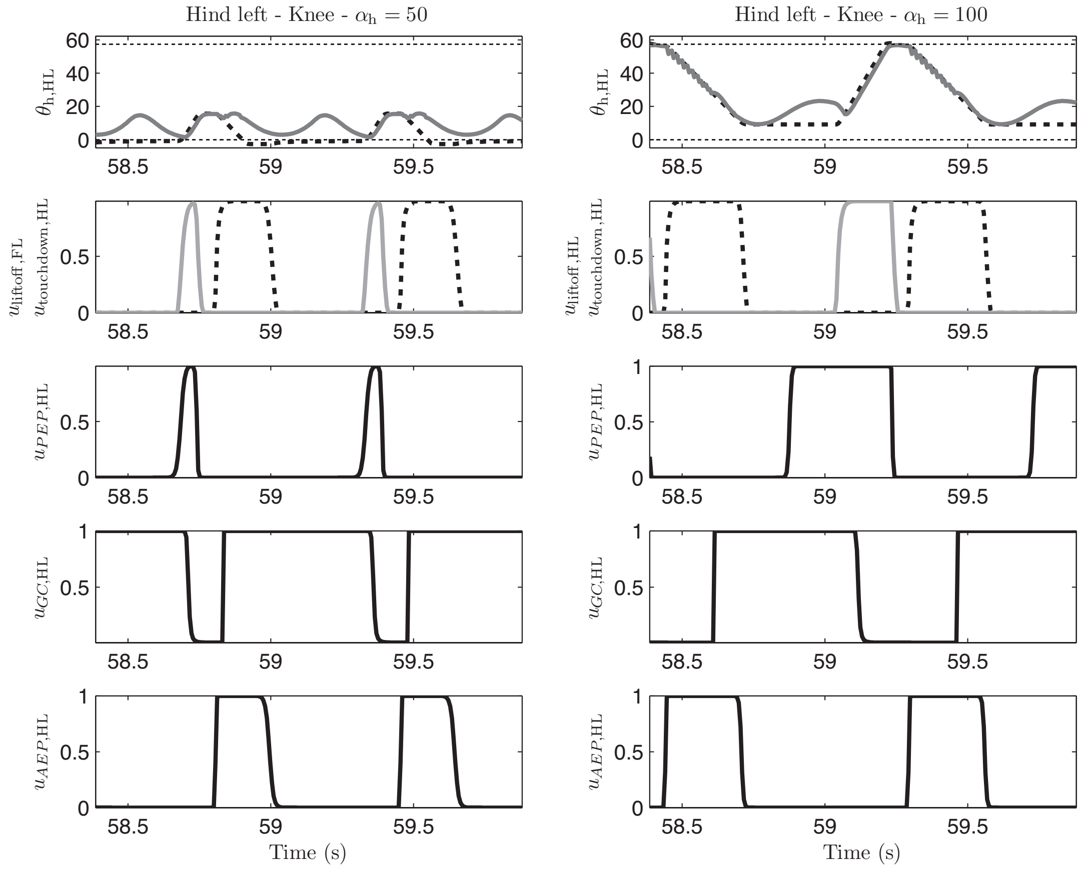

Figure 6.6: Neuron activity and motor output for the knee joint. Results from parameter set with $\alpha_h = 50$ are on the left, and with $\alpha_h = 100$ on the right. The first row presents the resulting motor output for the knee joint, dashed lines are the reference values, the solid lines the produced joint values and dotted lines represent the AEP and PEP values. In the second row, solid lines represent $u_{\text{liftoff,HL}}$ and dashed lines $u_{\text{touchdown,HL}}$. The neuron $u_{\text{touchdown,HL}}$ is activated when the hip reaches AEP. $u_{\text{liftoff,HL}}$ is activated by $u_{\text{PEP,HL}}$ and inhibited by the contralateral $u_{\text{GC,HR}}$.

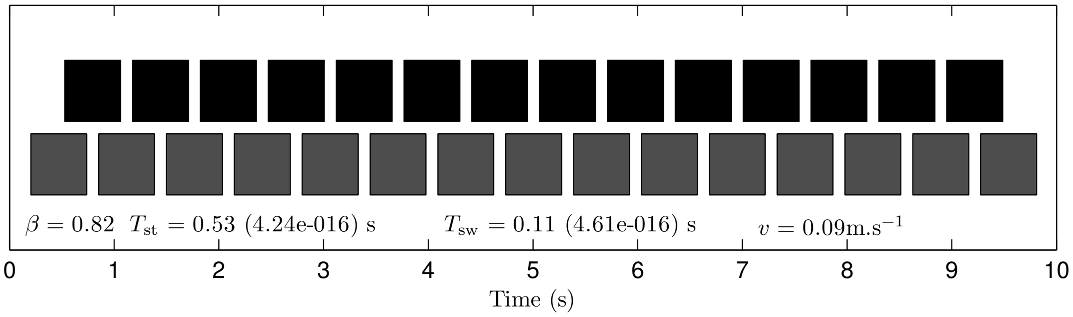

(a) $\alpha_{\mathrm{h}} = 50$

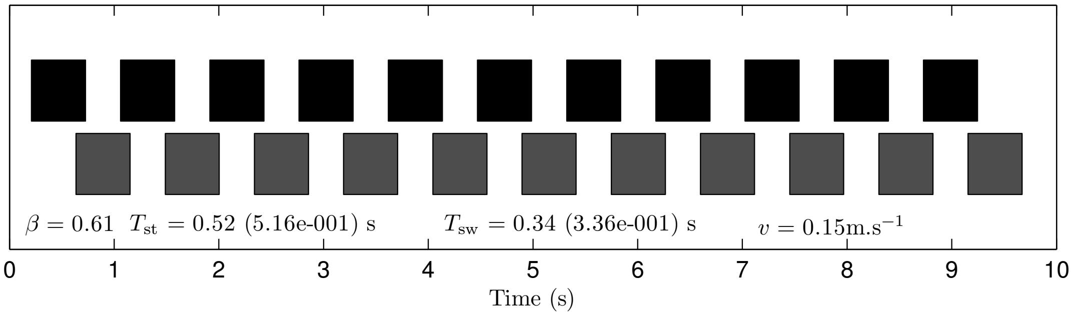

(b) $\alpha_{\mathrm{h}} = 100$

Figure 6.7: Stepping sequence of the hind girdle simulations.

6.3.2 Fore legs

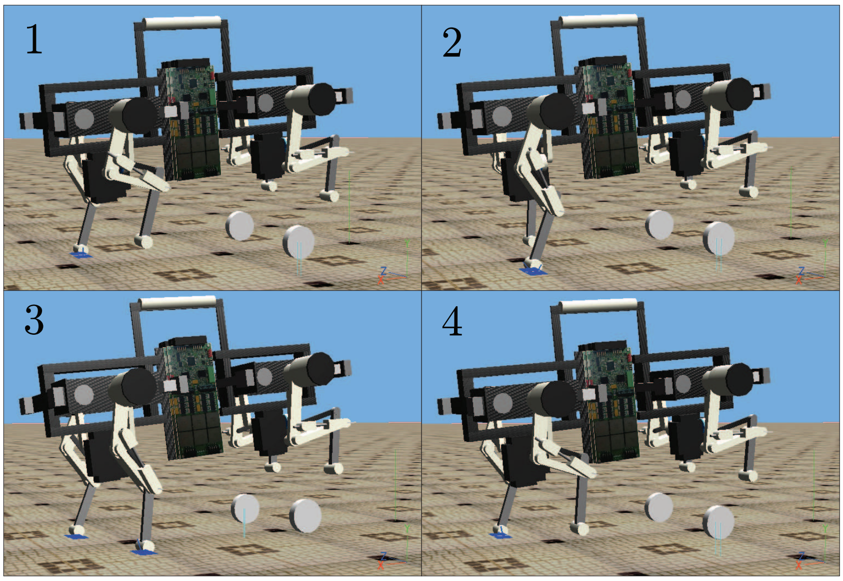

Figure 6.8: Snapshots from the simulation on the fore legs. The sequence of actions on the left leg: 1- swing, 2- touchdown, 3- stance, 4- lift-off.

Similar simulations were performed for the fore girdle (fig. 6.8), with the same parameter values as for hind girdle (table. 6.6), yielding distinct behavior when comparing to the hind legs.

Table 6.6: Neuron and joint output parameters for fore leg simulation.

	τ	Γ	Θ
liftoff	0.01	0.1	1
stance	0.01	0.1	1
touchdown	0.01	0.1	1
swing	0.01	0.1	1

Θ_{AEP}	Θ_{PEP}	$F_{\text{threshold}}$	α_{h}	γ_{h}	α_{k}	γ_{h}
15	5	1	60	500	300	500

Fig. 6.9 depicts the neuron activity and motor output from the hip joints, and fig. 6.10 depicts the activity and motor output from the knee joints. A striking difference when comparing to the hind simulation, is the excursion of the joint well beyond the AEP and PEP values (fig. 6.9).

Consider the results from the left leg. Initially the left leg produces no motor action, because the ground contact which activates $u_{\text{stance,FL}}$ hasn't been observed. When the foot is placed on the ground $u_{\text{stance,FL}}$ is activated and the hip joint propels the robot. When the hip passes PEP angle ($u_{\text{PEP,FR}} = 1$) and the contralateral leg is placed on the ground ($u_{\text{GC,FR}} = 1$), the *liftoff* neuron produces the flexion of the knee, releasing the ground contact, activating the *swing* neuron, producing the swing movement in the hip. The swing movement is halted after the hip having reached AEP, holding its position until a new ground contact is detected. $u_{\text{touchdown,FL}}$ is also activated and the leg is stretched.

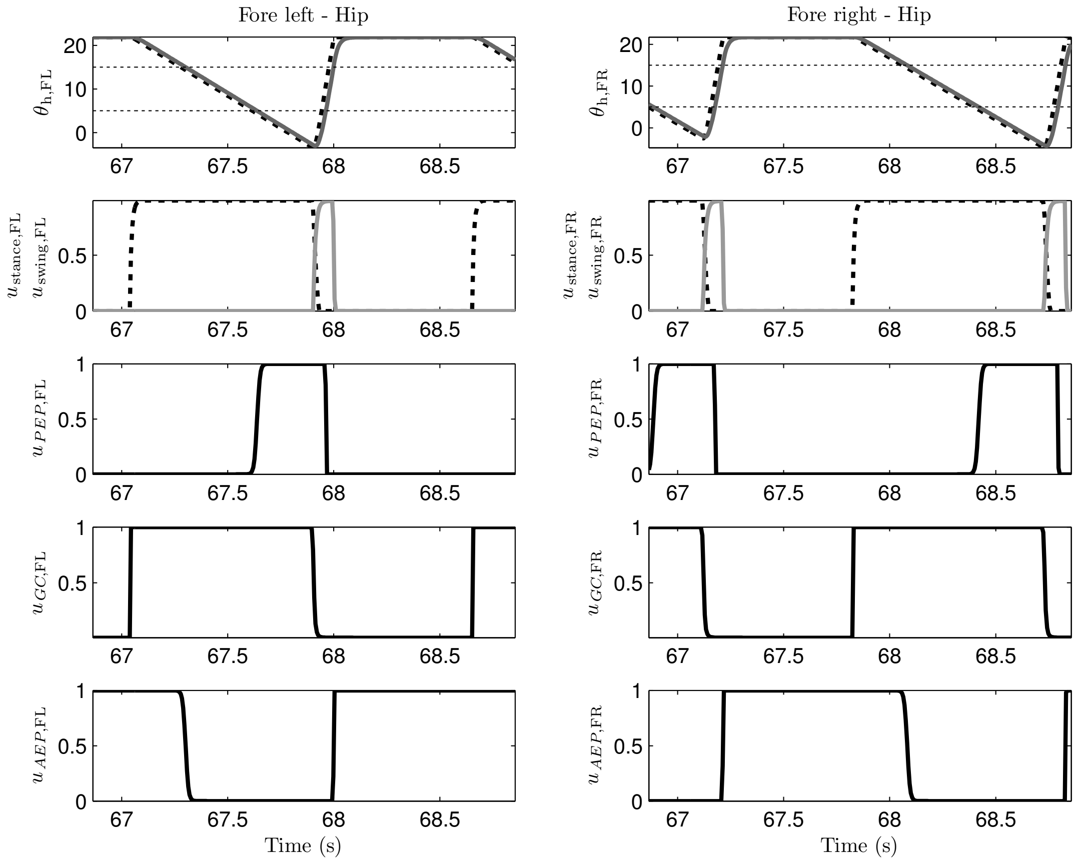

Figure 6.9: Neuron activity and motor output for the hip joints. The joint reference values are the dashed lines, and the performed joint movements are the solid lines (top row). Dotted lines represent the AEP and PEP values. $u_{\mathrm{stance},i}$ is represented with solid lines and $u_{\mathrm{swing},i}$ with dashed lines.

The obtained stepping sequence is presented in fig. 6.11. The robot walking on its fore legs achieves a velocity of 0.11 m.s^{-1}, greater than the 0.09 m.s^{-1} obtained in the walk with the hind legs and employing the same parameter values. The stepping pattern is also alternated, with a lower duty factor: 0.55 in the fore legs and 0.8 in the hind legs; larger swing duration: 0.85 s in fore and 0.11 s in hind legs; and stance duration: 0.85 s in fore and 0.75 s in hind legs .

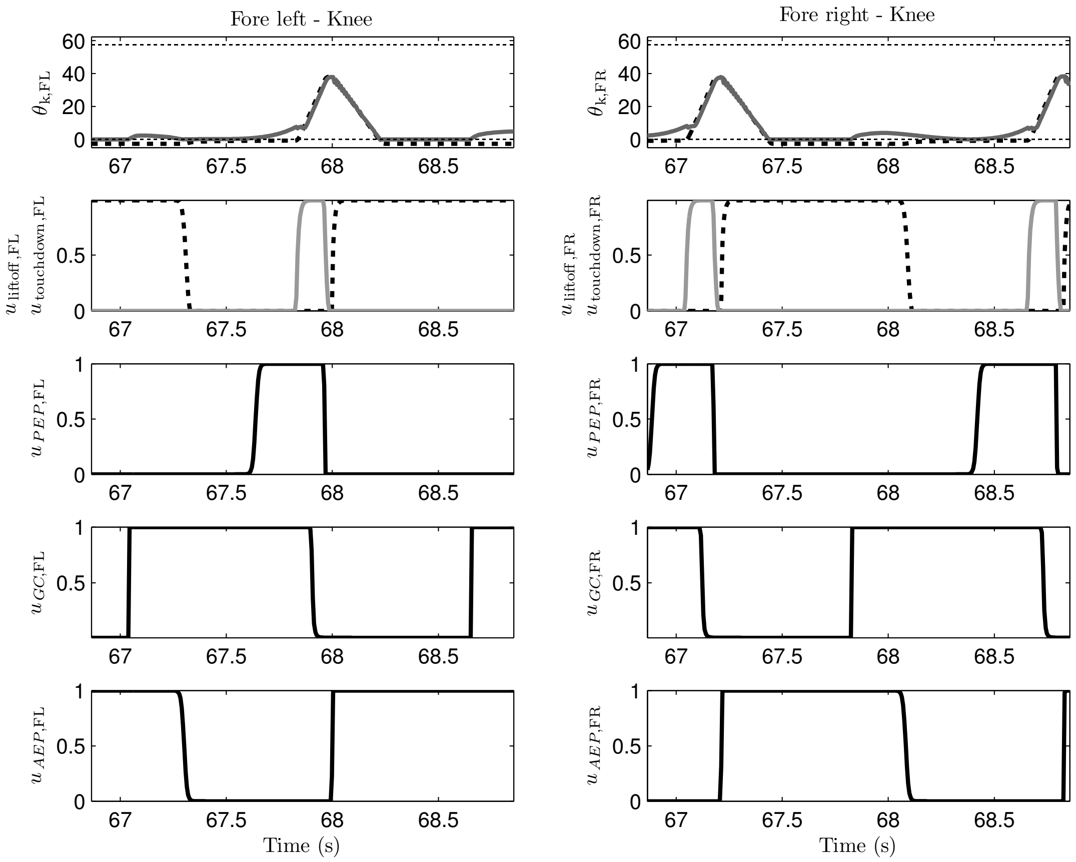

Figure 6.10: Neuron activity and motor output for the knee joints. Joint reference values are depicted by dashed lines and the performed knee joint angles by solid lines. $u_{\mathrm{liftoff},i}$ is represented with solid lines and $u_{\mathrm{touchdown},i}$ with dashed lines.

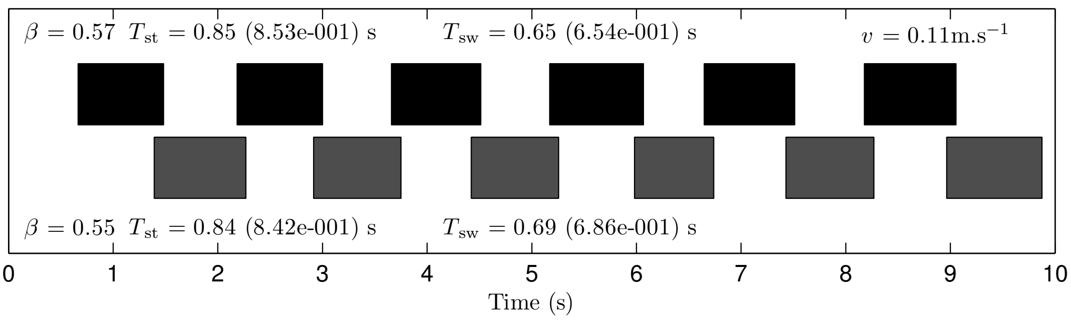

Figure 6.11: Alternated stepping sequence obtained from the fore girdle simulation.

6.3.3 Fore and hind legs

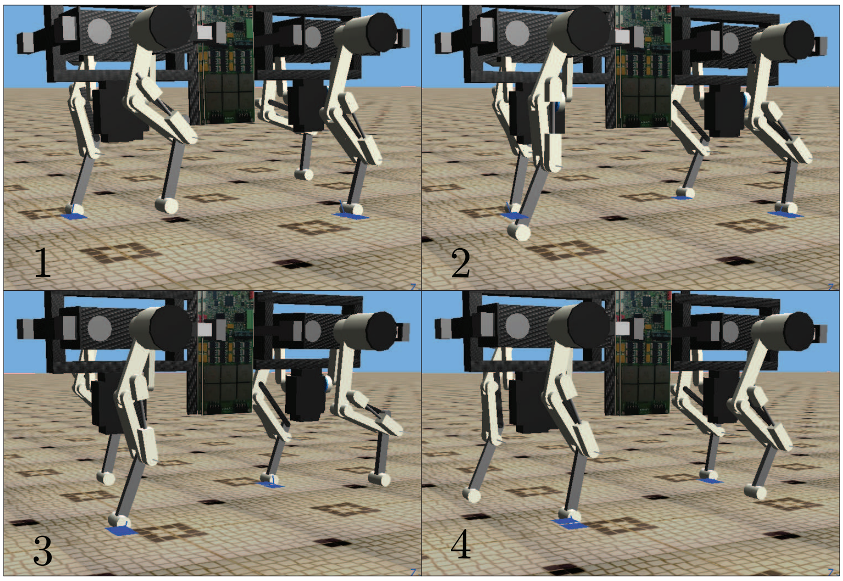

Figure 6.12: Simulation of quadruped walking using the reflex network.

The current simulation addresses the full quadruped walk, using both fore and hind girdles. The previous two simulation scenarios served to demonstrate the obtained motor behaviors when employing the same parameters from the two independent girdles. With this insight the parameter set for the gull quadruped scenario was established. The parameter set presented in table 6.7 accomplishes stepping motions of the legs while propelling and maintaining the robot's balance.

Table 6.7: Neuron and joint output parameters for fore leg simulation.

	τ	Γ	Θ
liftoff	0.01	0.1	1
stance	0.01	0.1	1
touchdown	0.01	0.1	1
swing	0.01	0.1	1

	Θ_{AEP}	Θ_{PEP}	$F_{\text{threshold}}$	α_{h}	γ_{h}	α_{k}	γ_{h}
Fore	15	5	1	50	300	300	500
Hind	10	0	1	50	300	300	500

The obtained motor behavior can be said to resemble a walk, despite the lack of a constant periodic pattern, as observable in fig. 6.13. From the stepping sequence it is possible to ascertain that the robot performs a walking behavior which resembles a mix between a trot and a diagonal sequence walk. The stepping sequence also evidences an asymmetry along the sagittal plane, concerning the fore legs. In the fore girdle, there is an asymmetry in duty factor, with one leg having a greater support duration, randomly alternating between the right fore and the left fore. In fig. 6.13 at around 25 s and at 55 s it is noticeable this asymmetric pattern (red boxes).

Despite a not ideal stepping sequence pattern, the robot effectively propels itself forward while maintaining an upright posture, without falling over. It is even resilient to falls in certain parameter configurations. The robot may stumble and delay a step, but the stepping movements elicited by the reflexes make the robot regain stability again.

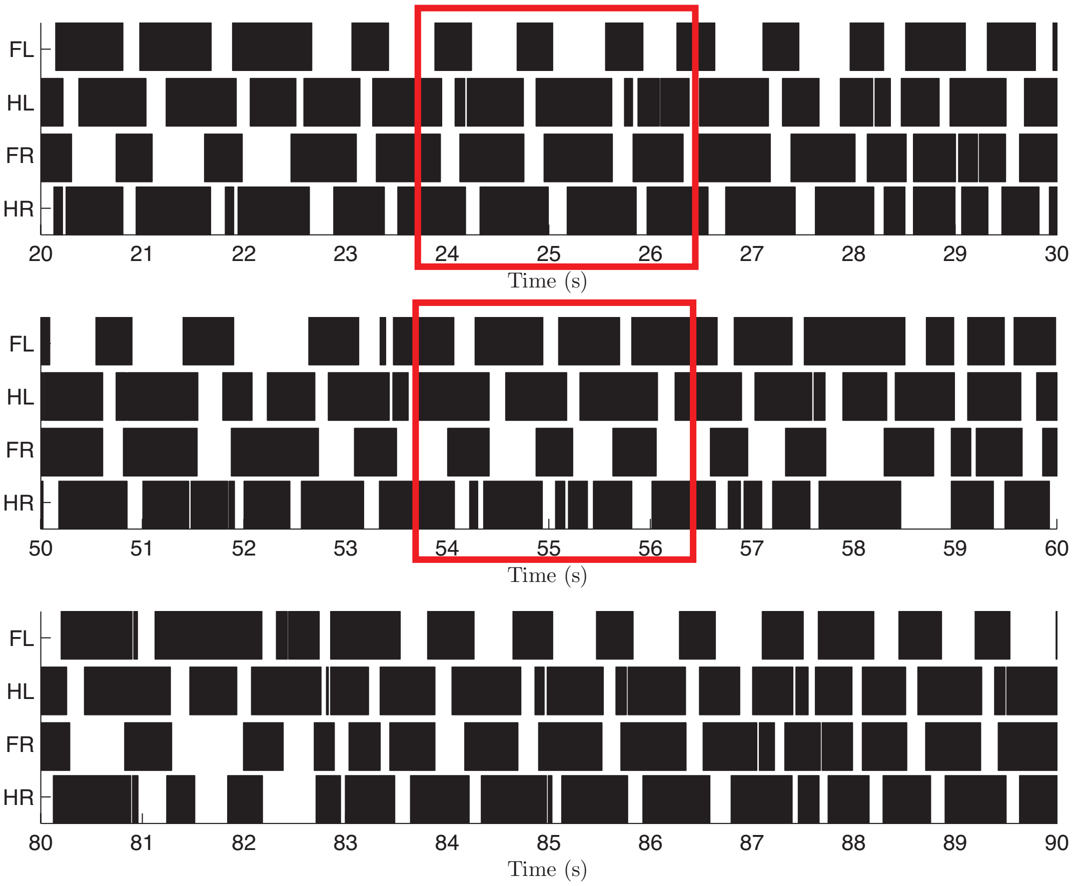

Figure 6.13: Stepping sequence from the full quadrupedal simulation.

6.4 Remarks on reflex-based quadruped walking

In this chapter was proposed and tested a reflex network for the walking of a compliant quadruped robot. The parsimonious reflex network is able to generate a sequence of motor actions triggered by external sensory events, accomplishing stepping motor behaviors. Although capable of generating quadrupedal stepping behaviors, the final stepping sequence pattern is not consistent and periodic.

When tested independently fore and hind girdles produce a dissimilar expression of the stepping patterns, and no set of parameters would produce similar stepping behaviors for the fore and hind legs in terms of duty factor, step period, stance and swing durations.

The range of possible parameter values was also much larger in single girdle setups, with the ability of producing high velocities and large step lengths. Such solutions were not possible in the quadrupedal scenario, resulting in a loss of balance and fall. However, in certain quadrupedal scenarios with appropriate parameter values, it was observed that the robot becomes quite resilient to external disturbances, such as small ramps and random height terrains.

The final exhibited posture on the quadruped robot is a result of the overall walking pattern and the interplay of the reflex chain and sensory input. It is not possible to specify a reference walking posture with the current approach, as the final motor behavior is not defined.

So far in the current implementation, the reflexes are always enabled and are not phase dependent. Because there is no control of the current state within a step cycle, the sensory events can influence the leg behavior in any moment of the step cycle. This ability may be relevant when considering certain phasic feedback mechanisms, such as corrective stumbling and stepping reflexes.

Also relevant, is the inclusion of other sources of sensory information, such as roll and pitch of the body, and leg load information. The inclusion of these feedback pathways could produce more adequate motor actions and contribute to the maintenance of posture and compensate external disturbances.

6.4.1 Integration of the reflex network with a CPG

The original aim concerned with the exploration of an alternative role for the CPG, acting as a regulator, or supervisor of the sensorimotor processes of a locomotor reflex network. This role can either be achieved by modulating the reflex magnitude, reflex activity and the respective feedback pathways. The CPG could alternatively serve as a possible endogenous rhythmic internal model, acting as a predictor of the expected sensory signals or the state. It could even have a role within the feedback loop, correcting imperfect sensory feedback and adapting peripheral inputs and feedback pathways [116].

The walking performance of the proposed reflex network is not satisfactory in the sense that it does not produce a consistent locomotor pattern. It also does not allow the modulation of walking behavior, lacking the mechanisms for changing rhythmic activity and performing more complex walking behaviors. The improvement of the reflex network was not sought, because its performance serves the initial goal of having an initial reflex network as a starting point for the integration of the CPG.

The proposed reflex network clearly presents some limitations, exacerbated by the lack of a well-defined step phase. The inclusion of a CPG can address these issues, e.g. producing a reference step phase, used to modulate phase dependent corrective reflexes such as stumbling correction.

In fig. 6.14 are represented three new conceptual suggestions on how the CPG can be integrated with the reflex network. All three suggestions are alternative formulations of the CPG, where the CPG does not produce directly a motor output, but instead acts as a process supervisor, entrained by the dynamic interactions between the body and environment.

These approaches are meant to differ from others, where the CPG produces the final motor output which is then corrected by a set of reflexes [110], or where the CPG produces the motor output of proximal joints and then modulates the reflex circuits of the distal joints [112].

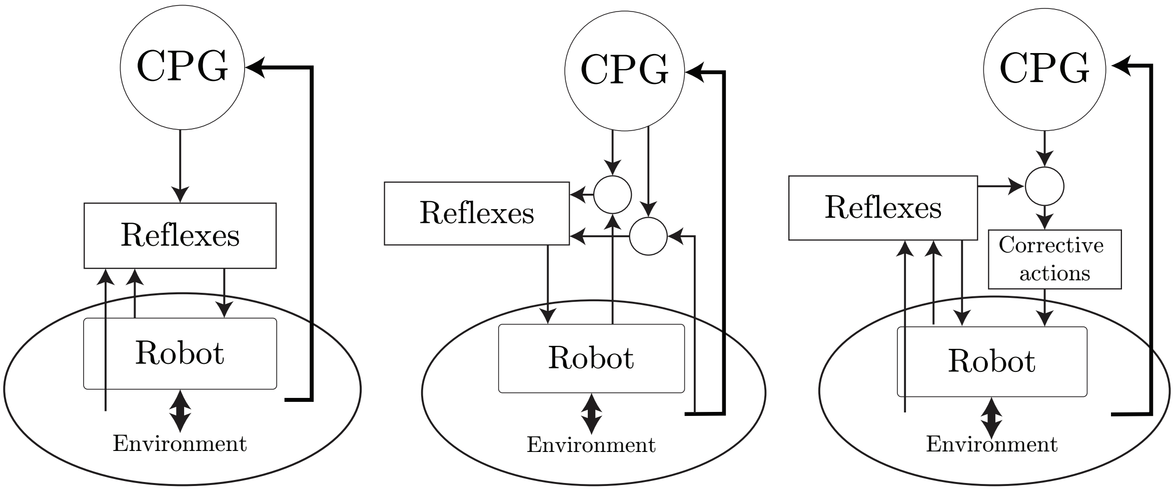

(a) CPG as modulator of the reflex network. The entrained rhythmic activity of the CPG establishes the step phase, and the CPG regulates the activity if the reflex circuits.

(b) CPG as forward model, receiving information from the motor actions and the robot interaction with the environment, and outputting predicted sensory information to the reflex network.

(c) CPG as an inverse model. Entrained by sensory information and the interaction with the environment, the CPG establishes the phase of the step cycle and outputs the expected motor actions.

Figure 6.14: Suggested approaches for the inclusion of the CPG within the reflex based solution.

Fig. 6.14(a) depicts the CPG role producing a feedforward modulation of the reflex network. The CPG receives sensory information about the robot's state and the body-environment interaction, entraining the CPG rhythmic activity with the exhibited motor behavior of the robot. The CPG produces a rhythmic modulation of the reflex network, governing the activity of reflexes' sensory pathways, controlling phasic reflexes, mediating the sensory information which elicits the reflexive actions, and even modulating motor gains.

In fig. 6.14(b) the CPG acts as a forward model, filtering and processing sensory information. The rhythmic of the CPG is entrained by the input signals relating to the motor state of the robot and its interaction with the environment. Sensory information is filtered and compared with the expected output from the CPG, and is then input to the reflex network.

Fig. 6.14(c) depicts the CPG as a predictor of the motor output from the reflex network, building an inverse model of the sensorimotor interactions. The CPG is entrained by sensory information and the interaction with the environment, and establishes the phase of the step cycle and outputs the expected motor actions. The predicted motor actions from the CPG are compared with the motor output from the reflex circuits, eliciting corrective motor actions when deemed necessary.

These possible methods of integrating the CPG within the reflex based solution, having the CPG as a mediating layer between higher-centers, the low-level reflexive motor actions and the dynamic body-environment interactions. As far the author is aware, this is an original endeavor, which has not been explored. They are conceptual proposals and require further work and thought on development and implementation, with no apparent advantages among each other.

CHAPTER 7

CONCLUSIONS

The work developed in this thesis was integrated in a team's research project endeavoring the exploitation of the concept of CPGs and the framework of dynamical systems to accomplish robust and adaptive legged locomotion in potentially unperceived and irregular terrains, for small position controlled robots. The research project aims to explore insights from neuroethology research on vertebrate motor control and from the concept of CPGs, trying to apply the knowledge on the functional description of the vertebrate CPGs, its organization, and most importantly, the sensorimotor interactions which adapt the locomotor behaviors to perturbations. The choice of using methods of dynamical systems and nonlinear oscillators is motivated by the fact that it presents interesting features for dynamic motor control of robots, while it allows to explore previously proposed mechanisms and contribute to further advancement of the framework.

Goals: The goals of this thesis concern with the design of a model free solution for legged robots, using dynamical system methods and oscillators to implement a CPG based controller. It intends to exploit the features provided by the oscillators' characteristics to accomplish a solution capable of generating coordinated motor patterns for walking robots. The final solution should be able to perform different locomotor behaviors, ultimately resulting in goal-oriented locomotion. It aims to include feedback mechanisms, contributing towards robust locomotion, stable foot placement, terrain adaptation, as well as equilibrium maintenance and posture control. The work has a strong focus on the application of the designed solutions to high gain position controlled robots, such as the addressed Sony AIBO and Robotis DARwIn-OP.

Contributions: The main contributions of this work is the proposal of a CPG based architecture for a quadruped robot, a CPG for humanoid biped robots and a reflex based network for a compliant quadruped.

The CPG based solution for quadrupedal walking is based on interconnected oscillators to drive the motor patterns for the whole leg, organized such that it produces the stepping motions of a leg, including the double peaks motions for the knee, without explicit low-level planning. The CPGs are included in the generation level of a structured architecture, divided by levels of abstraction, coordinated to produce the temporal relationships of quadruped symmetric gaits and the final goal-oriented locomotion. The regulation level feeds the CPGs with the parameters which specify the motor patterns and the temporal relationships among the CPGs, translating between task level goals and generation level parameters. This approach reduces the dimensionality of the control problem, decoupling low level trajectory generation from high level planning, as demonstrated in a navigation task.

Postural control of a standing quadruped is addressed by proposing a set of parallel postural responses, which define static equilibrium criteria which depends on sensory information. This method accomplishes the integration and fusion of several sensory modalities which contribute towards the balance maintenance of the robot. The proposed postural control system is also integrated with the CPG locomotor system, with its output projecting into the offset parameter of the oscillators. The capabilities of the postural system have been successfully demonstrated in a quadruped AIBO robot, subject to different types of postural disturbances.

The biped CPG solution employed a different approach for the CPG implementation, due to the stricter requirements in terms of balance and motor pattern complexity required to make the robot walk. The CPG is divided into rhythm generation and pattern generation, based on the idea of motion primitives and the modular construction of motor skills. A required minimum set of motion primitives is identified, which is able to produce goal-oriented walking, motivated by the fact that it should be used as an initial locomotor repertoire, and should later be improved and expanded using developmental methods, such as reinforcement learning methods. Within the proposed solution, a phase regulation mechanisms based on the phase transition reflexes observed in vertebrates is also proposed. The role of the proposed phase regulation mechanisms were evaluated, demonstrating an extended ability of the biped robot to walk on, and adapt to small unperceived slopes.

The capabilities of the proposed solution are demonstrated in several experiments in the DARwIn-OP humanoid robot, other simulated biped robot models, and is also applied within a whole-body control framework.

In the final chapter is proposed a network based on a chain of reflexes for producing the motor patterns of quadrupedal walking. This approach is meant as a means to initiate a discussion on possible alternative roles of the CPGs in the generation of legged locomotion. It provides a parsimonious framework for purely reflexive walking, where it is possible to study how the CPG could take part on the regulation of the reflex activity, or sensory signal filtering. The walking behavior produced by the reflex network is unpredictable, not possible to specify a motor behavior, and the walking performance has room for improvement in many aspects, e.g. in terms of regularity, stability and achieved velocity.

The inclusion of a CPG within the reflex framework is hoped to improve the limitations of a purely reflexive behavior, by introducing a reference rhythmic activity, making the locomotor pattern more regular and allowing the modulation of the rhythmic activity. It would also introduce a reference step phase which would allow the application of phasic feedback mechanisms.

Outlook: Robots have been usually built as fully actuated, high gain position controlled, rigid machines, including most of the legged robots. Legged locomotion is however a task which requires a high degree of agility and a dynamic interaction with the environment. Such interaction application demands from these kind of robots very fast control loops in order to neutralize the effects of disturbances.

This aspect has been observed as a limiting factor when applying the proposed CPG solutions on the biped and quadruped robots. The lack of planning on the task space of the end-effector position and orientation, the generation of simplified joint space trajectories, and the stiff actuation of the robots have demonstrated to be a detractor to accomplish the most stable locomotion. This is not a factor in other CPG solutions which define the motion of the end-effectors in the task space [15, 135, 215], and accurately establish joint position references. However, these approaches maintain the challenge of: i) designing feedback mechanisms to be integrated with the CPGs, ii) the requirement of a very fast control loop for reactive corrections, and iii) the limitation of high gain position controlled joints. On the quadruped postural task, the slow position control loop also demonstrated to be a limiting factor, reflected on how fast the postural corrections can be produced by the system.

Furthermore, it has been revealed to be quite difficult to propose analogous feedback mechanisms as those observed in animal locomotion due to the limited backdrivability and the stiff actuation of the joints. The inclusion of compliant elements in the robot's actuation can simplify the walking task and help on achieving agile locomotion, by passively rejecting small disturbances in a fast way, and exploring self-stabilization. On the other hand, it is not a trivial matter, as it hampers the control problem and state estimation. This is one area where oscillator based CPGs may present an advantage due to their entrainment properties [29], but has not been fully explored in more capable robots.

Throughout the period of development of the presented work, great advances have taken place in the topic of locomotion in legged robots, and the outlook seems promising. The capabilities of active compliance in walking robots have been developed and further explored [87, 193], ever improving the abilities towards agile locomotion.

Some CPG based approaches have recently been applied in hybrid solutions, employing CPGs and model based control methods in order to achieve active compliant behavior in torque controlled platforms, capable of addressing unperceived irregular terrains. Mostafa Ajallooeian et al. [2] implement the CPGs as coupled nonlinear oscillators, producing joint trajectories based on user defined piecewise Hermite polynomials with four knots. The outputs of the CPGs are transformed into actuation torques through a P-controller and adjusted with torques produced from a virtual model, which maintains the attitude of the trunk. Barasuol et al. [15] used a CPG producing task space trajectories mapped to joint space through a regular PD position and torque controller, and a floating-base inverse dynamics to provide the feed-forward commands. On top of the end effector controllers, there is a trunk controller to maintain the trunk's attitude and push recovery mechanisms based on capture points.

The most interesting feature on the concept of CPGs, remains yet an satisfactorily unanswered question. If devising a CPG solution for robotics, how should feedback mechanisms be designed, what effects should they have to produce adaptations and which corrections performed when facing disturbances? This key question may remain unanswered for the near future, while research on the neural organization of vertebrate motor control further studies the intricate processes of motor generation and adaptation in more depth. Meanwhile, independently of the implementation method chosen to model the behavior of CPGs, engineered solutions may continue to take the role of locomotion adaptation and disturbance rejection.

BIBLIOGRAPHY

[1] J. A. Acebrón, L. L. Bonilla, C. J. Pérez Vicente, F. Ritort, and R. Spigler. The kuramoto model: A simple paradigm for synchronization phenomena. *Reviews of Modern Physics*, 77(1):137–185, Apr. 2005.

[2] M. Ajallooeian, S. Pouya, A. Sproewitz, and A. Ijspeert. Central Pattern Generators Augmented with Virtual Model Control for Quadruped Rough Terrain Locomotion. In *2013 IEEE International Conference on Robotics and Automation (ICRA 2013)*, 2013.

[3] R. Alexander. The gaits of bipedal and quadrupedal animals. *The International Journal of Robotics Research*, 3(2):49–59, 1984.

[4] S. Aoi, S. Fujiki, T. Yamashita, T. Kohda, K. Senda, and K. Tsuchiya. Generation of adaptive splitbelt treadmill walking by a biped robot using nonlinear oscillators with phase resetting. In *Intelligent Robots and Systems (IROS), 2011 IEEE/RSJ International Conference on*, pages 2274–2279, 2011.

[5] S. Aoi, N. Ogihara, T. Funato, Y. Sugimoto, and K. Tsuchiya. Evaluating functional roles of phase resetting in generation of adaptive human bipedal walking with a physiologically based model of the spinal pattern generator. *Biological Cybernetics*, 102(5):373–387, 2010.

[6] S. Aoi, N. Ogihara, Y. Sugimoto, and K. Tsuchiya. Simulating adaptive human bipedal locomotion based on phase resetting using foot-contact information. *Advanced Robotics*, 22(15):1697–1713, 2008.

[7] S. Aoi, H. Sasaki, and K. Tsuchiya. A multilegged modular robot that meanders: Investigation of turning maneuvers using its inherent dynamic characteristics. *SIAM J. Applied Dynamical Systems*, 6(2):348–377, 2007.

[8] S. Aoi and K. Tsuchiya. Locomotion control of a biped robot using nonlinear oscillators. *Autonomous Robots*, 19(3):219–232, 2005.

[9] S. Aoi and K. Tsuchiya. Stability analysis of a simple walking model driven by an oscillator with a phase reset using sensory feedback. *Robotics, IEEE Transactions on*, 22(2):391–397, 2006.

[10] S. Aoi and K. Tsuchiya. Adaptive behavior in turning of an oscillator-driven biped robot. *Autonomous Robots*, 23(1):37–57, 2007.

[11] S. Aoi, T. Yamashita, A. Ichikawa, and K. Tsuchiya. Hysteresis in gait transition induced by changing waist joint stiffness of a quadruped robot driven by nonlinear oscillators with phase resetting. In *Intelligent Robots and Systems (IROS), 2010 IEEE/RSJ International Conference on*, pages 1915–1920, 2010.

[12] P. Arena. A mechatronic lamprey controlled by analog circuits. In *MED'01 9th Mediterranean Conference on Control and Automation*. IEEE, June 2001.

[13] P. Arena, L. Fortuna, M. Frasca, and G. Sicurella. An adaptive, self-organizing dynamical system for hierarchical control of bio-inspired locomotion. *Systems, Man, and Cybernetics, Part B: Cybernetics, IEEE Transactions on*, 34(4):1823–1837, 2004.

[14] Y. Arshavsky, T. Deliagina, and G. Orlovsky. Pattern generation. *Current Opinion in Neurobiology*, 7(6):781–789, 1997.

[15] V. Barasuol, J. Buchli, C. Semini, M. Frigerio, E. R. D. Pieri, and D. G. Caldwell. A reactive controller framework for quadrupedal locomotion on challenging terrain. In *2013 IEEE International Conference on Robotics and Automation (ICRA 2013)*, 2013.

[16] J. Bares and D. Wettergreen. Dante II: Technical description, results and lessons learned. *International Journal of Robotics Research*, 18(7):621–649, July 1999.

[17] R. D. Beer, H. J. Chiel, R. D. Quinn, and R. E. Ritzmann. Biorobotic approaches to the study of motor systems. *Current Opinion in Neurobiology*, 8(6):777 – 782, 1998.

[18] S. Behnke. Online trajectory generation for omnidirectional biped walking. In *Robotics and Automation, 2006. ICRA 2006. Proceedings 2006 IEEE International Conference on*, pages 1597–1603, 2006.

[19] K. Berns, W. Ilg, M. Deck, and R. Dillmann. Adaptive control of the four-legged walking machine BISAM. In *Control Applications, 1998. Proceedings of the 1998 IEEE International Conference on*, volume 1, pages 428–432 vol.1, 1998.

[20] P. A. Bhounsule, J. Cortell, and A. Ruina. Design and control of ranger: an energy-efficient, dynamic walking robot. In *15th International Conference on Climbing and Walking Robot - CLAWAR 2012*, 2012.

[21] E. Bicho, P. Mallet, and G. Schoner. Target representation on an autonomous vehicle with low-level sensors. *The International Journal of Robotics Research*, 19(5):424–447, May 2000.

[22] A. Biewener. *Animal Locomotion*. Oxford Animal Biology Series. OUP Oxford, 2003.

[23] E. Bizzi, V. Cheung, A. d'Avella, P. Saltiel, and M. Tresch. Combining modules for movement. *Brain Research Reviews*, 57(1):125 – 133, 2008.

[24] R. Blickhan. The spring-mass model for running and hopping. *Journal of Biomechanics*, 22(11-12):1217 – 1227, 1989.

[25] S. Boyd and L. Vandenberghe. *Convex Optimization*. Cambridge University Press, New York, NY, USA, 2004.

[26] G. Brambilla, J. Buchli, and A. Ijspeert. Adaptive four legged locomotion control based on nonlinear dynamical systems. In S. Nolfi, G. Baldassarre, R. Calabretta, J. Hallam, D. Marocco, J.-A. Meyer, O. Miglino, and D. Parisi, editors, *From Animals to Animats 9*, volume 4095 of *Lecture Notes in Computer Science*, pages 138–149. Springer Berlin Heidelberg, 2006.

[27] T. G. Brown. The intrinsic factors in the act of progression in the mammal. *Proceedings of the Royal Society of London. Series B, Containing Papers of a Biological Character*, 84(572):308–319, 1911.

[28] J. Buchli and A. Ijspeert. Distributed central pattern generator model for robotics application based on phase sensitivity analysis. In A. Ijspeert, M. Murata, and N. Wakamiya, editors, *Biologically Inspired Approaches to Advanced Information Technology*, volume 3141 of *Lecture Notes in Computer Science*, pages 333–349. Springer Berlin Heidelberg, 2004.

[29] J. Buchli and A. J. Ijspeert. Self-organized adaptive legged locomotion in a compliant quadruped robot. *Auton. Robots*, 25(4):331–347, 2008.

[30] J. Buchli, M. Kalakrishnan, M. Mistry, P. Pastor, and S. Schaal. Compliant quadruped locomotion over rough terrain. In *Intelligent Robots and Systems, 2009. IROS 2009. IEEE/RSJ International Conference on*, pages 814–820, 2009.

[31] J. Buchli, L. Righetti, and A. J. Ijspeert. Engineering entrainment and adaptation in limit cycle systems. *Biological Cybernetics*, 95(6):645–664, 2006.

[32] D. Bullock, R. M. Bongers, M. Lankhorst, and P. J. Beek. A vector-integration-to-endpoint model for performance of viapoint movements. *Neural Networks*, 12(1):1 – 29, 1999.

[33] P.-L. Buono and M. Golubitsky. Models of central pattern generators for quadruped locomotion I. primary gaits. *Journal of Mathematical Biology*, 42(4):291–326, 2001.

[34] R. E. Burke. Sir charles sherrington's the integrative action of the nervous system: a centenary appreciation. *Brain*, 130(4):887–894, 2007.

[35] K. Byl, A. Shkolnik, S. Prentice, N. Roy, and R. Tedrake. Reliable dynamic motions for a stiff quadruped. In O. Khatib, V. Kumar, and G. Pappas, editors, *Experimental Robotics*, volume 54 of *Springer Tracts in Advanced Robotics*, pages 319–328. Springer Berlin Heidelberg, 2009.

[36] L. Castro, C. P. Santos, M. Oliveira, and A. J. Ijspeert. Postural control on a quadruped robot using lateral tilt: A dynamical system approach. In *EUROS*, volume 44 of *Springer Tracts in Advanced Robotics*, pages 205–214. Springer, 2008.

[37] X. Chen, K. Watanabe, K. Kiguchi, and K. Izumi. Implementation of omnidirectional crawl for a quadruped robot. *Advanced Robotics*, 15(2):169–190, 2001.

[38] S. Chernova and M. Veloso. An evolutionary approach to gait learning for four-legged robots. In *Proceedings of IROS'04*, September 2004.

[39] A. Ciancio, L. Zollo, E. Guglielmelli, D. Caligiore, and G. Baldassarre. Hierarchical reinforcement learning and central pattern generators for modeling the development of rhythmic manipulation skills. In *Development and Learning (ICDL), 2011 IEEE International Conference on*, volume 2, pages 1–8, 2011.

[40] J. Cobano, J. Estremera, and P. Gonzalez de Santos. Accurate tracking of legged robots on natural terrain. *Autonomous Robots*, 28(2):231–244, 2010.

[41] A. H. Cohen and P. Wallen. The neuronal correlate of locomotion in fish: "fictive swimming" induced in an in vitro preparation of the lamprey spinal cord. *Exp Brain Res*, 41:11–18, 1980.

[42] H. Cruse, T. Kindermann, M. Schumm, J. Dean, and J. Schmitz. Walknet—a biologically inspired network to control six-legged walking. *Neural Networks*, 11(7–8):1435 – 1447, 1998.

[43] J. Dahl and L. Vandenberghe. cvxopt - python software for convex optimization, 2012. [Online]`http://abel.ee.ucla.edu/cvxopt/`.

[44] S. Degallier, L. Righetti, and A. J. Ijspeert. Hand placement during quadruped locomotion in a humanoid robot: A dynamical system approach. In *2007 IEEE/RSJ International Conference on Intelligent Robots and Systems, October 29 - November 2, 2007, Sheraton Hotel and Marina, San Diego, California, USA*, pages 2047–2052, 2007.

[45] S. Degallier, L. Righetti, L. Natale, F. Nori, G. Metta, and A. Ijspeert. A modular bio-inspired architecture for movement generation for the infant-like robot icub. In *Biomedical Robotics and Biomechatronics, 2008. BioRob 2008. 2nd IEEE RAS EMBS International Conference on*, pages 795–800, 2008.

[46] S. Degallier, C. P. Santos, L. Righetti, and A. J. Ijspeert. Movement generation using dynamical systems: a humanoid robot performing a drumming task. In *Humanoids*, pages 512–517. IEEE, 2006.

[47] F. Delcomyn. Neural basis for rhythmic behaviour in animals. *Science*, 210(4469):492–498, 1980.

[48] T. Deliagina, I. Beloozerova, P. Zelenin, and G. Orlovsky. Spinal and supraspinal postural networks. *Brain Research Reviews*, 57(1):212 – 221, 2008. Networks in Motion.

[49] T. G. Deliagina, G. N. Orlovsky, P. V. Zelenin, and I. N. Beloozerova. Neural bases of postural control. *Physiology*, 21(3):216–225, 2006.

[50] T. G. Deliagina, M. G. Sirota, P. V. Zelenin, G. N. Orlovsky, and I. N. Beloozerova. Interlimb postural coordination in the standing cat. *The Journal of Physiology*, 573(1):211–224, 2006.

[51] R. Dillmann, J. Albiez, B. Gaßmann, T. Kerscher, and M. Zöllner. Biologically inspired walking machines: design, control and perception. *Philosophical Transactions of the Royal Society A: Mathematical, Physical and Engineering Sciences*, 365(1850):133–151, 2007.

[52] M. R. Dimitrijevic, Y. Gerasimenko, and M. M. Pinter. Evidence for a spinal central pattern generator in humans. *Annals of the New York Academy of Sciences*, 860(1):360–376, 1998.

[53] T. Drew. Neuronal mechanisms for the adaptive control of locomotion in the cat. In *Proceedings of adaptive motion of animals and machines*, 2000.

[54] J. Duysens and H. Van de Crommert. Neural control of locomotion; the central pattern generator from cats to humans. *Gait Posture*, 7(2):131–141, 1998.

[55] Ö. Ekeberg. A combined neuronal and mechanical model of fish swimming. *Biological Cybernetics*, 69(5-6):363–374, 1993.

[56] Ö. Ekeberg and K. Pearson. Computer simulation of stepping in the hind legs of the cat: An examination of mechanisms regulating the stance-to-swing transition. *Journal of Neurophysiology*, 94(6):4256–4268, 2005.

[57] G. Endo, J. Morimoto, J. Nakanishi, and G. Cheng. An empirical exploration of a neural oscillator for biped locomotion control. In *Proceedings of the 2004 IEEE International Conference on Robotics and Automation, ICRA 2004, April 26 - May 1, 2004, New Orleans, LA, USA*, pages 3036–3042, 2004.

[58] G. Endo, J. Nakanishi, J. Morimoto, and G. Cheng. Experimental studies of a neural oscillator for biped locomotion with QRIO. In *Robotics and Automation, 2005. ICRA 2005. Proceedings of the 2005 IEEE International Conference on*, pages 596–602, 2005.

[59] J. Estremera and P. de Santos. Generating continuous free crab gaits for quadruped robots on irregular terrain. *Robotics, IEEE Transactions on*, 21(6):1067–1076, 2005.

[60] P. Estévez, J. C. Grieco, W. Medina-meléndez, and G. Fernández-López. Gait synthesis in legged robot locomotion using a CPG-based model, 2007.

[61] H. Feng and R. Wang. Construction of central pattern generator for quadruped locomotion control. In *Advanced Intelligent Mechatronics, 2008. AIM 2008. IEEE/ASME International Conference on*, pages 979–984, 2008.

[62] T. Flash and B. Hochner. Motor primitives in vertebrates and invertebrates. *Current Opinion in Neurobiology*, 15(6):660 – 666, 2005. Motor sytems / Neurobiology of behaviour.

[63] A. Frigon and S. Rossignol. Experiments and models of sensorimotor interactions during locomotion. *Biol. Cybern.*, 95(6):607–627, Dec. 2006.

[64] Y. Fukuoka, H. Kimura, and A. H. Cohen. Adaptive dynamic walking of a quadruped robot on irregular terrain based on biological concepts. *The International Journal of Robotics Research*, 22(3-4):187–202, 2003.

[65] S. Gay, S. Dégallier, U. Pattacini, A. Ijspeert, and J. Victor. Integration of vision and central pattern generator based locomotion for path planning of a non-holonomic crawling humanoid robot. In *Intelligent Robots and Systems (IROS), 2010 IEEE/RSJ International Conference on*, pages 183–189, 2010.

[66] T. Geng, B. Porr, and F. Wörgötter. Self-stabilized biped walking under control of a novel reflexive network. In *IROS*, pages 3269–3274, 2005.

[67] T. Geng, B. Porr, and F. Wörgötter. Fast biped walking with a sensor-driven neuronal controller and real-time online learning. *I. J. Robotic Res.*, 25(3):243–259, 2006.

[68] H. Geyer and H. Herr. A muscle-reflex model that encodes principles of legged mechanics produces human walking dynamics and muscle activities. *Neural Systems and Rehabilitation Engineering, IEEE Transactions on*, 18(3):263–273, 2010.

[69] H. Geyer, A. Seyfarth, and R. Blickhan. Compliant leg behaviour explains basic dynamics of walking and running. *Proceedings. Biological sciences / The Royal Society*, 273(1603):2861–2867, Nov. 2006.

[70] C. Graf and T. Röfer. A closed-loop 3D-LIPM gait for the robocup standard platform league humanoid. In E. Pagello, C. Zhou, S. Behnke, E. Menegatti, T. Röfer, and P. Stone, editors, *Proceedings of the Fifth Workshop on Humanoid Soccer Robots in conjunction with the 2010 IEEE-RAS International Conference on Humanoid Robots*, Nashville, TN, USA, 2010.

[71] S. Grillner, J. Hellgren, A. Ménard, K. Saitoh, and M. A. Wikström. Mechanisms for selection of basic motor programs – roles for the striatum and pallidum. *Trends in Neurosciences*, 28(7):364 – 370, 2005.

[72] S. Grillner, P. Wallén, K. Saitoh, A. Kozlov, and B. Robertson. Neural bases of goal-directed locomotion in vertebrates — an overview. *Brain Research Reviews*, 57(1):2 – 12, 2008. Networks in Motion.

[73] I. Ha, Y. Tamura, H. Asama, J. Han, and D. Hong. Development of open humanoid platform DARwIn-OP. In *SICE Annual Conference (SICE), 2011 Proceedings of*, pages 2178–2181, 2011.

[74] M. Habib. *Bioinspiration and Robotics: Walking and Climbing Robots*. I-Tech Education and Publishing, 2007.

[75] J. Hellgren, S. Grillner, and A. Lansner. Computer simulation of the segmental neural network generating locomotion in lamprey by using populations of network interneurons. *Biological Cybernetics*, 68(1):1–13, 1992.

[76] B. Hengst, D. Ibbotson, S. B. Pham, and C. Sammut. Omnidirectional locomotion for quadruped robots. In *RoboCup 2001: Robot Soccer World Cup V*, pages 368–373, London, UK, 2002. Springer-Verlag.

[77] A. Heralic, K. Wolff, and M. Wahde. Central pattern generators for gait generation in bipedal robots. In A. C. de Pina Filho, editor, *Humanoid Robots: New Developments*, chapter 17, pages 285–304. I-Tech Education and Publishing, Vienna, Austria, June 2007. Invited book chapter.

[78] M. Hersch and A. Billard. Reaching with multi-referential dynamical systems. *Autonomous Robots*, 25(1-2):71–83, 2008.

[79] M. Hersch and A. G. Billard. A model for imitating human reaching movements. In *Proceedings of the 1st ACM SIGCHI/SIGART conference on Human-robot interaction*, HRI '06, pages 341–342, New York, NY, USA, 2006. ACM.

[80] G. W. Hiebert and K. G. Pearson. Contribution of sensory feedback to the generation of extensor activity during walking in the decerebrate cat. *Journal of Neurophysiology*, 81(2):758–770, 1999.

[81] M. Hildebrand. The adaptive significance of tetrapod gait selection. *American Zoologist*, 20(1):255–267, 1980.

[82] M. Hirose and K. Ogawa. Honda humanoid robots development. *Philosophical Transactions of the Royal Society A: Mathematical, Physical and Engineering Sciences*, 365(1850):11–19, 2007.

[83] S. Hirose, Y. Fukuda, and H. Kikuchi. The gait control system of a quadruped walking vehicle. *Advanced Robotics*, 1(4):289–323, 1986.

[84] M. Hoffmann and R. Pfeifer. The implications of embodiment for behavior and cognition: animal and robotic case studies. *CoRR*, abs/1202.0440, 2012.

[85] G. Hornby, S. Takamura, J. Yokono, O. Hanagata, T. Yamamoto, and M. Fujita. Evolving robust gaits with AIBO, 2000.

[86] Y. Hu, W. Tian, J. Liang, and T. Wang. Learning fish-like swimming with a CPG-based locomotion controller. In *Intelligent Robots and Systems (IROS), 2011 IEEE/RSJ International Conference on*, pages 1863–1868, 2011.

[87] M. Hutter, C. Gehring, M. Bloesch, M. A. Hoepflinger, C. D. Remy, and R. Siegwart. StarlETH: A compliant quadrupedal robot for fast, efficient, and versatile locomotion. In *15th International Conference on Climbing and Walking Robot - CLAWAR 2012*, 2012.

[88] S. Hyon, J. Morimoto, and G. Cheng. Hierarchical motor learning and synthesis with passivity-based controller and phase oscillator. In *Robotics and Automation, 2008. ICRA 2008. IEEE International Conference on*, pages 2705–2710, 2008.

[89] S. Hyon, J. Morimoto, and M. Kawato. From compliant balancing to dynamic walking on humanoid robot: Integration of CNS and CPG. In *Robotics and Automation (ICRA), 2010 IEEE International Conference on*, pages 1084–1085, 2010.

[90] H. Igarashi, T. Machida, F. Harashima, and M. Kakikura. Free gait for quadruped robots with posture control. In *Advanced Motion Control, 2006. 9th IEEE International Workshop on*, pages 433–438, 2006.

[91] A. Ijspeert, J. Nakanishi, and S. Schaal. Movement imitation with nonlinear dynamical systems in humanoid robots. In *Robotics and Automation, 2002. Proceedings. ICRA '02. IEEE International Conference on*, volume 2, pages 1398–1403, 2002.

[92] A. J. Ijspeert. Central pattern generators for locomotion control in animals and robots: A review. *Neural Networks*, 21(4):642–653, 2008.

[93] A. J. Ijspeert, A. Crespi, D. Ryczko, and J.-M. Cabelguen. From swimming to walking with a salamander robot driven by a spinal cord model. *Science*, 315(5817):1416–1420, 2007.

[94] A. J. Ijspeert, J. Nakanishi, H. Hoffmann, P. Pastor, and S. Schaal. Dynamical movement primitives: Learning attractor models for motor behaviors. *Neural Computation*, 25(2):328–373, Nov. 2012.

[95] K. Inagaki and H. Kobayashi. A gait transition for quadruped walking machine. In *Intelligent Robots and Systems '93, IROS '93. Proceedings of the 1993 IEEE/RSJ International Conference on*, volume 1, pages 525–531 vol.1, 1993.

[96] S. Inagaki, H. Yuasa, and T. Arai. CPG model for autonomous decentralized multi-legged robot system—generation and transition of oscillation patterns and dynamics of oscillators. *Robotics and Autonomous Systems*, 44(3–4):171 – 179, 2003. Best papers presented at IAS-7.

[97] S. Inagaki, H. Yuasa, T. Suzuki, and T. Arai. Wave CPG model for autonomous decentralized multi-legged robot: Gait generation and walking speed control. *Robotics and Autonomous Systems*, 54(2):118 – 126, 2006. Intelligent Autonomous Systems 8th Conference on Intelligent Autonomous Systems (IAS-8).

[98] I. Iossifidis and G. Schöner. Reaching with a redundant anthropomorphic robot arm using attractor dynamics. In *Proceedings Of The 37Th International Symposium On Robotics Isr 2006 And 4Th German Conference On Robotics Robotik 2006, München, Germany, May 15-17, Vdi Verlag, 2006*, 2006.

[99] M. Ishida, S. Kato, M. Kanoh, and H. Itoh. Generating locomotion for biped robots based on the dynamic passivization of joint control. In *Systems, Man and Cybernetics, 2009. SMC 2009. IEEE International Conference on*, pages 3157–3162, 2009.

[100] T. Ishii, S. Masakado, and K. Ishii. Locomotion of a quadruped robot using CPG. In *Neural Networks, 2004. Proceedings. 2004 IEEE International Joint Conference on*, volume 4, pages 3179–3184 vol.4, 2004.

[101] S. Ito, H. Yuasa, Z. W. Luo, M. Ito, and D. Yanagihara. A mathematical model of adaptive behavior in quadruped locomotion. *Biological Cybernetics*, 78(5):337–347, 1998.

[102] J. V. Jacobs and F. B. Horak. Cortical control of postural responses. *Journal of Neural Transmission*, 114(10):1339–1348, 2007.

[103] T. K. Forebrain control of locomotor behaviors. *Brain Research Reviews*, 57(1):192–8, 2008.

[104] K. Kaneko, F. Kanehiro, S. Kajita, H. Hirukawa, T. Kawasaki, M. Hirata, K. Akachi, and T. Isozumi. Humanoid robot HRP-2. In *Robotics and Automation, 2004. Proceedings. ICRA '04. 2004 IEEE International Conference on*, volume 2, pages 1083–1090 Vol.2, 2004.

[105] T. Kano, K. Nagasawa, D. Owaki, A. Tero, and A. Ishiguro. A CPG-based decentralized control of a quadruped robot inspired by true slime mold. In *Intelligent Robots and Systems (IROS), 2010 IEEE/RSJ International Conference on*, pages 4928–4933, 2010.

[106] P. S. Katz. Neurons, networks, and motor behavior. *Neuron*, 16(2):245 – 253, 1996.

[107] O. Kiehn. Locomotor circuits in the mammalian spinal cord. *Annual Review of Neuroscience*, 29(1):279–306, 2006.

[108] H. Kimura and Y. Fukuoka. Adaptive dynamic walking of the quadruped on irregular terrain-autonomous adaptation using neural system model. In *Robotics and Automation, 2000. Proceedings. ICRA '00. IEEE International Conference on*, volume 1, pages 436–443 vol.1, 2000.

[109] H. Kimura and Y. Fukuoka. Biologically inspired adaptive dynamic walking in outdoor environment using a self-contained quadruped robot: 'tekken2'. In *Intelligent Robots and Systems, 2004. (IROS 2004). Proceedings. 2004 IEEE/RSJ International Conference on*, volume 1, pages 986–991 vol.1, 2004.

[110] H. Kimura, Y. Fukuoka, and A. H. Cohen. Adaptive dynamic walking of a quadruped robot on natural ground based on biological concepts. *The International Journal of Robotics Research*, 26(5):475–490, 2007.

[111] H. Kimura, Y. Fukuoka, and H. Katabuti. Mechanical design of a quadruped "tekken3 & 4" and navigation system using laser range sensor. In *Proceedings of International Symphosium of Robotics*, Tokyo, November 2005.

[112] T. J. Klein and M. A. Lewis. A physical model of sensorimotor interactions during locomotion. *Journal of Neural Engineering*, 9(4):046011, 2012.

[113] J. Kober and J. Peters. Policy search for motor primitives in robotics. *Machine Learning*, 84(1-2):171–203, 2011.

[114] T. Komatsu and M. Usui. Dynamic walking and running of a bipedal robot using hybrid central pattern generator method. In *Mechatronics and Automation, 2005 IEEE International Conference*, volume 2, pages 987–992 Vol. 2, 2005.

[115] I. Koo, T. Kang, G. Vo, T. Trong, Y. Song, and H. Choi. Biologically inspired control of quadruped walking robot. *International Journal of Control, Automation and Systems*, 7(4):577–584, 2009.

[116] A. Kuo. The relative roles of feedforward and feedback in the control of rhythmic movements. *Motor Control*, 2(6):1087–1640, 2002.

[117] A. D. Kuo. The six determinants of gait and the inverted pendulum analogy: A dynamic walking perspective. *Human Movement Science*, 26(4):617 – 656, 2007. European Workshop on Movement Science 2007 European Workshop on Movement Science 2007.

[118] A. D. Kuo, J. M. Donelan, and A. Ruina. Energetic consequences of walking like an inverted pendulum: step-to-step transitions. *Exercise and sport sciences reviews*, 33(2):88–97, Apr. 2005.

[119] M. Lafreniere-Roula and D. A. McCrea. Deletions of rhythmic motoneuron activity during fictive locomotion and scratch provide clues to the organization of the mammalian central pattern generator. *Journal of Neurophysiology*, 94(2):1120–1132, 2005.

[120] G. Lee, R. Lowe, and T. Ziemke. Modelling early infant walking: Testing a generic CPG architecture on the nao humanoid. In *Development and Learning (ICDL), 2011 IEEE International Conference on*, volume 2, pages 1–6, 2011.

[121] J. Lee, J.-Y. Kim, I.-W. Park, B.-K. Cho, M.-S. Kim, I. Kim, and J.-H. Oh. Development of a humanoid robot platform HUBO FX-1. In *SICE-ICASE, 2006. International Joint Conference*, pages 1190–1194, 2006.

[122] M. Lewis and G. Bekey. Gait adaptation in a quadruped robot. *Autonomous Robots*, 12(3):301–312, 2002.

[123] M. A. Lewis and L. S. Simo. Elegant stepping: A model of visually triggered gait adaptation. *Connect. Sci.*, 11(3-4):331–344, 1999.

[124] C. Maioli and R. E. Poppele. Parallel processing of multisensory information concerning self-motion. *Experimental Brain Research*, 87(1):119–125, oct 1991.

[125] V. A. Makarov, E. Del Río, M. G. Bedia, M. G. Velarde, and W. Ebeling. Central pattern generator incorporating the actuator dynamics for a hexapod robot. In *Proceedings of World Academy of Science Engineering and Technology*, pages 19–24, 2006.

[126] P. Manoonpong, T. Geng, T. Kulvicius, B. Porr, and F. Wörgötter. Adaptive, fast walking in a biped robot under neuronal control and learning. *PLoS Computational Biology*, 3(7), 2007.

[127] P. Manoonpong, F. Pasemann, and F. Wörgötter. Sensor-driven neural control for omnidirectional locomotion and versatile reactive behaviors of walking machines. *Robot. Auton. Syst.*, 56(3):265–288, 2008.

[128] E. Marder, D. Bucher, D. J. Schulz, and A. L. Taylor. Invertebrate central pattern generation moves along. *Current Biology*, 15(17):R685 – R699, 2005.

[129] J. Massion, K. Popov, J. C. Fabre, P. Rage, and V. Gurfinkel. Is the erect posture in microgravity based on the control of trunk orientation or center of mass position? *Experimental Brain Research*, 114(2):384–389, apr 1997.

[130] V. Matos and C. P. Santos. Central pattern generators with phase regulation for the control of humanoid locomotion. In *IEEE-RAS International Conference on Humanoid Robots*, Business Innovation Center Osaka, Japan, 2012.

[131] V. Matos, C. P. Santos, and C. Pinto. A brainstem-like modulation approach for gait transition in a quadruped robot. In *Intelligent Robots and Systems, 2009. IROS 2009. IEEE/RSJ International Conference on*, pages 2665 –2670, 2009.

[132] T. Matsubara, J. Morimoto, J. Nakanishi, M. Sato, and K. Doya. Learning CPG-based biped locomotion with a policy gradient method. In *Humanoid Robots, 2005 5th IEEE-RAS International Conference on*, pages 208–213, 2005.

[133] K. Matsuoka. Sustained oscillations generated by mutually inhibiting neurons with adaptation. *Biological Cybernetics*, 52(6):367–376, 1985.

[134] C. Maufroy, H. Kimura, and K. Takase. Towards a general neural controller for quadrupedal locomotion. *Neural Networks*, 21(4):667 – 681, 2008. Robotics and Neuroscience.

[135] C. Maufroy, H. Kimura, and K. Takase. Integration of posture and rhythmic motion controls in quadrupedal dynamic walking using phase modulations based on leg loading/unloading. *Autonomous Robots*, 28(3):331–353, 2010.

[136] C. Maufroy, T. Nishikawa, and H. Kimura. Stable dynamic walking of a quadruped robot kotetsu; using phase modulations based on leg loading/unloading. In *Robotics and Automation (ICRA), 2010 IEEE International Conference on*, pages 5225–5230, 2010.

[137] D. Mccrea, J. Quevedo, B. Fedirchuk, and S. Gosgnach. The stumbling correction reaction during fictive locomotion in the cat. *Annals of the New York Academy of Sciences*, 860(1):502–504, 1998.

[138] D. A. McCrea. Spinal circuitry of sensorimotor control of locomotion. *The Journal of Physiology*, 533(1):41–50, 2001.

[139] D. A. McCrea and I. A. Rybak. Organization of mammalian locomotor rhythm and pattern generation. *Brain Research Reviews*, 57(1):134 – 146, 2008.

[140] T. McGeer. Passive walking with knees. In *Robotics and Automation, 1990. Proceedings., 1990 IEEE International Conference on*, pages 1640–1645 vol.3, 1990.

[141] R. B. McGhee. Computer coordination of motion for omni-directional hexapod walking machines. *Advanced Robotics*, 1(2):91–99, 1986.

[142] P. McSharry, G. Clifford, L. Tarassenko, and L. Smith. A dynamical model for generating synthetic electrocardiogram signals. *Biomedical Engineering, IEEE Transactions on*, 50(3):289 –294, march 2003.

[143] D. A. McVea, J. M. Donelan, A. Tachibana, and K. G. Pearson. A role for hip position in initiating the swing-to-stance transition in walking cats. *Journal of Neurophysiology*, 94(5):3497–3508, 2005.

[144] A. Minetti. The biomechanics of skipping gaits: a third locomotor paradigm? *Royal society of London. Proceedings. B, Biological sciences*, 265(1402):1227 – 1235, 07 1998.

[145] H. L. More, J. R. Hutchinson, D. F. Collins, D. J. Weber, S. K. H. Aung, and J. M. Donelan. Scaling of sensorimotor control in terrestrial mammals. *Proceedings of the Royal Society B: Biological Sciences*, 277(1700):3563–3568, 2010.

[146] T. Mori, Y. Nakamura, M.-A. Sato, and S. Ishii. Reinforcement learning for a CPG-driven biped robot. In *Proceedings of the 19th national conference on Artifical intelligence*, AAAI'04, pages 623–630. AAAI Press, 2004.

[147] J. Morimoto, G. Endo, J. Nakanishi, and G. Cheng. A biologically inspired biped locomotion strategy for humanoid robots: Modulation of sinusoidal patterns by a coupled oscillator model. *Robotics, IEEE Transactions on*, 24(1):185–191, 2008.

[148] J. Morimoto, S. Hyon, C. Atkeson, and G. Cheng. Low-dimensional feature extraction for humanoid locomotion using kernel dimension reduction. In *Robotics and Automation, 2008. ICRA 2008. IEEE International Conference on*, pages 2711–2716, 2008.

[149] J. Nakanishi, J. Morimoto, G. Endo, G. Cheng, S. Schaal, and M. Kawato. Learning from demonstration and adaptation of biped locomotion. *Robotics and Autonomous Systems*, 47(2–3):79 – 91, 2004.

[150] R. Niiyama and Y. Kuniyoshi. A pneumatic biped with an artificial musculoskeletal system. In *Proc. 4th Int. Symposium on Adaptive Motion of Animals and Machines (AMAM 2008)*, pages 80–81, Cleveland, Ohio USA, June 2008.

[151] M. Ogino, Y. Katoh, M. Aono, M. Asada, and K. Hosoda. Reinforcement learning of humanoid rhythmic walking parameters based on visual information. *Advanced Robotics*, 18(7):677–697, 2004.

[152] M. Oliveira, C. P. Santos, L. Costa, and M. Ferreira. Multi-objective parameter CPG optimization for gait generation of a quadruped robot considering behavioral diversity. *2011 IEEE/RSJ International Conference on Intelligent Robots and Systems (IROS 2011)*, page 2286–2291, 2011.

[153] J. Or. A hybrid CPG-ZMP controller for the real-time balance of a simulated flexible spine humanoid robot. *Systems, Man, and Cybernetics, Part C: Applications and Reviews, IEEE Transactions on*, 39(5):547–561, 2009.

[154] G. N. Orlovskii, T. G. Deliagina, and S. Grillner. *Neuronal control of locomotion: from mollusc to man*. Oxford University Press, 1999.

[155] D. Owaki, T. Kano, K. Nagasawa, A. Tero, and A. Ishiguro. Simple robot suggests physical interlimb communication is essential for quadruped walking. *Journal of The Royal Society Interface*, 2012.

[156] M. Y. C. Pang and J. F. Yang. The initiation of the swing phase in human infant stepping: importance of hip position and leg loading. *The Journal of Physiology*, 528(2):389–404, 2000.

[157] P. Pastor, M. Kalakrishnan, F. Meier, F. Stulp, J. Buchli, E. Theodorou, and S. Schaal. From dynamic movement primitives to associative skill memories. *Robotics and Autonomous Systems*, 61(4):351 – 361, 2013. Models and Technologies for Multi-modal Skill Training.

[158] K. Pearson. Role of sensory feedback in the control of stance duration in walking cats. *Brain Research Reviews*, 57(1):222 – 227, 2008.

[159] K. G. Pearson. Proprioceptive regulation of locomotion. *Current Opinion in Neurobiology*, 5(6):786 – 791, 1995.

[160] K. G. Pearson. Generating the walking gait: role of sensory feedback. In S. Mori, D. G. Stuart, and M. Wiesendanger, editors, *Brain Mechanisms for the Integration of Posture and Movement*, volume 143 of *Progress in Brain Research*, pages 123 – 129. Elsevier, 2004.

[161] F. Petit, M. Chalon, W. Friedl, M. Grebenstein, A. Albu-Schäffer, and G. Hirzinger. Bidirectional antagonistic variable stiffness actuation: Analysis, design amp; implementation. In *Robotics and Automation (ICRA), 2010 IEEE International Conference on*, pages 4189–4196, 2010.

[162] R. Pfeifer, M. Lungarella, and F. Iida. Self-organization, embodiment, and biologically inspired robotics. *Science*, 318(5853):1088–1093, 2007.

[163] A. C. d. Pina Filho. Simulating the hip and knee behavior of a biped by means of nonlinear oscillators. *The Open Cybernetics & Systemics Journal*, 2:185–191, 2008.

[164] A. C. d. Pina Filho and M. S. Dutra. Study and modeling of the ankles movement pattern in the course of human locomotion. In *Proceedings of COBEM 2007, 19th International Congress of Mechanical Engineering*, 2007.

[165] C. Pinto and M. Golubitsky. Central pattern generators for bipedal locomotion. *Journal of Mathematical Biology*, 53(3):474–489, 2006.

[166] G. Pratt. Legged robots at MIT: what's new since raibert? *Robotics Automation Magazine, IEEE*, 7(3):15–19, 2000.

[167] G. A. Pratt. Low impedance walking robots. *Integrative and Comparative Biology*, 42(1):174–181, 2002.

[168] J. Pratt, P. Dilworth, and G. Pratt. Virtual model control of a bipedal walking robot. In *IEEE Conference on Robotics and Automation*, pages 193–198, 1997.

[169] M. Raibert, M. Chepponis, and H. B. Brown. Experiments in balance with a 3D one-legged hopping machine. *International Journal of Robotics Research*, 3:75–92, 1984.

[170] M. Raibert, M. Chepponis, and J. Brown, H.B. Running on four legs as though they were one. *Robotics and Automation, IEEE Journal of*, 2(2):70–82, 1986.

[171] C. D. Remy, K. W. Buffinton, and R. Y. Siegwart. Stability analysis of passive dynamic walking of quadrupeds. *The International Journal of Robotics Research*, in press, 2009.

[172] C. Ridderstrom and J. Ingvast. Quadruped posture control based on simple force distribution-a notion and a trial. In *Intelligent Robots and Systems, 2001. Proceedings. 2001 IEEE/RSJ International Conference on*, volume 4, pages 2326–2331 vol.4, 2001.

[173] L. Righetti and A. Ijspeert. Programmable central pattern generators: an application to biped locomotion control. In *Robotics and Automation, 2006. ICRA 2006. Proceedings 2006 IEEE International Conference on*, pages 1585–1590, 2006.

[174] L. Righetti and A. J. Ijspeert. Pattern generators with sensory feedback for the control of quadruped locomotion. In *IEEE International Conference on Robotics and Automation, 2008. ICRA 2008*, pages 819–824, May 2008.

[175] D. Robinson, J. Pratt, D. Paluska, and G. Pratt. Series elastic actuator development for a biomimetic walking robot. In *Advanced Intelligent Mechatronics, 1999. Proceedings. 1999 IEEE/ASME International Conference on*, pages 561–568, 1999.

[176] S. Rossignol, R. Dubuc, and J.-P. Gossard. Dynamic sensorimotor interactions in locomotion. *Physiological Reviews*, 86(1):89–154, 2006.

[177] A. Russell, G. Orchard, and R. Etienne-Cummings. Configuring of spiking central pattern generator networks for bipedal walking using genetic algorthms. In *Circuits and Systems, 2007. ISCAS 2007. IEEE International Symposium on*, pages 1525–1528, 2007.

[178] S. Rutishauser, A. Sprowitz, L. Righetti, and A. Ijspeert. Passive compliant quadruped robot using central pattern generators for locomotion control. In *Biomedical Robotics and Biomechatronics, 2008. BioRob 2008. 2nd IEEE RAS EMBS International Conference on*, pages 710–715, 2008.

[179] J. S. S. Barthélemy and A. Micaelli. Arboris-python, 2012. [Online]`https://github.com/salini/arboris-pyhton`.

[180] N. Saito, N. Saga, and T. Sato. Development of spherical joint robot using pneumatic artificial muscles. In *Industrial Electronics, 2008. IECON 2008. 34th Annual Conference of IEEE*, pages 1614–1619, 2008.

[181] J. Salini, S. Barthélemy, and P. Bidaud. LQP-Based controller design for humanoid whole-body motion. In *Advances in Robot Kinematics: Motion in Man and Machine*, pages 177–184. Springer, 2010.

[182] J. Salini, V. Padois, and P. Bidaud. Synthesis of complex humanoid whole-body behavior: A focus on sequencing and tasks transitions. In *Robotics and Automation (ICRA), 2011 IEEE International Conference on*, pages 1283–1290, 2011.

[183] C. P. Santos and M. Ferreira. Two vision-guided vehicles: temporal coordination using nonlinear dynamical systems. In *ICRA*, pages 14–19, 2007.

[184] C. P. Santos and V. Matos. Gait transition and modulation in a quadruped robot: A brainstem-like modulation approach. *Robotics and Autonomous Systems*, In Press, Accepted Manuscript:–, 2011.

[185] C. P. Santos and V. Matos. CPG modulation for navigation and omnidirectional quadruped locomotion. *Robotics and Autonomous Systems*, 60(6):912 – 927, 2012.

[186] C. P. Santos, M. Oliveira, A. M. A. C. Rocha, and L. Costa. Head motion stabilization during quadruped robot locomotion: Combining dynamical systems and a genetic algorithm. In *2009 IEEE International Conference on Robotics and Automation, ICRA 2009, Kobe, Japan, May 12-17, 2009*, pages 2294–2299, 2009.

[187] M. Sato, Y. Nakamura, and S. Ishii. Reinforcement learning for biped locomotion. In J. R. Dorronsoro, editor, *ICANN*, volume 2415 of *Lecture Notes in Computer Science*, pages 777–782. Springer, 2002.

[188] Saunders, V. T. Inman, and H. D. Eberhart. The major determinants in normal and pathological gait. *J Bone Joint Surg Am*, 35(3):543–558, July 1953.

[189] S. Schaal, S. Kotosaka, and D. Sternad. Nonlinear dynamical systems as movement primitives. In *Humanoids2000, First IEEE-RAS International Conference on Humanoid Robots*, 2000.

[190] S. Schaal and N. Schweighofer. Computational motor control in humans and robots. *Current Opinion in Neurobiology*, 15(6):675 – 682, 2005.

[191] S. Schaal, D. Sternad, and C. G. Atkeson. One-handed juggling: A dynamical approach to a rhythmic movement task. *Journal of Motor Behavior*, pages 165–183, 1996.

[192] G. Schöner, M. Dose, and C. Engels. Dynamics of behavior: Theory and applications for autonomous robot architectures. *Robotics and Autonomous Systems*, 16(2–4):213 – 245, 1995. Moving the Frontiers between Robotics and Biology.

[193] C. Semini, N. G. Tsagarakis, E. Guglielmino, M. Focchi, F. Cannella, and D. G. Caldwell. Design of HyQ – a hydraulically and electrically actuated quadruped robot. *Proceedings of the Institution of Mechanical Engineers, Part I: Journal of Systems and Control Engineering*, 225(6):831–849, 2011.

[194] J. Shan and F. Nagashima. Neural locomotion controller design and implementation for humanoid robot HOAP-1. *Nippon Robotto Gakkai Gakujutsu Koenkai Yokoshu*, 20:1C34, 2008.

[195] M. L. Shik, F. V. Severin, and G. N. Orlovskiĭ. Control of walking and running by means of electric stimulation of the midbrain. *Biofizika*, 11(4):659–666, 1966.

[196] S. Shimada, T. Egami, K. Ishimura, and M. Wada. Neural control of quadruped robot for autonomous walking on soft terrain. In H. Asama, T. Arai, T. Fukuda, and T. Hasegawa, editors, *Distributed Autonomous Robotic Systems 5*, pages 415–423. Springer Japan, 2002.

[197] R. Siegwart and I. R. Nourbakhsh. *Introduction to Autonomous Mobile Robots*. Bradford Company, Scituate, MA, USA, 2004.

[198] J. Silva, V. Matos, and C. P. Santos. Timed trajectory generation for a toy-like wheeled robot. In *IECON 2010 - 36th Annual Conference on IEEE Industrial Electronics Society*, pages 1645 –1650, nov. 2010.

[199] S.-M. Song and K. J. Waldron. *Machines that walk: the adaptive suspension vehicle*. MIT Press„ Cambridge, Mass., 1989.

[200] J. Sousa, V. Matos, and C. Peixoto dos Santos. A bio-inspired postural control for a quadruped robot: An attractor-based dynamics. In *2010 IEEE/RSJ International Conference on Intelligent Robots and Systems*, pages 5329 –5334, 2010.

[201] S. Strogatz. *Nonlinear Dynamics And Chaos*. Sarat Book House, 1994.

[202] N. Sugimoto and J. Morimoto. Phase-dependent trajectory optimization for CPG-based biped walking using path integral reinforcement learning. In *Humanoid Robots (Humanoids), 2011 11th IEEE-RAS International Conference on*, pages 255–260, 2011.

[203] L. Sun, M.-H. Meng, W. Chen, H. Liang, and T. Mei. Design of quadruped robot based CPG and fuzzy neural network. In *Automation and Logistics, 2007 IEEE International Conference on*, pages 2403–2408, 2007.

[204] G. Taga. A model of the neuro-musculo-skeletal system for human locomotion - I. emergence of basic gait. *Biological Cybernetics*, 73(2):97–111, 1995.

[205] G. Taga. A model of the neuro-musculo-skeletal system for human locomotion - II. real-time adaptability under various constraints. *Biological Cybernetics*, 73(2):113–121, 1995.

[206] G. Taga. A model of the neuro-musculo-skeletal system for anticipatory adjustment of human locomotion during obstacle avoidance. *Biological Cybernetics*, 78(1):9–17, 1998.

[207] G. Taga, Y. Yamaguchi, and H. Shimizu. Self-organized control of bipedal locomotion by neural oscillators in unpredictable environment. *Biological Cybernetics*, 65(3):147–159, 1991.

[208] H. Takemura, M. Deguchi, J. Ueda, Y. Matsumoto, and T. Ogasawara. Slip-adaptive walk of quadruped robot. *Robotics and Autonomous Systems*, 53(2):124–141, 2005.

[209] H. Takemura, J. Ueda, Y. Matsumoto, and T. Ogasawara. A study of a gait generation of a quadruped robot based on rhythmic control - optimization of CPG parameters by a fast dynamics simulation environment. In *Proceedings of 5th International Conference on Climbing and Walking Robots (CLAWAR 2002)*, pages 759–766, 2002.

[210] C. Tang, S. Ma, B. Li, and Y. Wang. A self-tuning multi-phase CPG enabling the snake robot to adapt to environments. In *Intelligent Robots and Systems (IROS), 2011 IEEE/RSJ International Conference on*, pages 1869–1874, 2011.

[211] C. Teixeira, L. Costa, and C. Santos. Self-Improving Biped Locomotion. In *11th International Conference of Numerical Analysis and Applied Mathematics (ICNAAM)*, 2013.

[212] E. Theodorou, J. Buchli, and S. Schaal. Reinforcement learning of motor skills in high dimensions: A path integral approach. In *Robotics and Automation (ICRA), 2010 IEEE International Conference on*, pages 2397–2403, 2010.

[213] D. T. Tran, I. M. Koo, G. L. Vo, S. gon Roh, S. Park, H. Moon, and H.-R. Choi. A new method in modeling central pattern generators to control quadruped walking robots. In *Intelligent Robots and Systems, 2009. IROS 2009. IEEE/RSJ International Conference on*, pages 129–134, 2009.

[214] M. Tresch, P. Saltiel, and E. Bizzi. The construction of movement by the spinal cord. *Nature Neuroscience*, 2(2):162–167, 1999.

[215] K. Tsujita, H. Toui, and K. Tsuchiya. Dynamic turning control of a quadruped locomotion robot using oscillators. *Advanced Robotics*, 19:1115–1133(19), October 2005.

[216] K. Tsujita, K. Tsuchiya, and A. Onat. Adaptive gait pattern control of a quadruped locomotion robot. In *Intelligent Robots and Systems, 2001. Proceedings. 2001 IEEE/RSJ International Conference on*, volume 4, pages 2318–2325 vol.4, 2001.

[217] M. Vukobratovic and B. Borovac. Zero-moment point - thirty five years of its life. *I. J. Humanoid Robotics*, 1(1):157–173, 2004.

[218] T. Wadden and Ö. Ekeberg. A neuro-mechanical model of legged locomotion: single leg control. *Biological Cybernetics*, 79(2):161–173, 1998.

[219] Webots. http://www.cyberbotics.com. Commercial Mobile Robot Simulation Software.

[220] P. B. Wieber. Trajectory free linear model predictive control for stable walking in the presence of strong perturbations. In *Humanoid Robots, 2006 6th IEEE-RAS International Conference on*, pages 137–142, 2006.

[221] M. Williamson. Rhythmic robot arm control using oscillators. In *Intelligent Robots and Systems, 1998. Proceedings., 1998 IEEE/RSJ International Conference on*, volume 1, pages 77–83 vol.1, 1998.

[222] D. Wooden, M. Malchano, K. Blankespoor, A. Howard, A. A. Rizzi, and M. Raibert. Autonomous navigation for BigDog. In *IEEE International Conference on Robotics and Automation, 2010. ICRA 2010*, pages 4736–4741. IEEE, 2010.

[223] K. Yoneda and S. Hirose. Dynamic and static fusion gait of a quadruped walking vehicle on a winding path. In *Robotics and Automation, 1992. Proceedings., 1992 IEEE International Conference on*, pages 143–148 vol.1, 1992.

[224] L. Zhang, S. Ma, and K. Inoue. Several insights into omnidirectional static walking of a quadruped robot on a slope. In *IROS*, pages 5249–5254, 2006.

[225] X. Zhang and H. Zheng. Walking up and down hill with a biologically-inspired postural reflex in a quadrupedal robot. *Autonomous Robots*, 25(1-2):15–24, 2008.

[226] M. Zhao and L. Sentis. A three dimensional foot placement planner for locomotion in very rough terrains. In *IEEE-RAS International Conference on Humanoid Robots*, Business Innovation Center Osaka, Japan, 2012.

APPENDIX A

LANDAU-STUART OSCILLATOR

The oscillator presented in chapter 3 and used for the quadruped CPG in chapter 4 is here analytically analyzed. A simple representation of the Landau-Stuart equation with amplitude independent frequency is presented in cartesian coordinates in equations (A.1) and (A.2). The mathematical expression defines an isochronous oscillator (frequency is independent of its amplitude) with an Hopf bifurcation, having a stable harmonic limit cycle solution or a stable fixed point at the origin $(x, z) = (O, 0)$.

$$\dot{x} = f_x = \alpha \left(\mu - ((x - O)^2 + z^2)\right)(x - O) - \omega z, \tag{A.1}$$

$$\dot{z} = f_z = \alpha \left(\mu - ((x - O)^2 + z^2)\right) z + \omega(x - O), \tag{A.2}$$

A.1 Behavior and stability of the oscillator

To study the behavior, the system is linearized about the fixed point $(x, z) = (O, 0)$, by computing the Jacobian matrix $J(f_x, f_z)$.

$$J(f_x, f_z) = \begin{bmatrix} \frac{\partial f_x}{\partial x} & \frac{\partial f_x}{\partial z} \\ \frac{\partial f_z}{\partial x} & \frac{\partial f_z}{\partial z} \end{bmatrix} \tag{A.3}$$

$$= \begin{bmatrix} -\alpha(z^2 - \mu + (O - x)^2) - \alpha(O - x)(2O - 2x) & 2\alpha z(O - x) - \omega \\ \omega + 2\alpha z(O - x) & -2\alpha z^2 - \alpha(z^2 - \mu + (O - x)^2) \end{bmatrix} \tag{A.4}$$

The eigenvalues of the Jacobian at the fixed point are used to determine the behavior of the system:

$$J(O, 0) = \begin{bmatrix} \alpha\mu & -\omega \\ \omega & \alpha\mu \end{bmatrix} \tag{A.5}$$

The eigenvalues given by $\det|\lambda \mathrm{I} - J| = 0$ are $\lambda = \alpha\mu \pm i\omega$, giving the necessary information for the system's classification at the fixed point. The imaginary part of the eigenvalues reveals a periodic behavior in the linearized approximation. The real part denotes wether it behaves as a source or sink at the fixed point.

- For $\alpha\mu > 0$ the fixed point behaves as source (repeller). Trajectories spiral outwards from the fixed point.
- For $\alpha\mu = 0$ stability can not be determined by linearization.
- For $\alpha\mu < 0$ the fixed point behaves as sink (attractor). Trajectories spiral towards the fixed point.

To further study the periodic behavior of the system, a change to polar coordinates is performed, for an easier analysis.

Let $x = O + r\cos(\theta)$, $z = r\sin(\theta)$ and $r = \sqrt{(x-O)^2 + z^2}$. Substituting in eqs. (A.1) and (A.2) yields:

$$\dot{r}\cos(\theta) - r\dot{\theta}\sin(\theta) = \alpha\left(\mu - r^2\right)r\cos(\theta) - \omega r\sin(\theta) \tag{A.6}$$

$$\dot{r}\sin(\theta) + r\dot{\theta}\cos(\theta) = \alpha\left(\mu - r^2\right)r\sin(\theta) + \omega r\cos(\theta) \tag{A.7}$$

Multiplying eqs. (A.6) and (A.7) by $\cos(\theta)$ and by $\sin(\theta)$ respectively, results in:

$$\dot{r}\cos^2(\theta) - r\dot{\theta}\sin(\theta)\cos(\theta) = \alpha\left(\mu - r^2\right)r\cos^2(\theta) - \omega r\sin(\theta)\cos(\theta) \tag{A.8}$$

$$\dot{r}\sin^2(\theta) + r\dot{\theta}\sin(\theta)\cos(\theta) = \alpha\left(\mu - r^2\right)r\sin^2(\theta) + \omega r\sin(\theta)\cos(\theta) \tag{A.9}$$

Then, adding both equations yields:

$$\dot{r}\left(\cos^2(\theta) + \sin^2(\theta)\right) = \alpha(\mu - r^2)r\left(\cos^2(\theta) + \sin^2(\theta)\right) \tag{A.10}$$

$$\implies \dot{r} = \alpha\left(\mu - r^2\right)r \tag{A.11}$$

Multiplying again eqs. (A.6) and (A.7), this time by $\sin(\theta)$ and by $\cos(\theta)$, becomes:

$$\dot{r}\sin(\theta)\cos(\theta) - r\dot{\theta}\sin^2(\theta) = \alpha\left(\mu - r^2\right)r\sin(\theta)\cos(\theta) - \omega r\sin^2(\theta) \tag{A.12}$$

$$\dot{r}\sin(\theta)\cos(\theta) + r\dot{\theta}\cos^2(\theta) = \alpha\left(\mu - r^2\right)r\sin(\theta)\cos(\theta) + \omega r\cos^2(\theta) \tag{A.13}$$

Then, adding both equations yields:

$$\dot{\theta}r\left(\cos^2(\theta) + \sin^2(\theta)\right) = \omega r\left(\cos^2(\theta) + \sin^2(\theta)\right) \tag{A.14}$$

$$\implies \dot{\theta} = \omega \tag{A.15}$$

Equations (A.11) and (A.15) are the polar representation of the oscillator, making it easier to analyze because the radius (r) and phase motion (θ) are independent. Classifying the behavior of the oscillator is a matter of analyzing the behavior of the radius and phase.

In terms of phase, the behavior defined by the differential equation (A.15) is easy to be analyzed. The phase of the periodic solution increases with a constant rate of change ω.

The fixed points described by eq. (A.11) define the steady state of the oscillator's radius. Making $\dot{r} = 0$, yields the fixed points: $r_{*1} = 0$, $r_{*2} = \pm\sqrt{\mu}$. Given that $r = \sqrt{(x - O^2) + z^2}$, the fixed point $r_{*2} = -\sqrt{\mu}$ is not considered. The linearized system is studied at the fixed points:

$r_{*1} = 0$:

$$\frac{d}{dr}\left(\alpha(\mu - r^2)r\right)\bigg|_{r=r_{*1}} = \alpha(\mu - 3 \times 0^2) \tag{A.16}$$

$$= \alpha\mu \tag{A.17}$$

The fixed point $r = 0$ is stable if $\alpha\mu < 0$, and unstable if $\alpha\mu > 0$. Given the previously determination of the origin's behavior, the fixed point at the origin $(x, z) = (O, 0)$ is a sink when $\alpha\mu < 0$ and the radius of the periodic solution will converge to the stable fixed point $r = 0$. When $\alpha\mu > 0$ the $(x, z) = (O, 0)$ behaves as a periodic source and the fixed point $r = 0$ is unstable.

$r_{*2} = \sqrt{\mu}$:

$$\frac{d}{dr}\left(\alpha(\mu - r^2)r\right)\bigg|_{r=r_{*2}} = \alpha(\mu - 3\sqrt{\mu}^2) \tag{A.18}$$

$$= -2\alpha\mu \tag{A.19}$$

The fixed point $r = \sqrt{\mu}$ is stable if $\alpha\mu > 0$, and unstable if $\alpha\mu < 0$. This means that the fixed point at the origin $(x, z) = (O, 0)$ acts as a source when $\alpha\mu < 0$, producing a periodic solution which then stabilizes with a radius of $r = \sqrt{\mu}$. When $\alpha\mu < 0$ the fixed $r = \sqrt{\mu}$ becomes unstable, and the radius converges to the other fixed point $r = 0$.

The radius of the periodic solution is determined by the value of $\sqrt{\mu}$, established at all times that $\mu > 0$. The oscillator behavior is then specified by the sign of α, controlling the supercritical Hopf bifurcation [201].

- The oscillator produces a periodic motion, for $\alpha > 0$, centered at $(x, y) = (O, 0)$ with ω frequency and a radius $\sqrt{\mu}$.
- The oscillator produces an oscillatory convergent solution towards $(x, y) = (O, 0)$, for $\alpha < 0$.

A.2 Phase coupling into Landau-Stuart oscillator

The coupling established in section 4.5, in chapter 4, is here demonstrated. Consider the oscillator in polar coordinates, coupled with a phase reference ψ, for an easier addition of the coupling term:

$$\begin{aligned} \dot{r} &= \alpha\left(\mu - r^2\right) r \\ \dot{\theta} &= \omega + k\sin(\psi - \theta) \end{aligned} \tag{A.20}$$

The oscillator is then changed to cartesian coordinates, considering $\theta = \cos^{-1}\left(\frac{x}{r}\right)$, $\theta = \sin^{-1}\left(\frac{z}{r}\right)$, $r = \frac{x}{\cos(\theta)}$, and $r = \frac{z}{\sin(\theta)}$.

$$\begin{aligned} \dot{x} &= \dot{r}\cos(\theta) - r\dot{\theta}\sin(\theta) \\ \dot{z} &= \dot{r}\sin(\theta) - r\dot{\theta}\cos(\theta) \end{aligned} \tag{A.21}$$

$$\implies \begin{aligned} \dot{x} &= \alpha(\mu - r^2) r\cos(\cos^{-1}(\tfrac{x}{r})) - \tfrac{z}{\sin(\theta)}\left[\omega + \sin(\psi - \theta)\right]\sin(\theta) \\ \dot{z} &= \alpha(\mu - r^2) r\sin(\sin^{-1}(\tfrac{x}{r})) - \tfrac{x}{\cos(\theta)}\left[\omega + \sin(\psi - \theta)\right]\cos(\theta) \end{aligned} \tag{A.22}$$

$$\implies \begin{aligned} \dot{x} &= \alpha(\mu - r^2)x - z\left[\omega + \sin(\psi - \theta)\right] \\ \dot{z} &= \alpha(\mu - r^2)z - x\left[\omega + \sin(\psi - \theta)\right] \end{aligned} \tag{A.23}$$

Using the trigonometric identity $\sin(\alpha - \beta) = \sin(\alpha)\cos(\beta) - \cos(\alpha)\sin(\beta)$:

$$\begin{aligned} \sin(\psi - \theta) &= \sin(\psi)\cos(\theta) - \cos(\psi)\sin(\theta) \\ &= \tfrac{x}{r}\sin(\psi) - \tfrac{z}{r}\cos(\psi) \\ &= \tfrac{1}{r}\left(x\sin(\psi) - z\cos(\psi)\right) \end{aligned} \tag{A.24}$$

Substituting in equations (A.23):

$$\begin{aligned} \dot{x} &= \alpha(\mu - r^2)x - z\left[\omega + \tfrac{k}{r}\left(x\sin(\psi) - z\cos(\psi)\right)\right] \\ \dot{z} &= \alpha(\mu - r^2)z - x\left[\omega + \tfrac{k}{r}\left(x\sin(\psi) - z\cos(\psi)\right)\right] \end{aligned} \tag{A.25}$$

We have then the oscillator coupled with a phase reference ψ in cartesian representation:

$$\dot{x} = \alpha(\mu - r^2)x - z\overline{\omega} \tag{A.26}$$

$$\dot{z} = \alpha(\mu - r^2)z - x\overline{\omega} \tag{A.27}$$

$$\overline{\omega} = \omega + \frac{k}{r}\left(x\sin(\psi) - z\cos(\psi)\right) \tag{A.28}$$

$$r = \sqrt{x^2 + z^2} \tag{A.29}$$

APPENDIX B

PHASE OSCILLATOR COUPLING

Synchronization and phase locking of two phase oscillators is here analytically studied and phase locking properties demonstrated, in the particular case which both have the same frequency.

The dynamics of the two coupled phase oscillators are described by the nonuniform phase oscillators [1]:

$$\dot{\phi} = \omega + K\sin\left(\theta - \phi + \Psi\right), \tag{B.1}$$

$$\dot{\theta} = \omega + K\sin\left(\phi - \theta - \Psi\right), \tag{B.2}$$

where ϕ and θ are the phase of the oscillators, ω is the phase speed, or frequency, as given by the period of oscillations $\omega = \frac{2\pi}{T}$, Ψ is the desired phase difference, and K the coupling strength.

The phase relationship resulting from the coupling between ϕ and θ phase oscillators can be easily analyzed in terms of dynamical system stability. Consider the phase difference dynamics between the two oscillators as:

$$\psi = \phi - \theta \tag{B.3}$$

$$\dot{\psi} = \dot{\phi} - \dot{\theta} \tag{B.4}$$

Performing the variable substitution from eq. (B.1) and eq. (B.2) in eq.(B.4), obtains:

$$\dot{\psi} = \omega + K\sin\left(-\psi + \Psi\right) - \omega - K\sin\left(\psi - \Psi\right) \tag{B.5}$$

$$\Rightarrow \dot{\psi} = -2K\sin\left(\psi - \Psi\right) \tag{B.6}$$

The value of a stable phase difference between ϕ and θ is achieved when $\dot{\psi} = 0$. In other words, the stable fixed points from $\dot{\psi}$ in eq. (B.6).

$$-2K\sin(\psi-\Psi) = 0 \tag{B.7}$$

$$\Rightarrow \psi-\Psi = k\pi \tag{B.8}$$

$$\Rightarrow \psi = \Psi + k\pi \tag{B.9}$$

The fixed points for the phase relationship are found to be $\Psi + k\pi$ with $k \in \mathbb{Z}$.

To find which of these fixed points are stable, a linear approximation is performed around the fixed points:

$$\frac{\mathrm{d}}{\mathrm{d}\psi}\left(-2K\sin(\psi-\Psi)\right) < 0 \tag{B.10}$$

$$\left(-2K\cos(\psi-\Psi)\right) < 0 \tag{B.11}$$

Therefore, with $K > 0$, the stability of the fixed points follows that for:

$$-2K\cos(\psi-\Psi)\big|_{(\psi-\Psi)=k\pi, k\in\mathbb{Z}} \tag{B.12}$$

- The fixed point is unstable, when k is even.
- The fixed point is stable, when k is odd.

The stable fixed points are found analytically to be periodic, with period 2π. This is also possible to be verified through visual inspection in fig. B.1.

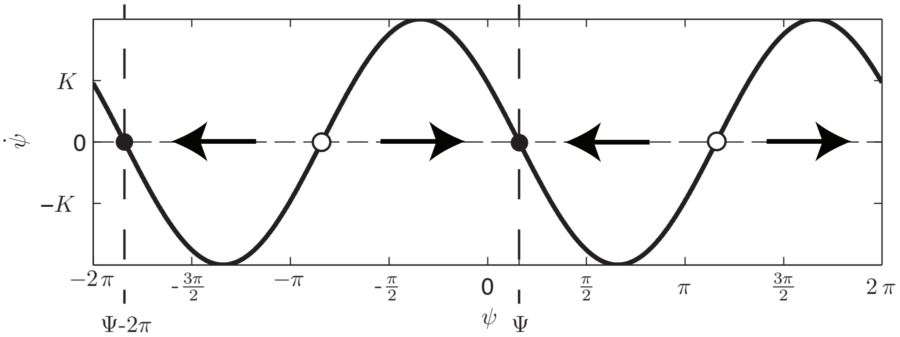

Figure B.1: Phase plot of the phase difference between the two oscillator.

This means that two phase oscillators with equal frequencies, using the coupling method in eq.(B.1), will always maintain the desired phase relationship of Ψ, regardless of initial conditions.